STUDIES OF MASS TRANSPORT IN SOME POLY (ETHYLENEOXIDE)- BASED POLYMER ELECTROLYTES

Martin Thomas Hardgrave

A Thesis Submitted for the Degree of PhD
at the
University of St Andrews

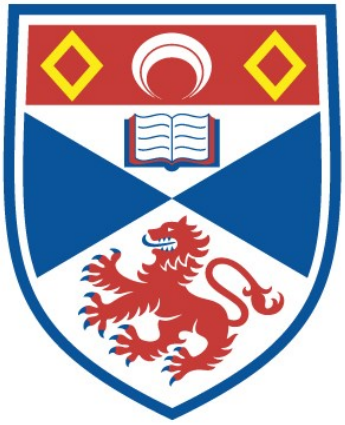

1991

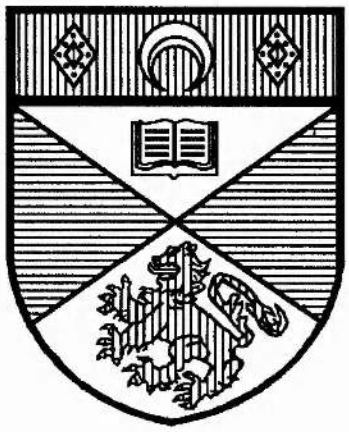

STUDIES OF MASS TRANSPORT IN SOME POLY(ETHYLENEOXIDE)–BASED POLYMER ELECTROLYTES

A thesis presented for the degree of

Doctor of Philosophy

in the Faculty of Science of the University of St Andrews

by Martin Thomas Hardgrave, *B.Sc.*

United College of St. Salvator and St. Leonard

St Andrews

November 1990

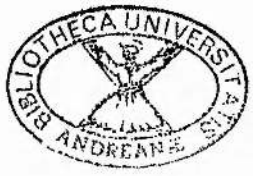

LIBRARY DECLARATION

In submitting this thesis to the University of St Andrews I understand that I am giving permission for it to be made available for use in accordance with the regulations of the University Library for the time being in force, subject to any copyright vested in the work not being affected thereby. I also understand that the title and abstract will be published, and that a copy of the work may be made and supplied to any *bona fide* library or research worker.

Signed:

DECLARATION

I, Martin Thomas Hardgrave, certify that this thesis has been composed by myself, that it is a record of my own work, and that it has not been submitted in any previous application for a Higher Degree.

This thesis describes the results of research carried out in the Department of Chemistry, United College of St. Salvator and St. Leonard, University of St Andrews, under the supervision of Professor C. A. Vincent since 1st October 1987.

November 1990 Signed:

I was admitted to the Faculty of Science in the University of St Andrews under Ordinance General no. 12 on 1st October 1987, and as a candidate for the degree of Doctor of Philosophy on 29th September 1988.

Signed:

CERTIFICATION

I hereby certify that Martin Thomas Hardgrave, *B.Sc.*, has spent twelve terms of research work under my supervision, and that he has fulfilled the conditions of the Resolution and Regulations appropriate to the degree of Doctor of Philosophy.

November 1990 Signed:

C. A. Vincent
Director of Research

Acknowledgements

I would like to thank my supervisor, Professor Colin Vincent, for his guidance and patience throughout the three years of this project. He emphasized that it was to be *my* project.

Thanks must go to Dr Fiona Gray whose advice and expertise in the laboratory were very welcome.

Drs Christiane Poinsignon, Jean-Claude Lassègue and José Dianoux introduced me to quasielastic neutron scattering with great forebearance.

I also learned much from Drs Peter Bruce, Marek Lieder and Michael Rogers and James Evans.

Much of the experimental work could not have been carried out without the use of excellent equipment made by James Rennie and the Departmental Mechanical Workshop. Sylvia Smith performed hundreds of atomic absorption analyses, and gave advice as to how the technique could be made to work.

My family have supported me financially and morally during seven years of further education, which is why this is their thesis. The support of friends in St Andrews and Dundee kept me going during the darker moments.

I would like to thank the Science and Engineering Reasearch Council for a research studentship.

To my parents

"With all your heart honour your father,
never forget the birthpangs of your mother.
Remember that you owe your birth to them;
how can you repay them for what they have done for you?"

Ecclesiasticus 7:27—28

ABSTRACT

The work in this thesis relates to the transport of salt species in polymer electrolytes, which are solid ionic conductors in which mass transport is similar to that in liquids, rather than in ion-conducting glasses.

A brief examination of some of the experimental techniques which have been used to study polymer electrolytes is given before examining in more detail the processes involved when these materials are polarised between non-blocking electrodes.

A theoretical treatment is given for various models of polymer electrolytes, in particular polymer electrolytes containing free ions and polymer electrolytes containing free ions and ion-pairs. Non-ideality has been considered for the free ion model. Computer simulations of the free ion and ion-pair model predict that the steady-state current that these materials pass may be proportional to the applied potential difference for many tens of volts, in contrast with the free ion model, where the potential difference limit is of the order of millivolts. The use of the terms "transference number" and "transport number" is discouraged, because of the effect of the motion of uncharged species in practical systems. A new parameter, the current fraction, is defined for steady-state polarisation experiments.

An experimental study of amorphous polymer electrolytes is described, in which electrolytes were polarised to steady-state using non-blocking electrodes. The application of the Hittorf technique to these materials has been demonstrated, with true transference numbers determined for some electrolytes.

Conductivity and neutron scattering experiments suggest that the reported unusual conductivity behaviour of lithium triflate-based electrolytes does not exist or is not generally displayed.

CONTENTS

CHAPTER 1

INTRODUCTION

Polymer electrolytes (PEs) are a relatively new type of solid ionic conductor, formed by the dissolution of salts in suitable high molecular weight (solid) coordinating host polymers (usually polyethers). Complexes between simple sodium and potassium salts and poly(ethyleneoxide) (abbreviated to PEO, $-(CH_2CH_2O)-_n$) were first reported by Fenton *et al.* [1] in 1973, who noted the conducting properties of these materials. It was suggested some years later, in 1978, by Armand *et al.* [2] that these materials were potentially useful as electrolytes in solid-state secondary batteries.

Since then, interest in these materials has increased greatly, with a large number of electrolytes having been reported, and many experimental procedures adopted to study them. PEs have been the subject of extensive reviews [3]—[6], which are recommended for providing a more thorough introduction and exposition of literature results than may be provided in this thesis, and conferences have taken place which were dedicated wholly or partly to these materials (for example, the Solid State Ionics conferences and the International Symposia on Polymer Electrolytes).

Most interest has been shown towards the study of alkali metal salts in PEO; and in particular towards lithium salts (typically lithium perchlorate, $LiClO_4$; and lithium trifluoromethanesulphonate (lithium triflate), $LiCF_3SO_3$), because of the relatively high conductivity electrolytes they produce, and because the low density and high reduction potential of lithium should allow high energy-density batteries to be fabricated. Other salts still attract study, and recently multivalent-cation electrolytes (containing, for example, Hg^{2+}, Cu^{2+}, Pb^{2+} and La^{3+}) have been prepared (see, for example, Farrington and Linford in reference [4] and references therein, [7]—[9]). Polymers other than PEO are now commonly used to produce PEs, in an attempt to improve their conductive and mechanical properties (see, for example, Cowie and Gray, both in reference [3] and Booth *et al.* in reference [4] and references therein).

1.1 NOMENCLATURE

The usual nomenclature adopted to describe the composition of PEs is to regard the material as consisting of a given number of (coordinating) polymer repeat units *per* cation of the salt. Thus, the chemical formula of an electrolyte in which there are nine (ethyleneoxide) units for every sodium ion in sodium perchlorate, say, would be written as PEO_9NaClO_4; and called a 9:1 electrolyte (it being understood that in this case the polymer was PEO and the salt sodium perchlorate).

It is sometimes the case that the number of salt cations *per* coordinating polymer unit is used to provide the chemical formula, which would result in the formula of the compound in the above example being written as $PEO(NaClO_4)_{0.11}$. This is an unsatisfactory style of expressing electrolyte compositions, as it almost invariably results in numbers less than unity being used to express compositions, and this style has not been adopted in this thesis.

1.2 APPLICATIONS OF POLYMER ELECTROLYTES

Armand *et al.* [2] suggested that PEs could be used as ion-conducting electrolytes in all-solid batteries, because they possess relatively high conductivities. Thin films of PEs should therefore have small resistances, allowing the fabrication of thin batteries. Batteries would basically consist of a metal anode, a PE based on a salt of the metal, and an intercalation material as a cathode, permitting frequent recharging of the battery. If alkali metal anodes are used, relatively high energy-density batteries may be produced, because of the low density of these metals—lithium, for example, is over twenty times less dense than lead—and because of their large reduction potentials. For use in batteries, PEs should have the following properties:

(i) Good ionic conductivities, preferably at room-temperature

(ii) Poor electronic conductivities (to prevent self-discharge)

(iii) A large electrochemical stability window

(iv) The ability to be formed and processed in a practical manner

Much effort has been expended in attempting to produce electrolytes with good ionic conductivities, either by varying the salt chosen or modifying the polymers used as the solvent. Conductivities of the order of 10^{-3} S cm^{-1} may be achieved at moderately high temperatures (>100°C) using PEO, though conductivities tend to be low at room temperature using this polymer, as explained below.

Ionic conductivities are usually several orders of magnitude higher than electronic conductivities, because there is usually no suitable conduction path for electrons through the electrolyte. Copper-based electrolytes, though, display high electronic conductivities [10]. If electronic conductivities and self-discharge rates are low, long shelf-lives may be anticipated for commercial batteries.

Armand [3] reported that the electrochemical stability window of PEO is 4 V (relative to Li/Li^+), making it suitable for use in lithium batteries. However, the addition of salts may promote the chemical degradation of the polymer [11].

Whilst possibly not an important point for the laboratory study of PEs, the ease of production and handling of PE films is likely to be a relevant factor for the industrial production of PE-based batteries.

Reviews of PE batteries have been reported elsewhere (Scrosati in reference [3], Belanger *et al.* in reference [4] and references therein), and the reporting of PE-based batteries is now a regular occurrence in the literature (see, for example, [12]—[18].

The use of PEs in electrochromic and photoelectrochemical devices has also been reported [19]—[24]. In the former example lithium ions from the PE intercalate into a metal oxide (typically a tungsten bronze) as the result of the application of a potential difference, producing a colour change; such devices have uses as "smart windows". This colour change would be reversed by the application of an opposite potential difference, forcing the ions back into the electrolyte. In the latter example the PE contains a redox couple in contact with a semiconductor. Holes generated by illumination of the semiconductor interface cause the oxidation of species in the PE, allowing the liberated electrons to pass through an external circuit before returning to

reduce species in the PE at another electrode.

It seems likely that many and varied uses of polymer electrolytes will be found in the future.

1.3 THIS WORK

It is still not clear what ionic species are produced when a salt dissolves in a polyether to produce an ion-conducting medium. This thesis has sought to examine what the effect of the transport of various salt species is on the conductive properties of PEs from a theoretical viewpoint, and then to examine the experimentally determined parameters from PEs in light of this theoretical treatment.

Chapter 2 provides a brief summary of some literature results about mass transport in PEs derived from a variety of experimental techniques, such as radiotracer diffusion, NMR, conductivity measurements*etc.* and discusses the validity of some of the techniques for the evaluation of transference numbers.

In Chapter 3 the response of various PEs to the application of a potential difference is examined from a theoretical viewpoint, and computer simulations of PEs containing free ions and ion-pairs are given to contrast the difference between such PEs and the free ions case, which has been studied in detail by Bruce and Vincent [25]. Non-ideality is briefly touched upon. A discussion about transference and transport numbers is presented in that Chapter, and an argument given that such terms should not initially be used when interpreting the results from polarisations of real PE cells.

Chapter 4 details the experimental procedures adopted to produce and study various PEs; including sample preparation, equipment, and treatment of experimental data.

Chapter 5 contains the results from the polarisation of PE cells to steady-state, and discusses them in light of what has been covered in Chapter 3.

Chapter 6 details the procedures adopted in the study of non-steady-state polarisations of PEs using a Hittorf cell, and examines the results which this procedure

provides and compares them with results from cross-linked and liquid PEs.

Chapter 7 presents some results from a quasielastic neutron scattering study of some $PEO_xLiCF_3SO_3$ electrolytes, which was undertaken to examine conductivity anomalies in this system reported by Robitaille and Fauteux [11].

Chapter 8 discusses the results presented in this thesis, and suggests how the study of PEs should proceed from this point.

A list of references and an appendix, containing miscellaneous experimental data, follow this final Chapter.

CHAPTER 2

MASS TRANSPORT IN POLYMER ELECTROLYTES

The mass transport of species in solid polymer electrolytes occurs principally *via* migration in an electric field and diffusion in a concentration gradient (strictly a chemical potential gradient). Convection does not occur in these systems, because the polymer in which the species are transported is too viscous to deform under the density gradients which are responsible for convection. The long-range transport of species in a PE is envisaged as being due to the facile restructuring of the polymer environment around the species, allowing their transfer from one polymer segment to another, thus allowing long-range motion of the species. This facile restructuring of the polymer has led to the description of the polymer as a "liquid" on a microscopic scale, though obviously a macroscopic solid. Long-range motion of the polymer itself does not occur, due to chain entanglement, and in this respect PEs are substantially different to conventional liquid electrolytes, in which the long-range transport of salt species may occur concomitantly with that of the solvent.

The subject of mass transport in PEs may be broken down into two fundamental questions: *what exactly* is *the mechanism of mass transport?* and *what species* undergo *mass transport?* The first question has received the most attention in the literature, and it has been shown [26] that mass transport only occurs to any great extent in the amorphous part of the PE. This was implied by Fenton *et al.* [1] in their original paper, when they observed that the conductivity increased with the amount of amorphous material present. Since then, much work has been carried out to study the dynamics of polymer motion and relate them to the conductivity; and several conduction mechanisms have been suggested (these are reviewed by Ratner in reference [3]).

The question of what species are being transported is a difficult one to answer. Ideally, the PE would only conduct a single cationic species, and PEs in which this is so have been prepared, but their conductivities tend to be low [27] [28]. The fact that good conductors are conductors of both cations and anions means that it is important to examine what exactly the charged species are, and how they contribute to the conductivity.

The dielectric constant (ε) of PE-forming polymers tends to be low ($\varepsilon \approx 5$)

compared to other polar solvents (for water, $\varepsilon \approx 80$). This suggests that PEs are going to be weak electrolytes, with extensive ion association (or little salt dissociation) taking place at even low concentrations. Although higher salt aggregates may be produced in PEs they are likely to be immobile due to their size, so the mobile species responsible for conductivity may indeed be quite simple salt species, such as free ions and triple ions. Neutral ion-pairs may also occur to a large extent. The polarisation of PEs containing such species is considered in Chapter 3.

Before examining more closely mass transport in PEs, the polymer-salt system itself will be examined, to show how the complexities of composition have consequences for the study of mass transport in these materials.

2.1 THE POLYMER-SALT SYSTEM

The production of PEs is usually achieved by the casting of a non-aqueous solution of the polymer and salt into a suitable former; leaving the PE as a thin film when the solvent is removed.

PEO in one form or another remains the polymer most widely studied. Polymer-salt interactions are greatest in $-[(CH_2)_nO]-_m$ for $n = 2$ [5], and even high conductivity polyphosphazene-based polymers rely on pendant ethyleneoxide chains for their ion transport [29].

Not all salts will dissolve in PEO: the dissolution of salts in solvents requires that the lattice energy of the salt be overcome by the enthalpy and entropy of the solvation of the species formed, and Papke *et al.* [30] observed that the maximum lattice energy that a salt may possess and still dissolve in PEO is about 750 kJ mol^{-1}.

It is not sufficient for the dissolution of a salt in the host polymer to take place for a PE to be produced. As well as having good coordination to the polymer, some of the salt species must easily break free of this for transfer to another polymer segment (hence for long-range motion) to take place. In liquid PE systems the long-range motion of ions coordinated to polymer segments may occur by migration of the whole

polymer-ion entity, without the breaking of the ion-polymer bond. This long-range polymer-ion motion may not occur in solid PEs, so polymer-ion bonds must be relatively labile in these systems. This is discussed in §2.1.1.

When dissolution of a salt in PEO takes place, various solid phases may be produced, such as crystalline PEO, crystalline PEO-salt complexes, amorphous PEO, amorphous PEO-salt phases, and undissolved salt. Because the amorphous electrolyte is solely responsible for the ionic conductivity, the presence of non-conducting phases complicates the study of PEs: the kinetics involved when the proportions of these phases change with temperature are complicated, and often considerable hysteresis in the conductivity is displayed when the temperature is cycled, because a substantial amorphous phase (produced by heating to high temperature) may be retained for a long time on cooling (see, for example, data in references [6] and [31]). Also, if the proportions of the different phases are not known accurately, the actual conducting part of the electrolyte may have a different composition to the bulk composition; further, the presence of other phases may increase the tortuosity for ionic conduction between electrodes, thus producing a smaller apparent conductivity. If this is the case, two electrolytes of identical bulk composition but with differing proportions of amorphous material may give very different results under the same experimental conditions.

This problem of differing bulk and conducting compositions may account for the difficulty in reproducing results reported in the literature. The use of wholly amorphous electrolytes is more likely to lead to reproducible and interpretable results.

Another reason why reproducibility has been poor is that the presence of small amounts of residual solvent from the solvent casting may affect transport in the electrolyte. The presence of solvent in the PE may have an effect on the salt species present or act as a plasticiser in the polymer, consequently affecting the conductivity. The solvent may be difficult to remove; for example, the dissolution of copper (II) triflate in liquid PEO produces a yellow solution [32], but its dissolution in acetonitrile produces a blue solution, and solvent casting into PEO from acetonitrile produces a blue PE [33] [34]. Samples hot-pressed from a ground mixture of the polymer and salt

are yellow-green [35]. This suggests that acetonitrile remains coordinated to the copper (II) ions, which prevents transport processes from being discussed in terms of copper species–PEO interactions, and requires the PE to be regarded as a conductor of solvated ions. This problem of solvent retention is likely to make itself more apparent in transition metal electrolytes, as their coordination compounds tend to be coloured; however, it indicates that the removal of solvent must be thorough, because alkali metal-based electrolytes do not show a tell-tale colour change in the presence of coordinated solvent. Solvent casting has also been shown to influence the conductivity of the resultant PE, depending on the purity of the solvent and the casting regimen [37].

Huq and Farrington [9] contrast transport numbers obtained for zinc in anhydrous electrolytes and electrolytes in which the zinc salt was a hydrate. The anhydrous PEs showed a zinc transport number of nearly zero, whereas the electrolyte prepared from the hydrated salt showed a transport number of about 0.9.

The hydration and dehydration of PEO_8NiBr_2 electrolytes was found to have a profound effect on the cation transport number [37]: the electrolyte had a transport number of about zero before hydration and dehydration, and about 0.6 afterwards.

There is nothing wrong in having electrolytes with a transport number of 0.9, even if it arises from the presence of solvent, but the task of examining the salt-polymer processes responsible for conduction in PEs is not likely to be made easier if these materials are cited as typical "solvent-free electrolytes" and provide results which are in conflict with those provided from the study of truly solvent-free materials.

2.1.1 Polymer-Salt Bond Lability

It has been mentioned at the start of the Chapter how the restructuring of the polymer-salt environment was required for mass transport in solid PEs. Sudies show that the interactions in PEs are predominantly between cation-containing species and the polymer, with little anion-polymer interaction [38]. This means that the interactions or "bonds" between the cations and the ether-oxygens must be labile for these species to move through the electrolyte.

AC impedance studies [7] of PEO-based lanthanum perchlorate PEs with blocking electrodes show that these PEs possess quite high conductivities, but dc conductivity studies [7] with lanthanum electrodes show that there is no sustainable steady-state current, and consequently no lanthanum-based conductivity. This electrolyte is thus a perchlorate ion conductor. Similar observations have been found for calcium and magnesium PEs [7] [39]. This observation highlights the point that salt dissolution is not a sufficient condition for the production of a PE which conducts cations.

Bruce *et al.* [40] suggested that the rate at which ions exchange their inner solvation sphere of water [41] may be used as a general guide to how easily cations would exchange their coordinating sites in PEs. Ions such as those of the alkali metals exhibit rapid exchange, and indeed form cation-conducting PEs. Divalent ions such as Cu^{2+} and Hg^{2+} would also be assumed to follow this principle, and they produce moderately good electrolytes, whereas magnesium (which does not exchange water rapidly) should produce poor PEs which do not conduct cations. This was the basis for studying lanthanum-based PEs, which might also have been expected to produce reasonable PEs on the basis of their water exchange rate. Whilst comparisons between different systems should not be taken too far (Farrington and Linford [4] remark that the water exchange rate is not the only important factor in determining whether PEs are ion-conductors), the comments by Bruce *et al.* highlight the point that the easy making and breaking of polymer-salt bonds is necessary for the formation of ion-conducting PEs.

2.1.2 Phase Diagrams of Some PEO-based Polymer Electrolytes

The electrolytes used in this study were based on PEO, and the salts used were lithium perchlorate, lithium triflate, and sodium tetraphenylborate. The phase diagrams of PEO_xLiClO_4 [11], $PEO_xLiCF_3SO_3$ [11] and PEO_xNaBPh_4 [112] are shown in Figures 2-1 to 2-3. It may be observed that substantial regions of amorphous electrolyte exist, the amounts of which generally increase above 65°C, the melting point

of PEO.

The phase diagrams must be treated with some caution, because the electrolytes tend not to be at equilibrium—it has already been mentioned that more amorphous material may be retained on cooling than might be expected, due to the slow recrystallisation kinetics of the electrolyte. The use of the lever rule is unlikely to yield the actual proportions of phases present in the electrolyte at a given temperature.

2.1.2.1 Phase Diagram of PEO_xLiClO_4

In this system, where $x \geq 6$, the electrolyte is completely amorphous above 65°C, which is the melting temperature of the 6:1 complex observed to be present with PEO below this temperature for these compositions. When the complex melts it dissolves in the PEO to produce an amorphous electrolyte of uniform composition. The wide range of compositions and temperatures over which this electrolyte is amorphous made it an ideal candidate for study, with the prospect of obtaining reproducible results.

2.1.2.2 Phase Diagram of $PEO_xLiCF_3SO_3$

The phase diagram of this system, with $x \geq 3$, shows that PEO and 3:1 complex are present below 65°C, and above this temperature the 3:1 complex gradually dissolves in the amorphous PEO as the temperature increases, eventually producing a completely amorphous electrolyte. It is seen that, for most practical compositions and temperatures, electrolytes will not be uniform in composition, complicating the interpretation of the results obtained from these materials.

2.1.2.3 Phase Diagram of PEO_xNaBPh_4

The phase diagram of this electrolyte, with $x \geq 8$, shows an 8:1 complex and PEO present at low temperatures, and like the lithium triflate-based PEs this crystalline complex gradually dissolves in the PEO above 65°C to produce an amorphous electrolyte. The temperature range over which the electrolyte may be studied using

sodium electrodes is limited by the low melting point of sodium metal (≈ 97°C). This may necessitate the use of sodium alloy electrodes which are solid at elevated temperatures.

The largest amorphous region in the above systems exists for PEO_xLiClO_4, which is why this PE was chosen for most of the experimental studies in this project. It should be possible to attribute experimental observations to the polymer electrolyte itself, rather than to changes in the phase composition; something which may occur in the other electrolytes. The limited amorphous ranges of the other electrolytes prevent useful studies from being carried out on them over a large composition and temperature range.

2.2 MASS TRANSPORT IN SOLID POLYMER ELECTROLYTES

Studies of mass transport occurring in solid PEs are hampered by the fact that it is not known with any certainty what salt species are present. Also, most PEs are of high concentration (even $PEO_{100}LiClO_4$ has a salt concentration of 0.26 M) so there is always concern that the interpretation of the results from some of the techniques used to study them are inappropriate [43].

In a complementary study to that of MacCallum *et al.* for low concentration liquid electrolytes [44], Gray [45] carried out a conductivity study of low-concentration solid polymer electrolytes. It was found that the same type of conductivity behaviour with concentration occurred in solid PEs as in liquid PEs; that is, an initial drop in molar conductivity as the concentration increased, followed by a subsequent rise (as is illustrated in Figure 2-4), and the data were interpreted in terms of the initial production of neutral ion-pairs (reducing the molar conductivity) followed by the production of mobile triple ions as the salt concentration increased, which caused the molar conductivity to rise. The implication of these results is that extensive ion association

may occur at high salt concentrations, which is also indicated by Raman spectroscopy [46].

Of the various techniques used to study mass transport in PEs the ac and dc polarisation techniques are probably the most widely used. AC polarisation of PEs using blocking and non-blocking electrodes provides information about the conductivity of the PE, and dc polarisations also provide useful information, even if the interpretation of these results is difficult, as is shown in Chapter 3.

Some experimental methods and their results will be briefly considered in the following sections.

2.2.1 NMR Studies

Nuclear magnetic resonance (NMR) can be used to observe a given type of atomic nucleus in the polymer, and various results may be obtained using this technique. The free induction decay (fid) may be used to determine the relative amounts of the resonant nucleus in crystalline and amorphous phases [26] [47], because the spin-lattice relaxation time is longer in ordered phases than in unstructured ones; a short fid component superimposed on a long fid may be found for a mixed-phase PE, and the strengths of the two components may be used to determine the crystalline to amorphous ratio.

Pulsed Field Gradient NMR (PFG-NMR) may be used to determine diffusion coefficients [48] by dephasing the nuclear spins in a magnetic field gradient, and rephasing them a short time later in an opposite field gradient; the amount of dephasing is dependent on the strength of the magnetic field (which is distance-dependent through the sample), so if the resonant nucleus moves to a different position (*i.e.* to a different rephasing magnetic field) the rephasing of the sample will not be perfect, and the amount of imperfect rephasing may be used to determine a diffusion coefficient for the resonant species. Interpretation of these results is complicated by the fact that NMR is indiscriminate in its detection of the resonant nuclei, so that all mobile species containing the nucleus under investigation will contribute to the diffusion coefficient

obtained, and assigning diffusion coefficients to individual species is difficult; if not impossible.

As Bruce and Vincent have observed [49], the use of NMR diffusion coefficients in the equation for the cation transport number:

$$t_+ = \frac{D_+}{D_+ + D_-} \qquad 2\text{-}1$$

will tend to result in a transport number of 0.5 if ion-pairs predominate, a value which has been reported by NMR [50], because in this case the cation and anion diffusion coefficients will be equal (to the ion-pair diffusion coefficient).

A description of the use of NMR in the study of mass transport in solids is given in references [3] and [51].

2.2.2 Radiotracer Studies

In radiotracer experiments a radioactively-labelled salt is allowed to diffuse into the PE, and sectioning of the PE followed by the determination of the radioactivity in each segment may be used to determine the diffusion coefficients of the ions under investigation. This method suffers from the same problem as the NMR experiment in that the diffusion of all species containing the labelled element will be registered, so that the diffusion coefficient is not attributable to any one species. Chadwick *et al.* [3] [52], who performed many experiments of this type, obtained results which suggested that preferential salt diffusion took place along crystallite boundaries, rather than through the electrolyte, demonstrating the problems which may occur when using mixed-phase materials. However, the sectioning procedure used in this technique is not suited to fully amorphous materials, because they are too soft for fine sectioning.

It is often the case that the diffusion coefficients found from this technique differ greatly from those found from the conductivity *via* the Nernst-Einstein equation. In reference [52], where a rubidium salt was studied, agreement was found from the tracer diffusion data and ac conductivity data, possibly because the rubidium ion is so

large that no ion association exists in this system.

2.2.3 Conductivity Studies

In conductivity experiments, on ideal dissociated electrolytes, the Nernst-Einstein equation may be used to determine a cation and anion diffusion coefficient. However, because the Nernst-Einstein equation contains a term in the concentration of the diffusing species:

$$\sigma = \frac{nq^2}{kT}D \qquad 2\text{-}2$$

and because the composition and amount of the salt species present in an electrolyte are normally unknown, the use of the Nernst-Einstein equation is likely to yield ambiguous results.

DC measurements with non-blocking electrodes are complicated by the fact that the diffusion of neutral species may result in transport of the non-blocked species [53]—[55], so it may not be assumed that the steady-state current is due to the non-blocked ion alone. There is also evidence that the use of concentration rather than activity is not fully justified [56]—[58].

Molar conductivity measurements on low concentration solid and liquid PEs [44] [45] have been mentioned as showing the existence of extensive ion association. At higher concentrations increases in viscosity cause a decrease in the molar conductivity even though the conductivity itself increases.

The temperature variation of the conductivity of mixed-phase electrolytes tends to be of an Arrhenius type ($\log(\sigma)$ *vs* $1/T$ is linear), with two linear regions of differing slope, with an intercept around the melting point of PEO (see, for example, references [8] and [59]), as shown in Figure 2-5. Amorphous electrolytes tend to show a non-linear response for the variation in conductivity with temperature ($\log(\sigma)$ *vs* $1/T$ plots are curved) [60], as shown in Figure 2-6. The curved response has been fitted to WLF and VTF equations, which were originally derived for the temperature-dependent

mechanical properties of polymers [61] [62]. This type of response has been shown to be consistent with free-volume or configurational entropy mechanisms of mass transport (see, for example, Ratner in reference [3] and references therein), but the examination of conductivity-temperature data tends to concentrate on the polymer, with no consideration given to any change in the species content of the PE, even though spectral data suggest that the amounts of the various species present in PEs change with temperature [63].

2.2.4 DC Polarisation Studies

DC polarisation studies are very practical procedures to perform, either using blocking or non-blocking electrodes. Blocking electrodes may be used to determine the electronic conductivity of the electrolyte, because ionic discharge may not occur at the electrodes.

The use of non-blocking electrodes in the dc polarisation of PEs may be used to determine the ionic conductivity of the electrolyte when a concentration polarisation exists across the cell, as is detailed in Chapter 3. In an electrolyte containing free ions the ratio of steady-state to initial conductivity provides a measure of the non-blocked species transport number; however, this is not so when species other than free ions are present, as shown in the next Chapter.

A four-point conductivity cell utilising the van der Pauw method [64] has been used to determine the conductivity of PEs and ion-conducting glasses [65].

2.3 MASS TRANSPORT IN LIQUID POLYMER ELECTROLYTES

Polymer electrolytes formed by the dissolution of salts in liquid polyethers have been used for low-concentration conductivity studies and as possible model systems for the study of solid PEs [44] [45] [66]. Liquid PEs have several advantages over solid PEs; they are easier to produce with a uniform composition, and their conductivity is

higher, allowing dilute solutions to be studied. However, as has been mentioned, the motion of species which may be immobile in solid PEs may occur in liquid PEs by the long-range motion of polymer-ion entities. This must be remembered if conclusions about solid PEs are being inferred from data obtained from liquid PEs. Liquid PEs have been studied using light scattering techniques (see Torell and Schantz in reference [4] and references therein), in an attempt to quantify ion association in the system. Results suggest that the proportions of ion-pairs increase as the temperature is raised [67]. Solid PEs have not been studied this way because they are relatively opaque to laser radiation.

Cameron *et al.* [66] studied liquid PEs based on sodium salts using the Hittorf method, and found that the anion transference number was approximately unity. This study, being a non-equilibrium one, only considered the transport of charged species in the polymer; this being difficult to do in solid PEs because of the possibility of the transport of neutral species in the concentration gradients which form rapidly during the polarisation of a thin cell to steady-state [53] [54]; however, Chapter 6 details preliminary measurements using this technique for some solid electrolytes.

2.4 COMMENTS

It is apparent that the various experimental techniques produce results which are difficult to interpret, and often contradictory results are obtained from different techniques because it is not known what salt species are present. Very dilute electrolytes have been characterised by MacCallum *et al.* [44] and Gray [45], and these electrolytes contain known salt species, making their examination desirable using some of the various techniques described above; however, their dilute nature may make it impractical to do so. Their dilute nature is likely to make them relatively ideal, again making their study desirable, especially considering the results derived in Chapter 3.

Figure 2-1. Phase diagram of PEO_xLiClO_4 (from reference [11]).

(●) phase transitions determined using optical microscopy

(+) phase transitions determined using conductivity measurements

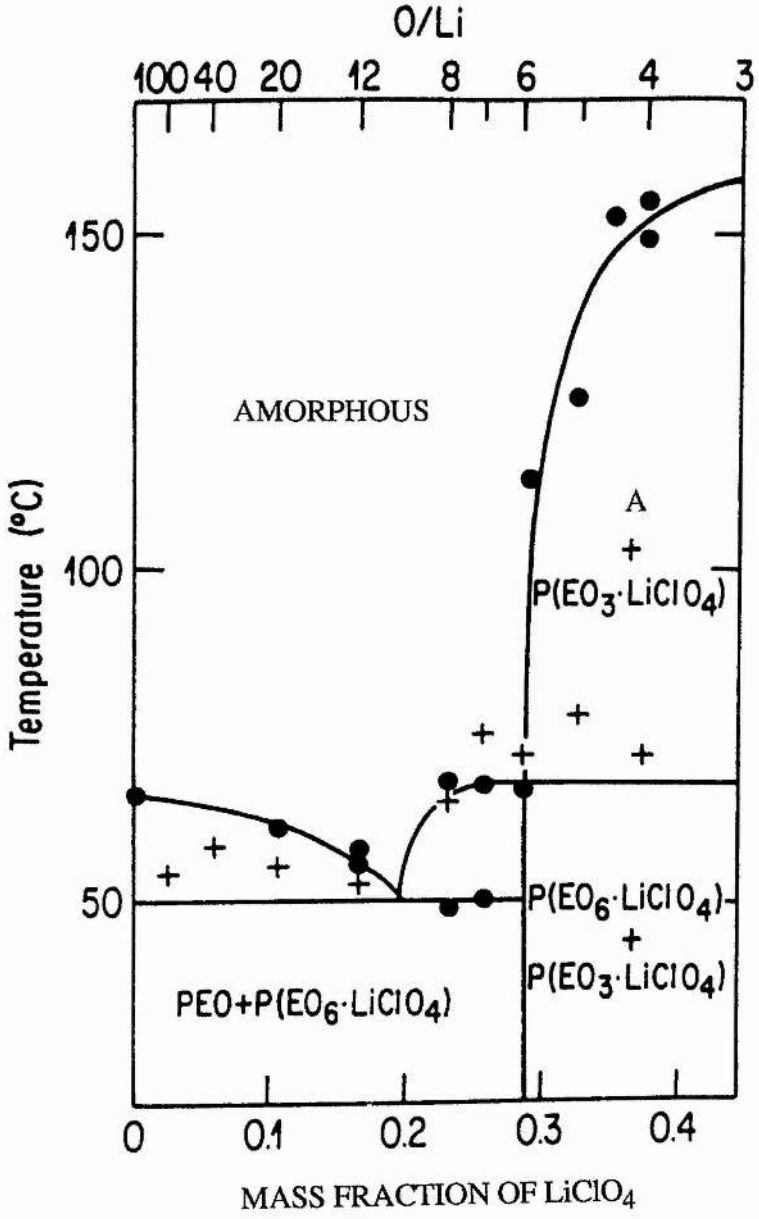

Figure 2-2. Phase diagram of $PEO_xLiCF_3SO_3$ (from reference [11]).

(+) (■) phase transitions determined using optical microscopy

(x) (o) (▲) phase transitions determined using conductivity measurements

(⊡) phase transitions determined using NMR

(●) (△) (⊗) phase transitions determined using DTA or DSC

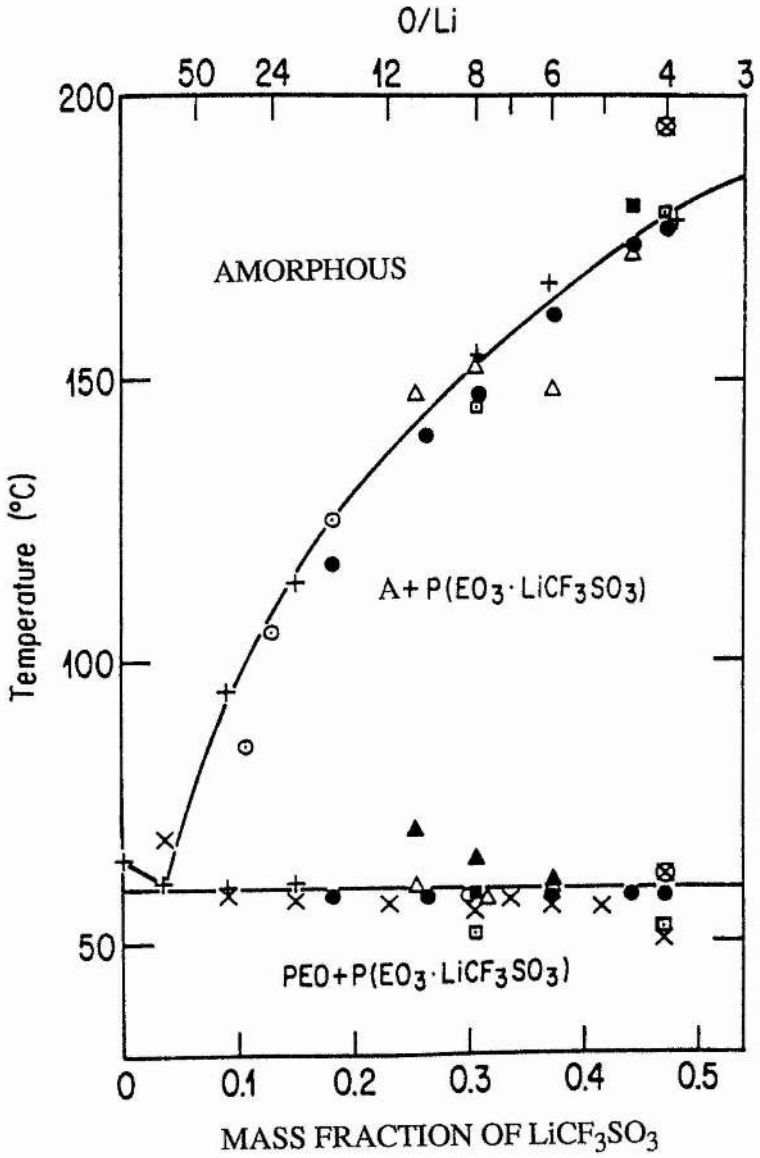

Figure 2-3. Phase Diagram of PEO_xNaBPh_4 (from reference [112]).

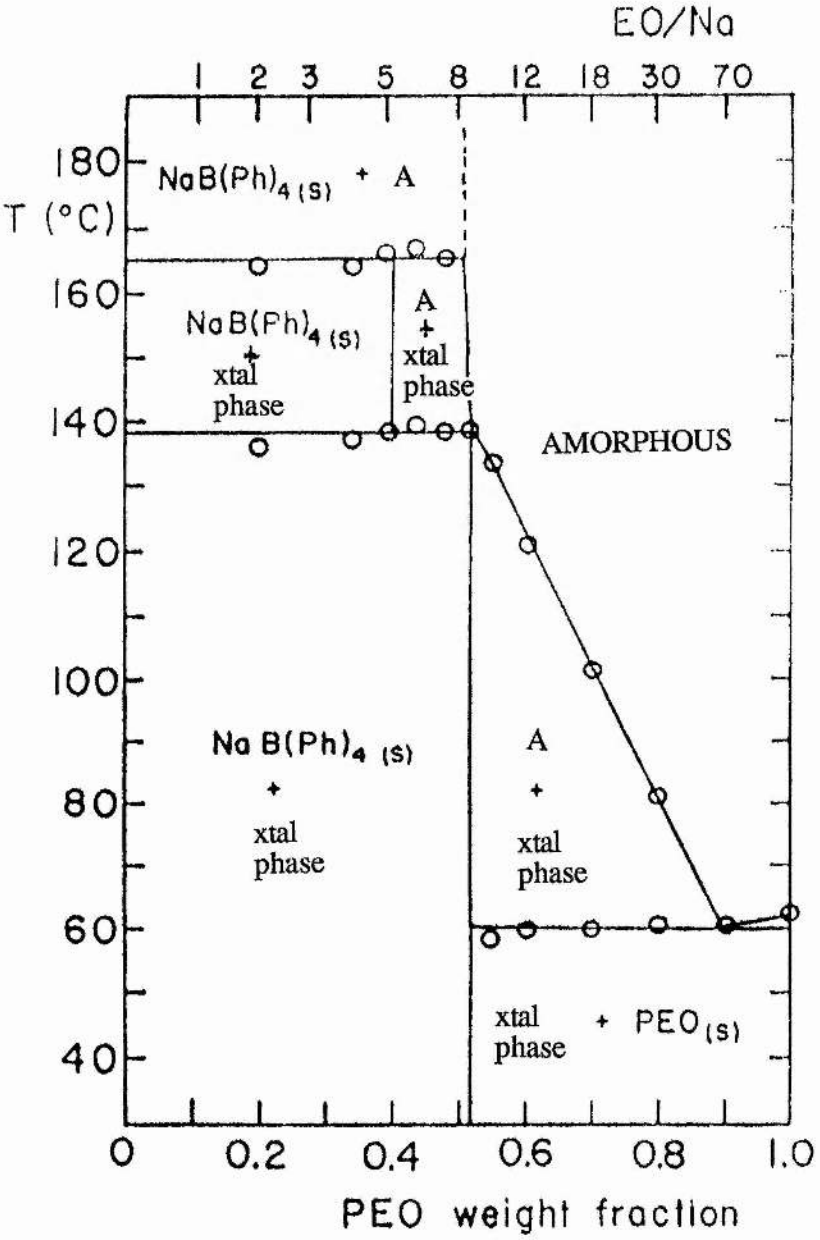

Figure 2-4. Variation in Molar Conductivity with Concentration for Low Concentration Polymer Electrolytes (after reference [44]).

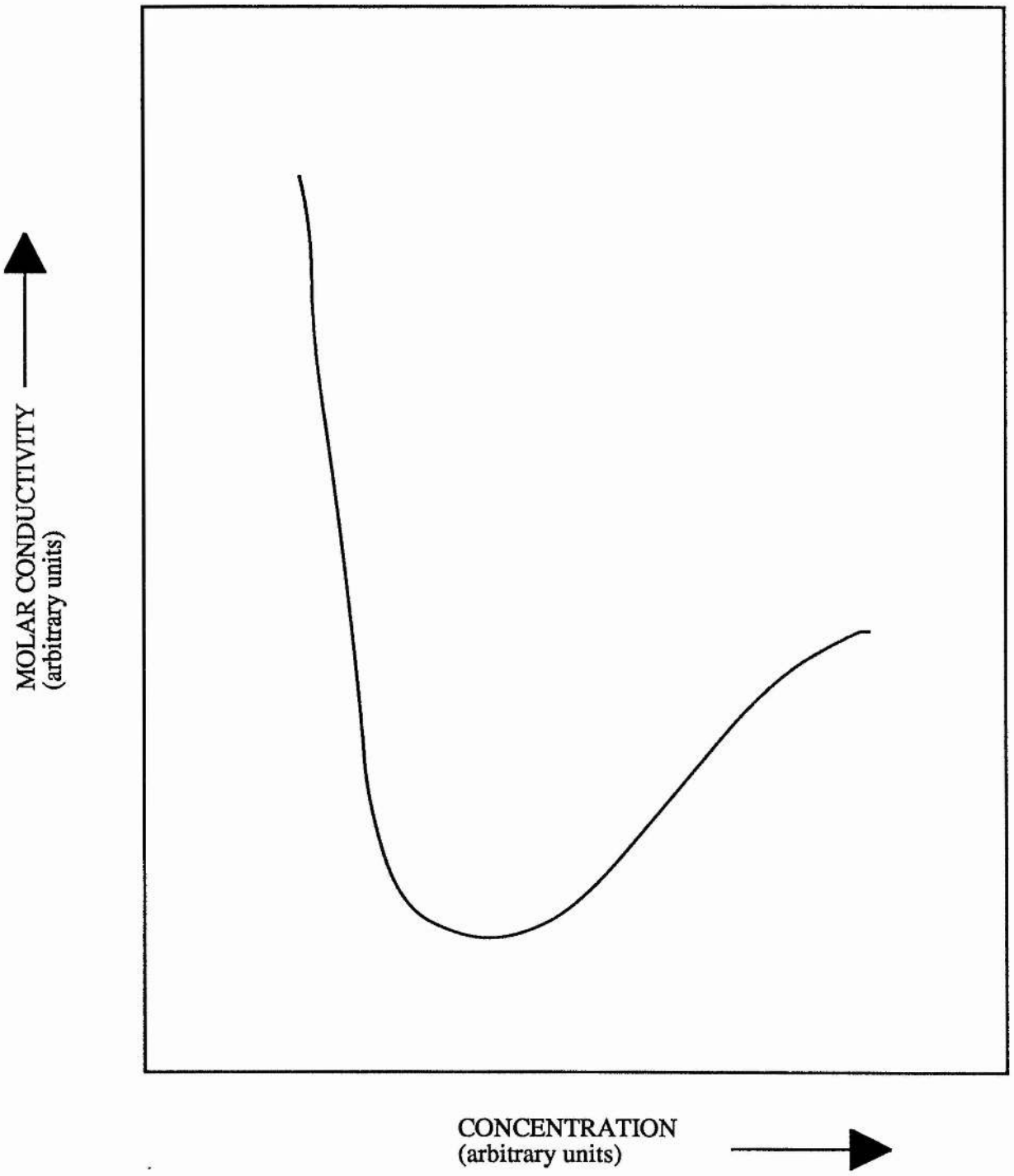

Figure 2-5. Variation in Conductivity with Temperature for a Polymer Electrolyte Displaying an Arrhenius Response.

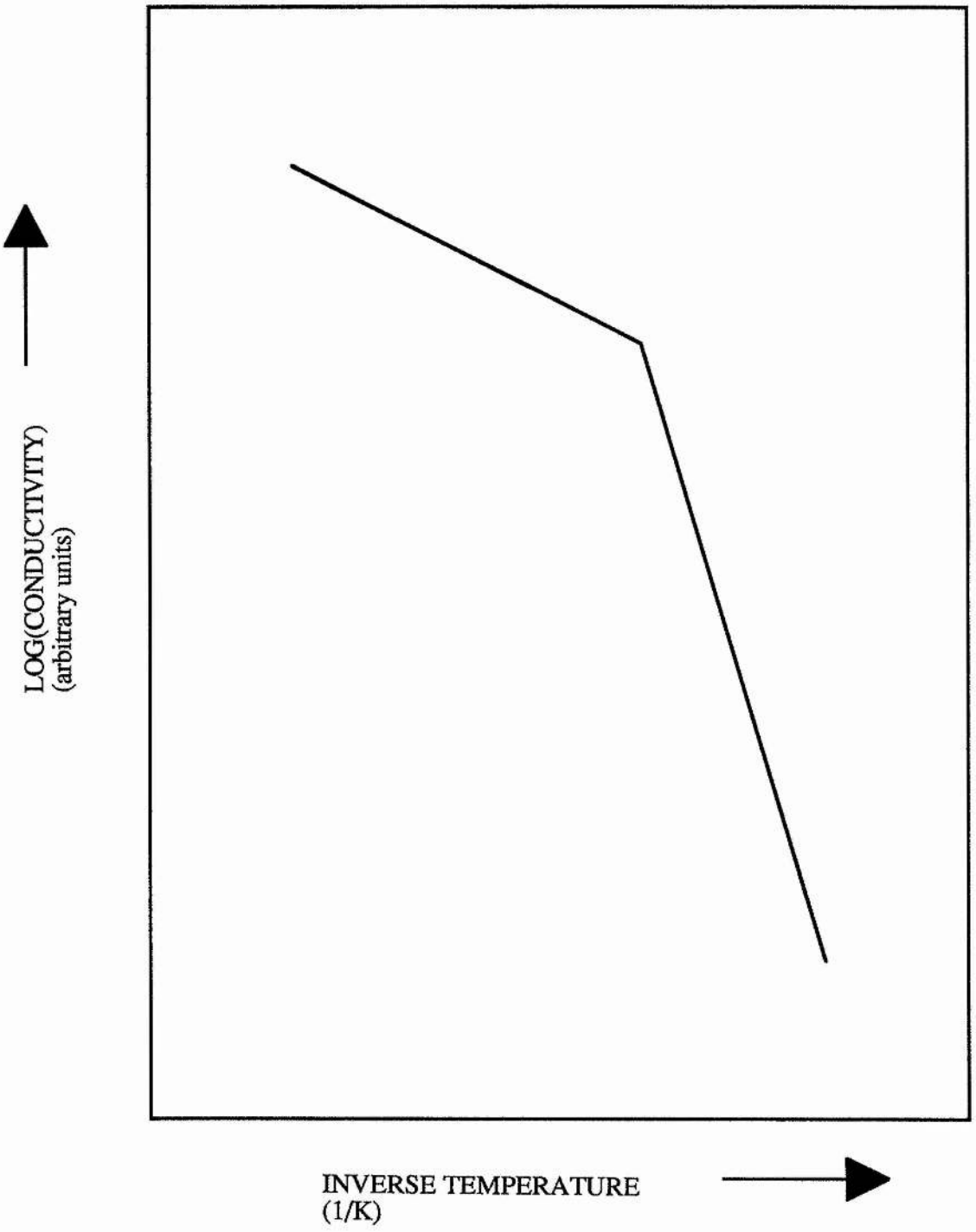

Figure 2-6. Variation in Conductivity with Temperature for a Polymer Electrolyte Displaying a VTF-type Response.

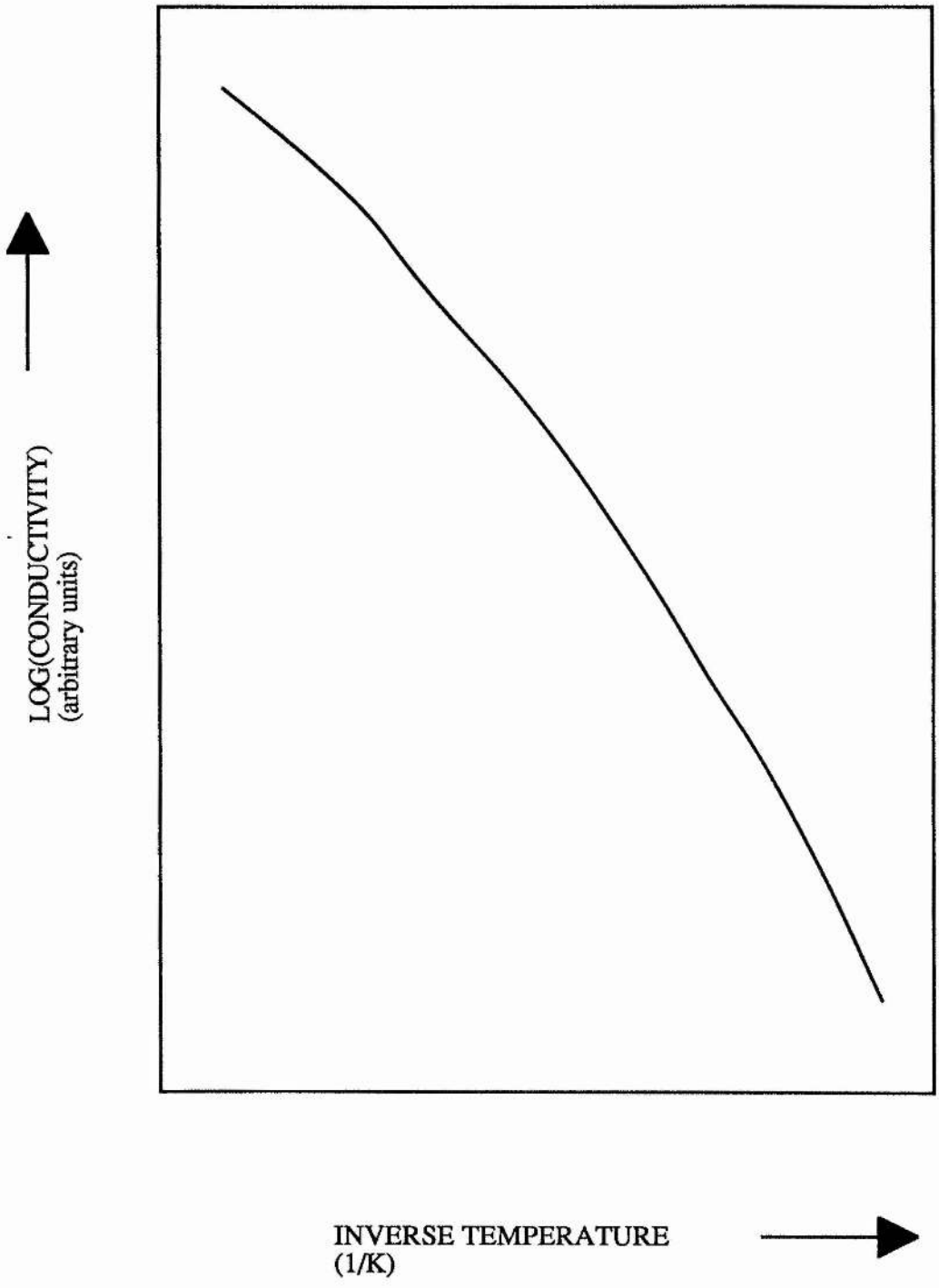

CHAPTER 3

STEADY-STATE DC POLARISATION OF POLYMER ELECTROLYTE CELLS

In this Chapter the polarisation to steady-state of PE cells of the type M|PEO_XMX|M with non-blocking electrodes is considered from a theoretical viewpoint. In §3.1 the establishment of concentration gradients and the reduction in current when a constant potential difference is applied to the electrodes, are demonstrated for two types of PE: one containing only free ions; and one containing free ions and neutral species, to show that the transport of neutral species must be taken into consideration at steady-state.

After this introduction, the steady-state situation is described quantitatively in §3.2 by using the Nernst-Einstein equation (for field-driven mass transport) and Fick's 1st law (for diffusion-driven mass transport). It has been observed that the use of the Nernst-Einstein equation for what are very concentrated electrolytes is not entirely appropriate [43], though it may be thought of as a good first approximation. The effect of non-ideality (inclusion of Onsager cross-terms, and the use of activity rather than concentration) is discussed in §3.3.

The results of computer simulations of PE cells are presented in §3.4, rather than in Chapter 5, because they were generated from equations derived in this Chapter, and it is well to examine the results they anticipate for ideal cells before experimental data from real cells are presented. Such simulations are particularly useful for a PE containing free ions and ion-pairs, because mathematical equations dealing with this type of PE may not be solved exactly (as they can be for the free ion case), requiring the use of computer simulations.

The distinction between transport numbers and transference numbers is discussed in §3.5, in light of the results derived in the previous sections, and in light of the way such terms are used in the literature.

3.1 QUALITATIVE DC POLARISATION OF POLYMER ELECTROLYTE CELLS

In this section the polarisation to steady-state of a symmetrical two-electrode cell of the type M|PEO-MX|M is considered, in which the electrolyte contains mobile species, and in which the electrodes are reversible to the M^+ ion. The electrolyte is assumed to be of a uniform composition.

3.1.1 The Steady-state DC Polarisation of a Polymer Electrolyte Cell Containing M^+ and X^- Ions.

This situation has been described quantitatively by Bruce and Vincent [25], and by Buck [55], and it is the most straightforward situation to study, though the assumption that only free ions are present in the electrolyte is probably not a realistic one for most PEs.

When a cell such as that described above is polarised by the application of a constant potential difference between the electrodes a current flows which decreases with time to a steady-state value (illustrated in Figure 3-1). At steady-state there must be no net transport of X-containing species through the cell, because the electrodes are only non-blocking to the cations.

Consider Figure 3-2, which depicts the changes occurring in a polarised cell as time proceeds. In Figure 3-2a, which depicts the equilibrium situation at time $t = 0$ before a potential difference is applied to the cell, there is no net motion of the ions, and the concentration of the ions is uniform across the cell (indicated by the horizontal line in the Figure). At a time $t > 0$ the potential difference is applied and the ions begin to migrate to their respective electrodes. Cations are removed at the cathode and are injected at the anode, and anions accumulate at the anode and become depleted at the cathode. This process, because the anions may not be discharged at the electrodes, leads to a concentration gradient starting to form across the cell [68]. This is depicted in Figure 3-2b. Macroscopic charge neutrality requires that the cation and anion concentration gradients be equal.

The ionic concentration gradients promote ionic diffusion away from the anode, so that at steady-state (when there must be no net anionic motion in the cell) the migrational and diffusional fluxes of the anions must be equal and opposite. For the cations, the steady-state current is composed of a migrational flux assisted by a diffusional flux. In §3.2 the migrational flux will be expressed by the Nernst-Einstein equation, and the diffusional flux by Fick's 1st law. The concentration gradient exists throughout the electrolyte at steady-state, a situation represented in Figure 3-2c.

Because the concentration of the electrolyte is not the same at both electrodes, a concentration potential difference ΔE exists between them, which is expressed by the Nernst equation. As the applied potential difference is constant, the effect of the development of the electrode potential difference is to reduce the electrolyte potential difference $\Delta\phi$ from its initial value to a steady-state value. Because the potential difference acting over the electrolyte has fallen, the migrationary cation current is also expected to fall, though this may be offset to some extent by the promotion of cation diffusion in the concentration gradient which forms as the polarisation proceeds. The reduction and eventual cessation of the net migration of anions also causes the current to decrease. The distribution of the applied potential difference between the electrode and electrolyte potential differences in PE cells is discussed in §3.1.3.

3.1.2 The Steady-state DC Polarisation of a Polymer Electrolyte Cell Containing M^+ and X^- Ions and MX Ion-pairs.

This is the simplest extension from the above case. We now consider the effect of the presence of neutral ion-pairs, which are formed by the association of free ions, and which are in a fast equilibrium with the free ions. Again a constant potential difference is applied to the cell, which is depicted in Figure 3-3, and again the electrodes are reversible to M^+ ions alone. Figure 3-3a represents the situation at time $t = 0$ before the potential difference is applied. When the potential difference is applied at a time $t > 0$ the ions start to migrate to their respective electrodes, as shown in Figure 3-3b, causing an ionic concentration gradient to form between the electrodes. Because

there is a fast equilibrium between the ions and ion-pairs, the formation of an ionic concentration gradient promotes the simultaneous establishment of an ion-pair concentration gradient, which promotes the diffusion of ion-pairs in the direction of the cathode, as shown in Figure 3-3c, where the cell is at steady-state.

The steady-state condition must now take the diffusion of ion-pairs into consideration. In this case the steady-state condition is that no discharge of any X-containing species (X^- and MX) may occur. It is seen from Figure 3-3c that, for X-containing species, the migration of anions must be balanced by the diffusion of anions and ion-pairs. For the cations at steady-state, it should be realised that the ion-pairs transport M across the cell, so the mass transport processes constituting the steady-state current are the migration and diffusion of cations and the diffusion of ion-pairs. The potentially important rôle played by neutral species during the passage of current was stressed by Cameron *et al.* [53], Bruce *et al.* [54], and Buck [69].

More advanced cases may be treated in a similar manner, but there is little benefit in doing so qualitatively. These two examples have shown generally what processes occur at steady-state for PEs containing ions and PEs containing ions and neutral species. In §3.2 the steady-state situations described above are treated mathematically.

3.1.3 The Distribution of Applied Potential Difference Over Polymer Electrolyte Cells.

In this section the distribution that the applied potential difference takes over a PE cell during polarisation is demonstrated. A real PE cell, such as Li|PEO_xLiClO_4|Li, will possess an interfacial resistance due to passivation of the lithium in contact with the PE, which serves to reduce that part of the applied potential which acts over the electrolyte. As may be seen from the impedance diagram in Figure 3-4, the resistance at the interface may greatly exceed the resistance of the electrolyte itself (impedance diagrams are discussed in §4.4).

Consider a PE cell such as that described above. If the interface resistance is R_i

and the bulk electrolyte resistance R_b, then the current I^o which flows initially, when a potential difference of ΔV_a is applied, is given by:

$$I^o = \frac{\Delta V_a}{R_i + R_b} \qquad 3\text{-}1$$

and the potential difference acting over the interface resistance, ΔV_i is given by:

$$\Delta V_i = I^o R_i \qquad 3\text{-}2$$

so the potential difference ΔV_b (conveniently written as ΔV) acting over the bulk electrolyte is given by:

$$\Delta V = I^o R_b = \Delta V_a - \Delta V_i$$

i.e.

$$\Delta V = \Delta V_a - I^o R_i \qquad 3\text{-}3$$

In this way the effect of the interface resistances may be corrected for, allowing the examination of the electrolyte itself. Initially, all of the corrected potential difference acts over the electrolyte, so $\Delta V = \Delta\phi^o$ at time t = 0. At steady-state a current I^s flows, which means that the interface resistance at steady-state drops potential by an amount ΔV_i^s, given by:

$$\Delta V_i^s = I^s R_i^s \qquad 3\text{-}4$$

R_i^s may not be the same as R_i, because the interface resistance may change with time. It is also assumed that the only effect of the interface resistance is to drop potential in an ohmic fashion; that no steady-state processes (the reduction and cessation of the net motion of anion-containing species, and the formation of a concentration gradient) actually take place in the layer. Fauteux [70] cautioned that the diffusional impedance found by low-frequency ac analysis of such PEs [71] may arise from diffusion in the interfacial layer at steady-state, rather than such diffusion occurring in the PE; but the interpretation of dc polarisation data in this thesis suggests that the interface does simply act as a resistor, with no active steady-state processes occurring in it.

Thus the potential difference ΔV^s acting over the electrolyte at steady-state is given by:

$$\Delta V^s = \Delta V_a - I^s R_i^s \qquad 3\text{-}5$$

and it is composed of an electrode potential difference ΔE, due to the different concentrations of electroactive ion at the electrodes, together with a steady-state electrolyte potential difference, $\Delta\phi^s$.

The electrode potential difference, ΔE, for an ideal electrolyte, may be expressed as:

$$\Delta E = \frac{RT}{F} \ln\left(\frac{c_a}{c_c}\right) \qquad 3\text{-}6$$

so the total potential difference may be written as:

$$\Delta V^s = \Delta E + \Delta\phi^s \qquad 3\text{-}7$$

The qualitative distributions of potential difference at the onset of polarisation and at steady-state are depicted in Figure 3-5. Quantitative relationships between ΔE, $\Delta\phi$, and ΔV will be derived in §3.2.

3.2 QUANTITATIVE DC POLARISATION OF POLYMER ELECTROLYTE CELLS

In this section the steady-state dc polarisation of PEs containing various species is considered quantitatively, having established above the processes which occur in the PE when steady-state is achieved. The electrolyte is assumed to be ideal, with concentration-independent diffusion coefficients and no ion-ion interactions.

3.2.1 The Steady-state DC Polarisation of a Polymer Electrolyte Cell Containing M^+ and X^- Ions.

Consider a cell M|PEO-MX|M containing free M^+ and X^- ions, and in which the electrodes are non-blocking to M^+ and blocking to X^-. This treatment has been undertaken by Bruce and Vincent [25], but it is useful to have an exposition of it here, to allow comparisons to be made with it when more advanced models are examined. It is also assumed that an interfacial resistance is not present or has been corrected for by

noting the potential difference dropped over it.

The cell is considered to lie along, and be symmetrical about, the x-axis, with the cathode at x = 0, and the anode at x = t. Because the polarisation is applied only along the x-axis, this is the only direction that need be considered for the diffusion and migration of species.

It is known that for the anions at steady-state their diffusion balances their migration, resulting in no net anionic transport. Describing the diffusion using Fick's 1st law, and the migration by the Nernst-Einstein equation, it may be written that:

$$FD_{-}\frac{dc_{-}}{dx} = \frac{F^2}{RT}D_{-}c_{-}\frac{d\phi}{dx} \qquad 3\text{-}8$$

Charge neutrality requires that the cation and anion concentrations, c_+ and c_-, be equal. They may be written as c, which is also the salt concentration in this free ion model, allowing an expression for the potential difference gradient, $d\phi/dx$, acting over the electrolyte to be derived from equation (3-8), such that:

$$\frac{d\phi}{dx} = \frac{RT}{Fc}\frac{dc}{dx} \qquad 3\text{-}9$$

From this expression the potential difference may be found by integration; *i.e.*

$$\int_c^a d\phi = \frac{RT}{F}\int_c^a \frac{1}{c}\,dc$$

which implies that:

$$\Delta\phi = \frac{RT}{F}\ln\left(\frac{c_a}{c_c}\right) \qquad 3\text{-}10$$

Thus the potential difference acting over the electrolyte at steady-state is equal to the Nernst potential difference (3-6) due to the concentration differences at the cathode and anode, and is thus equal to half the applied potential difference, ΔV, from equation (3-7): *i.e.*:

$$\Delta V = \Delta\phi + \Delta E = \frac{2RT}{F}\ln\left(\frac{c_a}{c_c}\right) \qquad 3\text{-}11$$

It is known for the cations that their migration and diffusion both contribute to the

steady-state current, I^s, such that:

$$-\frac{I^s}{A} = FD_+\frac{dc}{dx} + \frac{F^2}{RT}D_+c\frac{d\phi}{dx} \qquad 3\text{-}12$$

Substituting for $d\phi/dx$ from equation (3-9), equation (3-12) becomes:

$$-\frac{I^s}{A} = 2FD_+\frac{dc}{dx} \qquad 3\text{-}13$$

It may thus be noted that the migration and diffusion processes of the cations are of equal magnitude. Because the steady-state current is a constant, dc/dx in equation (3-13) must be a constant, which means that the concentration varies linearly across the cell. Two equations immediately follow from this observation:

$$c_a + c_c = 2c_o \qquad 3\text{-}14$$

and $$dc/dx = (c_a - c_c)/t \qquad 3\text{-}15$$

In equation (3-11) we have an expression for the potential difference applied to the cell, and in equation (3-13) we have an expression for the steady-state current, which, using equation (3-15), may be written as:

$$-I^s = \frac{2AFD_+}{t}(c_a - c_c) \qquad 3\text{-}16$$

It would be useful to examine the current-voltage response of the electrolyte at steady-state by relating equations (3-11) and (3-16), because the current and voltage are easily determined for a real electrolyte. However, equation (3-11) contains a difference in the natural logarithms of the electrode concentrations, and equation (3-16) a difference in the electrode concentrations themselves, and it is not readily apparent how to relate the two.

Bruce and Vincent [25] found that for small $(c_a - c_c)$, the two equations could be related in:

$$(c_a - c_c) \approx \frac{1}{2}(c_a + c_c)\ln\left(\frac{c_a}{c_c}\right) \qquad 3\text{-}17$$

From equations (3-14) and (3-17), equations (3-11) and (3-16) may be related in a single expression. Calling $-I^st/A\Delta V$ the steady-state conductivity, σ^s, it is apparent

that:

$$\sigma^s = \frac{F^2}{RT} D_+ c_o \qquad 3\text{-}18$$

Thus, for small concentration differences at the electrodes, the steady-state conductivity is constant; *i.e.*, the steady-state current is a linear function of the applied potential difference. Equation (3-18) may be compared to the equation for the initial conductivity, σ^o, when both cations and anions are mobile:

$$\sigma^o = \frac{F^2}{RT} (D_+ + D_-) c_o \qquad 3\text{-}19$$

and it is seen that the steady-state conductivity is the same as that part of the initial conductivity which arises from the cations. This means that the ratio of steady-state to initial conductivities provides a measure of the cation transference number, and if parameters from a real cell (*i.e.* one in which electrode interfaces exist and must be corrected for) are employed, the ratio of equations (3-18) and (3-19) may be written as:

$$\frac{\sigma^s}{\sigma^o} = \frac{I^s (\Delta V_a - I^o R_i^o)}{I^o (\Delta V_a - I^s R_i^s)} \qquad 3\text{-}20$$

which is the transference number equation quoted by Evans *et al.* [72].

Equations (3-10) and (3-14) may be used to express the electrode concentrations c_a and c_c in terms of $\Delta\phi$ so that the accuracy of equation (3-17) may be assessed as $\Delta\phi$ increases (thus as $(c_a - c_c)$ increases). It may be shown that:

$$c_c = \frac{2c_o}{1 + \exp\left(\frac{F\Delta\phi}{RT}\right)} \quad \text{and} \quad c_a = \frac{2c_o}{1 + \exp\left(\frac{-F\Delta\phi}{RT}\right)} \qquad 3\text{-}21$$

so for a given electrolyte concentration and temperature the electrode concentrations may be determined as a function of $\Delta\phi$, and these accurate values from equation (3-21) may be used in equation (3-17) to assess its accuracy as $\Delta\phi$ increases. Bruce and Vincent [25] found that for an applied potential difference of 20 mV the error in equation (3-17) was 1%; but by 60 mV the error was 10%. This rapid rise in error is due to the non-linear nature of the natural logarithm. Thus, as the applied potential

difference is increased, the logarithmic term in the voltage expression increases at a greater rate than the difference term in the current expression, and a fall in the steady-state conductivity (defined as I^s/I^o corrected for interface resistances, rather than equation (3-18)) occurs. In this case the ratio of the steady-state conductivity to the initial conductivity is less than that found at lower applied potentials, causing equation (3-20) to decrease as the potential difference increases.

This is not to suggest that the cation transference number is decreasing as the applied potential difference increases, but rather that equation (3-20) is only equal to the cation transference number (defined as $D_+/(D_+ + D_-)$) at low applied potentials.

Although a low limit of applied potential difference for a constant steady-state conductivity was indicated by theory in reference [25], an experimental verification of this prediction was not sought at the time. It is shown in the following section that this low applied potential limit may be exceeded when ion-pairs are present, possibly making the experimental determination of the potential difference limit of constant steady-state conductivity a useful procedure for establishing the species content of PEs, or at least in distinguishing between models. Experimental results of these determinations are presented in Chapter 5.

In conclusion: it has been shown that, for a PE containing mobile free ions:

(i) the steady-state current is proportional to the applied potential difference only for small values ($\approx$ 20 mV) of the latter.

(ii) the applied potential difference is distributed equally over the electrolyte potential difference and the electrode potential difference.

3.2.2 The Steady-state DC Polarisation of a Polymer Electrolyte Cell Containing M^+ and X^- Ions and MX Ion-pairs.

We next consider a PE cell like that in §3.2.1, but in which the electrolyte now contains free ions and ion-pairs, with a fast equilibrium existing between them such that the following equation holds:

$$[MX] = K[M^+][X^-] \qquad 3\text{-}22$$

i.e. $$i = Kc_+c_- = Kc^2 \qquad 3\text{-}23$$

Again the cation and anion concentrations must be equal, because of charge neutrality. It has already been seen qualitatively what occurs during the polarisation of such a cell; with the diffusion of ion-pairs transporting M across the cell.

Now there is no net transport of X-containing species across the cell at steady-state, so the migration of X^- ions is countered by the diffusion of X^- ions and MX ion-pairs.

For the species containing X:

$$\frac{F^2}{RT}D_-c\frac{d\phi}{dx} = FD_-\frac{dc}{dx} + FD_o\frac{di}{dx} \qquad 3\text{-}24$$

and noting that di/dx is given by:

$$\frac{di}{dx} = \frac{d(Kc^2)}{dx} = 2Kc\frac{dc}{dx} \qquad 3\text{-}25$$

It may be written that, for dϕ/dx:

$$\frac{d\phi}{dx} = \frac{RT}{Fc}\frac{dc}{dx}\left(1 + 2Kc\frac{D_o}{D_-}\right) \qquad 3\text{-}26$$

Equation (3-26) may be solved in a similar manner to equation (3-9) such that:

$$\Delta\phi = \frac{RT}{F}\ln\left(\frac{c_a}{c_c}\right) + 2\frac{KRTD_o}{FD_-}(c_a - c_c). \qquad 3\text{-}27$$

Equation (3-27) may be compared to equation (3-10) for the case of no ion-pairing. It may be noted that the effect of ion-association is to introduce a linear term in the concentration difference between the electrodes into the expression for the electrolyte potential difference. In the event of K being small (implying that few ion-pairs are present) equation (3-27) tends to equation (3-10), as would be expected. Equations (3-6) and (3-27) may be combined to provide an expression for the applied potential difference across the cell:

$$\Delta V = \Delta\phi + \Delta E = \frac{2RT}{F}\left[\ln\left(\frac{c_a}{c_c}\right) + \frac{KD_o}{D_-}(c_a - c_c)\right] \qquad 3\text{-}28$$

Here the electrolyte potential difference, $\Delta\phi$, is always greater than the electrode potential difference, ΔE, because the second term in equation (3-27) is always greater than zero.

The steady-state current is composed of M^+ and MX diffusion and M^+ migration, so for the cations:

$$-\frac{I^s}{A} = FD_+\frac{dc}{dx} + FD_o\frac{di}{dx} + \frac{F^2}{RT}D_+c\frac{d\phi}{dx} \qquad 3\text{-}29$$

From equation (3-26), equation (3-29) becomes:

$$-\frac{I^s}{A} = 2FD_+\frac{dc}{dx} + 2KFD_oc\left(1 + \frac{D_+}{D_-}\right)\frac{dc}{dx} \qquad 3\text{-}30$$

Because equation (3-30) contains a term in c(dc/dx), the concentration gradient is not linear, so an equation of the form of equation (3-14) cannot be written in the case of free ions and ion-pairs. Equation (3-30) may be solved for 'c' to yield an equation comparable to equation (3-16):

$$-\frac{I^s}{A}\int_0^x dx = 2FD_+\int_{c_c}^{c_x} dc + 2KFD_o\left(1 + \frac{D_+}{D_-}\right)\int_{c_c}^{c_x} c\ dc$$

i.e.

$$-\frac{I^s}{A}x = 2FD_+(c_x - c_c) + KFD_o\left(1 + \frac{D_+}{D_-}\right)\left(c_x^2 - c_c^2\right) \qquad 3\text{-}31$$

For x = t, the electrolyte thickness, c_x may be written as c_a, the ionic concentration at the anode, so equation (3-31) becomes:

$$-\frac{I^s t}{A} = 2FD_+\Delta c + KFD_o\left(1 + \frac{D_+}{D_-}\right)\Delta c\Sigma c \qquad 3\text{-}32$$

where Δc is the difference between the ionic concentrations at the electrodes, and Σc is the sum of these concentrations.

We now have expressions for the applied potential difference (3-28) and the

steady-state current (3-32), and these may be related using equation (3-17) as before, to provide an expression for the steady-state conductivity, σ^s:

$$\sigma^s = -\frac{I^s t}{A\Delta V} = \frac{F^2 D_+}{2RT}\Sigma c\left(1 + \frac{KD_o\Sigma c}{2D_+\left(1 + \frac{KD_o\Sigma c}{2D_-}\right)}\right) \qquad 3\text{-}33$$

Equation (3-33) is similar in form to equation (3-18), but now Σc cannot be equated to $2c_o$, because of the non-linear concentration gradient. If, however, Σc is relatively independent of ΔV (as is likely to be the case at low potential differences, where Σc will tend to $2c_o$) we find again that the steady-state conductivity is independent of the applied potential difference. It may be noted that for $K = 0$ (no ion-pairs present) equation (3-33) becomes the same as equation (3-18), which was derived for the free ion case. It may also be noted that if KD_o is large (either due to the predominance of ion-pairs or their rapid diffusion) equation (3-33) becomes equal to:

$$\sigma^s = \frac{F^2}{RT}\frac{\Sigma c}{2}(D_+ + D_-) \qquad 3\text{-}34$$

which is simply the initial conductivity, σ^o. The interpretation of this is that no concentration gradients are established in the electrolyte, because they are dispersed by ion-pair diffusion as quickly as they are formed. In this case the current remains at its initial value throughout the polarisation. Cameron *et al.* [53] have observed that in such a case the use of equation (3-20) yields a cation transference number of unity, even though the cations themselves are relatively immobile. This paradox is resolved by remembering that equation (3-20) was derived for a completely dissociated electrolyte, so it is not valid to apply it to more complicated systems; however, as will be discussed in §3.5, data may be usefully applied to equation (3-20) whether or not the salt is fully ionised.

No expression of c_a and c_c in terms of $\Delta\phi$ may be found in this case, to provide equivalent expressions to the equations in (3-20). This makes it difficult to assess the linearity range of equation (3-17) in the case of free ions and ion-pairs. What may be

done, however, is to examine the response of a cell using a computer simulation with known (or reasonably assigned) experimental parameters. The results of this study are presented in detail in §3.4. These results show that, whereas a 20 mV limit was found for a linear I^s-ΔV response in PEs containing free ions, a linear I^s-ΔV response may be displayed for up to tens of volts when ion-pairs are present. The exact linear range is dependent on the particular variables, but the extended linear ranges are ultimately due to the presence of the ion-pairs.

The main conclusions from the examination of PE cells containing mobile free ions and ion-pairs are:

(i) the applied potential difference is not evenly distributed over the electrode potential difference and the electrolyte potential difference: the electrode potential difference is less than the electrolyte potential difference, and consequently less than half of the applied potential difference.

(ii) the potential difference range of a linear I^s-ΔV response may not be determined exactly, but it may be as large as several tens of volts, depending on the experimental parameters.

(iii) the steady-state conductivity is not that part of the initial conductivity arising from the cations: a contribution from neutral ion-pairs is present.

3.2.3 The Steady-state DC Polarisation of a Polymer Electrolyte Cell Containing M^+, X^-, MX_2^-, and M_2X^+ Ions and MX Ion-pairs.

It is not possible to examine the full case of five species present in a PE because the mathematics involved is too complicated. What may be done, however, is to examine specific combinations of the species which may be present; for example, examining the behaviour of a cell containing M^+ and MX_2^- ions, or one containing M^+, M_2X^+ and X^- ions.

If one examines the number of possible combinations of any species from the five in the section title it is found that 31 combinations are possible. Some may be eliminated on the grounds of simple physical impossibility; such as only M^+ ions or

only X^- and MX_2^- ions being present, leaving 18 possible combinations to be considered. Discounting the two models already discussed, 16 remain. These are:

(1)	M^+, MX_2^-	(2)	X^-, M_2X^+
(3)	M_2X^+, MX_2^-	(4)	M^+, MX, MX_2^-
(5)	M^+, X^-, MX_2^-	(6)	M^+, X^-, M_2X^+
(7)	M^+, M_2X^+, MX_2^-	(8)	X^-, MX, M_2X^+
(9)	X^-, M_2X^+, MX_2^-	(10)	MX, M_2X^+, MX_2^-
(11)	M^+, X^-, MX, M_2X^+	(12)	M^+, X^-, MX, MX_2^-
(13)	M^+, X^-, M_2X^+, MX_2^-	(14)	X^-, MX, M_2X^+, MX_2^-
(15)	M^+, MX, M_2X^+, M_2X^+	(16)	M^+, X^-, MX, MX_2^-, M_2X^+

The most straightforward models to study involve M^+ ions, as their absence requires the postulation of chemical reactions which produce M^+ ions at the electrode from the species already present in the electrolyte, such that the electrode reactions remain the oxidation and reduction of lithium and lithium ions.

Even in these more straightforward cases equilibria between the various species in the electrolyte must be proposed (such as that between the free ions and ion-pairs in §3.2.2) which may lead to the production of overly complicated mathematical expressions. Thus, of the sixteen models above, only two (nos. 1 and 4) were able to be given a thorough mathematical treatment. Of the rest, expressions for the steady-state current and electrolyte potential difference could only be obtained for models 2, 3, and 8.

3.2.3.1 The Steady-state DC Polarisation of a Polymer Electrolyte Cell Containing M^+ and MX_2^- Ions.

In this model charge neutrality requires that $[M^+] = [MX_2^-] = c$, where c is seen to be half the salt concentration. It is only in this respect that this model differs from the free ion case. The expressions for the steady-state current and the applied, electrode, and electrolyte potential differences are the same; *i.e.*:

$$\Delta V = \frac{2RT}{F} \ln\left(\frac{c_a}{c_c}\right) \qquad 3\text{-}35$$

and

$$-I^s = \frac{2FAD_+}{t}\Delta c \qquad 3\text{-}36$$

The implication of this result is that again a low potential-limit of a linear steady-state current-applied potential difference response will be found.

3.2.3.2 *The Steady-state DC Polarisation of a Polymer Electrolyte Cell Containing M^+ and MX_2^- Ions and MX Ion-pairs.*

Again, macroscopic charge neutrality requires that $[M^+] = [MX_2^-] = c$. In this case the salt concentration is given by $[M^+] + [MX_2^-] + [MX]$. It is suggested that the ions and ion-pairs are in a fast equilibrium, such that the following equation holds:

$$[MX]^2 = K'[M^+][MX_2^-] \qquad 3\text{-}37$$

i.e.

$$[MX] = Kc \quad \text{where} \quad K = \sqrt{(K')} \qquad 3\text{-}38$$

In this case the variation in ionic concentration across the cell is linear, even though ion-pairs are present. This suggests that a limited range of linear steady-state current-applied potential difference response will be found.

The steady-state current is found to be:

$$-I^s = \frac{FA\Delta c}{t}\left[2D_+ + \frac{KD_o}{2} + \frac{KD_oD_+}{2D_N}\right] \qquad 3\text{-}39$$

and the applied potential difference is:

$$\Delta V = \frac{RT}{F}\left(2 + \frac{KD_o}{2D_N}\right)\ln\left(\frac{c_a}{c_c}\right) \qquad 3\text{-}40$$

where ΔE is less than $\Delta\phi$.

3.2.3.3 *The Steady-state DC Polarisation of a Polymer Electrolyte Cell Containing M_2X^+ and X^- Ions.*

In this model charge neutrality requires that $[M_2X^+] = [X^-] = c$, where c is equal to half of the salt concentration. The steady-state current is found to be:

$$-I^s = \frac{4AFD_PD_-}{t(D_- - D_P)}\Delta c \qquad 3\text{-}41$$

and the electrolyte potential difference, $\Delta\phi$, is found to be:

$$\Delta\phi = \frac{RT}{F}\left(\frac{D_- + D_P}{D_- - D_P}\right)\ln\left(\frac{c_a}{c_c}\right) \qquad 3\text{-}42$$

3.2.3.4 *The Steady-state DC Polarisation of a Polymer Electrolyte Cell Containing M_2X^+ and MX_2^- Ions.*

In this model charge neutrality requires that the two ionic concentrations are equal, *i.e.* that $[M_2X^+] = [MX_2^-] = c$, where c is now two thirds of the salt concentration. The steady-state current is found to be:

$$-I^s = \frac{FA}{t}\left(\frac{6D_ND_P}{2D_N - D_P}\right)\Delta c \qquad 3\text{-}43$$

and the electrolyte potential difference is:

$$\Delta\phi = \frac{RT}{F}\left(\frac{2D_N + D_P}{2D_N - D_P}\right)\ln\left(\frac{c_a}{c_c}\right) \qquad 3\text{-}44$$

3.2.3.5 *The Steady-state DC Polarisation of a Polymer Electrolyte Cell Containing M_2X^+ and X^- Ions and MX Ion-pairs.*

In this model the ionic concentrations are equal, i.e. $[M_2X^+] = [X^-] = c$, and the salt concentration is given by $2[M_2X^+] + [MX]$. It is assumed that the equilibrium relating the species is:

$$[MX]^2 = K'[M_2X^+][X^-] \qquad 3\text{-}45$$

such that:

$$[MX] = Kc, \text{ where } K = (K')^{1/2} \qquad 3\text{-}46$$

The steady-state current is found to be:

$$-I^s = \frac{FA}{t}\left[\frac{KD_o(D_p + D_-) + 4D_pD_-}{D_- - D_p}\right]\Delta c \qquad 3\text{-}47$$

and the electrolyte potential difference:

$$\Delta\phi = \frac{RT}{F}\left(\frac{D_p + KD_o + D_-}{D_- - D_p}\right)\ln\left(\frac{c_a}{c_c}\right) \qquad 3\text{-}48$$

The examination of PEs containing triple ions in addition to the free ions and ion-pairs has shown that the increase in complexity is great, with only a few specific models capable of full or partial mathematical treatment. Of the models fully examined, the electrode potential difference remains less than the electrolyte potential difference. It might prove to be the case that, when M^+ ions are not present in the electrolyte, the suggested reactions giving rise to M^+ ions at the electrodes result in electrode potential differences greater than the electrolyte potential differences, though no examples of this were found. It is found experimentally that ΔE is usually greater than $\Delta\phi$.

3.3 NON-IDEALITY IN POLYMER ELECTROLYTES

Polymer electrolytes are not likely to be ideal electrolytes: strong electrolytes (such as salts like sodium chloride dissolved in liquids of high dielectric constant) are virtually ideal in concentrations of up to tens of millimolar, but PEs are not strong electrolytes; PEs have low dielectric constants, which will prevent the screening of ionic charges, possibly causing extensive ion association in the electrolyte. The concentrations of PEs are typically of the order of 1-3 M, again meaning that non-ideality is a likely occurrence. Sources of non-ideality are likely to arise from the invalidity of two assumptions which were used in the previous sections:

(i) that concentrations may be used instead of activities, and

(ii) that no ion-ion interactions occur, such that Onsager's cross-terms are zero.

The first point is discussed in §3.3.1, and the second in §3.3.2.

3.3.1 Effect of Activity on Polymer Electrolyte Cells Containing Free Ions at Steady-state.

For an electrolyte which contains only free ions it is found that the effect of considering activity alone does not alter the equality of the electrolyte and electrode potential differences, though the non-ideal equations do differ from the ideal ones.

For the anions at steady state it may be written that:

$$RT\ d\ln a - F\ d\phi = 0 \qquad 3\text{-}49$$

from which it follows that:

$$\frac{d\phi}{dx} = \frac{RT}{F}\frac{d\ln a}{dx} \qquad 3\text{-}50$$

and also:

$$\frac{d\phi}{dx} = \frac{RT}{F}\frac{d\ln a}{d\ln c}\frac{d\ln c}{dx} \qquad 3\text{-}51$$

If dlna/dlnc is a constant, this expression may be integrated to provide an expression for $\Delta\phi$ as before:

$$\Delta\phi = \frac{RT}{F}\frac{d\ln a}{d\ln c}\ln\left(\frac{c_a}{c_c}\right) \qquad 3\text{-}52$$

The electrode potential difference, ΔE, may be written as:

$$\Delta E = \frac{RT}{F}\ln\left(\frac{a_a}{a_c}\right) \qquad 3\text{-}53$$

and it follows that it may also be written as:

$$\Delta E = \frac{RT}{F}\frac{d\ln a}{d\ln c}\ln\left(\frac{c_a}{c_c}\right) \qquad 3\text{-}54$$

Thus the two potential terms remain equal. If dlna/dlnc is greater than unity it necessarily follows that $\ln(c_a/c_c)$ is not as great in the non-ideal case as it was in the

ideal case, because the magnitude of ΔE remains one half of the applied potential difference. The effect of this decrease in $\ln(c_a/c_c)$ for a given potential difference is to increase the potential difference range over which the steady-state current is linearly related to the potential difference, because equation (3-17) will break down at higher potential differences. However, the fact that ΔE and $\Delta\phi$ remain equal means that the ideal and non-ideal free ion electrolytes can not be distinguished from ΔE measurements if only the activity is considered.

Measurements of the potential difference between electrolytes of differing concentrations indicate a dlna/dlnc term greater than unity [57] [58].

3.3.2 The Effect of Onsager's Cross Terms on Cells at Steady-state.

Phenomenological equations may be written [43] [73] to examine the ion fluxes occurring in a cell during a polarisation. These relate how the mass transport of one species is related to the transport of another species. In general terms, if there are 'j' species in the electrolyte, the flux of species 'i' may be written as:

$$J_i = -\sum_j L_{ij} \nabla \tilde{\mu}_j \qquad 3\text{-}55$$

However, as the cell is considered to have a single dimension which lies along the x-axis, this equation may be writen as:

$$J_i = -\sum_j L_{ij} \left(\frac{d\tilde{\mu}_j}{dx} \right) \qquad 3\text{-}56$$

If two species are present (*e.g.* M^+ and X^-) the equations which result are:

$$J_+ = - L_+ \frac{d\tilde{\mu}_+}{dx} - L_{\pm} \frac{d\tilde{\mu}_-}{dx} \qquad 3\text{-}57$$

and

$$J_- = - L_- \frac{d\tilde{\mu}_-}{dx} - L_{\pm} \frac{d\tilde{\mu}_+}{dx} \qquad 3\text{-}58$$

A strong electrolyte such as aqueous sodium chloride has a small, but not negligible, cross-term at high concentrations ($\approx$ 1 M) [73]. Such terms are likely to be of more

importance in PEs. Dudley and Steele [74] demonstrate how these cross-terms reveal themselves in solid conductors, and how they may be measured using suitable electrodes. However, if PEs are considered, and it is taken that a number of species are present, electrodes reversible to these species must be found. This may be possible for M^+ and X^- ions if these are the only species present, but unlikely for other, more complex, associated species.

On initial polarisation only field-driven transport will occur in the electrolyte, *i.e.*:

$$J_- = FL_-\frac{d\phi}{dx} - FL_\pm\frac{d\phi}{dx} \qquad 3\text{-}59$$

and

$$J_+ = -FL_+\frac{d\phi}{dx} + FL_\pm\frac{d\phi}{dx} \qquad 3\text{-}60$$

so the initial current, which is related to the algebraic sum of these fluxes, is proportional to:

$$(L_+ + L_- - 2L_\pm)\frac{d\phi}{dx} \qquad 3\text{-}61$$

At steady-state the net anion flux is zero, but a net cation flux exists.

For $d\mu_+/dx = d\mu_-/dx = d\mu/dx$, it is seen that for the anions at steady-state:

$$\frac{d\mu}{dx} = \left(\frac{L_- - L_\pm}{L_- + L_\pm}\right)\frac{d\phi}{dx} \qquad 3\text{-}62$$

Integration of this equation reveals an electrode potential difference less than the electrolyte potential difference.

For the cations, the flux at steady-state may be shown to be:

$$-J_+ = F\frac{d\phi}{dx}\left(\frac{2L_+L_- - 2L_\pm^2}{L_- + L_\pm}\right) \qquad 3\text{-}63$$

In the case where $L_\pm$ is zero equation (3-63) becomes:

$$- J_+ = 2FL_+\frac{d\phi}{dx} \qquad 3\text{-}64$$

which may be compared to the equation derived for the ideal case (equation 3-13).

The ratio of steady-state to initial current does not yield the transport number of the non-blocked species when $L_\pm$ is not zero:

$$\frac{I^s}{I^o} = \frac{J_+^s}{J_+^o + J_-^o} = \frac{L_+L_- - 2L_\pm^2}{L_+L_- - 2L_\pm^2 + L_-^2 - L_\pm L_- + L_\pm L_+} \qquad 3\text{-}65$$

Dudley and Steele [74] demonstrate how the transport numbers may be measured with appropriate electrodes.

The more types of species there are present in a PE the more complicated the phenomenological equations become.

In conclusion: for an electrolyte containing free ions in the presence of cross-terms, the electrode and electrolyte potential differences are not equal, with the electrolyte potential difference being the greater. The ratio of I^s:I^o does not yield the transport number of the non-blocked species. This is also true if the effects of activity and cross-terms are considered together [75].

3.4 COMPUTER SIMULATIONS OF POLYMER ELECTROLYTE CELLS CONTAINING FREE IONS AND ION-PAIRS

Because it is not possible to yield comparable equations to equation (3-20) for the free ions and ion-pairs model, it is more difficult to examine the applied potential difference range over which a constant steady-state conductivity occurs (which was found to be ≈ 20 mV for the free ion case). What may be done is to use computer simulations to model a specific electrolyte and determine this range. The procedure for doing this is outlined below.

3.4.1 Determination of the Salt Concentration Profile in a Polymer Electrolyte Containing Free Ions and Ion-pairs.

It may be seen that equation (3-31) is a quadratic equation in c_x, the ionic concentration at a point x between the electrodes, which may be used to give the salt concentration at any point x, s_x. From equation (3-22) it is known that:

$$s_x = c_x + Kc_x^2 \qquad 3\text{-}66$$

If equation (3-31) is recast in terms of c_x, the quadratic equation is found to be:

$$c_x^2 + \vartheta c_x - c_c^2 - \vartheta c_c + \frac{I^s x \vartheta}{2AFD_+} = 0 \qquad 3\text{-}67$$

where:

$$\vartheta = \frac{2D_+D_-}{KD_o(D_+ + D_-)}$$

i.e.:

$$c_x = \frac{\vartheta}{2}\left[-1 + \left(1 - \frac{2I^s x}{AFD_+\vartheta} + \frac{4c_c}{\vartheta} + \frac{4c_c^2}{\vartheta^2}\right)^{1/2}\right] \qquad 3\text{-}68$$

This equation may be used to determine the salt concentration profile across the cell, and the amount of salt in the cell if the variables it contains are known.

3.4.2 Determination of the Amount of Salt in a Polymer Electrolyte Containing Free Ions and Ion-pairs.

The amount of salt in the electrolyte must be conserved during a polarisation, because of electroneutrality and the non-discharge of anion-containing species. Thus, no matter what the salt concentration profile across the electrolyte is, the integral of it across the entire cell must yield the initial amount of salt present; *i.e.*:

$$\int_c^a s_x \, dx = s_o t \qquad 3\text{-}69$$

where t is the electrolyte thickness, and the limits of the integral are the cathode and anode.

It is not possible to insert equation (3-66) into equation (3-69) and solve the integral. However, the integral may be evaluated numerically if suitable values of parameters are chosen. For each simulation, the parameters which must be defined are:

I^s	the steady-state current
t	the electrode separation
A	the area of the electrodes
K	the ion-pair association constant
D_+	the cation diffusion coefficient
D_0	the ion-pair diffusion coefficient
D_-	the anion diffusion coefficient
c_c	the cation concentration at the cathode
s_0	the initial salt concentration

However, not all of these variables are independent. The initial salt concentration, the electrode separation, and the area of the electrodes may be regarded as known parameters (in an experiment they are under the control of the experimentalist), and the diffusion coefficients and association constant may be varied from simulation to simulation, but with reasonable values chosen (the diffusion coefficients are likely to be in the region of 10^{-8} cm^2 s^{-1} [48] [58]). If this is done, the only variable is the current density, because the cation concentration at the cathode may be determined now that the other parameters are known.

The integral of the salt concentration profile across the cell may be determined by dividing the salt concentration–distance graph into N strips, as shown in Figure 3-6. The salt concentration at each position in the electrolyte is known from equation (3-66), so the area of a strip 'n' may be approximated using the following equation:

$$\text{area of strip n} = (s_n - s_{n-1})\frac{t}{2N} + (s_{n-1})\frac{t}{N} \qquad 3\text{-}70$$

The total area is then found by the summation of the individual strip areas, *i.e.*:

$$\text{total area} = \sum_{n=1}^{N} (s_n - s_{n-1})\frac{t}{2N} + (s_{n-1})\frac{t}{N} \qquad 3\text{-}71$$

which, for the electrolyte shown in Figure 3-6, is:

$$\frac{t}{N}\sum_{n=0}^{N-1} s_n + \frac{t}{2N}(s_a - s_c) \qquad 3\text{-}72$$

For a chosen current there must exist a cation concentration at the cathode which allows the summation in equation (3-72) to be equal to the initial amount of salt in the electrolyte. The cation concentration at the cathode, c_c, must be increased from zero to a value at which the summation holds. It may happen that the current chosen is so large that even a c_c of zero will not satisfy the summation (the larger the current the smaller the cation concentration at the cathode will tend to get); in this case the current is unsustainable and must be reduced, and the calculation repeated.

Thus for a suitable current a value of c_c will be found for which the summation is satisfied, and now all the parameters needed to solve equation (3-31) in terms of the cation concentration at the anode are found. As c_a and c_c are now known, the applied potential difference equation (equation (3-27)) may now be solved, and the steady-state conductivity determined. The variation in the steady-state conductivity with the applied potential difference may be established by increasing the current from zero in steps, and determining c_c at each value (all other parameters being given), and then determining the steady-state conductivity. Because all of the parameters are now known accurately, the error in using equation (3-33) may be assessed as the potential difference is increased. This has been done for various parameters, as detailed in the following section.

3.4.3 Results of Computer Simulations of Polymer Electrolyte Cells Containing Free Ions and Ion-pairs.

The numerical integration method was used to determine the ionic concentrations at the electrodes, allowing accurate and approximate values for the steady-state conductivity to be determined (*cf.* equation (3-33) and equations (3-28) and (3-32)). The potential difference at which these two values differed by 1% was taken to be the limit of the linear I^s-ΔV response of the electrolyte. The computer simulations

calculated parameters at differing current densities, usually requiring the interpolation of data points to provide the values at 99.0% accuracy (typically interpolation between data at ≈ 99.5% and ≈ 98.5% accuracies). Occasionally extrapolation was required, but this was not performed if a large data range was not available (*i.e.* where the only data were greater than 99.9% accurate).

Small ionic concentrations (where the association constant is high) result in the salt concentrations through the electrolyte being very dependent on the values of the ionic concentration at the cathode, such that a small change in this ionic concentration will produce a large change in the salt concentrations, and consequently data in these cases may not be as reliable as data from high ionic concentration simulations.

Salt concentrations of 0.1, 0.5, and 1.0 M were chosen. Diffusion coefficients of 10^{-7}, 10^{-8}, and 10^{-9} $cm^2\ s^{-1}$ were permuted, in the belief that they represented a sufficient spread about the actual diffusion coefficients. The electrolyte thickness was chosen to be 0.25 mm, because this is a typical thin film value and close to the actual electrolyte thickness used in the experimental study. The values of the association constant K determine the initial proportions of free ions and ion-pairs in the electrolyte. The effect of the magnitude of K on the amount of free ions present is shown in Table 3-A. The electrolyte was divided into 100 strips for determining the salt content.

The results are contained in Table 3-B. It is seen that, in general, an increase in the amount or diffusion coefficient of the ion-pairs results in an increase in the potential difference range through which the steady-state conductivity is constant. This is because significant mass transport through the electrolyte in the form of neutral species occurs without the ionic concentrations at the electrodes differing by a great deal, which prevents equation (3-17) from breaking down.

3.5 THE USE OF THE TERMS TRANSPORT NUMBER AND TRANSFERENCE NUMBER.

In the literature the terms transport number and transference number have been

used almost interchangeably, thus frequently incorrectly. The transport number, t, of a species, n, is defined as the fraction of the total current carried by that species; *i.e.*

$$t_n = \frac{i_n}{\sum i} \qquad 3\text{-}73$$

and t is necessarily positive and less than or equal to unity.

The transference number, T, of an ion-constituent n_+ (n_-) is defined by Spiro [76] as the net number of faradays carried by all species which contain n across an imaginary reference plane in the electrolyte, in the direction of the cathode (anode) when one faraday passes through the plane*. The transference number of a species n thus considers the overall effect of the transport of species a, b, c, *etc.* which contain n. The transport number of n then has no meaning (unless n exists itself as one of the species), and only the transport numbers of a, b, c, *etc.* may be referred to.

The transference number of an ion-constituent n may be related to the transport numbers of all the species i, which each contain $N_{n/i}$ atoms of the ion-constituent, by the equation:

$$T_n = \sum_i N_{n/i} t_i (z_n/z_i) \qquad 3\text{-}74$$

The transference number of a species may be negative; Spiro [76] quotes the example of an aqueous solution of potassium silver cyanide polarised in a Hittorf experiment, in which the Ag^+ transference number is negative (because $Ag(CN)_2^-$ ions carry silver to the anode). The example also illustrates that the Hittorf method may sometimes be used to provide an insight as to the actual species present in solution: the fact that the silver transference number was negative but with a magnitude one half that of the cyanide clearly suggested that $Ag(CN)_2^-$ ions were present. This use is not likely

---

* The cation and anion ion-constituents are species from which all other species present may be built up. For example, if the species present in a lithium-based electrolyte are Li^+, Li_2X^+ and LiX_2^-, the ion-constituents would be Li^+ and X^-, since all the other species may be represented as combinations of them. The ion-constituents themselves do not have to be present as species in the electrolyte. If the species were LiX_2^-, Li^+, and $Li_3X_4^-$, the ion-constituents could be Li^+ and X^- or Li^+ and LiX_2^-, because either choice allows the production of all the other species from the ion-constituents.

to be possible in a PE where several types of salt species may be present.

3.5.1 Why I^s/I^o May Not Generally Be Used as a Measure of the Transport Number or Transference Number of the Non-blocked Species in a Polymer Electrolyte.

Shriver *et al.* [77] suggested that the ratio of steady-state current to initial current in a PE cell could be used as a measure of the (cation) transport number in the electrolyte, because (it was reasoned) the initial current is due to the motion of all charged salt species and the steady-state current is due to transport of the non-blocked salt species alone. There are several problems with this treatment, a relatively minor one being that any interfacial resistances between the electrodes and electrolyte (which affect the current passed from the application of a constant potential difference) must be corrected for, before the effect of the potential difference on the electrolyte can be considered, as shown earlier in this Chapter, and it is not clear if this was done for the data presented.

Evans *et al.* [72] identified the ratio of I^s:I^o in a symmetrical lithium PE cell containing free ions, correcting this ratio for changes in electrode interface resistances (which affect the current), as the cation transference number. The equation the authors quote is:

$$T_+ = \frac{I^s}{I^o}\left(\frac{\Delta V - I^o R_i^o}{\Delta V - I^s R_i^s}\right) \qquad 3\text{-}75$$

It is seen that this is simply the ratio of the initial electrolyte conductivity to the steady-state electrolyte conductivity, as was shown in §3.2.

Another problem with the treatment by Shriver *et al.* is that the term transport number is not strictly suitable, because there is no *prima facie* evidence of free ions being the predominant species in PEs. The term transference number, as used by Evans *et al.*, is also not an acceptable general term for the corrected ratio of I^s/I^o, because the results provided from steady-state and non-steady-state experiments are likely to be different, as explained below (in the case of a dissociated salt this equation

does yield, at low applied potential differences, the cation transference number).

It has been shown above that in a steady-state experiment the transport of neutral species may contribute to the steady-state current, such that the corrected value of I^s/I^o is not simply the cationic contribution to the current—but the Spiro definition of transference number refers to the net number of faradays carried by the ion-constituents through a reference plane in the cell. One cell in which the Spiro definition may be contrived is a Hittorf cell; in order to establish the net number of faradays carried by the ion-constituent some suitable technique, such as chemical analysis, is used to determine the concentration change of the ion-constituent in the electrolyte (which is described in more detail in Chapter 6). In order that all the concentration change is detected, the reference plane must be in an electrolyte region where no concentration changes occur during the timescale of the experiment. If this is so, only the transport of charged species may occur through the plane because no salt concentration differences exist across it which would promote the diffusion of neutral species.

Thus, because neutral species are important for mass transport in one experiment (steady-state) and irrelevant for mass transport in the other (non-steady-state), the experiments are likely to yield different "transference numbers". It is the Hittorf experiment which meets the Spiro definition of transference number, so it may be said that the steady-state experiment will not generally measure transference numbers.

3.5.2 The Use of I^s/I^o as a Practical Electrolyte Parameter—The "Current Fraction".

Steady-state experiments, therefore, are not likely to give a measurement of transference numbers. It is not apparent how, at steady-state, the ionic contribution to the transport of cation-containing species through the electrolyte may be separated from the neutral contribution, so it is suggested here that equation (3-75) be called the *"current fraction"* i_F, to allow the use of the equation without it necessarily claiming to measure something which it does not.

To all practical intents and purposes the current fraction is a transference number, though it will not agree with the results from a Hittorf experiment (which is why it should not be *called* a transference number); for example, in the case discussed above where ion-pairs are present and diffuse rapidly in an electrolyte, preventing a fall in the current with time, it is seen that a current fraction of unity follows from equation (3-75). The lack of a current decrease superficially suggests that only cations are mobile in the electrolyte, giving rise to a "transference number" of unity. If a Hittorf experiment were carried out on the same electrolyte the results would be different: the massive contribution of the ion-pairs to transport in the electrolyte would be irrelevant, and the true ionic transference numbers would be determined. If the cations are relatively immobile, with nearly all of the charge being transported by the anions, a cation transference number of zero would be found, even though in a steady-state experiment the transference number is apparently unity [53]! This example illustrates why equation (3-75) should be referred to as a different parameter.

Equation (3-75) is a useful experimental parameter, as it shows what proportion of the initial current can be expected to be maintained at steady-state in a real thin-electrolyte cell, where the anticipated cell dimensions are likely to allow the rapid attainment of a steady-state concentration profile between the electrodes [68]. In an electrolyte operating under load in a real cell one is not so much concerned with what species are transporting charge through the cell so long as the current itself is satisfactory, so it is not important if the actual cation transference number is small providing the current fraction (with its contribution from neutral species) is large.

However, it will be remembered that the steady-state current is only a linear function of the electrolyte potential difference for a finite range of the latter, which, as has been shown already, may be a small range (of the order of millivolts). When the linear range has been exceeded the steady-state current is found to be less than anticipated by the simple use of Ohm's law, causing a fall in the current fraction. For i_F to be a useful parameter its variation with the electrolyte potential difference must be known, but because PEs display a potential difference range over which i_F is constant,

i_F may be further defined as the corrected value of I^s/I^o determined in the potential difference range where an ohmic response of the steady-state current to the applied potential difference occurs. In this situation i_F may be referred to as the *"limiting current fraction"*, i_{FI}, and it is a property of the electrolyte independent of the applied potential difference (for some unspecified potential difference range which must be determined for each electrolyte) but likely to be temperature and concentration dependent.

This observation implicitly suggests that the potential difference range of the limiting current fraction should be determined as a matter of course for PEs which may eventually be used in batteries, because PEs which display a small voltage range of constant i_F response may perhaps only pass miniscule amounts of current at steady-state if a large potential difference acts across the electrolyte, even though it may possess an excellent unpolarised ac conductivity and good low-potential i_F. This has been done for several amorphous lithium perchlorate and lithium triflate electrolytes at the same temperature, and the results are presented in Chapter 5.

Table 3-A: Variation in cation concentration with ion-pair association constant for three salt concentrations.

SALT CONCENTRATION mol m^{-3}	ASSOCIATION CONSTANT K m^3 mol^{-1}	CATION CONCENTRATION mol m^{-3}
100	0.001	91.6
100	0.1	27.0
100	10.0	3.1
500	0.001	366
500	0.1	65.9
500	10.0	7.0
1000	0.001	618
1000	0.1	95.1
1000	10.0	10.0

Table 3-B: Applied Potential Difference Limits at 99% Accuracy for PE Cells Containing Free Ions and Ion-pairs.

Simulations denoted * have been found by interpolation.

Simulations denoted † have been found by extrapolation.

c = 100 mol m^{-3}, K = 0.001 m^3 mol^{-1}, 91.6% free ions.

I^s / 10^{-3} A m^{-2}	ΔV mV	D_+ / 10^{-13} m^2 s^{-1}	D_- / 10^{-13} m^2 s^{-1}	D_o / 10^{-13} m^2 s^{-1}	%	
3.0	27.3	1	1	1	98.9	
6.0	40.0	1	1	10	98.9	
40	206.8	1	1	100	99.1	
2.3	21.1	1	10	1	99.0	*
3.5	18.7	1	10	10	99.0	*
19	31.8	1	10	100	99.0	*
2.4	21.5	1	100	1	99.0	*
3.2	16.5	1	100	10	99.0	*
14	14.7	1	100	100	99.0	
24	23.9	10	1	1	99.0	*
44	41.4	10	1	10	99.0	*
245	221.3	10	1	100	99.0	
24	23.4	10	10	1	98.9	
27	24.5	10	10	10	98.9	
60	40.0	10	10	100	98.9	
24	23.4	10	100	1	98.9	
23	20.9	10	100	10	90.0	*
35	18.7	10	100	100	90.0	*
240	23.6	100	1	1	99.0	
440	42.8	100	1	10	99.0	*
2300	224	100	1	100	99.0	*
240	23.6	100	10	1	98.9	
240	23.9	100	10	10	99.0	*
440	41.4	100	10	100	99.0	*
240	23.6	100	100	1	98.9	
240	23.4	100	100	10	98.9	
270	24.5	100	100	100	98.9	

c = 100 mol m^{-3}, K = 0.1 m^3 mol^{-1}, 27.0% free ions.

I^s / 10^{-3} A m^{-2}	ΔV mV	D_+ / 10^{-13} m^2 s^{-1}	D_- / 10^{-13} m^2 s^{-1}	D_o / 10^{-13} m^2 s^{-1}	%	
3.3	62.8	1	1	1	99.0	*
30	510	1	1	10	99.0	
300	5020	1	1	100	99.0	
1.4	14.6	1	10	1	99.0	*
12	48.2	1	10	10	99.1	
150	457	1	10	100	99.0	*

1.3	11.5	1	100	1	99.0 *
10	15.0	1	100	10	99.0
130	33.7	1	100	100	99.0 *
22	67.6	10	1	1	99.0 *
180	548	10	1	10	98.9
1500	4557	10	1	100	99.0 *
8	22.0	10	10	1	99.0
23	43.2	10	10	10	99.0 *
300	510	10	10	100	99.0
6	15.8	10	100	1	99.0
17.3	18.5	10	100	10	99.0 *
120	48.2	10	100	100	99.1
210	69.6	100	1	1	98.9
1500	496	100	1	10	99.0
33000	10826	100	1	100	99.0 †
68	22.1	100	10	1	99.0 *
220	67.6	100	10	10	99.0 *
1800	548	100	10	100	98.9
60	19.5	100	100	1	98.9
80	22.0	100	100	10	99.0
330	62.7	100	100	100	99.0 *

c = 100 mol m^{-3}, K = 10 m^3 mol^{-1}, 3.1% free ions.

I^s / 10^{-3} A m^{-2}	ΔV mV	D_+ / 10^{-13} m^2 s^{-1}	D_- / 10^{-13} m^2 s^{-1}	D_o / 10^{-13} m^2 s^{-1}	%
4	588	1	1	1	99.0
40	5807	1	1	10	98.9
400	57975	1	1	100	99.0
2	67.6	1	10	1	99.0
21	570	1	10	10	98.9
210	5548	1	10	100	99.0
1	11.7	1	100	1	99.1
16.8	63.5	1	100	10	99.0 *
175	518	1	100	100	99.0 *
21.7	574	10	1	1	99.0 *
140	3672	10	1	10	99.0
2100	55320	10	1	100	99.0
4	65.9	10	10	1	99.0
40	588	10	10	10	99.0
400	5807	10	10	100	98.9
1.8	15.0	10	100	1	99.0 *
18.7	63.2	10	100	10	99.0 *
210	570	10	100	100	98.9
210	602	100	1	1	99.0
2100	6034	100	1	10	98.9
49000	139804	100	1	100	99.0 †
26	70.0	100	10	1	99.0 *
217	574	100	10	10	99.0 *
2100	5535	100	10	100	99.0

9.7	22.8	100	100	1	99.0 *
40	65.9	100	100	10	99.0
400	588	100	100	100	99.0

c = 500 mol m^{-3}, K = 0.001 m^3 mol^{-1}, 73.2% free ions.

I^s / 10^{-3} A m^{-2}	ΔV mV	D_+ / 10^{-13} m^2 s^{-1}	D_- / 10^{-13} m^2 s^{-1}	D_o / 10^{-13} m^2 s^{-1}	%
13.6	26.4	1	1	1	99.0 *
66.7	92.0	1	1	10	99.0 *
600	748	1	1	100	99.0
10.7	19.4	1	10	1	99.0 *
33.3	22.4	1	10	10	99.0 *
300	83.4	1	10	100	99.0
10.3	18.6	1	100	1	99.0 *
27.1	14.7	1	100	10	99.0 *
218	19.4	1	100	100	99.0 *
120	28.8	10	1	1	99.1
440	100.6	10	1	10	99.0 *
3500	786	10	1	100	99.0 *
92	21.9	10	10	1	99.0 *
136	26.4	10	10	10	99.0 *
686	94.7	10	10	100	99.0 *
88	20.9	10	100	1	99.0 *
107	19.4	10	100	10	99.0 *
329	22.0	10	100	100	99.0 *
1200	29.5	100	1	1	99.0
4000	97.7	100	1	10	99.0
55000	1331	100	1	100	99.0 †
889	21.8	100	10	1	99.0 *
1200	28.8	100	10	10	99.0
4000	91.2	100	10	100	99.1
900	22.1	100	100	1	99.0
920	21.9	100	100	10	99.0 *
1357	26.4	100	100	100	99.0 *

c = 500 mol m^{-3}, K = 0.1 m^3 mol^{-1}, 13.2% free ions.

I^s / 10^{-3} A m^{-2}	ΔV mV	D_+ / 10^{-13} m^2 s^{-1}	D_- / 10^{-13} m^2 s^{-1}	D_o / 10^{-13} m^2 s^{-1}	%
18.2	133.4	1	1	1	99.0 *
180	1241	1	1	10	99.0
1800	12330	1	1	100	99.0
8.7	23.9	1	10	1	99.0 *
90	127.1	1	10	10	99.1
1000	1262	1	10	100	99.0 *

6.5	12.5	1	100	1	99.0 *
60	20.1	1	100	10	99.1
800	124.8	1	100	100	99.0 *
120	151.3	10	1	1	98.9
1020	1271	10	1	10	99.0 *
10000	12430	10	1	100	99.0 †
30	29.4	10	10	1	99.0
182	133.4	10	10	10	99.0 *
1800	1241	10	10	100	99.0
19.8	16.8	10	100	1	99.0 *
86.7	23.9	10	100	10	99.0 *
900	127.1	10	100	100	99.0
1067	145	100	1	1	99.0 *
10000	1356	100	1	10	98.9
		100	1	100	
231	30.5	100	10	1	99.0 *
1200	151.3	100	10	10	98.9
10111	1245	100	10	100	99.1
146	18.8	100	100	1	99.0 *
300	29.4	100	100	10	99.0
1820	133.4	100	100	100	99.0 *

c = 500 mol m^{-3}, K = 10.0 m^3 mol^{-1}, 1.4% free ions.

I^s / 10^{-3} A m^{-2}	ΔV mV	D_+ / 10^{-13} m^2 s^{-1}	D_- / 10^{-13} m^2 s^{-1}	D_o / 10^{-13} m^2 s^{-1}	%
100	646	1	1	1	99.1
		1	1	10	
		1	1	100	
8	105.2	1	10	1	99.1
6	71	1	10	10	99.0
		1	10	100	
2	6.1	1	100	1	99.0
>10	>14	1	100	10	
		1	100	100	
>10	>116	10	1	1	
		10	1	10	
		10	1	100	
9.6	65.9	10	10	1	99.0 *
		10	10	10	
		10	10	100	
5	12.5	10	100	1	99.0
>10	>13.1	10	100	10	
		10	100	100	
		100	1	1	
		100	1	10	
		100	1	100	
>10	>11.8	100	10	1	
		100	10	10	
		100	10	100	

100	100	1
100	100	10
100	100	100

c = 1000 mol m^{-3}, K = 0.001 m^3 mol^{-1}, 61.8% free ions.

I^s / 10^{-3} A m^{-2}	ΔV mV	D_+ / 10^{-13} m^2 s^{-1}	D_- / 10^{-13} m^2 s^{-1}	D_o / 10^{-13} m^2 s^{-1}	%	
30	31.7	1	1	1	98.9	
180	141	1	1	10	99.0	
1800	1324	1	1	100	99.0	
20	18.5	1	10	1	99.0	*
80	24.2	1	10	10	99.1	
900	136.7	1	10	100	99.0	
26.7	16.9	1	100	1	99.0	*
65.5	14.0	1	100	10	99.0	*
600	22.3	1	100	100	99.1	
240	33.7	10	1	1	99.0	
1067	143.3	10	1	10	99.0	*
10000	1329	10	1	100	99.0	
154	21.3	10	10	1	99.0	*
300	31.7	10	10	10	98.9	
1800	141.1	10	10	100	99.0	
146	20.0	10	100	1	99.0	*
200	18.5	10	100	10	99.0	*
800	24.2	10	100	100	99.1	
2400	34.9	100	1	1	99.0	
10000	144.6	100	1	10	99.0	
>10000	>143.1	100	1	100		
1500	21.8	100	10	1	99.0	*
2400	33.7	100	10	10	99.0	
11670	157	100	10	100	99.0	†
1500	21.8	100	100	1	99.0	
1543	21.3	100	100	10	99.0	*
3000	31.7	100	100	100	98.9	

c = 1000 mol m^{-3}, K = 0.1 m^3 mol^{-1}, 9.5% free ions.

I^s / 10^{-3} A m^{-2}	ΔV mV	D_+ / 10^{-13} m^2 s^{-1}	D_- / 10^{-13} m^2 s^{-1}	D_o / 10^{-13} m^2 s^{-1}	%	
40	197.1	1	1	1	99.0	
400	1908	1	1	10	98.9	
4000	18993	1	1	100	98.9	
17.6	28.4	1	10	1	99.0	*
190	179.3	1	10	10	99.0	*
2100	1827	1	10	100	99.0	
14	13.7	1	100	1	98.9	
140	26.7	1	100	10	99.0	*
1800	186.5	1	100	100	99.0	

240	208.8	10	1	1	98.9
2100	1811	10	1	10	99.0
>10000	>8553	10	1	100	
51.4	32.8	10	10	1	99.0 *
400	199.1	10	10	10	99.0
4000	1908	10	10	100	98.9
30.9	15.7	10	100	1	99.0 *
176	28.4	10	100	10	99.0 *
2100	198.4	10	100	100	99.0
2100	197.3	100	1	1	99.0
>10000	>932	100	1	10	
>10000	>930	100	1	100	
400	36.2	100	10	1	99.0
2400	208.8	100	10	10	98.9
>10000	>857	100	10	100	
231	20.2	100	100	1	99.0 *
514	32.8	100	100	10	99.0 *
4000	199.1	100	100	100	99.0

c = 1000 mol m^{-3}, K = 10 m^3 mol^{-1}, 1.0% free ions.

I^s / 10^{-3} A m^{-2}	ΔV mV	D_+ / 10^{-13} m^2 s^{-1}	D_- / 10^{-13} m^2 s^{-1}	D_o / 10^{-13} m^2 s^{-1}	%
210	1733	1	1	1	98.9
2100	17300	1	1	10	99.0
6000	49400	1	1	100	99.1
40	190.1	1	10	1	98.9
350	1595	1	10	10	99.0 *
3500	15877	1	10	100	99.0 *
14.4	21.8	1	100	1	99.0 *
210	189	1	100	10	98.9
2100	1746	1	100	100	99.0
2100	1884	10	1	1	99.0
10000	8974	10	1	10	99.0
>10000	>8960	10	1	100	
160	132.7	10	10	1	99.1
2100	1733	10	10	10	98.9
>10000	>8203	10	10	100	
40	24.2	10	100	1	99.0
400	190.1	10	100	10	98.9
3500	1596	10	100	100	90.0 *
2000	1792	100	1	1	99.1
>10000	>8906	100	1	10	
>10000	>8889	100	1	100	
		100	10	1	
3000	2470	100	10	10	99.1
>10000	>8172	100	10	100	
		100	100	1	
		100	100	10	
4000	1820	100	100	100	99.1

Figure 3-1. Decrease in magnitude of current with time to steady-state for an Na|$PEO_{100}NaBPh_4$|Na cell at 85°C polarised at -60mV.

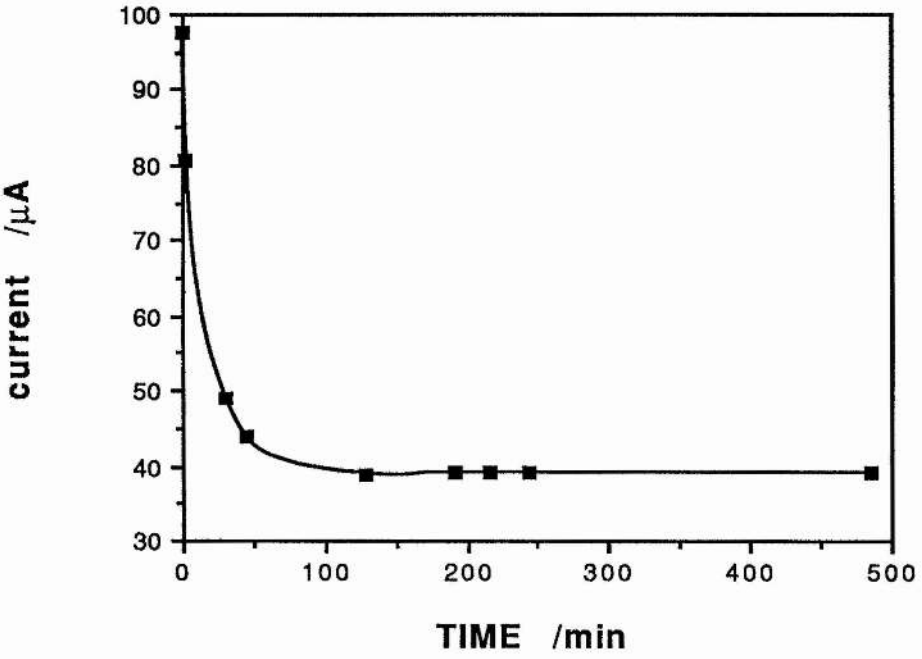

Figure 3-2. Transport processes in a cell M|PEO-MX|M containing free ions as steady-state is achieved.

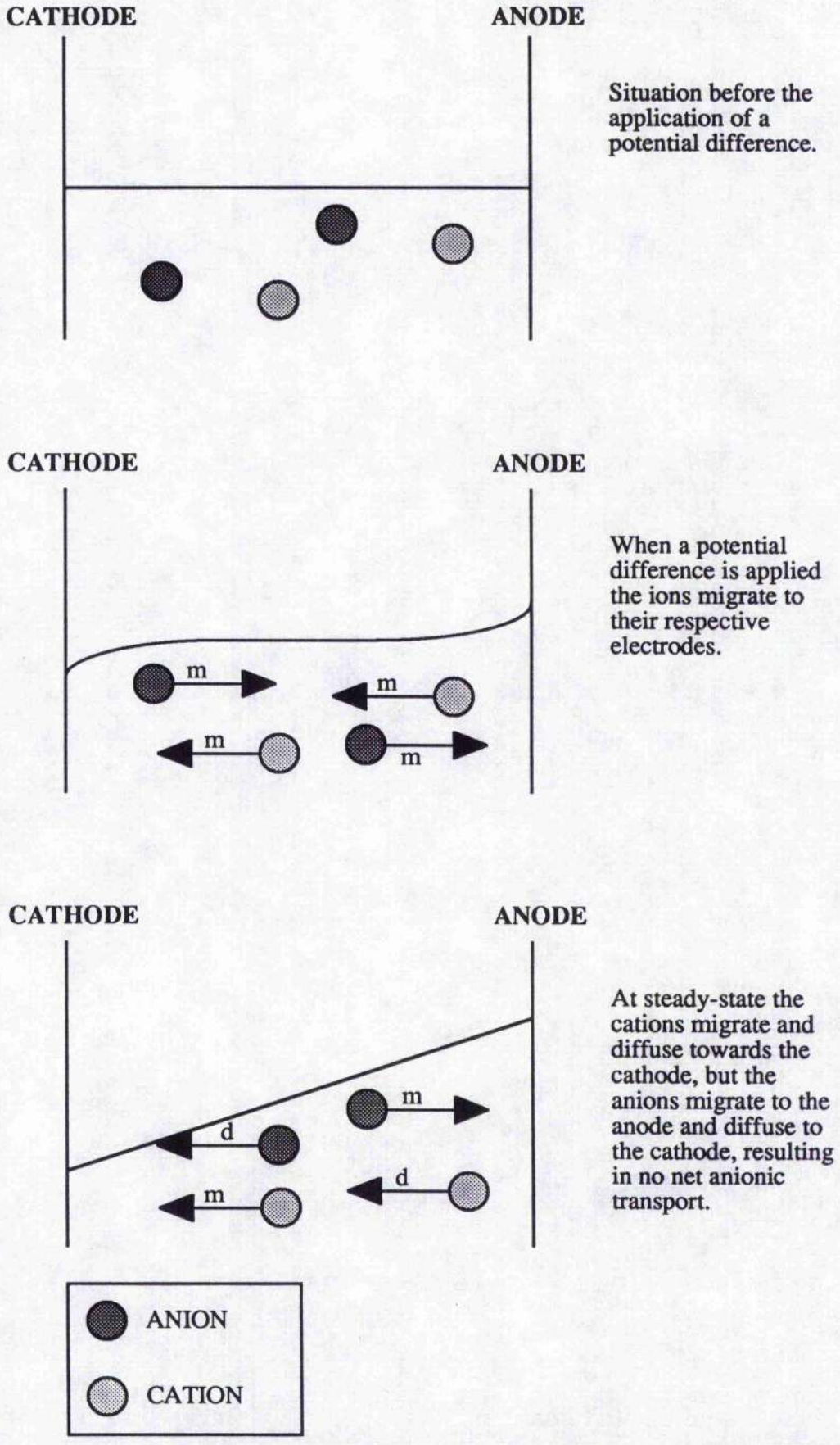

Figure 3-3. Transport processes in a cell M|PEO-MX|M containing free ions and ion-pairs as steady-state is achieved.

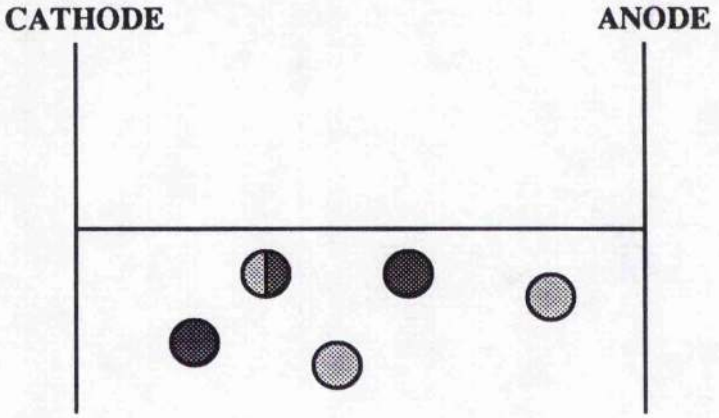

Situation before the application of a potential difference.

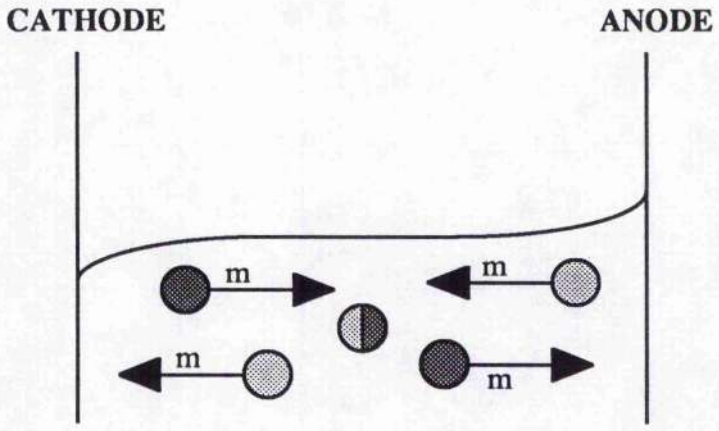

When a potential difference is applied the ions migrate to their respective electrodes.

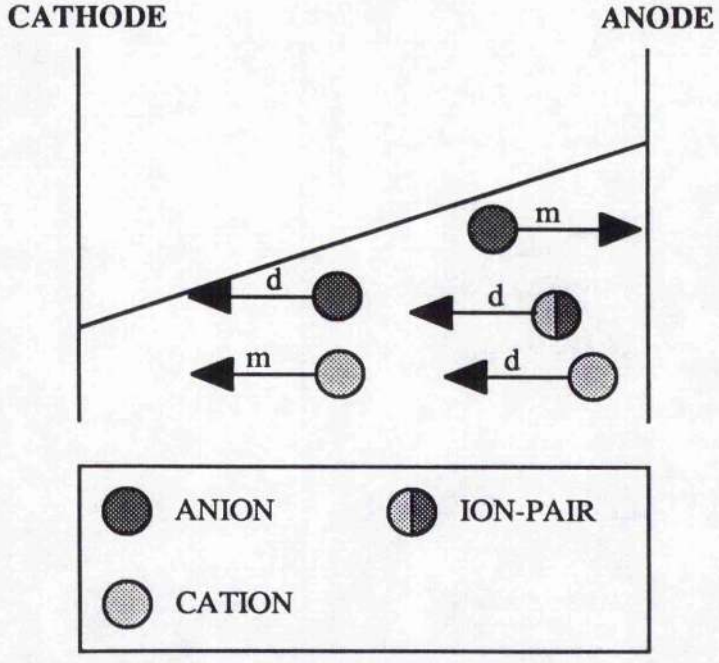

At steady-state the cations migrate and diffuse towards the cathode and the ion-pairs diffuse towards the cathode, but the anions migrate to the anode and diffuse to the cathode.
The anionic migration is balanced by the anionic diffusion and the diffusion of ion-pairs, resulting in no net anionic transport.

Figure 3-4. Impedance diagram showing a greater interface resistance than electrolyte resistance.

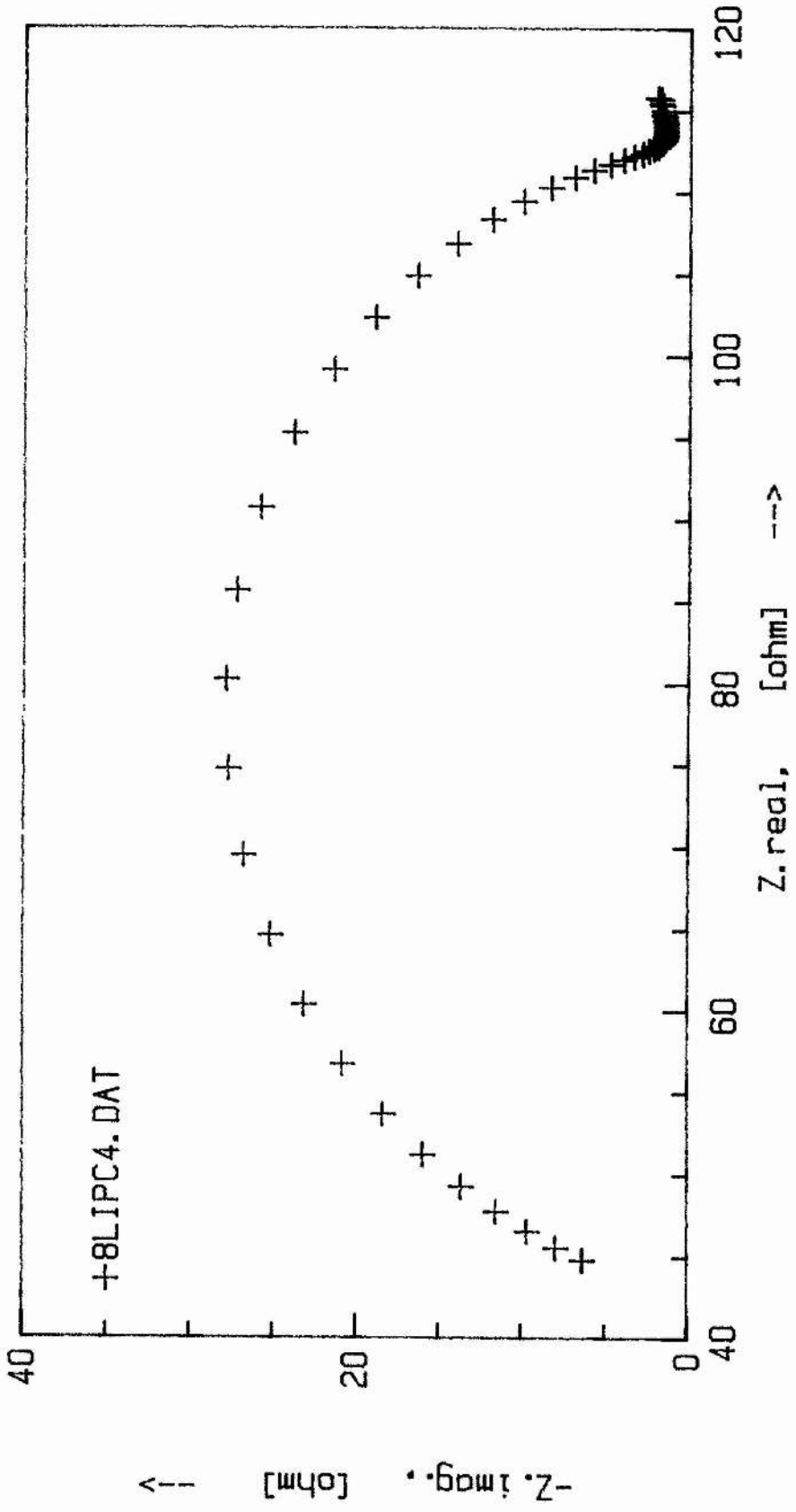

Figure 3-5. Distribution of the applied potential difference over an M|PE-MX|M cell initially and at steady-state.

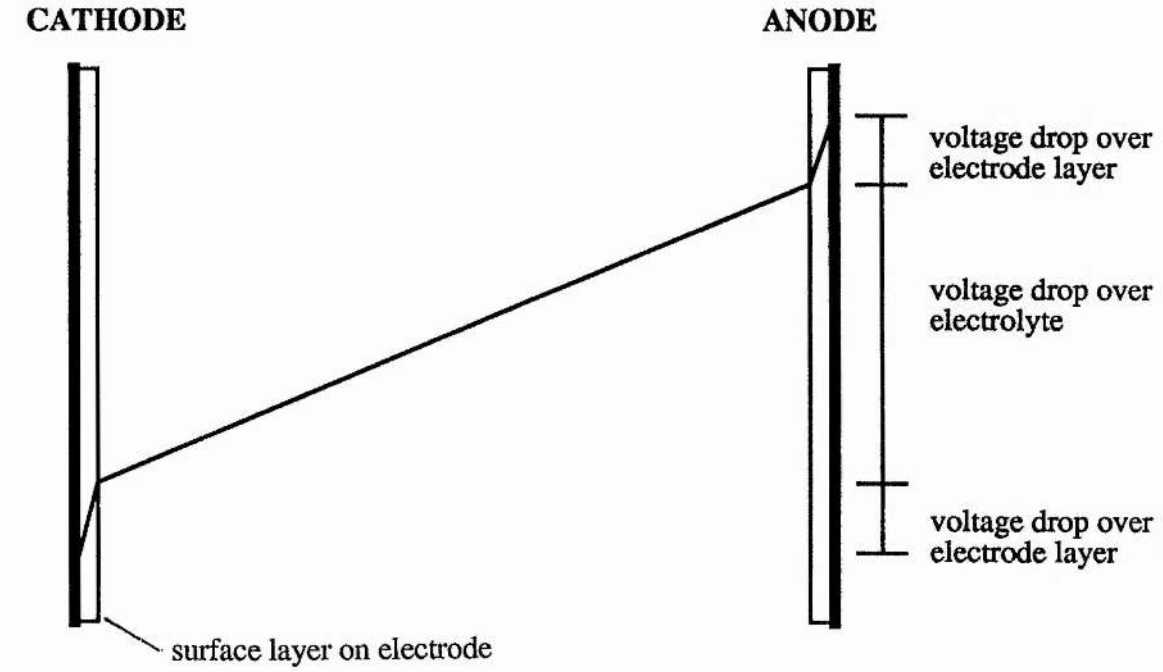

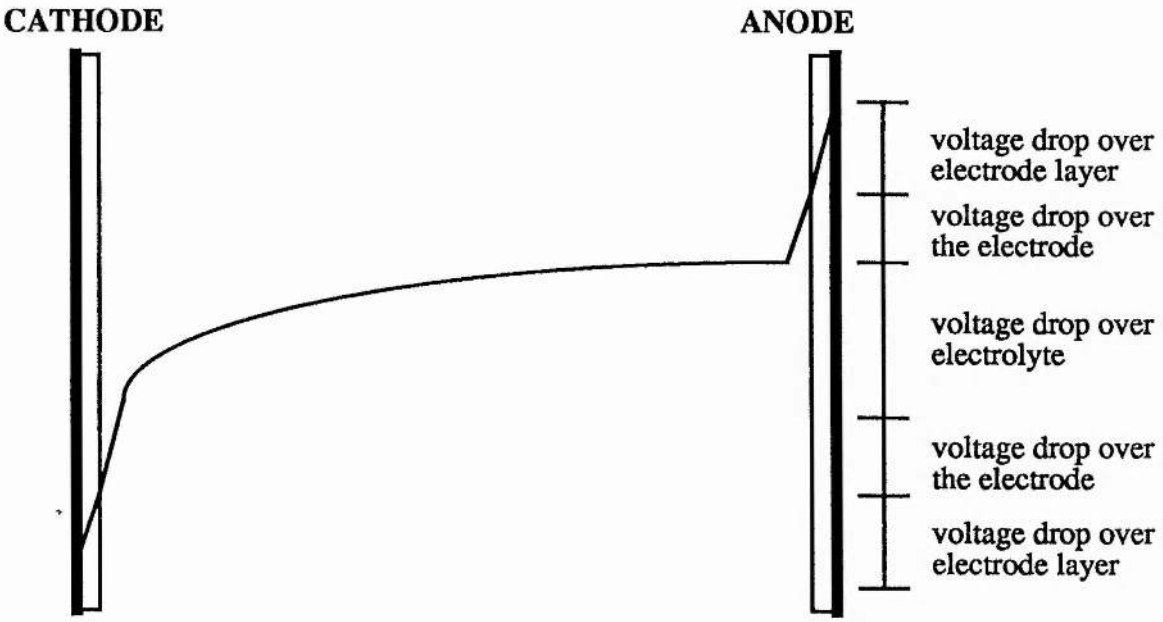

Figure 3-6. Determination of the amount of salt in a polymer electrolyte by numerical integration.

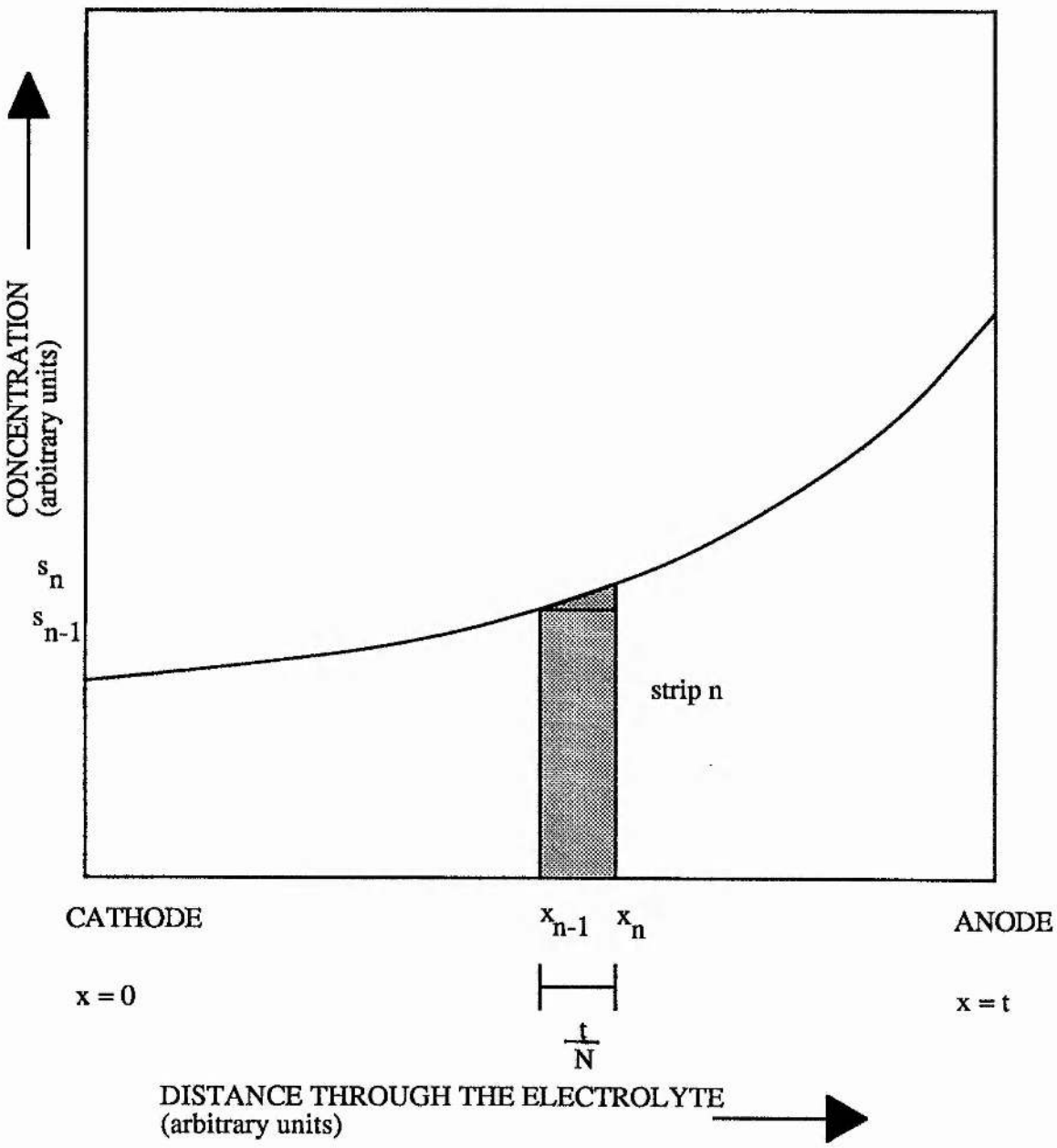

CHAPTER 4

EXPERIMENTAL PROCEDURES, EQUIPMENT, AND INSTRUMENTATION

This chapter details the treatment given to the chemicals used in this study and the experimental procedures adopted in the production of polymer electrolytes. A section about equipment and instrumentation, and the experimental techniques employed in the project is included.

Experiments on PEs were carried out in an argon-filled Faircrest drybox fitted with two copper catalyst columns (to remove oxygen) and two molecular seive columns (to remove water). The argon supply was greater than 99.998% pure (with $H_20 < 3$ ppm, $O_2 < 3$ ppm, $N_2 < 8$ ppm and hydrocarbons < 1 ppm), and the operating argon atmosphere was believed to be less than 10 ppm in water [78].

4.1 CHEMICAL SAMPLES

Lithium perchlorate (Aldrich Chemical Company Ltd.). This was dried by melting *in vacuo* at 300°C for 8 hours, and then ground in a mortar and pestle and stored in an argon-filled drybox. Prior to use it was re-ground.

Lithium triflate (3M Ltd.). This was dried by heating to 120°C for 24 hours and then stored in an argon-filled drybox. As a powder it received no further treatment prior to use.

Sodium tetraphenylborate (Aldrich Chemical Company Ltd.). This was dried by heating *in vacuo* at 80°C for 24 hours, after which it was transferred to an argon-filled drybox.

Poly(ethyleneoxide) (BDH Ltd., av. mol. wt. 4×10^6). This was dried by standing *in vacuo* over P_2O_5 for at least several weeks before being transferred to an argon-filled drybox in bulk, as required. This treatment has been shown to produce as dry a polymer as is possible [79].

Lithium (Alfa Metals). The metal foil (19 mm wide, 0.75 mm thick) was stored under paraffin in an argon-filled drybox. Prior to use the paraffin was removed and the lithium refreshed by scraping away its dull surface to reveal the fresh shiny metal underneath.

Sodium (Aldrich Chemical Company Ltd.). This was stored under paraffin in the form of spheres, 3-6 mm in diameter, in an argon-filled drybox. Prior to use the paraffin was removed and the surface refreshed by scraping its dull surface to reveal the shiny metal underneath.

Lead (Fisons Ltd.). The metal foil (0.15 mm thick) was used as received, and cut to size when required.

Sulphuric acid (Aristar Grade, BDH Chemicals Ltd.) and *perchloric acid* (Analar Grade, BDH Chemicals Ltd.), were used as received; they contained no lithium as impurity, and in total had less than 12 ppm of impurities.

4.2 SAMPLE PREPARATION

4.2.1 Production of Polymer Electrolytes by Grinding.

Polymer electrolyte samples were produced by a grinding/hot-pressing technique developed in these laboratories [80][81]. This procedure allowed the easy production of relatively thick electrolyte films—something which would be difficult to achieve by the more widespread method of solvent-casting. However, the grinding procedure did not produce uniform electrolytes of very large oxygen:metal ratios (> 100:1).

In the grinding process about 5 grams of material (either PEO or ground-PEO/salt mixture of known composition) were sealed by a rubber bung in a steel test-tube containing ≈ 50 steel ball-bearings of typical diameter 5 mm, under argon, and

shaken at liquid nitrogen temperatures for 10-20 minutes to thoroughly mix (and grind) the components. The bung was tied down to prevent its expulsion on warming to room temperature.

The low temperature resulted in the sample becoming brittle, and it fractured easily under the impact of the ball-bearings. After grinding, the tube was allowed to rise to room temperature, and it was returned to the drybox after the removal of water which had condensed on the outside of the tube, and the electrolyte was removed and stored. Electrolytes of O:M ratios of up to 100:1 were produced in this way. The grinding apparatus is shown in Figure 4-1.

4.2.2 Hot-Pressing of Polymer Electrolyte Discs.

To produce an electrolyte disc of 13 mm diameter, the required amount of PE for the desired disc thickness (≈ 0.05 g for an ≈ 300 μm thick film) was first of all pressed in a Specac die of 5 mm inner diameter, to 2 tonnes at room temperature for several seconds. This produced a manageable pill several millimetres thick which was used to produce a uniform 13 mm diameter disc on further treatment. The resultant 5 mm pill was centred in the 13 mm diameter die and pressed to 5 tonnes at room temperature for several seconds—the simple pressing of electrolyte powder in the 13 mm die was reported not to produce uniform PE discs [78], because the electrolyte was not evenly distributed in the die. The die was then enclosed in an aluminium jacket and heated rapidly by an electrical hotplate under no applied pressure to 120°C, at which temperature it was held for 3 hours. The aluminium jacket fitted closely around both the 5 mm and 13 mm dies, which had the same outer diameter and shared the same baseplate, and the jacket sat tightly on the hot-plate. The hot-plate itself fitted into the Specac press. After this heating the die was allowed to cool at its own rate to room temperature, a process usually performed overnight. When the sample had cooled to 70°C it was pressed to 1—2 tonnes, and then allowed to cool under this force.

The annealling and subsequent pressing produced a uniform (usually translucent; or almost transparent in the case of lithium perchlorate electrolytes) disc of

electrolyte 13 mm in diameter with the desired thickness, which was then assembled in a two-electrode cell.

To produce 20 mm diameter discs (for use in Hittorf cells) the procedure was almost unchanged. The required amount of electrolyte (≈ 0.42 g for 8:1 discs 1.0 mm thick) was placed in the 13 mm die and pressed to 5 tonnes at room temperature for several seconds, and the resulting pill centred in the 20 mm die, which was then pressed to 5 tonnes at room temperature for several seconds. At this stage the electrolyte did not fill the space between the anvils. Due to the large bulk of the 20 mm die it was heated to about 120°C for a short time (≈ 10 minutes) and then allowed to cool to room temperature, with 2 tonnes being applied at 70°C. The large size of the 20 mm die made accurate temperature control impractical, as the 20 mm die could not fit in the press on the hot-plate. This treatment produced uniform discs 20 mm in diameter, which were translucent to opaque (being 3-4 times as thick as the usual 13 mm diameter discs).

The dimensions of hot-pressed discs used in this study are greater than those easily and typically produced by solvent casting (50-100 μm). The hot-pressing arrangements are shown in Figure 4-2.

4.3 TWO-ELECTRODE CELLS

In this project PEs were most commonly studied *via* the use of non-blocking two-electrode cells. These were used for the frequency response analysis and the dc polarisation of electrolytes. In ac operation for frequency response analysis, real and imaginary impedances in the cell can be determined, as shown in §4.4. In dc operation the potential difference between the electrodes and the current flowing between them can be measured. The two techniques (ac and dc) together provided a useful means of studying polymer electrolytes.

Blocking electrodes are used in two-electrode cells for the determination of electrolyte conductivities and their variation with temperature. No chemical or

electrochemical reactions occur at the electrodes at the potential differences commonly employed in their operation. Metals such as platinum or stainless steel are taken to be suitable for use as blocking electrodes, but the nature of the electrolyte must be taken into account—stainless steel electrodes, for example, are unsuitable for use with copper triflate-based electrolytes [35]. Non-blocking electrodes (*e.g.* lithium for lithium-based electrolytes, sodium for sodium-based electrolytes *etc.*) were used throughout this study because they provide a means of determining the electrolyte conductivity as before, but may also be used to pass current through the electrolyte.

Two distinct types of two-electrode cell were used in this study; a cell for the polarisation of an electrolyte to a steady-state current (of which constant pressure and constant volume types were built), and a cell for non-steady-state polarisations (a Hittorf Cell). These cells are described below.

4.3.1 Constant Pressure Cell.

This cell is shown in Figure 4-3. With this arrangement pressure is applied to the electrodes *via* the two teflon halves of the cell, which are in turn kept under pressure by the screw and bayonet lock. The pressure is applied to ensure a good contact between the electrodes and the electrolyte. The pressure continually acting on the cell resulted in several disadvantages when using it; notably that the cell constant varied with time and depended on the initial electrolyte disc thickness, and the cell could not be cycled with temperature.

The electrolytes used in this study softened at elevated temperatures, and they deformed easily under applied pressure. Thus, in the constant pressure cell, the electrolyte was forced from between the electrodes at elevated temperatures. The applied pressure reduced the electrode separation, and therefore the cell constant, in an unknown manner as time went by, preventing conductivities from being determined from measured conductances. In extreme cases this electrolyte extrusion allowed the electrodes to touch, short-circuiting the cell (because the equilibrium arrangement of the cell—*i.e.* when the two teflon halves were in contact—was such that the two lithium

electrodes would be in contact).

The inability of the cell to be cycled with temperature was due to this electrolyte extrusion and possible thermal expansion of the electrolyte. It was thought that as the cell cooled from operation at high temperatures the electrolyte would contract, tending to pull itself away from the electrodes, diminishing the good contact. The fact that much electrolyte had been extruded anyway at high temperatures meant that the final electrode gap was relatively small, making the re-entry of electrolyte into the gap as the cell cooled difficult. Thus a cell could not be used at high temperatures, cooled, and then used again at high temperature.

All of these problems were solved by producing a constant volume cell. A constant volume cell whose electrode separation varied by only 0.2% with temperature was devised by Armstrong and Clarke [31], though the one described below is not as sophisticated as that described in the reference and the temperature variation in its electrode separation was not determined.

4.3.2 Constant Volume Cell.

This cell is shown in Figure 4-4. It was constructed from a machinable ceramic (Macor, Corning Inc.), because it was found that the lithium electrodes reacted with the teflon in the constant pressure cell. To operate effectively, an electrolyte disc of slightly greater thickness than the electrode separation of the empty cell ($\approx$ 0.26 mm in the cell commonly used) was prepared and assembled in the cell. The screw and bayonet lock applied pressure to the two halves of the cell and thence to the electrodes, as in the constant pressure cell. At high temperatures, if the electrolyte disc were thicker than the electrode separation, the pressure on the electrodes would cause the electrolyte to extrude until the two halves of the cell touched, at which time no more pressure would be acting on the electrodes. This produced a cell whose electrode separation—therefore whose cell constant—was indeed constant *. The fact that the electrode separation was

* The cell constant was invariant at a given temperature. It was not possible to determine the change in cell constant with temperature, so it was assumed that the cell

constant was verified by observing the electrolyte resistance over time using FRA, as shown in the impedance diagrams in Figure 4-5 and Figure 4-6 by the constant high-frequency intercepts. Impedance diagrams are described in §4.4.

Figure 4-5 incidentally shows the growth of the resistive surface layers with time more clearly than with the use of a constant pressure cell [82] because of the constant electrolyte resistance at the high-frequency intercept on the real axis. The fixed and known cell constant meant that the resistances found from the FRA could be used to determine electrolyte conductivities.

4.3.2.1 Temperature Cycling of the Constant Volume Cell.

The ability of the cell to be cycled in temperature was investigated. Because the electrode separation is constant and relatively large, compared to the constant pressure cell, it was hoped that any electrolyte extruded by thermal expansion would be able to contract and re-enter the electrode gap before the electrolyte pulled itself away from the electrodes. The conductance of the electrolyte with temperature is displayed in Figure 4-7 for three temperature sweeps; from 70°C to 140°C and back, and then to 140°C again. The sharp rise in conductance at the end of the first sweep is due to extrusion of the excess electrolyte, because the cell had not been left for a sufficient time at each of the temperatures on the first sweep for extrusion to ocour—the cell was simply allowed to achieve thermal equilibrium before a resistance measurement and then the temperature was increased. At the end of the first sweep the cell was left for a time, and electrolyte extrusion was allowed to occur. Extrusion is likely to be more rapid at elevated temperatures, because the electrolyte is softer at higher temperatures. There was no apparent difference between the following sweeps, showing that the cell was cyclable with temperature at least between 70°C and 140°C (the temperature range over which most lithium perchlorate and lithium triflate electrolytes are amorphous). Subsequently it was found that cooling the cell to room temperature had no adverse

---

constant was equal to that of the empty cell at room temperature.

effect on the cell when it was raised in temperature again, showing that any extruded electrolyte had re-entered the cell on cooling and contraction.

4.3.2.2 The Use of Sodium as an Electrode Material.

When sodium electrolytes were examined the electrodes were produced by tamping an oil-free sodium sphere into the space normally occupied by the lithium until a uniform circular surface of sodium was produced, flush with the macor surface. Small amounts of sodium had to be removed if the sphere was too large. Once the sodium was in place its surface was refreshed by light scraping with a spatula, and the electrolyte disc was placed on top, and the other macor cell half brought down to form a tight fit. In this case, because the electrodes were flush with the surface of the cell, a thicker electrolyte disc (≈ 400 μm thick) was required (because the lithium electrodes were not flush with the surface). In spite of the method of production of the electrodes satisfactory cells were assembled, as shown by the good semicircle in the impedance diagram of a $PEO_{100}NaBPh_4$ cell shown in Figure 4-8.

4.3.3 Hittorf Cell.

This two-electrode cell is shown in Figure 4-9a. It was constructed from Macor ceramic, and was difficult to produce because of the thin slots in the upper section, which tended to make this section fragile. These vertical slots allowed the easy segmentation by razor blade of the electrolyte slab into four pieces at the end of a polarisation, to prevent any concentration differences from dispersing. The steel contacts were held in contact with the electrodes under slight pressure, to ensure good steel-electrode and electrode-electrolyte contacts. No apparent electrolyte extrusion under this pressure was observed when the cell was dismantled, because the interior of the cell held the slab in shape, and extrusion through the vertical slits was disfavoured by the slit thinness.

The cell is much smaller than conventional Hittorf cells for the study of liquid electrolytes, which may be tens of centimetres in length (one is illustrated in §6.1).

There are several reasons for this:

(i) mass transport in a PE is very slow, so it will take a long time for concentration changes to travel the few millimetres between compartment boundaries, and

(ii) the analytical technique chosen to examine these concentration changes only required the presence of a small amount of lithium.

The slab of electrolyte was produced from a 20 mm diameter disc of electrolyte (whose preparation was described above) by means of a 12 x 16 mm rectangular steel template which was held on the disc, allowing its outline to be scored onto the sample by means of a scalpel. The edges were then trimmed to produce a slab of the required dimensions.

The electrode arrangement in this cell prevented useful FRA from being carried out, and the electrolyte resistance was determined from the initial current established when the cell was polarised with a small potential difference between two lithium electrodes. Resistances of $\approx 10\ k\Omega$ at 120°C may be attributed to the electrolyte alone, because the electrodes, each of area 9 mm^2, would possess an interfacial resistance of less than 10 Ω.

Often a lead metal cathode was used in the cell, so that the amount of lithium deposited on the electrode during the passage of current could be determined by analysis, in order to verify that the current at the cathode was indeed due to a lithium ion flux, as opposed to an electronic current or proton current produced by the breakdown of the polymer at the electrode-electrolyte interface. The lead cathode was prepared by folding a piece of lead foil around the steel contact, as shown in Figure 4-9b.

4.4 FREQUENCY RESPONSE ANALYSER AND ELECTROCHEMICAL INTERFACE: THE AC ANALYSIS OF POLYMER ELECTROLYTE CELLS

The ac analysis and dc polarisation of PE cells were carried out using a combined FRA-ECI setup under microcomputer control using commercial (Schlumberger) and in-house [83] software. The FRA was a Schlumberger 1250 or 1255, and the ECI was a Schlumberger 1286. The use of ac methods in the study of PE cells is outlined below.

4.4.1 The Use of AC Impedance Spectroscopy in the Study of Polymer Electrolyte Cells.

AC impedance studies are a very practical means of examining the conductivities of PEs. A PE cell may be treated as a combination of simple electronic components (capacitors, resistors *etc.*), and the response of the cell to an ac potential difference of varying frequency provides details of the real and imaginary impedances which are properties of the cell. The use of ac impedance spectroscopy for the examination of solid electrolytes has been reviewed elsewhere (see, for example, [84] [85] or Bruce in reference [3]) and a basic exposition of the technique is given below.

4.4.1.1 A Polymer Electrolyte Between Two Blocking Electrodes.

An electrolyte between two blocking electrodes will possess an electrolyte resistance, and a geometrical capacitance due to the electrodes. Because the impedance due to the capacitor is frequency-dependent, it varies as the frequency of the applied potential difference is swept, and the variation in real and imaginary impedances may be determined using suitable instrumentation. If this is done for a blocking system, a plot of imaginary *vs* real impedance will look like that shown in Figure 4-10.

The intercepts on the real impedance axis are at zero and the electrolyte resistance, R; and the maximum of the semicircle is dependent on the geometrical capacitance, such that the following equation holds:

$$\omega_{max} = \frac{1}{RC} \qquad 4\text{-}1$$

This type of response may be modelled by a resistor and capacitor in parallel. It is this electrolyte resistance that determines the initial current that would flow if the electrodes were non-blocking. Because the electrodes are blocking, a vertical spike appears at low frequencies—the lower the frequency gets the more dc character the potential difference displays, but no current flows because the electrodes are blocking. A double-layer capacitance is formed, with ions of one charge being adjacent to an electrode bearing the opposite charge. The capacitance acts in series with the parallel RC element described above. In real cells the spike tends to fall towards the real axis as a result of electrode roughness. The circuit representation of the cell would thus look like that shown in Figure 4-11.

4.4.1.2 A Polymer Electrolyte Between Two Non-Blocking Electrodes.

If non-blocking electrodes are used, a current may be maintained at low frequencies of applied potential difference (the ac potential difference effectively becomes dc) such that the dc resistance is greater than the ac resistance found from the semicircle, as above. The type of impedance plot found for such an example is shown in Figure 4-12.

A semicircle appears as before due to the electrolyte, but rather than a spike appearing at low frequencies, a line at 45° to the real axis is found, curving down to the real axis at the dc limit of the resistance is found. This is referred to as a Warburg impedance, and it arises from the diffusion of electroactive species within the electrolyte (or within the electrode, if it is an intercalation electrode, say). This feature is generally observable at very low frequencies (of the order of mHz) [71].

Real PE cells tend to display a second semicircle in an impedance diagram attributed to a resistive layer formed by passivation of the metal electrode in contact with the PE [84], as is depicted in Figure 4-13. This is particularly apparent in the impedance spectra of lithium cells, where the typical frequency range of the applied potential difference (65 kHz—1 Hz) does not permit the observation of the electrolyte

semicircle or the diffusion arc, as shown in Figure 4-14 for a real cell*. In cases such as this the first intercept is taken to be the electrolyte resistance, with the difference between the two intercepts being the interface resistance.

4.4.1.3 A Polymer Electrolyte Between Two Non-Blocking Electrodes—Experimental Observations.

The impedance diagrams usually observed for real electrolytes tended to display a single semicircle, attributed to the electrolyte/electrode interface, because of the limited frequency range of operation. This semicircle would increase with time until a steady-state value was reached, as shown in Figure 4-5. After a dc polarisation at relatively large potential differences this interface resistance would decrease, suggesting that a resistive layer on the electrode had been broken down. The semicircles observed tend to be flattened, with a centre below the real axis. The determination of intercepts was performed by simple extrapolation using a pair of compasses and a printout of the semicircle, or (more frequently) by using computer fitting programs to obtain the best semicircle [86].

For some dilute electrolytes (*e.g.* 50:1, 100:1 PEO-$LiClO_4$) a semicircle was initially observed, but after several polarisations the impedance plot continued below the imaginary axis to form another loop, as is shown in Figures 4-15 and 4-16. This was a particular problem for $PEO_{50}LiClO_4$, as is detailed in Chapter 5. It is not known why this occurred, but it did not occur in the majority of electrolytes, and only in the dilute systems.

---

* It may be shown using equation (4-1) that the maximum of the semicircle for an electrolyte of resistance 100 Ω between electrodes of area 1 cm^2 and separation 0.25 mm occurs at a frequency of tens of megahertz.

4.4.1.4 *Experimental Parameters for the ac Examination of Polymer Electrolytes.*

The ac analysis of PE cells was carried out using a potential difference of amplitude 5 mV r.m.s.. The frequency was decreased logarithmically from 65 kHz to 1 Hz, with either the number of points *per* decade or the total number of points being specified. An integration time of 200 cycles or 5 s *per* point was used, depending on the software controlling the experiment.

Real and imaginary impedances were determined by the FRA and stored, together with the frequencies, on floppy discs. This allowed the examination of the data using a commercial fitting program.

4.5 THE DETERMINATION OF THE LITHIUM CONTENT OF POLYMER ELECTROLYTES USING ATOMIC ABSORPTION SPECTROMETRY

Lithium atomic absorption spectrometry (Li-AAS) was thought to be an accurate and straightforward method of determining the lithium content of a PE; in particular of PEs from their Hittorf analysis. The technique has been used for determining the lithium content of plasma-polymerised PEs [87], though in this case the polymer did not enter solution (an occurrence whose importance is discussed later) and the salt was simply leached out of the thin PE film (≈1 μm thick) by water, to produce an aqueous lithium perchlorate solution which was introduced to the AA spectrometer [88].

The AA spectrometer used in this study was a Pye Unicam PU9000 AAS using an air/acetylene mixture, with a gas flow rate of 0.8 l min^{-1}, operating at wavelength 670.8 nm with a bandwidth of 0.5 nm. The concentration of lithium required for the analysis (0–5 ppm w/v) is of the order of 10 mg of PEO_8LiClO_4 in 100 cm^3 of water, and is a sixth of the amount of material in one of the electrolyte segments from the Hittorf Cell. The fact that an electrolyte compartment could be divided into several pieces would allow the uniformity of any concentration changes to be assessed along the electrode-electrolyte interfaces. The lithium concentration would generally be less

than 2 ppm, and reference solutions of 0.50, 1.00, and 2.00 ppm were required for calibrating the AA-spectrometer. These were prepared by the dilution of 1000 ppm Li solution (Aldrich Chemical Company Ltd.). Samples of PE were weighed on a 7-figure analytical balance (Sartorius Microbalance) to an accuracy of greater than 99.99% (± 0.001 mg).

The lithium was initially introduced to the AA-spectrometer as an aqueous solution of the PE: the PE was completely soluble in water, and the concentration of the resultant solution was sufficiently low that there was no apparent difference between the physical properties of the solution and the water; there was no obvious increase in viscosity, and no threads of polymer solution formed when the solution was poured (providing that samples of the size of a Hittorf cell compartment (1x4x12 mm) were used). After problems were encountered with the analysis (see §4.5.1), the PEO was destroyed by acid treatment (see §4.5.2), and the acidic solution diluted with water and introduced to the spectrometer as before.

The accuracy of the Li-AAS was ± 0.01 ppm, and a difference in concentration between electrode and middle compartments of the order of 10% was expected*, being of the order of 0.10 ppm. It was thought that such a difference would be distinguishable from a background variation of the order of 0.01 ppm.

4.5.1 The Effect of PEO on Lithium Atomic Absorption Spectrometry

The initial results of Li-AAS suggested that ≈ 10 ppm lithium solutions (known from the PE composition) were actually ≈ 0.4 ppm in lithium, with hardly any colouration of the AAS flame occurring when the solution was introduced. This suggested that the presence of the polymer was somehow suppressing the registration of the lithium. In order to examine this a series of aqueous solutions of PEs of

---

* Each Hittorf compartment is ≈ 60 mg, 130 μmol of which is lithium. A current of 50 μA flowing for 10 hours corresponds to a charge of 1.8 C, or 19 μmol of electrons. If all of the current is carried by the anions this is the change in the number of moles of lithium which will occur, which is of the order of 10%.

composition PEO_xLiClO_4 (x = 8, 18, and 50) were prepared such that they were each ≈ 10 ppm in lithium. Separate solutions of roughly the same composition were prepared by dissolving PEO and $LiClO_4$ together in distilled water, to determine if the PE production procedure gave rise to the detection problem. Finally, two solutions of ≈ 8:1 composition were prepared: one being PEO and $LiClO_4$ acidified with 10 cm^3 of 5 M H_2SO_4 with a total volume of 100 cm^3, in an attempt to depolymerise the polymer; and the other being $LiClO_4$ and $CH_3O(CH_2CH_2O)_4CH_3$, in an attempt to model a depolymerised electrolyte.

Analysis of these solutions (whose results are in Table 4-A) confirmed that the presence of PEO suppressed the detection of lithium, with the higher PEO-concentration solutions producing a lower response. There was no significant difference between the electrolyte solutions and the mixed solutions, suggesting that the procedure for producing the electrolyte did not account for the signal suppression. The acidified sample, which had been stirred at room temperature overnight, gave a proportionately greater response than the other 8:1 samples; but at an apparent lithium concentration of 0.85 ppm rather than 10.26 ppm there was no significant resolution of the problem. The solution prepared using the tetramer gave a strong response, being out of the calibration range of the spectrometer (5 ppm), but the colour of the flame (bright crimson) suggested that little, if any, suppression of the lithium signal took place.

The problem with the lithium detection was an initially surprising occurrence, because the actual PEO concentration was only ≈ 10 mM, and in an aqueous solution little salt-polymer interaction was anticipated. Such interferences in AAS may arise from physical or chemical processes, and they are briefly described below.

4.5.1.1 Physical Interferences in Atomic Absorption Spectrometry.

Physical interferences may arise due to the viscosity of the sample solutions; if the solution is too viscous the nebulisation efficiency of the spectrometer is affected, and this influences the number of free atoms in the flame. The 8:1 samples did not

seem unduly viscous, so this is not likely to be the source of the twenty-fold reduction in the detected lithium level. Solutions of 50:1 electrolyte were noticeably more viscous than those of the 8:1 electrolyte, which may account for the greater reduction in the lithium detection for solutions of higher PEO content. The use of an electrothermal atomiser, in which atoms from the sample are produced in a furnace rather than from aspiration into a flame, circumvents this problem, and this method (which is more sensitive) has been used to detect copper, iron, and chromium in PEO [89]. Metals which were added to the polymer were recovered at an efficiency of greater than 95% using this technique. The method of standard addition [90] may have circumvented this problem, but it would have been time-consuming, and a sample signal of the order of 0.40 ppm would probably not have permitted the accurate differentiation of electrode compartment and reference compartment results.

4.5.1.2 Chemical Interferences in Atomic Absorption Spectrometry.

Chemical interference may arise from processes occurring in the sample solution or the flame, such as the formation of thermally stable oxides, carbides, or nitrides. Any ionisation of the metal atoms in the flame will reduce the number of atoms available for excitation, and this may be circumvented by adding to the solution elements which are more ionisable (*e.g.* potassium). Interactions with cations or anions from the matrix may occur, enhancing or suppressing the absorption of metals in the flame, depending if the associated species produced are easy or hard to dissociate in the flame: it is reported [91] that glucose present at a concentration of $< 10^{-6}$ M causes a marked decrease in the absorption of calcium present at a concentration of 10^{-4} M. In this case small amounts of glucose may complex or form compounds with the calcium salt present, suppressing the calcium absorption. It is also known [92] that surfactants with 8–40 ethoxy units form ion-association complexes with cations (in this case zinc), and interfere with their detection. It is, therefore likely that chemical interference between PEO (or fragments from the decomposition of PEO in the flame) and the lithium was the source of the signal supression. An experiment which may

confirm this would be the introduction into the spectrometer of an aqueous solution of lithium perchlorate in the presence of a lithium-specific crown ether. Suppression of this signal would support the idea that chemical interactions between PEO fragments and lithium atoms occurred.

4.5.2 Quantitative Lithium Analysis Using Atomic Absorption Spectrometry

A severe method was adopted to destroy the PEO present in samples, with a view to allowing the lithium to be detected quantitatively. Initially, 3 mg samples of PEO_8LiClO_4 were heated electrically in Kjeldahl flasks with 3 cm^3 concentrated (98%) sulphuric acid and 0.5 cm^3 of concentrated (70%) perchloric acid behind a blast screen, or with the sulphuric acid alone, in an attempt to destroy the PEO. The PE, in the form of very thin 5 mm diameter discs prepared by pressing stock PE in a Specac press under hand force at room temperature, quickly dissolved, and the clear colourless liquid turned yellow then colourless in the mixed acid samples; or yellow then brown in the neat sulphuric acid samples.

The brown colouration was probably due to carbon from the polymer being deposited in the solution—samples of PEO of mass ≈ 10 mg undergoing the sulphuric acid treatment produced a flocculent brown deposit when diluted with distilled water and left to stand. The PE samples, being of a lower PEO content, remained brown and did not produce a precipitate on dilution and standing. The presence of the perchloric acid would seem to promote oxidation of the PEO to water and carbon dioxide (some bubbling was just visible in some samples). The heating was carried out at ≈ 100°C (samples of water rather than acid attained this temperature under the same heating régime, and it was assumed that the experimental samples did also; although the decomposition would be exothermic, the temperature would not be greatly increased over the timescale of the heating), under the control of a Variac, for two hours. After this time the solutions were allowed to cool, and then made up to 25 cm^3 with distilled water and submitted for AAS.

It was found that these samples (< 2 ppm Li) gave a much better analysis than in the previous cases (see Table 4-B), but were still in error by ≈ –30%. It was suggested that this may have been due to errors in the washing of the flasks (only ≈ 20 cm^3 of water to wash each flask) or to the standards not being as acidic as the samples, mineral acids being a possible source of interference in the AAS [90]. The fact that a PEO sample was apparently 0.08 ppm in lithium (distilled water being < 0.02 ppm) suggested that inappropriate standards were used.

When acidified standards were used, the apparent lithium content of the PE samples increased and that of the PEO sample decreased, as shown in Table 4-B, but a discrepancy between the actual and apparent lithium concentrations remained. In order to reduce any contribution from washing errors the volume of the final solution was increased to 100 cm^3, which allowed more water to be used for rinsing the flasks, and diluted the acids present (the 25 cm^3 solutions were exhibiting the presence of sodium in the AAS flame after they had been standing for a time; presumably leached from the glass flask in the presence of the perchloric and sulphuric acids). The larger final volume of solution allowed larger samples to be used for the same lithium concentration range (0 – 2 ppm).

A repeat experiment, using ≈ 6 mg samples of PE made up to 100 cm^3 with distilled water, with acidified standards produced measurements of lithium concentration which agreed closely with the expected values, as shown in Table 4-C. The samples denoted 8:1 PE (Li) were taken from the electrode segments of a failed cell through which negligible current had been passed, and they had been in contact with the lithium electrodes. These samples were taken to determine if any lithium contamination of the electrolyte segments from the electrodes took place. No lithium contamination was apparent.

The results of these analyses led to the belief that a Hittorf experiment could be undertaken with some hope of success, in that a lithium concentration difference as low as ≈ 0.02 ppm should be detectable using this technique, especially when several measurements from each compartment were taken.

In subsequent experiments this direct reproduction of the known lithium content by the AA spectrometer did not occur, requiring the production of a calibration graph to relate the experimentally determined lithium concentrations to known lithium concentrations. As well as using the data from the reference compartments, electrolyte was taken from the remains of the disc from which the electrolyte slab was taken; this allowed samples of a wide weight range to be taken, producing a wider range of lithium content data and consequently a more reliable fit between the indicated and known lithium contents. A fresh calibration graph was needed for each experiment, and on occasion the calibration chart was curved rather than linear. The reasons why this was so and why only one exact set of data were obtained are not known, and have not been investigated further, because the calibration graphs proved to be a satisfactory solution to the discrepancy.

Another problem with using Li-AAS to determine the lithium content of the PE was that of the solutions spoiling with time. This was apparent when one set of solutions was left in darkness for one month and re-submitted for analysis. Figure 4-17 shows both data sets—the initial linear set which was used for calibration, and the same solutions one month later. It is seen that the latter set consists of random scatter, demonstrating that the solutions should be tested immediately after their preparation. It is believed that this spoiling was responsible for one poor set of data obtained from a Hittorf experiment (see Chapter 6). Given that sodium was being leached from the glass it is possible that some reaction with the wall of the flask was responsible for the spoiling. This problem might be alleviated by the use of non-vitreous flasks.

4.5.3 Final Experimental Technique for Determining the Lithium Content of Polymer Electrolytes

The compartments from the Hittorf cell were cut into 6 pieces, with a range of masses deliberately chosen in order to provide a good spread of data points from the analysis. These pieces were then heated in the mixture of perchloric and sulphuric acids and diluted to 100 cm^3 with distilled water. Pieces of unpolarised electrolyte

were sometimes used and treated in the same way to provide more data points for calibration purposes.

The lead cathode underwent the same acid treatment, producing a fine, slightly pink precipitate (assumed to be predominantly lead sulphate). After dilution the lead cathode sample was decanted to prevent solids entering the AAS.

Within two days of the preparation the solutions were analysed using the AAS, with two readings taken from each solution. These readings agreed to within ± 0.02 ppm, and usually to within ± 0.01 ppm. The reading error was taken to be 0.02 ppm to ensure that all of the data points were contained in the error bound. Results from both middle compartments were compared, to verify that they were of the same composition, and that they were of the same composition as the unpolarised electrolyte. These data were used to prepare a calibration graph for relating the indicated lithium contents of the anode and cathode compartments (and of the lead cathode) to their actual lithium contents. The calibration graphs of actual Hittorf experiments are given in Chapter 6.

Figure 4-1. Schematic diagram of grinding apparatus for the preparation of polymer electrolytes.

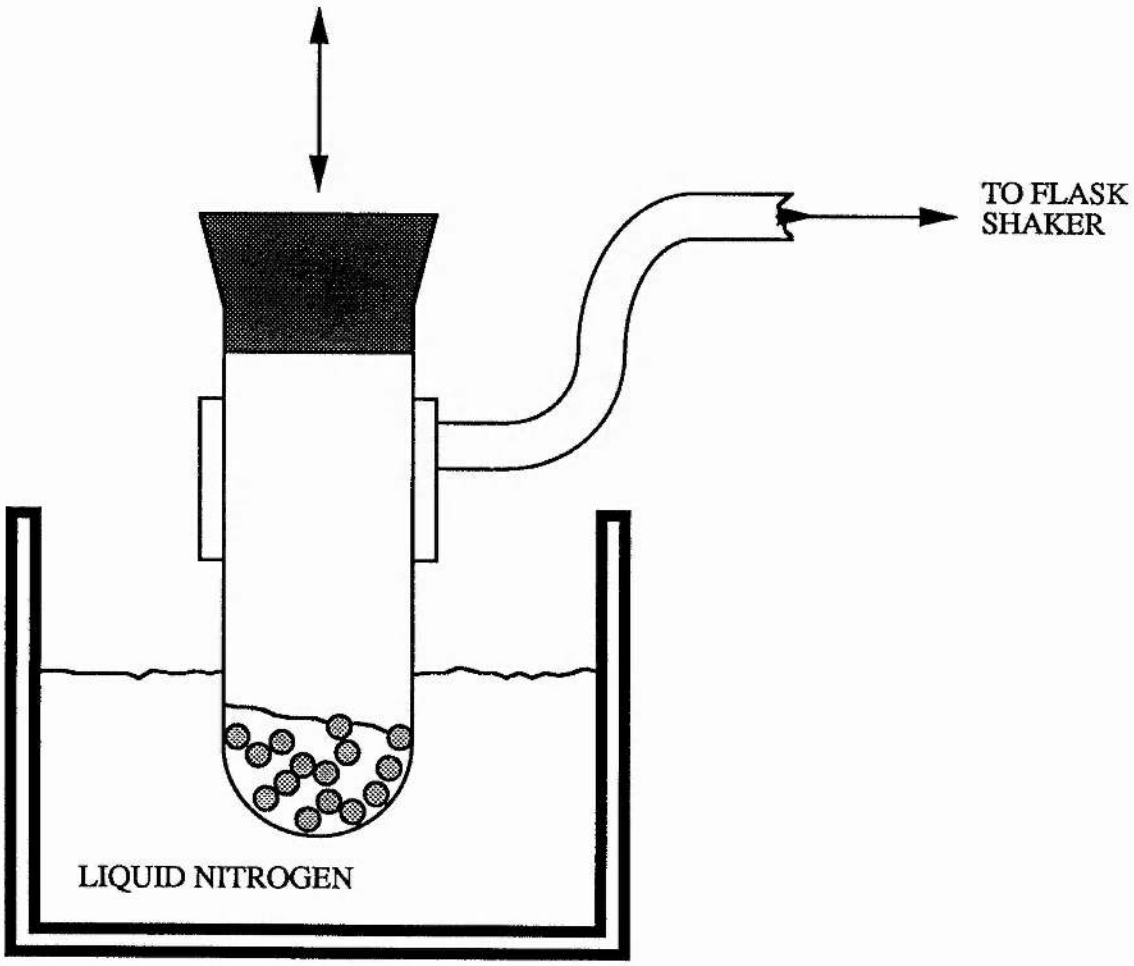

Figure 4-2. Hot-pressing arrangements for the production of polymer electrolyte discs.

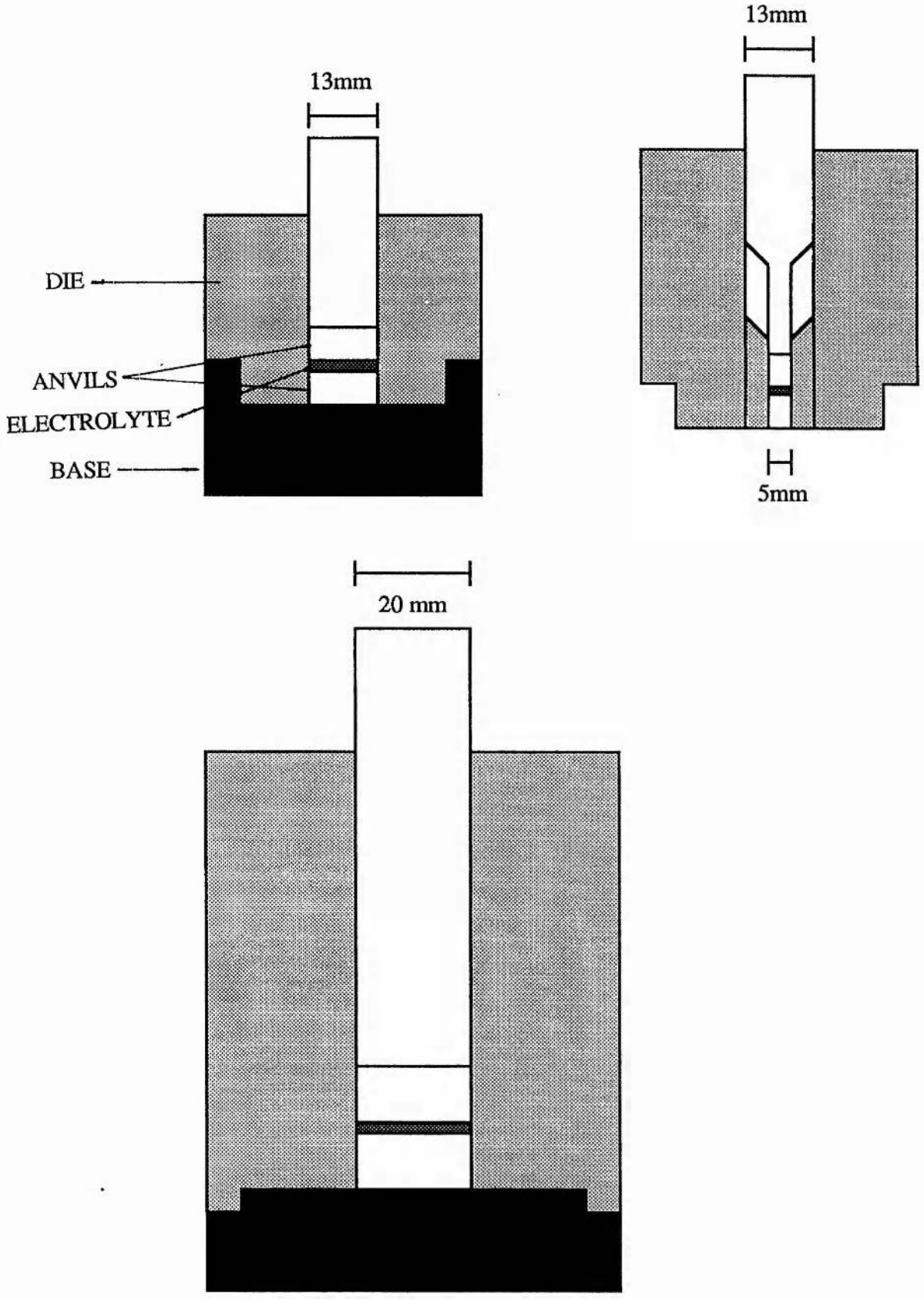

Figure 4-3. Constant pressure cell for the ac and dc analysis of polymer electrolytes.

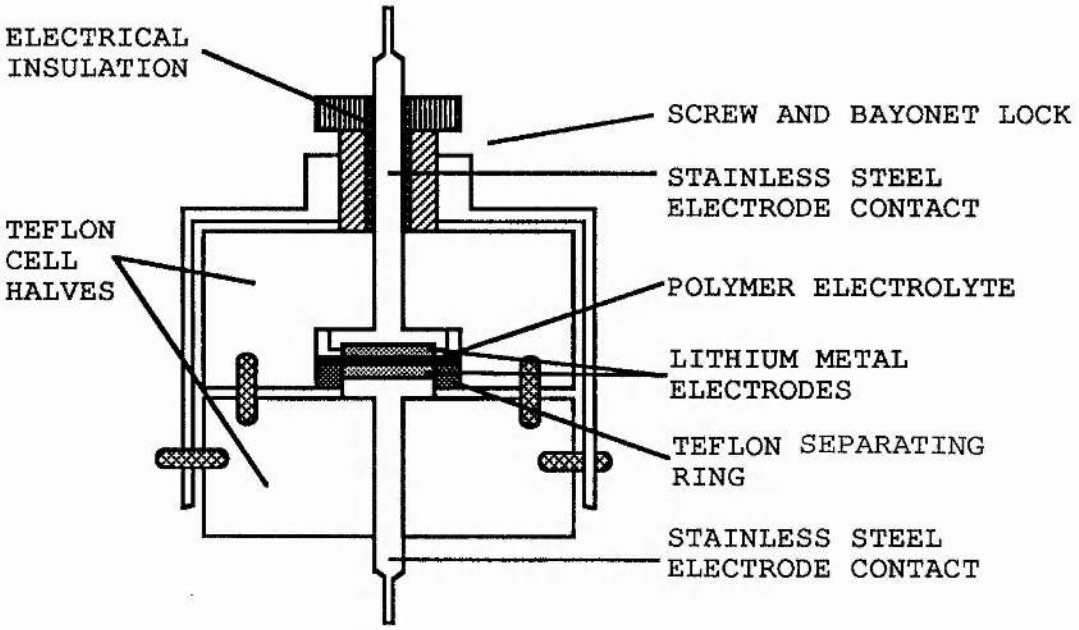

Figure 4-4. Constant volume cell for the ac and dc analysis of polymer electrolytes.

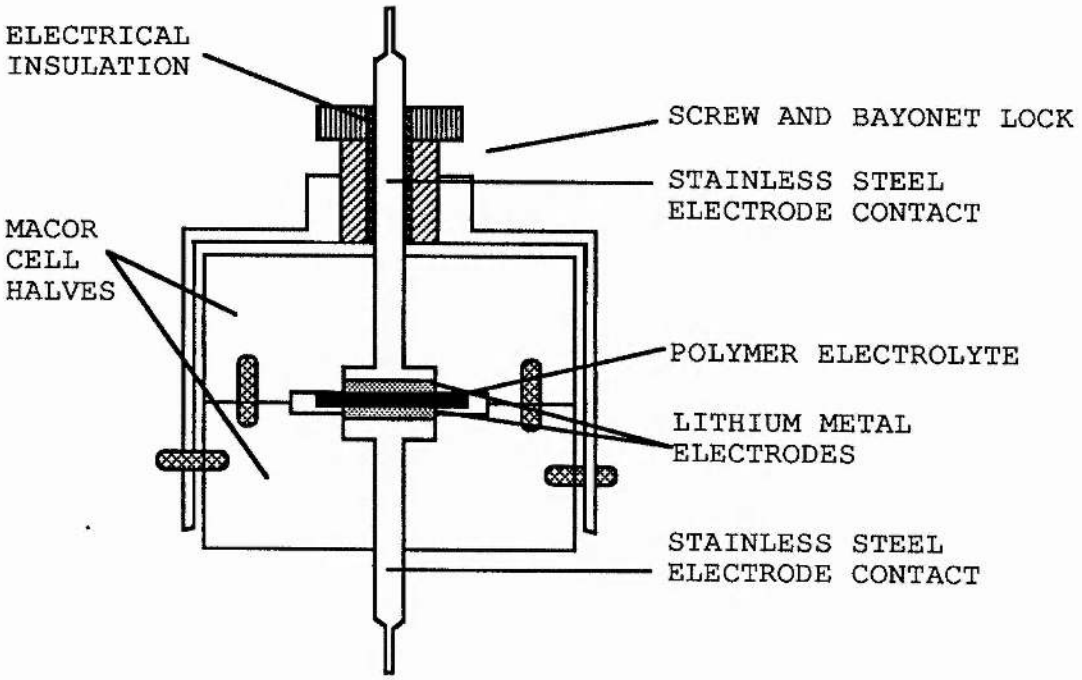

Figure 4-5. The growth with time of the interface resistance of an Li|PEO$_8$LiClO$_4$|Li cell at 95°C. Plots are taken at a time t, t + 30 mins, t + 2.5 hrs, t + 4 hrs, t + 5 hrs, and t + 22 hrs.

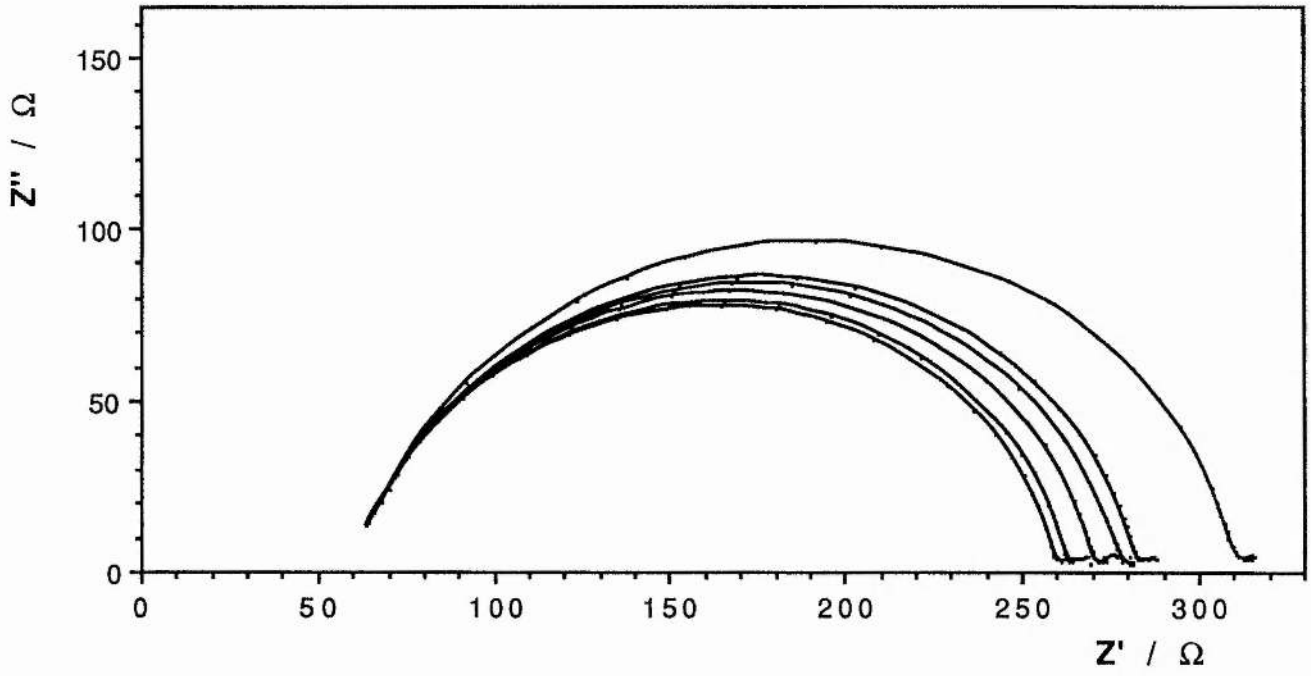

Figure 4-6. Impedance at 65 kHz of an Li|PEO$_8$LiClO$_4$|Li cell at 127.5°C, showing the small spread of impedances over time. Point A is a value at 65 kHz before thermal equilibrium had been attained. Impedances were measured at 60 minute intervals.

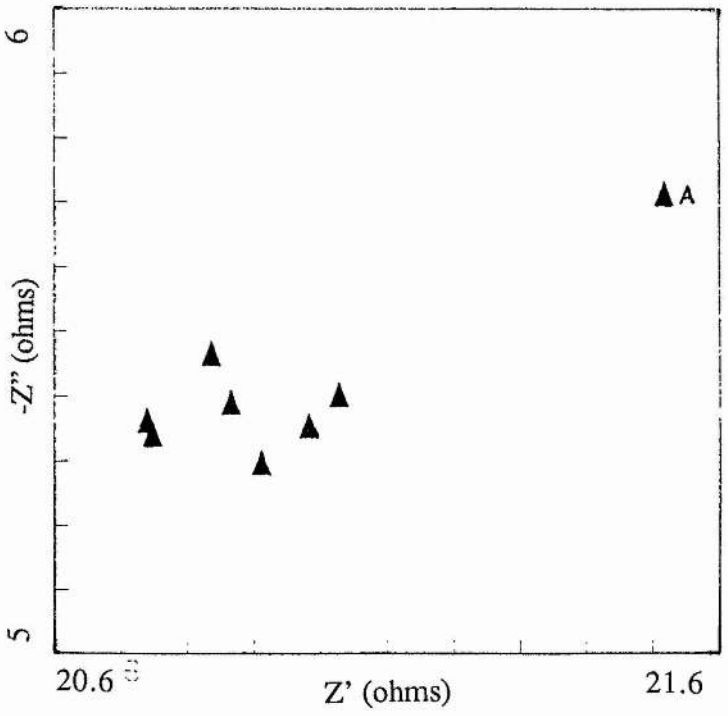

Figure 4-7. Variation in the conductance of a PEO_8LiClO_4 electrolyte with temperature during three temperature sweeps.

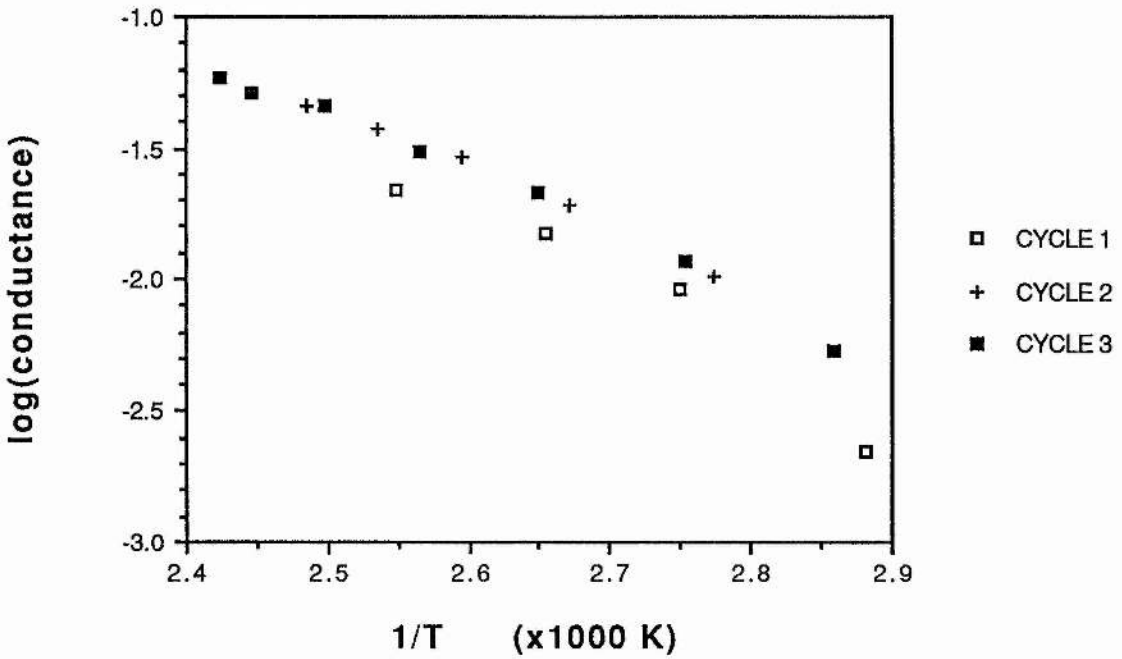

Figure 4-8. Impedance diagram of an Na|$PEO_{100}NaBPh_4$|Na cell at 85°C.

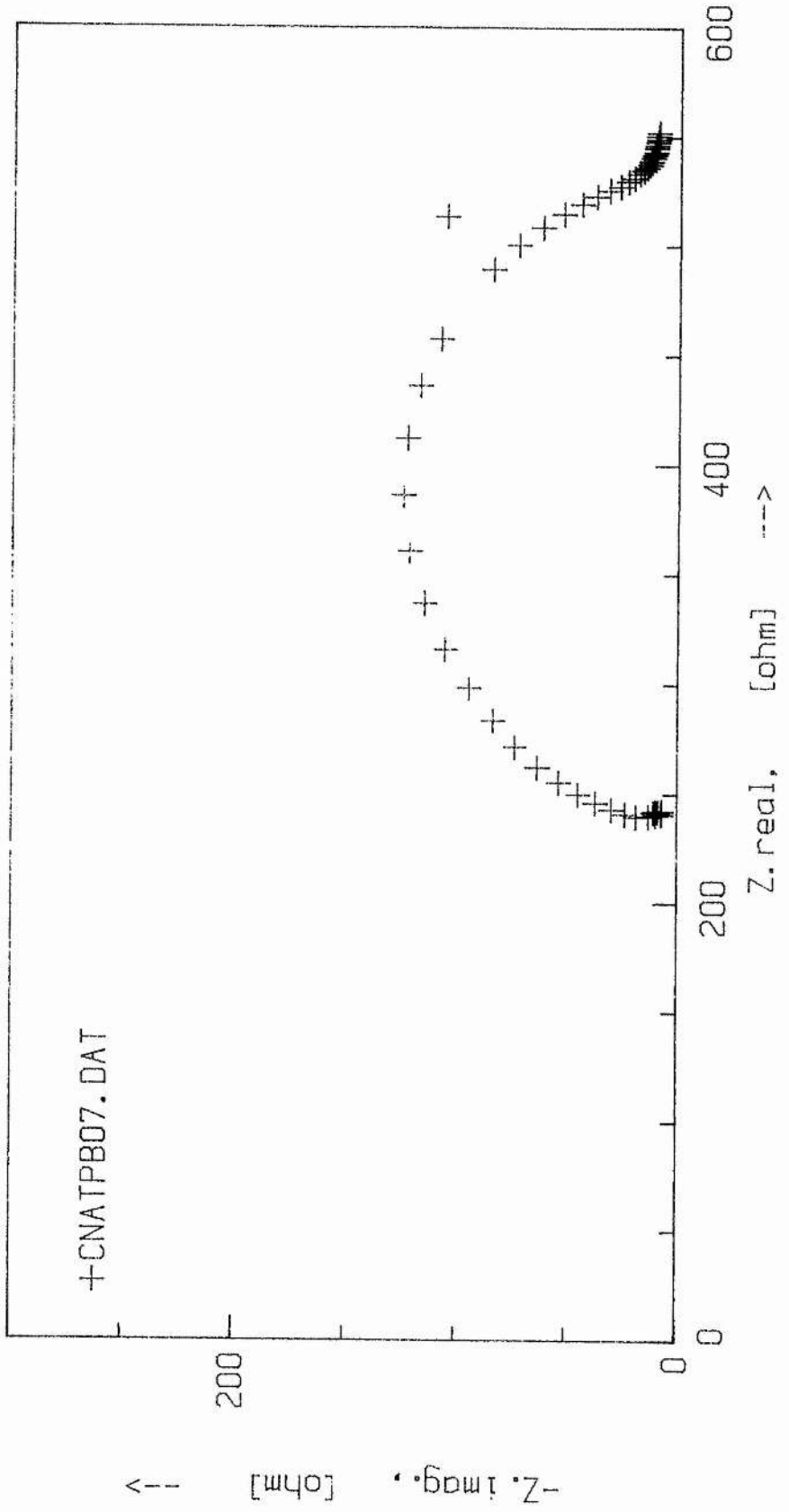

Figure 4-9a. Diagram showing the design of the Hittorf cell for transference number determinations.

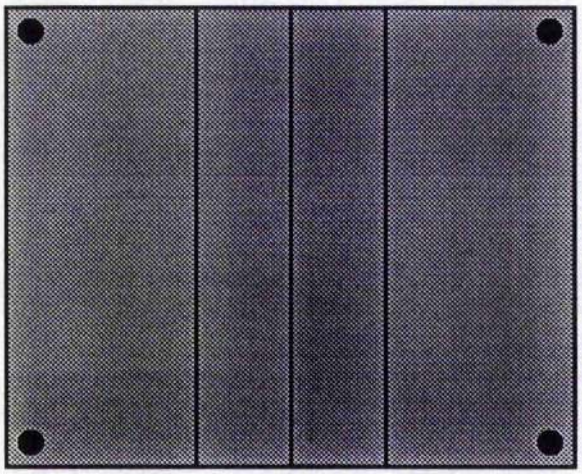

UPPER SECTION OF CELL (UPPER & SIDE VIEWS) SHOWING POSITIONS OF SCREW HOLES AND SECTIONING SLITS

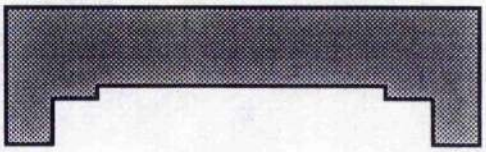

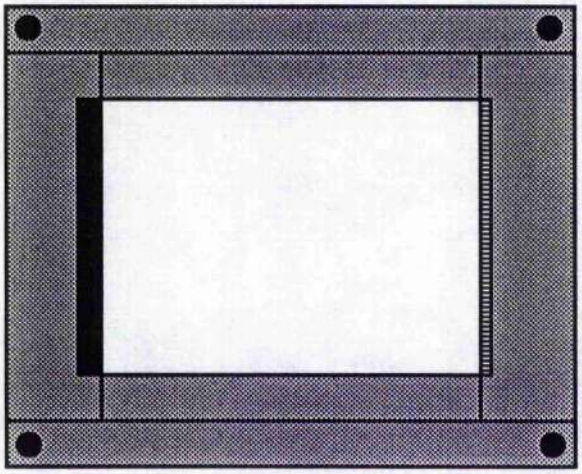

LOWER SECTION OF CELL (UPPER & SIDE VIEWS) SHOWING ELECTRODE AND ELECTROLYTE ARRANGEMENT & POSITIONS OF SCREW AND THERMO-COUPLE HOLES, & DEPRESSION FOR HOLDING THE ELECTROLYTE SLAB

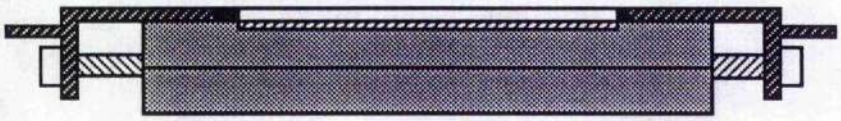

LOWER SECTION OF CELL SHOWING STEEL ELECTRODE CONTACTS

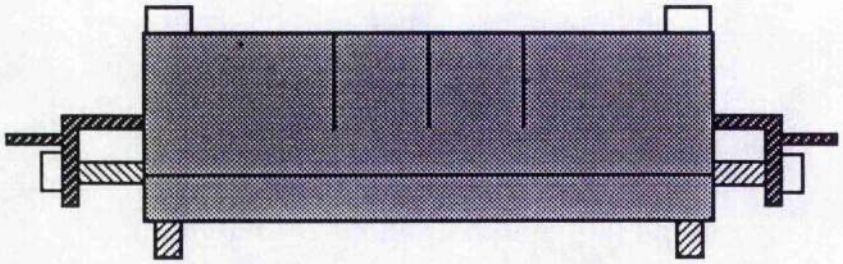

ASSEMBLED CELL

Figure 4-9b. Production of the lead cathode using lead foil and the steel electrode contact.

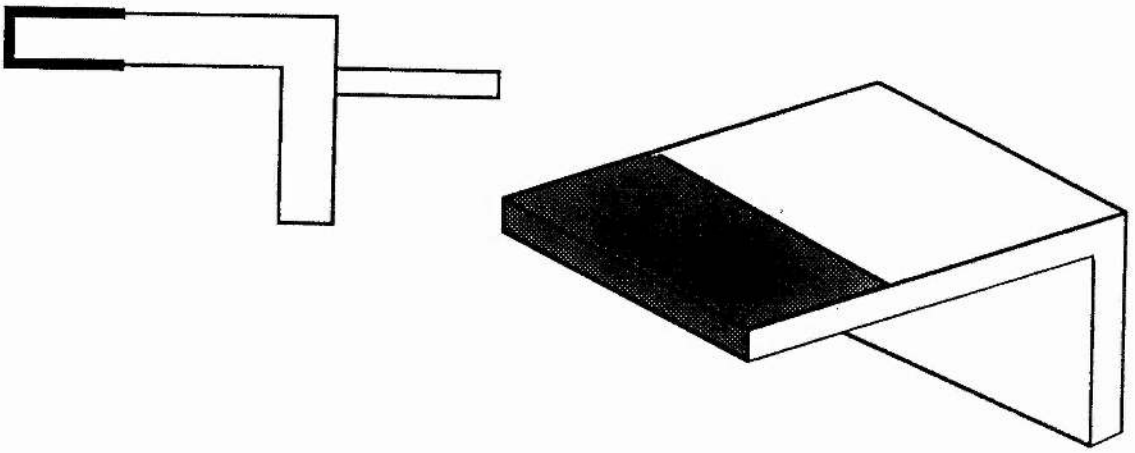

Figure 4-10. Impedance diagram of a polymer electrolyte between two blocking electrodes.

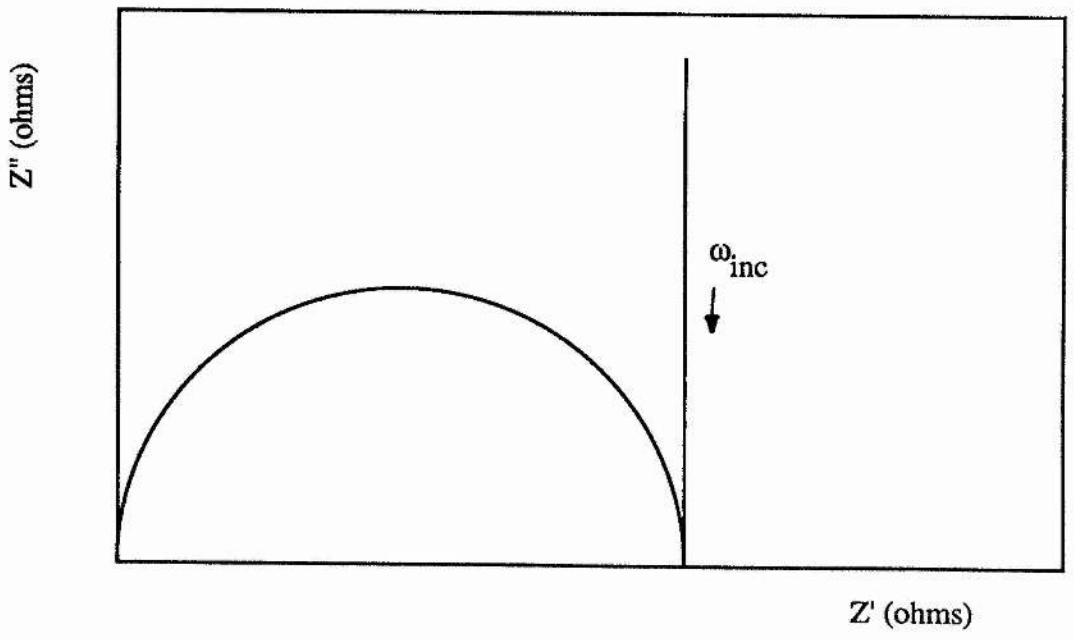

Figure 4-11. Circuit representation of the impedance diagram in Figure 4-10.

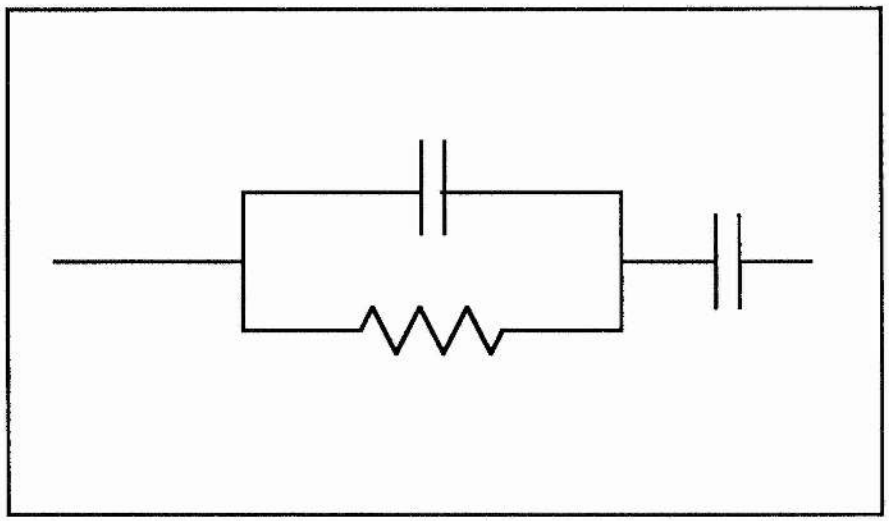

Figure 4-12. Impedance diagram of a polymer electrolyte between two non-blocking electrodes.

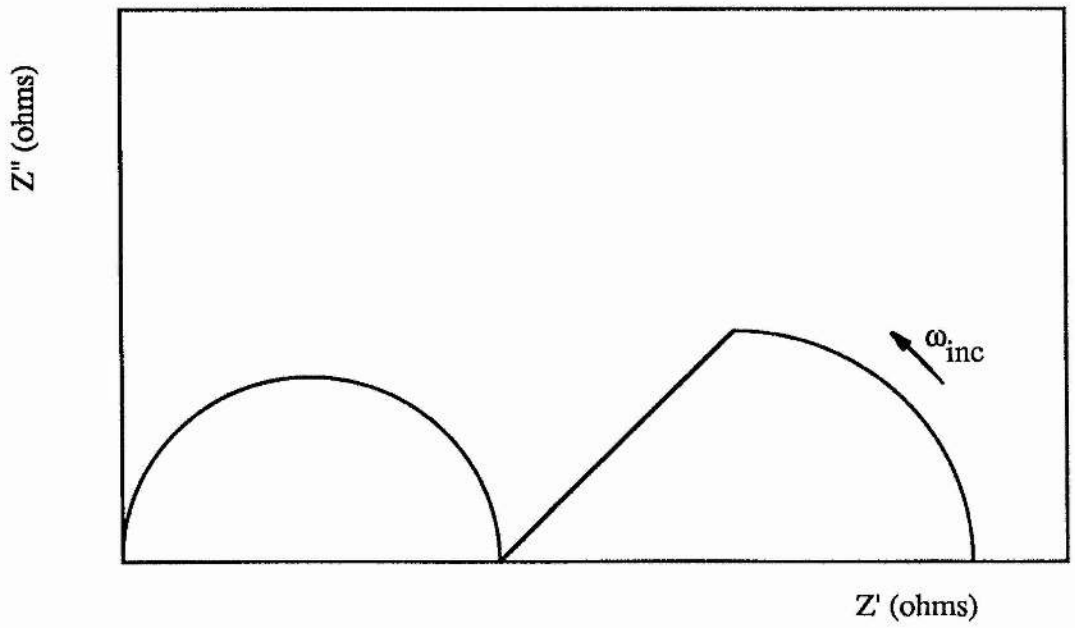

Figure 4-13. Impedance diagram of a polymer electrolyte between two non-blocking electrodes displaying an interfacial resistance.

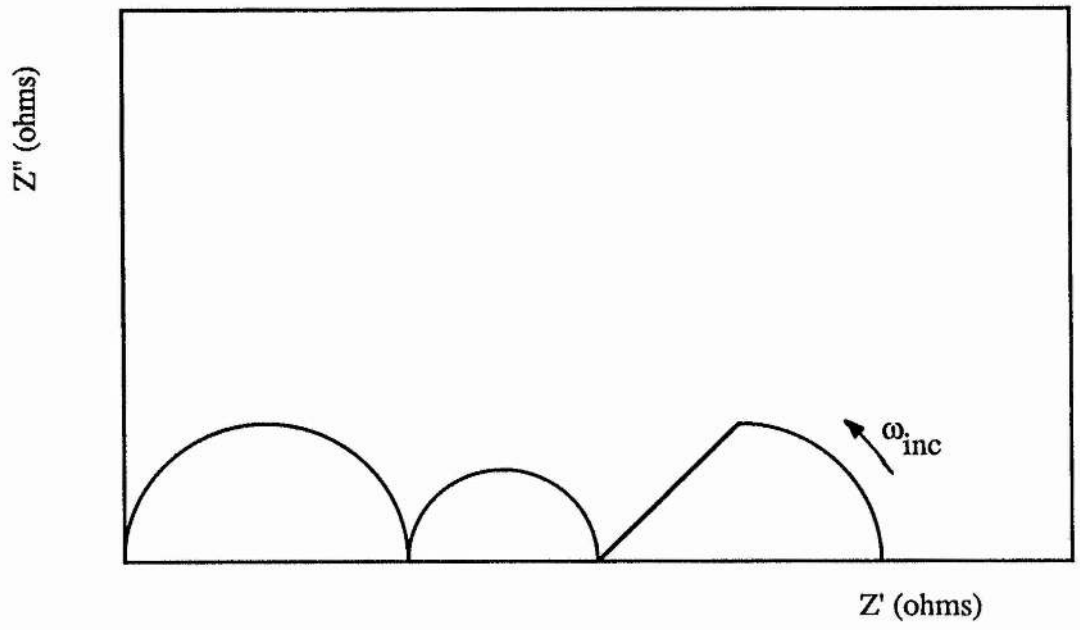

Figure 4-14. Impedance diagram for a real polymer electrolyte between two non-blocking electrodes for frequencies of 65kHz–1Hz.

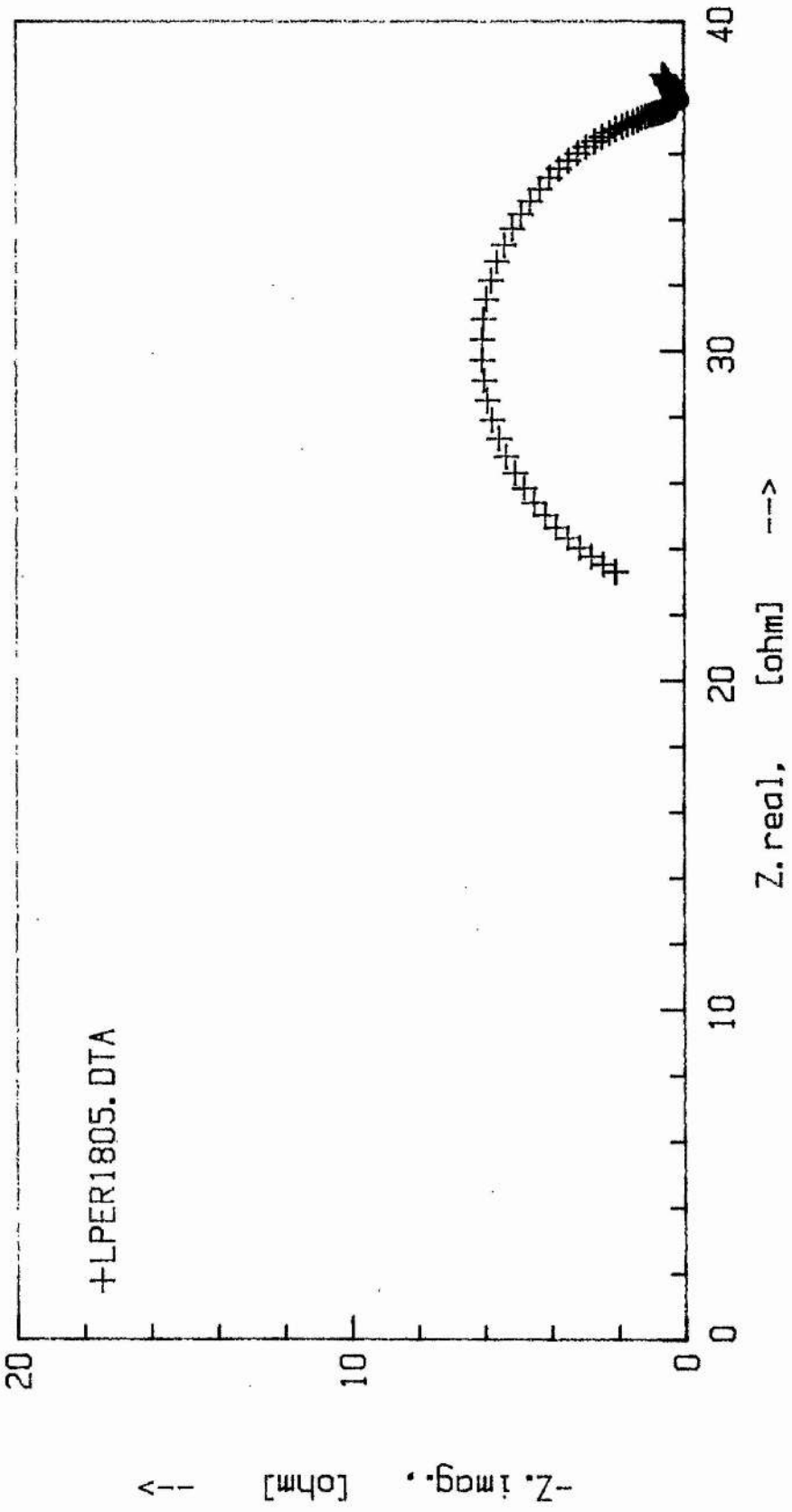

Figure 4-15. Impedance diagram of an Li|$PEO_{50}LiClO_4$|Li cell before dc polarisations have been performed.

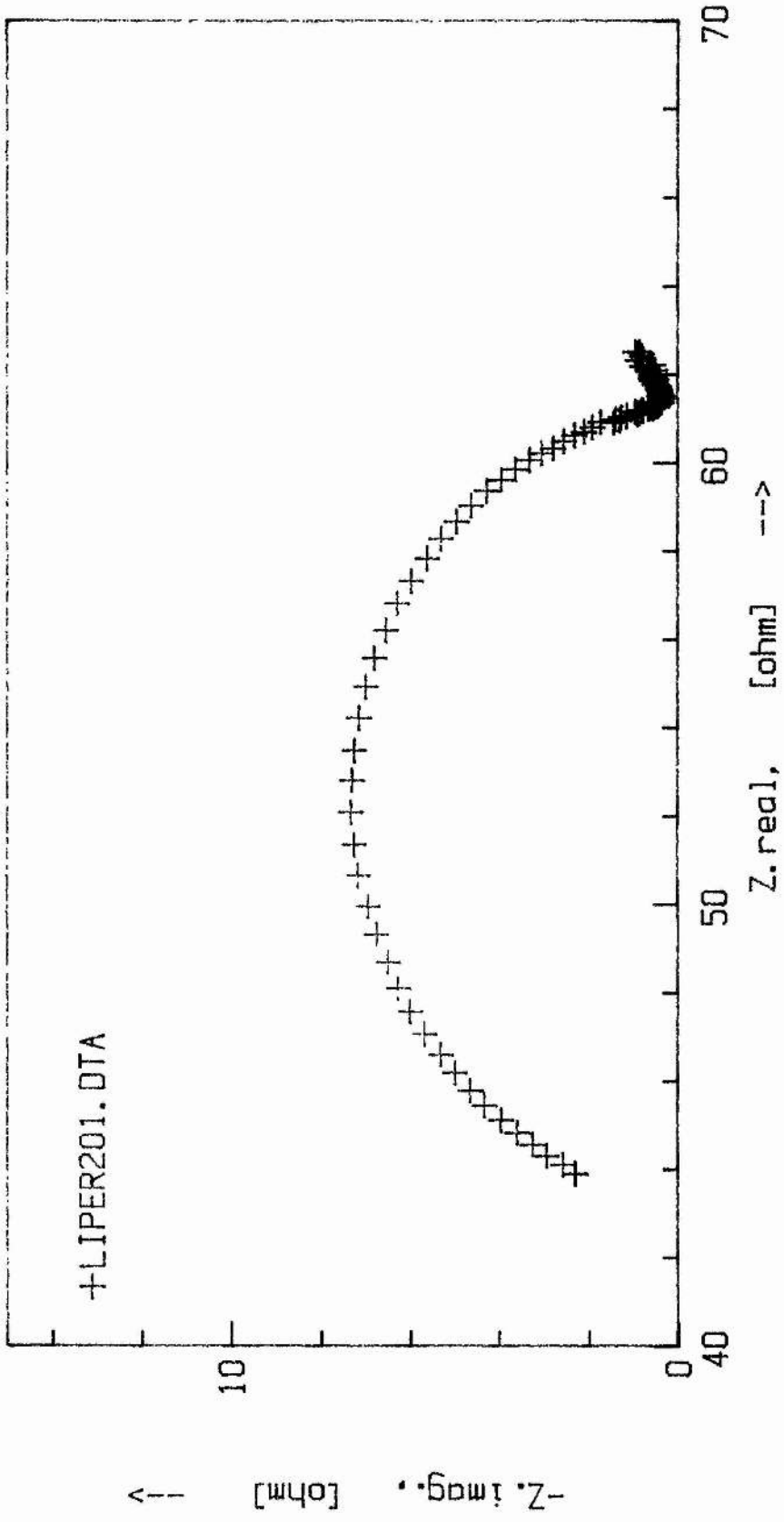

Figure 4-16. Impedance diagram of the cell in Figure 4-15 after several dc polariasations.

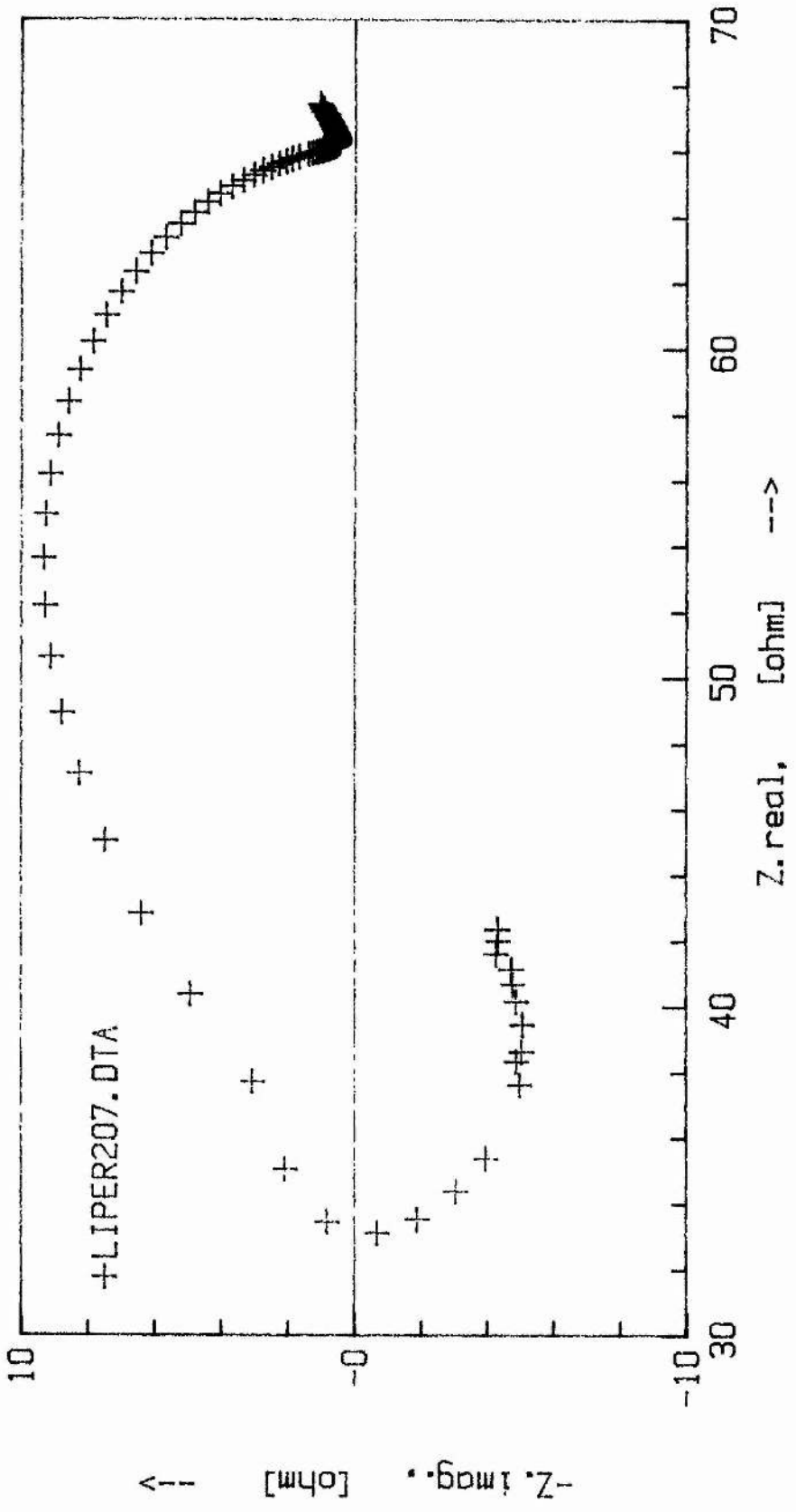

Figure 4-17. Measured (Li-AAS) *vs* actual (composition) lithium content of PEO_8LiClO_4 samples 2 days and 1 month after preparation.

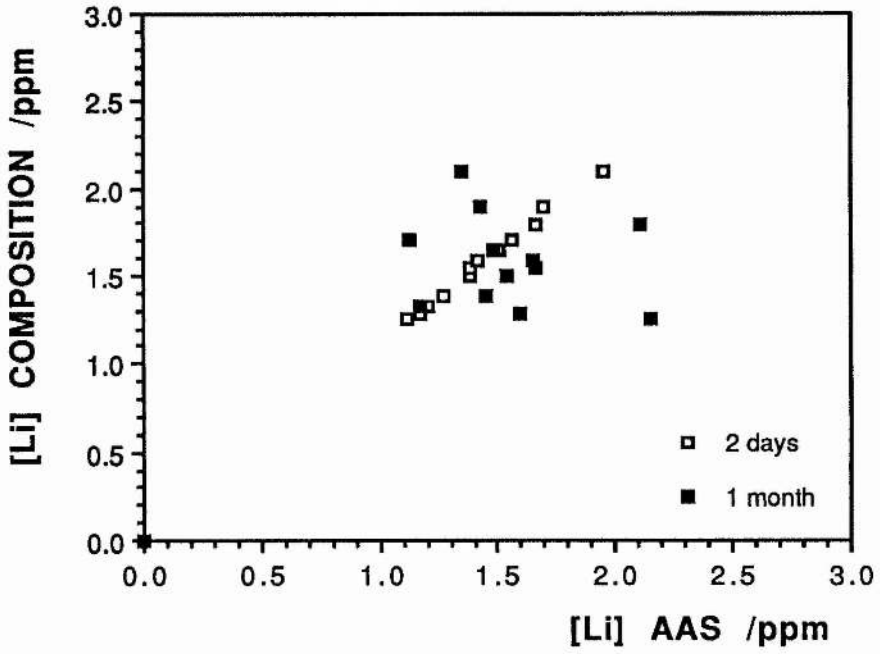

Table 4-A: Actual and Apparent Lithium Concentrations for Various Aqueous PEO_xLiClO_4 Solutions.

SAMPLE	ACTUAL Li CONCENTRATION /ppm	APPARENT Li CONCENTRATION /ppm
DISTILLED WATER	zero?	<0.02
8:1 ELECTRODE	≈10	0.92
8:1 MIDDLE	≈10	0.36
8:1 MIDDLE	≈10	0.47
8:1 PE	10.28	0.70
18:1 PE	10.28	0.20
50:1 PE	9.91	0.04
8:1 MIXTURE (actually 7:1)	12.46	0.69
18:1 MIXTURE (actually 15:1)	12.85	0.20
8:1 PE (ACIDIFIED)	10.26	0.85
8:1 TETRAMER MIXTURE (actually 7:1)	16.11	HIGH

Table 4-B: Actual and Apparent Lithium Concentrations for Various Samples Having Undergone Acid Digestion.

SAMPLE	ACTUAL Li CONCENTRATION /ppm	APPARENT Li CONCENTRATION /ppm	
PEO (i)	0.00	0.08	(0.00)
8:1 PE	1.84	1.29	
8:1 PE (i)	1.03	0.85	(0.94)
8:1 PE	0.97	0.85	(0.88)
8:1 PE (i)	1.93	1.57	

(i) These samples were treated with 0.5 cm^3 $HClO_4$ in addition to 3.0 cm^3 H_2SO_4

Figures in parentheses denote subsequent analysis using acidified standards

Table 4-C: Actual and Apparent Lithium Concentrations for Various Samples Having Undergone Acid Digestion.

SAMPLE	ACTUAL Li CONCENTRATION /ppm	APPARENT Li CONCENTRATION /ppm
PEO	0.00	0.01
8:1 PE	1.66	1.66
8:1 PE	1.12	1.08
8:1 PE	1.13	1.18
8:1 PE	1.18	1.16
8:1 PE	1.27	1.23
8:1 PE (Li)	1.04	1.01
8:1 PE (Li)	1.20	1.23

Samples denoted (Li) were taken from electrolyte which had been in contact with Li electrodes.

CHAPTER 5

THE STEADY-STATE DC POLARISATION OF POLYMER ELECTROLYTE CELLS—RESULTS

In this chapter the results from the dc polarisation of PEO-based lithium triflate, lithium perchlorate, and sodium tetraphenylborate PE cells of the form M|PEO-MX|M are presented, and discussed in light of the theory covered in Chapter 3. There are three main parameters which may be found from these experiments:

i the values of ΔE (directly) and $\Delta\phi$ (indirectly) constituting ΔV for each polarisation potential,

ii the values of the current fractions (defined as I^s/I^o corrected for interface resistances) for each polarisation potential, and

iii the range of linear I^s-ΔV response for a series of polarisation potentials.

These parameters are found using a combination of frequency response analysis (FRA) and dc polarisation. The FRA determines the electrolyte and interface resistances before and after the polarisation, and the dc polarisation determines the steady-state current and electrode potential difference at the end of the polarisation. The potential difference dropped over the interface resistance is corrected for by subtracting an amount ΔV_i, given by $I^s R_i^s$, from the applied potential difference, allowing the results to be discussed in terms of the potential difference acting over the electrolyte, ΔV.

The initial current is determined from the applied potential difference and the initial total (electrolyte plus interface) resistance, rather than from the display on the ECI, because the current is changing rapidly at the commencement of the polarisation, *i.e.*:

$$I^o = \frac{\Delta V}{R_b^o + R_i^o} \qquad 5\text{-}1$$

However, the indicated initial current was in close agreement with the calculated current.

In experiments undertaken to determine the linearity range of I^s-ΔV response, the applied potential difference was sometimes applied in a positive sense and sometimes in a negative sense between the electrodes, to ensure that the cell remained symmetrical, as it was feared that the continual passage of current (sometimes quite

large) only in one sense through the cell might lead to the growth of dendrites, contributing to an eventual short-circuit of the cell. Short-circuiting was a frequent occurrence at high potentials for high conductivity electrolytes.

The polarisation experiments were performed in a constant volume cell (described in Chapter 4) placed in a Büchi TO-50 oven, which was contained in an argon-filled drybox.

5.1 . THE DC POLARISATION OF POLYMER ELECTROLYTES

When a PE cell reaches steady-state, a concentration gradient must exist across the cell if a current fraction (see §3.5) of less than unity is obtained for the species to which the electrode is reversible (*e.g.* lithium in a PEO_xLiClO_4 PE cell with lithium electrodes): *i.e.*, for a steady-state electrolyte conductivity less than the initial electrolyte conductivity. The consequences of the existence of the concentration gradient are:

i diffusion coefficients will vary throughout the cell, if these values are concentration-dependent, and

ii the electrolyte conductivity will vary throughout the cell, if it is concentration dependent.

These effects will not be important if small potential differences are applied to the cell (because these will produce small concentration gradients and consequently minimal change in diffusion coefficients and conductivities). If, however, the conductivity is changing from point to point through the electrolyte (normal to the electrodes), the total electrolyte conductivity may be changed. Any change in the gross electrolyte conductivity may be evaluated by FRA at the end of a dc polarisation before concentration gradients have dispersed.

5.1.1 Potential Difference Range of Constant Electrolyte Resistance at Steady-State.

It is found that, for low concentration electrolytes, a small potential range of constant steady-state electrolyte resistance exists, usually of the order of 20 mV. Above this potential it is found that the electrolyte resistance, determined by FRA, increases. It is also found that this potential range of constant electrolyte resistance increases as the electrolyte concentration increases. However, for very low concentration electrolytes, Gray has found that this potential range increases again as the electrolyte concentration decreases towards the concentration at which a minimum in the molar conductivity of the PE occurs (≈ 10 mM) [32].

After high polarisation potentials have been applied, the electrolyte often displays a dramatic increase in its resistance, such that just one impedance diagram is not capable of recording the electrolyte resistance and the interface resistance at the end of a polarisation. This is because in the time it takes for the frequency to fall from 65 kHz at the electrolyte resistance intercept to 1 Hz at the ac resistance intercept, the whole cell resistance has fallen, and this causes the impedance diagram to loop back on itself, preventing the determination of the total resistance at the end of a polarisation. This looping behaviour is shown in Figure 5-1. Another impedance diagram must be taken after the total resistance has stopped falling, with the assumption that the interface resistance has not changed in the ten or so minutes needed to bring this about.

At moderately low concentrations (≈ 0.2 M *i.e.* ≈ 100:1) the increase in electrolyte resistance may be attributed to the fact that a concentration difference between the electrodes of 0.1 M, say, produced by the applied potential difference would have a more significant effect on an electrolyte of low concentration than on an electrolyte of high concentration (2.13 M in the case of $PEO_{12}LiClO_4$).

An increase in resistance at steady-state may be demonstrated by examining the schematic resistivity-concentration graph in Figure 5-2. If an electrolyte of concentration c_E and resistivity ρ_E is polarised, salt concentrations at the electrodes of c_a and c_c will arise. The total electrolyte resistance is related to the area under the graph

(Figure 5-2a), such that if the average resistivity, ρ_{av}, is greater than the initial resistivity, an increase in the electrolyte resistance will occur (Figure 5-2b).

An interesting observation about the conductivity–concentration diagram of $PEO_xLiCF_3SO_3$, as reported by Robitaille and Fauteux [11], may be made here. The conductivity–concentration graph reported gives rise to a resistivity–concentration graph of the form of Figure 5-3a. The indicated local maximum of resistivity occurs at 36:1. If an electrolyte of this composition is polarised, the salt concentrations at the electrodes will be forced towards values which possess lower resistivities (Figure 5-3b), such that the average electrolyte resistivity will fall (Figure 5-3c), causing the electrolyte resistance to fall at steady-state.

The initial and steady-state electrolyte resistances at various polarisation potentials are shown in Figure 5-4 for PEO_xLiClO_4, Figure 5-5 for $PEO_xLiCF_3SO_3$, and in Figure 5-6 for PEO_xNaBPh_4. The data are also contained in Tables 5-A to 5-K. It is seen that for some electrolytes the initial electrolyte resistance varied slightly over time from polarisation to polarisation, but the steady-state resistance at the end of a polarisation was the same as the initial resistance that was found for that polarisation (*i.e.* for electrolytes which had an "invariant" electrolyte resistance, this resistance did not significantly change over the timescale of an individual polarisation, though over the course of several days minor changes in the resistance were found).

Because the electrolyte resistance sometimes increased at steady-state, care must be taken to interpret the deviation from linearity of the I^s-ΔV response. The increase in resistance of the electrolyte at steady-state will reduce the steady-state current from a value which it would have taken had the resistance not increased. This is illustrated in Figure 5-7 which shows impedance diagrams for two electrolytes, which are identical save that one has a larger electrolyte resistance. Because the dc limits are different, due to this resistance increase, different steady-state currents would be passed if the same polarisation potential were applied to each. This deviation from linearity of the I^s-ΔV response in the presence of a varying electrolyte resistance is thus not indicative of the state of ion-pairing in the electrolyte.

Occasionally the semicircle found from FRA used to determine the electrolyte resistance continued below the real axis, as shown in Figure 5-8. In these cases the high frequency intercept with the real axis was taken as the electrolyte resistance. For $PEO_{50}LiClO_4$ an inductive semicircle was displayed, extending above the real axis, making it difficult to determine the electrolyte resistance (Figure 4-16). In this case the data at low frequencies were used to define a semicircle whose high frequency intercept with the real axis was taken to be the electrolyte resistance (as shown in Figure 5-9). It is not known why this behaviour was observed, and the extrapolation of the low frequency data to a high frequency intercept may not be appropriate, possibly making the results for the low concentration electrolytes unreliable.

5.1.2 ΔE-ΔV Variation with Applied Potential Difference

ΔE values were obtained from the steady-state dc polarisation experiments carried out to determine the linearity range of I^s-ΔV response. The potentiostat (an electrochemical interface) applied the potential difference across the cell, and the potential difference between the electrodes was measured by the inbuilt digital voltmeter (DVM). At the end of an experiment the polarisation potential was removed with the DVM still running; the DVM displayed the potential difference between the electrodes, which fell from the polarisation potential to the concentration potential difference, which decreased with time until little potential difference existed between the electrodes (typically ≈ 0.2 mV). This decrease with time in the potential difference across the cell is shown in Figure 5-10 for a PEO_xLiClO_4 electrolyte.

The variation in ΔE with ΔV is shown in Figures 5-11 to 5-13 for the electrolytes studied. The data are contained in Tables 5-A to 5-K. The low ΔV regions of these graphs are linear, and these portions were used to provide a constant value of ΔE/ΔV. These constant ΔE/ΔV values are shown in Table 5-L, and the data plotted in Figure 5-14 *vs* the salt concentration of the electrolyte. It is generally found that as the salt concentration in a PE increases, the ratio of ΔE:ΔV also increases.

In Figures 5-11 to 5-13 it is often found that at high potential differences ΔE is

less than would be found by extrapolation of the low potential data. If this is the case, the electrolyte potential difference must be greater than anticipated from the low potential data, which may serve to increase the steady-state current from its value calculated from low potential I^s-ΔV data. However, because deviation from a linear ΔE-ΔV response (with its tendency to increase the steady-state current) occurs at the same potentials as increases in the electrolyte resistance (which serve to decrease the steady-state current), the effect may not be noticeable.

5.1.2.1 How ΔE May Be Made Greater Than Δϕ for a Polymer Electrolyte Containing M^+ and X^- Ions and MX Ion-pairs.

In the model electrolytes examined in Chapter 3, ΔE was always found to be less than or equal to $\Delta\phi$, but the results from sodium tetraphenylborate- and lithium perchlorate-based PEs show that ΔE is usually greater than $\Delta\phi$. It was also suggested that a reaction producing M^+ ions at the electrodes (for models which did not consider M^+ ions to exist in the electrolyte) may give rise to a value of ΔE greater than $\Delta\phi$, but that none were found. One model which may be used to give a greater ΔE value, at least mathematically, is a modified version of the one described in §3.2.2.

In this modified model enhanced ionisation of ion-pairs in the vicinity of the electrodes is assumed to take place, giving rise to a greater amount of free ions, as shown in the concentration-distance plot in Figure 5-15. The ions have concentrations of c_a and c_c just away from the electrodes and enhanced concentrations c_a' and c_c' at the electrodes. The increased ion concentration is assumed to be given by the original ion concentration plus a term due to the breaking up of a fraction, α, of the ion-pairs; *i.e.*:

$$c_c' = c_c + \alpha K c_c^2 \quad \text{and} \quad c_a' = c_a + \alpha K c_a^2 \qquad 5\text{-}2$$

If this is the case then the concentration potential difference between the electrodes will be given by:

$$\Delta E = \frac{RT}{F}\ln\left(\frac{c_a'}{c_c'}\right) = \frac{RT}{F}\ln\left(\frac{c_a}{c_c}\right) + \frac{RT}{F}\ln\left(\frac{1 + \alpha K c_a}{1 + \alpha K c_c}\right) \qquad 5\text{-}3$$

The second term in equation (5-3) is seen to be greater than zero for an α greater than zero. If the αKc terms are much greater than unity, the concentration potential difference will be double the value expected in the absence of this ion-pair breakdown, so possibly greater than the electrolyte potential difference, $\Delta\phi$.

Whilst this provides a mathematical solution to the experimental observation that ΔE tends to be greater than $\Delta\phi$, it is not a totally unrealistic model. In the presence of large electric fields weak electrolytes such as acetic acid show an enhanced conductivity due to the increase in the ionisation of the species, this being called the second Wien effect, or dissociation field effect [93]. The potential differences required are of the order of 10 kV cm^{-1}, which is the same as 1 mV acting over 1 nm.

5.1.3 The Applied Potential Difference Range of Linear Steady-State Current—Applied Potential Difference Response.

Before examining the experimental results found in this project concerning the potential difference range of linear I^s-ΔV response it worth considering some of the data in the literature. The data tend to be reported in terms of the potential difference range over which transport numbers have been determined using either equation (3-75) or a simple ratio of steady-state to initial currents [42] [94]—[97]. If no corrections for the interface resistance have been applied then the actual potential range over the electrolyte for a linear I^s-ΔV response may be much less than indicated.

Bonino *et al.* [33] report that a copper (II) triflate-based PE shows a linear I^s-ΔV response up to 250 mV, but it is not clear if the substantial interface resistances in this system were corrected for.

An interesting result was reported by Watanabe *et al.* [98] for a lithium perchlorate electrolyte based on a network polymer; the electrolyte was dilute, being estimated at $\approx$ 0.15 M, (which might lead to the expectation that a small potential range of I^s-ΔV response might be displayed because of changes in electrolyte resistance—see §5.1.1) but a constant response was found up to 100 mV. In this system, then, the presence of neutral species may occur.

In this project the variation in steady-state current with the applied potential difference has been determined for lithium- and sodium-based PEs at a constant temperature (≈ 120°C for the lithium-based PEs and ≈ 85°C for the sodium-based PEs). These results are shown in Figures 5-16 to 5-18 and in Tables 5-A to 5-K. It is seen that the linear portions of the graphs show an extended linear range of I^s-ΔV response as the concentrations of the PEs increase, with low (≈ 20 mV) potential ranges for low concentration electrolytes. However, the breakdown in linearity in these electrolytes is probably due to the increase in the electrolyte resistance, as well as to any deviation from linearity of the equations used in Chapter 3.

Gray has found [32] that as the concentration of lithium perchlorate-based PEs decreases (O:M » 100:1), the potential difference range of a linear I^s-ΔV response increases, and no increase in electrolyte resistance occurs. This again suggests that the effects of neutral species may become important and distinguishable from other effects at low concentrations.

It may be concluded then that the deviation from linearity of the I^s-ΔV response may not be usefully interpreted in terms of the species content of electrolytes at potential differences where the electrolyte resistance is increasing.

5.2 CURRENT FRACTION MEASUREMENTS IN POLYMER ELECTROLYTES

The equation used by Evans *et al.* [72] as a measurement of the cation transference number (now referred to as the current fraction) in PEs, *i.e.* equation (3-75) has been used to determine such values for PEs based on $LiClO_4$, $LiCF_3SO_3$, and $NaBPh_4$. These results are shown in Tables 5-M to 5-W, and in Figures 5-19 to 5-21 where they are plotted against the electrolyte potential difference. It is seen that these current fractions are potential-dependent above a particular potential; the increase in electrolyte resistance at steady-state reduces the anticipated steady-state current, thus reducing the values of i_F from their low-potential values. The low-potential values of

i_F are constant, and these are referred to as limiting current fractions, i_{FI}. These i_{FI} values are contained in Table 5-X and displayed in Figure 5-22, where they are plotted against the salt concentration of the PE at 120°C for PEO_xLiClO_4 and $PEO_xLiCF_3SO_3$. As the concentration decreases, i_{FI} increases.

A study of the variation in limiting current fraction with temperature was undertaken for four PEO_xLiClO_4 electrolytes at various temperatures between 90°C and 140°C. The data are contained in Table 5-Y and shown in Figure 5-23, together with the values found from the I^s-ΔV polarisation study at ≈ 120°C. The only discrepancy between the two sets of results are the values obtained for the $PEO_{12}LiClO_4$ samples. All of the I^s-ΔV electrolyte discs were produced from different stock samples than were used in the i_F study, so the reproducibility of the results is generally good. It is seen that as the temperature increases, i_F increases.

It is seen that, for the lithium-based electrolytes, the limiting current fraction decreases with increasing concentration. The values obtained for lithium triflate electrolytes are consistent with those obtained by Bruce *et al.* [99] for PEs of higher concentration, which were mixtures of crystalline and amorphous electrolyte. The limiting current fractions of lithium perchlorate PEs are approximately half the value of those shown by lithium triflate PEs, but the lithium perchlorate PEs possess a higher steady-state conductivity than the lithium triflate PEs.

The variation in current fractions between sodium tetraphenylborate PEs is not as large as those shown for the lithium electrolytes, but the temperature of the sodium measurements is not comparable to that of the lithium measurements, and the amorphous range of the sodium PEs is not as extensive as those possessed by the lithium electrolytes. These results are not usefully compared to the lithium results, and they were undertaken to evaluate the observation by Killis *et al.* [100] that this system seemed to be predominantly ionised. The fact that $\Delta E > \Delta\phi$ suggests that this may not be the case.

Some determinations of I^s/I^o have appeared in the literature, either arising from simple ratios of the steady-state to initial current (for example references [42] [77] [94])

or by using the corrected equation of Evans *et al.* (for example [34] [72] [99] [101]). Some publications even report the potential difference at which the measurements were carried out, or report the potential difference range over which the measurements were taken (indicating that the measurement is constant over this range) [42] [95]—[97].

Farrington's group [42] [95]—[97], working with multivalent cation electrolytes (Zn^{2+}, Ni^{2+}, Pb^{2+}) have reported current fractions which are constant up to several hundred millivolts, suggesting that ion association is significant in these systems. However, the data in reference [42] seem to be direct ratios of steady-state to initial currents, with no corrections for the effect of interface resistances. Zinc-based electrolytes in contact with zinc electrodes are known to form large interfacial resistances [102], which would possibly more than halve the potential difference range of limiting current fraction. Yet large potential differences may cause disruption of the interface, making the interface resistance smaller and causing more of the applied potential difference to act over the electrolyte.

5.2.1 The Effect of ΔE on Current Fractions.

The steady-state current is experimentally found to be close to the value that would be passed if the steady-state value of $\Delta\phi$ acted over the electrolyte initially; so the reduction in the current as the cell approaches steady-state gives the appearance that it is due mainly to the reduction in electrolyte potential difference from its initial value of ΔV caused by the establishment of the electrode potential difference. Thus, the diffusion of cation-containing species in the cell at steady-state almost overcomes the effect of the reduction in the migration of cation-containing species by the fall in $\Delta\phi$, and the stoppage of the net transport of anion-containing species in the cell. A steady-state conductivity may be defined using $\Delta\phi$, which is different to that defined in Chapter 3 in terms of ΔV, such that:

$$\sigma_{\Delta\phi} = -\frac{I^{s}t}{A\Delta\phi} \qquad 5\text{-}4$$

It is seen from Table 5-Z that the resistance that this expression provides is similar to

the actual steady-state electrolyte resistance determined using FRA. If this is the case the ratio of I^s/I^o is approximately given by:

$$\frac{I^s}{I^o} \approx 1 - \frac{\Delta E}{\Delta V} \qquad 5\text{-}5$$

The close relationship between i_{FI} and $\Delta E/\Delta V$ is demonstrated in Figure 5-24, which shows a plot of $\Delta E/\Delta V$ *vs* i_{FI} for PEO-based lithium perchlorate and lithium triflate PEs at 120°C. The graph is surprisingly linear considering that two different salts are examined and only several data points are present, showing that i_{FI} has a strong dependence on the relative magnitude of the electrode potential difference. A least mean squares fit to the data has an intercept at an i_{FI} value of 0.98, but the line has been drawn through unity to demonstrate the anticipated fit.

It is not apparent why the fall in current should match the fall in the electrolyte potential difference—for an ideal free ion PE this would necessarily mean that the cation transference number is 0.5. It would be interesting to see if this behaviour arises in other electrolytes, where a large amorphous composition range exists to allow a wide spread of data to be obtained.

Table 5-A. Steady-state polarisation data for $PEO_{100}LiCF_3SO_3$ at 121-122°C.

ΔV_a	ΔV	ΔE	$\Delta\phi$	I°	I^s	R_e^s	R_e°	R_i^s	R_i°
/ mV	/ mV	/ mV	/ mV	/ μA	/ μA	/ Ω	/ Ω	/ Ω	/ Ω
5	4.8	1.9	2.9	17.3	10.7	272.8	270.4	19.3	19.4
-10	-9.7	-3.5	-6.3	-33.8	-21.2	283.9	273.2	12.9	23.0
20	19.2	7.1	12.1	67.4	41.9	282.7	274.3	19.5	22.6
-40	-38.1	-13.7	-24.4	-133.0	-79.8	292.9	274.8	23.6	25.9
50	47.5	16.7	30.8	165.3	98.7	305.4	274.4	25.1	28.0
60	57.6	20.0	37.6	201.3	96.6	307.5	272.3	25.1	25.7
60	56.9	19.8	37.1	198.5	116.3	319.0	274.3	26.9	27.9
-70	-66.6	-22.9	-43.7	-230.3	-120.0	334.6	274.0	28.6	30.0
-80	-76.6	-25.8	-50.8	-267.1	-134.3	354.4	271.7	25.5	27.8
100	96.1	31.2	64.9	325.1	160.3	372.4	280.7	24.6	26.9

Table 5-B. Steady-state polarisation data for $PEO_{50}LiCF_3SO_3$ at 120-121°C.

ΔV_a	ΔV	ΔE	$\Delta\phi$	I°	I^s	R_e^s	R_e°	R_i^s	R_i°
/ mV	/ mV	/ mV	/ mV	/ μA	/ μA	/ Ω	/ Ω	/ Ω	/ Ω
5	4.6	2.2	2.4	40.3	22.2	105.2	107.3	18.9	16.7
10	9.3	4.4	4.9	81.2	44.6	107.3	106.7	16.7	16.5
20	18.7	8.6	10.1	158.5	88.8	110.6	110.8	14.5	15.4
40	37.7	16.8	20.9	319.7	169.0	116.0	110.6	13.7	14.5
-60	-57.4	-24.1	-33.3	-486.6	-225	130.3	105.1	11.5	18.2
-80	-77.3	-30.6	-46.7	-644.1	-277	136.7	106.1	9.6	18.1
100	97.1	36.7	60.4	813.7	318	145.7	106.6	9.1	16.3
-120	-111.0	-41.9	-69.1	-958.5	-333	142.5	105.7	26.9	19.5

Table 5-C. Steady-state polarisation data for $PEO_{36}LiCF_3SO_3$ at 120-121°C.

ΔV_a	ΔV	ΔE	$\Delta\phi$	I°	I^s	R_e^s	R_e°	R_i^s	R_i°
/ mV	/ mV	/ mV	/ mV	/ μA	/ μA	/ Ω	/ Ω	/ Ω	/ Ω
5	4.7	2.2	2.5	52.4	28.2	86.3	85.7	11.7	9.7
-10	-9.3	-4.7	-4.6	-98.3	-50.0	88.7	86.0	13.8	15.7
20	17.8	9.0	8.8	194.9	103.7	83.4	83.1	21.2	19.5
-40	-37.2	-17.6	-19.6	-382.8	-165.6	94.1	85.5	17.2	19.0
-40	-35.9	-17.2	-18.7	-367.0	-204	86.3	86.7	20.3	22.3
60	54.0	25.0	29.0	555.0	294	89.9	86.0	20.5	22.1
-80	-73.5	-32.2	-41.3	-735.3	-321	109.6	86.1	20.4	22.7
100	90.8	38.2	52.6	909.9	377	115.2	85.5	24.4	24.4

Table 5-D. Steady-state polarisation data for $PEO_{18}LiCF_3SO_3$ at 120-121°C.

ΔV_a	ΔV	ΔE	$\Delta\phi$	I^o	I^s	R_e^s	R_e^o	R_i^s	R_i^o
/ mV	/ mV	/ mV	/ mV	/ μA	/ μA	/ Ω	/ Ω	/ Ω	/ Ω
5	4.6	2.5	2.1	78.1	37.6	53.5	54.9	10.3	9.1
-10	-8.9	-4.8	-4.1	-148.8	-77.2	51.1	52.7	14.6	14.5
20	17.6	9.7	7.9	304.4	149.2	49.5	50.5	15.9	15.2
-40	-36.3	-18.9	-17.4	-595.2	-309	53.6	51.0	11.9	16.2
-60	-54.0	-27.8	-26.2	-916.0	-468	51.9	49.1	12.9	16.4
-70	-59.2	-29.2	-30.0	-1005.7	-633	47.2	46.0	17.0	23.6
80	72.4	36.6	35.8	1253.9	446	69.6	48.3	17.1	15.5
-80	-74.0	-35.7	-38.3	-1118.9	-444	77.4	56.5	13.6	15.0
90	71.2	36.7	34.5	1195.2	690	43.5	45.8	27.2	29.5
100	87.8	43.3	44.5	1432.7	684	63.8	53.4	17.8	16.4

Table 5-E. Steady-state polarisation data for $PEO_{100}LiClO_4$ at 121-122°C.

ΔV_a	ΔV	ΔE	$\Delta\phi$	I^o	I^s	R_e^s	R_e^o	R_i^s	R_i^o
/ mV	/ mV	/ mV	/ mV	/ μA	/ μA	/ Ω	/ Ω	/ Ω	/ Ω
5	4.6	3.0	1.6	37.7	14.7	101.1	106.5	28.9	26
-10	-9.1	-5.9	-3.2	-72.7	-30.1	101.1	103.6	28.9	34
20	17.9	11.7	6.2	149.8	53.9	101.8	96.1	38.1	37.4
40	36.0	22.6	13.4	288.8	94.6	121.8	97.1	42.0	41.4
-80	-73.7	-43.0	-30.7	-571.0	-163.8	153.4	96.9	38.3	43.2
120	113.1	61.9	51.2	839.7	178.9	194.3	100.2	38.7	42.7
200	191.1	99.8	91.3	1434.7	207.8	199.4	96.7	42.7	42.7
-300	-289.5	-139.0	-150.5	-2117.1	-227.0	244.1	104.7	46.4	37.0
600	592.1	245.5	346.6	4273.5	216.0	245.5	100.6	36.8	39.8

Table 5-F. Steady-state polarisation data for $PEO_{50}LiClO_4$ at 121-122°C.

ΔV_a	ΔV	ΔE	$\Delta\phi$	I^o	I^s	R_e^s	R_e^o	R_i^s	R_i^o
/ mV	/ mV	/ mV	/ mV	/ μA	/ μA	/ Ω	/ Ω	/ Ω	/ Ω
5	4.4	3.2	1.2	81.6	30.8	43.3	43.1	19.4	18.4
-10	-8.9	-6.1	-2.8	-159.0	-57.9	43.7	43.5	19.9	19.5
20	16.3	12.2	4.1	300.8	111.0	44.8	42.1	22.5	24.4
-40	-35.3	-23.7	-11.6	-602	-203	49.8	43.4	23.2	23.0
60	53.6	34.8	18.8	867	206	52.2	42.7	26.2	26.5

Table 5-G. Steady-state polarisation data for $PEO_{18}LiClO_4$ at 121-122°C.

ΔV_a	ΔV	ΔE	$\Delta\phi$	I°	I^s	R_e^s	R_e°	R_i^s	R_i°
/ mV	/ mV	/ mV	/ mV	/ μA	/ μA	/ Ω	/ Ω	/ Ω	/ Ω
5	4.4	3.3	1.1	139.3	45.2	22.8	23.0	13.2	12.9
-10	-8.7	-6.5	-2.2	-274.0	-84.5	22.6	22.6	14.9	13.9
20	16.6	12.5	4.1	461.9	168.3	22.6	22.6	20.1	20.7
-40	-33.1	-24.6	-8.5	-879.1	-328	23.4	22.7	21.0	22.8
-60	-50.6	-37.0	-13.6	-1373.0	-437	23.6	22.5	21.5	21.2
80	69.5	49.5	20.0	1742.9	526	24.5	22.6	20.0	23.3

Table 5-H. Steady-state polarisation data for $PEO_{15}LiClO_4$ at 120-122°C.

ΔV_a	ΔV	ΔE	$\Delta\phi$	I°	I^s	R_e^s	R_e°	R_i^s	R_i°
/ mV	/ mV	/ mV	/ mV	/ μA	/ μA	/ Ω	/ Ω	/ Ω	/ Ω
5	4.1	3.1	1.0	124.1	43.3	19.1	18.9	20.9	21.4
-10	-8.1	-6.1	-2.0	-238.7	-90.4	19.0	19.1	21.5	22.8
20	17.2	12.8	4.4	591.7	203	19.1	19.1	14.0	14.7
-40	-34.4	-25.7	-8.7	-1208.5	-405	19.2	18.9	13.8	14.2
60	55.8	41.4	14.4	2264.2	633	20.6	20.0	6.6	6.5
-80	-68.9	-50.9	-18.0	-2185.8	-785	19.5	19.0	14.1	17.6
100	83.5	60.1	23.4	2493.8	889	19.8	19.0	18.6	21.1
-140	-121.6	-57.8	-63.8	-3325.4	-1380	19.4	18.3	13.3	23.8

Table 5-I. Steady-state polarisation data for $PEO_{12}LiClO_4$ at 119-120°C.

ΔV_a	ΔV	ΔE	$\Delta\phi$	I°	I^s	R_e^s	R_e°	R_i^s	R_i°
/ mV	/ mV	/ mV	/ mV	/ μA	/ μA	/ Ω	/ Ω	/ Ω	/ Ω
5	4.1	3.1	1.0	127.6	43.7	18.5	18.6	20.8	20.6
-10	-8.1	-6.0	-2.1	-232.6	-86.7	19.6	19.8	21.6	23.2
20	15.2	11.5	3.7	414.9	167.8	19.4	19.6	28.6	28.6
-40	-31.0	-23.3	-7.7	-823.0	-340.2	19.7	19.5	26.4	29.1
80	65.9	49.2	16.7	1877.9	715.8	19.5	19.2	19.7	23.4

Table 5-J. Steady-state polarisation data for $PEO_{100}NaBPh_4$ at 81-83°C.

ΔV_a / mV	ΔV / mV	ΔE / mV	$\Delta\phi$ / mV	I^o / μA	I^s / μA	R_e^s / Ω	R_e^o / Ω	R_i^s / Ω	R_i^o / Ω
10	7.8	5.9	1.9	18.8	7.32	237.1	235.4	303.5	296.7
20	14.6	10.9	3.7	33.5	14.3	239.1	233.3	379.9	364.3
-40	-31.5	-23.3	-8.2	-73.3	-28.4	250.3	237.9	299.9	307.6
-60	-47.1	-34.6	-12.5	-99.8	-39.3	255.2	235.7	328.1	365.4
80	65.6	48.7	16.9	144.8	53.4	275.5	240.6	270.1	312.0
-100	-77.3	-57.1	-20.2	-151.3	-54.9	275.8	237.2	414.1	423.8

Table 5-K. Steady-state polarisation data for $PEO_{36}NaBPh_4$ at 85-86°C.

ΔV_a / mV	ΔV / mV	ΔE / mV	$\Delta\phi$ / mV	I^o / μA	I^s / μA	R_e^s / Ω	R_e^o / Ω	R_i^s / Ω	R_i^o / Ω
10	7.7	5.8	1.9	30.7	12.35	146.9	143.4	187.2	182.0
40	31.0	23.3	7.7	123.5	51.2	144.7	143.0	175.9	181.0
-60	-48.6	-36.1	-12.5	-189.9	-94.2	123.0	141.9	121.5	174.1
80	62.8	47.0	15.8	244.6	95.6	155.0	143.4	179.9	183.7

Table 5-L. Ratio of ΔE to ΔV for PEO_xLiClO_4, $PEO_xLiCF_3SO_3$, at 120°C and PEO_xNaBPh_4 at 80-85°C.

PEO_xLiClO_4		$PEO_xLiCF_3SO_3$		PEO_xNaBPh_4	
O:M ratio	$\Delta E/\Delta V$	O:M ratio	$\Delta E/\Delta V$	O:M ratio	$\Delta E/\Delta V$
100	0.628	100	0.367	100	0.738
50	0.648	50	0.421	36	0.746
18	0.718	36	0.509		
15	0.727	18	0.551		
12	0.747				

Table 5-M. Steady-state current fractions of $PEO_{100}LiCF_3SO_3$ at 121-122°C.

ΔV_a / mV	ΔV^s / mV	ΔV^o / mV	I^o /μA	I^s /μA	i_F
5	4.8	4.7	17.3	10.7	0.61
-10	-9.7	-9.2	-33.8	-21.2	0.59
20	19.2	18.5	67.4	41.9	0.60
-40	-38.1	-36.6	-133.0	-79.8	0.58
50	47.5	45.4	165.3	98.7	0.57
60	57.6	54.8	201.3	96.6	0.46
60	56.9	54.5	198.5	116.3	0.56
-70	-66.6	-63.1	-230.3	-120.0	0.49
-80	-76.6	-72.6	-267.1	-134.3	0.48
100	96.1	91.3	325.1	160.3	0.47

Table 5-N. Steady-state current fractions of $PEO_{50}LiCF_3SO_3$ at 120-121°C.

ΔV_a / mV	ΔV^s / mV	ΔV^o / mV	I^o /μA	I^s /μA	i_F
5	4.6	4.3	40.3	22.2	0.51
10	9.3	8.7	81.2	44.6	0.51
20	18.7	17.6	158.5	88.8	0.53
40	37.7	35.4	319.7	169.0	0.50
-60	-57.4	-51.1	-486.6	-225	0.41
-80	-77.3	-68.3	-644.1	-277	0.38
100	97.1	86.7	813.7	318	0.35
-120	-111.0	-101.3	-958.5	-333	0.32

Table 5-O. Steady-state current fractions of $PEO_{36}LiCF_3SO_3$ at 120-121°C.

ΔV_a / mV	ΔV^s / mV	ΔV^o / mV	I^o /μA	I^s /μA	i_F
5	4.7	4.5	52.4	28.2	0.51
-10	-9.3	-8.5	-98.3	-50.0	0.46
20	17.8	16.2	194.9	103.7	0.48
-40	-37.2	-32.7	-382.8	-165.6	0.38
-40	-35.9	-31.8	-367.0	-204	0.49
60	54.0	47.7	555.0	294	0.47
-80	-73.5	-63.3	-735.3	-321	0.38
100	90.8	77.8	909.9	377	0.36

Table 5-P. Steady-state current fractions of $PEO_{18}LiCF_3SO_3$ at 120-121°C.

ΔV_a / mV	ΔV^s / mV	ΔV^o / mV	I^o /μA	I^s /μA	i_F
5	4.6	4.3	78.1	37.6	0.45
-10	-8.9	-7.8	-148.8	-77.2	0.45
20	17.6	15.4	304.4	149.2	0.43
-40	-36.3	-30.4	-595.2	-309	0.43
-60	-54.0	-45.0	-916.0	-468	0.43
-70	-59.2	-46.3	-1005.7	-633	0.49
80	72.4	60.6	1253.9	446	0.30
-80	-74.0	-63.2	-1118.9	-444	0.34
90	71.2	54.7	1195.2	690	0.44
100	87.8	76.5	1432.7	684	0.42

Table 5-Q. Steady-state current fractions of $PEO_{100}LiClO_4$ at 121-122°C.

ΔV_a / mV	ΔV^s / mV	ΔV^o / mV	I^o /μA	I^s /μA	i_F
5	4.6	4.0	37.7	14.7	0.34
-10	-9.1	-7.5	-72.7	-30.1	0.34
20	17.9	14.4	149.8	53.9	0.29
40	36.0	28.0	288.8	94.6	0.25
-80	-73.7	-55.3	-571.0	-163.8	0.22
120	113.1	84.1	839.7	178.9	0.16
200	191.1	138.7	1434.7	207.8	0.11
-300	-289.5	-221.7	-2117.1	-227.0	0.08
600	592.1	429.9	4273.5	216.0	0.04

Table 5-R. Steady-state current fractions of $PEO_{50}LiClO_4$ at 121-122°C.

ΔV_a / mV	ΔV^s / mV	ΔV^o / mV	I^o /μA	I^s /μA	i_F
5	4.4	3.5	81.6	30.8	0.30
-10	-8.9	-6.9	-159.0	-57.9	0.28
20	13.2	12.7	300.8	111.0	0.36
-40	-26.0	-26.1	-602	-203	0.34
60	54.6	37.0	867	206	0.16

Table 5-S. Steady-state current fractions of $PEO_{18}LiClO_4$ at 121-122°C.

ΔV_a / mV	ΔV^s / mV	ΔV^o / mV	I^o /μA	I^s /μA	i_F
5	4.4	3.2	139.3	45.2	0.24
-10	-8.7	-6.2	-274.0	-84.5	0.22
20	16.6	10.4	461.9	168.3	0.23
-40	-33.1	-20.0	-879.1	-328	0.23
-60	-50.6	-30.9	-1373.0	-437	0.19
80	69.5	39.4	1742.9	526	0.17

Table 5-T. Steady-state current fractions of $PEO_{15}LiClO_4$ at 120-122°C.

ΔV_a / mV	ΔV^s / mV	ΔV^o / mV	I^o /μA	I^s /μA	i_F
5	4.1	2.3	124.1	43.3	0.20
-10	-8.1	-4.6	-238.7	-90.4	0.22
20	17.2	11.3	591.7	203	0.23
-40	-34.4	-22.8	-1208.5	-405	0.22
60	55.8	45.3	2264.2	633	0.23
-80	-68.9	-41.5	-2185.8	-785	0.22
100	83.5	47.4	2493.8	889	0.20
-140	-121.6	-60.9	-3325.4	-1380	0.21

Table 5-U. Steady-state current fractions of $PEO_{12}LiClO_4$ at 119-120°C.

ΔV_a / mV	ΔV^s / mV	ΔV^o / mV	I^o /μA	I^s /μA	i_F
5	4.1	2.4	127.6	43.7	0.20
-10	-8.1	-4.6	-232.6	-86.7	0.21
20	15.2	8.1	414.9	167.8	0.22
-40	-31.0	-16.1	-823.0	-340.2	0.21
80	65.9	36.1	1877.9	715.8	0.21

Table 5-V. Steady-state current fractions of $PEO_{100}NaBPh_4$ at 81-83°C.

ΔV_a / mV	ΔV^s / mV	ΔV^o / mV	I^o /μA	I^s /μA	i_F
10	7.8	4.4	18.8	7.32	0.22
20	14.6	7.8	33.5	14.3	0.23
-40	-31.5	-17.5	-73.3	-28.4	0.22
-60	-47.1	-23.5	-99.8	-39.3	0.20
80	65.6	34.8	144.8	53.4	0.20
-100	-77.3	-35.9	-151.3	-54.9	0.17

Table 5-W. Steady-state current fractions of $PEO_{36}NaBPh_4$ at 85-86°C.

ΔV_a / mV	ΔV^s / mV	ΔV^o / mV	I^o /μA	I^s /μA	i_F
10	7.7	4.4	30.7	12.35	0.23
40	31.0	17.6	123.5	51.2	0.24
-60	-48.6	-26.9	-189.9	-94.2	0.27
80	62.8	35.1	244.6	95.6	0.22

Table 5-X. Limiting current fractions of PEO_xLiClO_4 and $PEO_xLiCF_3SO_3$ at 120°C.

$LiClO_4$		$LiCF_3SO_3$	
O:M ratio	i_{Fl}	O:M ratio	i_{Fl}
100	0.34	100	0.60±0.01
50	0.29±0.01	50	0.52±0.01
18	0.23±0.01	36	0.49±0.02
15	0.22±0.01	18	0.44±0.01
12	0.21±0.01		

Table 5-Y. Limiting current fractions of PEO_xLiClO_4 at various temperatures.

O:M ratio	T /°C	i_{Fl}
8	95.4	0.16 ± 0.02
	110.5	0.18 ± 0.02
	127.5	0.20 ± 0.02
	141.8	0.21 ± 0.02
12	95.5	0.20 ± 0.02
	107.0	0.22 ± 0.01
	121.0	0.26 ± 0.01
	137.0	0.30 ± 0.01
50	98.0	0.23 ± 0.01
	108.8	0.26 ± 0.01
	123.7	0.30 ± 0.01
	138.6	0.33 ± 0.01
100	91.2	0.26 ± 0.01
	103.2	0.29 ± 0.01
	114.5	0.32 ± 0.01
	129.0	0.36 ± 0.01
	140.0	0.39 ± 0.01

Table 5-Z. Comparison of electrolyte resistances found from FRA* and $\Delta\phi/I^s$† for $LiClO_4$- and $LiCF_3SO_3$-based polymer electrolytes.

$LiCF_3SO_3$

O:M ratio	Resistance (FRA) /Ω	Resistance ($\Delta\phi/I^s$) / Ω
100	274	286
50	107.4	110.6
36	85.6	89.3
18	50.8	53.6

$LiClO_4$

O:M ratio	Resistance (FRA) /Ω	Resistance ($\Delta\phi/I^s$) / Ω
100	100.3	110.1
50	43.0	41.4
18	22.7	26.3
15	19.0	22.9
12	19.3	23.0

* These are averages of the electrolyte resistances before polarisation.

† These are averages of data before deviation of the I^s-ΔV response.

Figure 5-1. Looping behaviour of FRA due to finite time required for analysis.

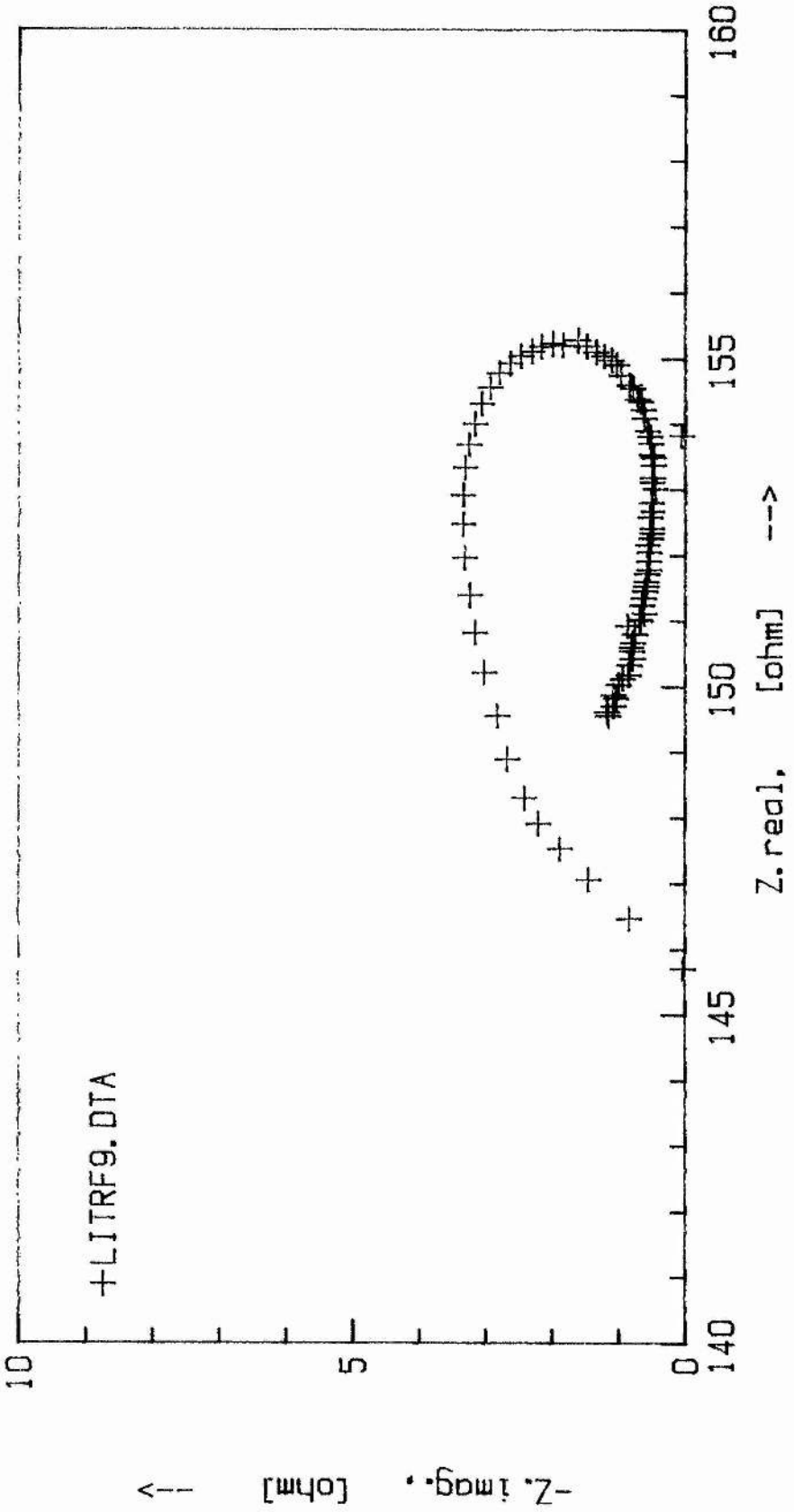

Figure 5-2. Schematic resistivity-concentration graph for a polymer electrolyte, demonstrating increase in average resistivity due to polarisation.

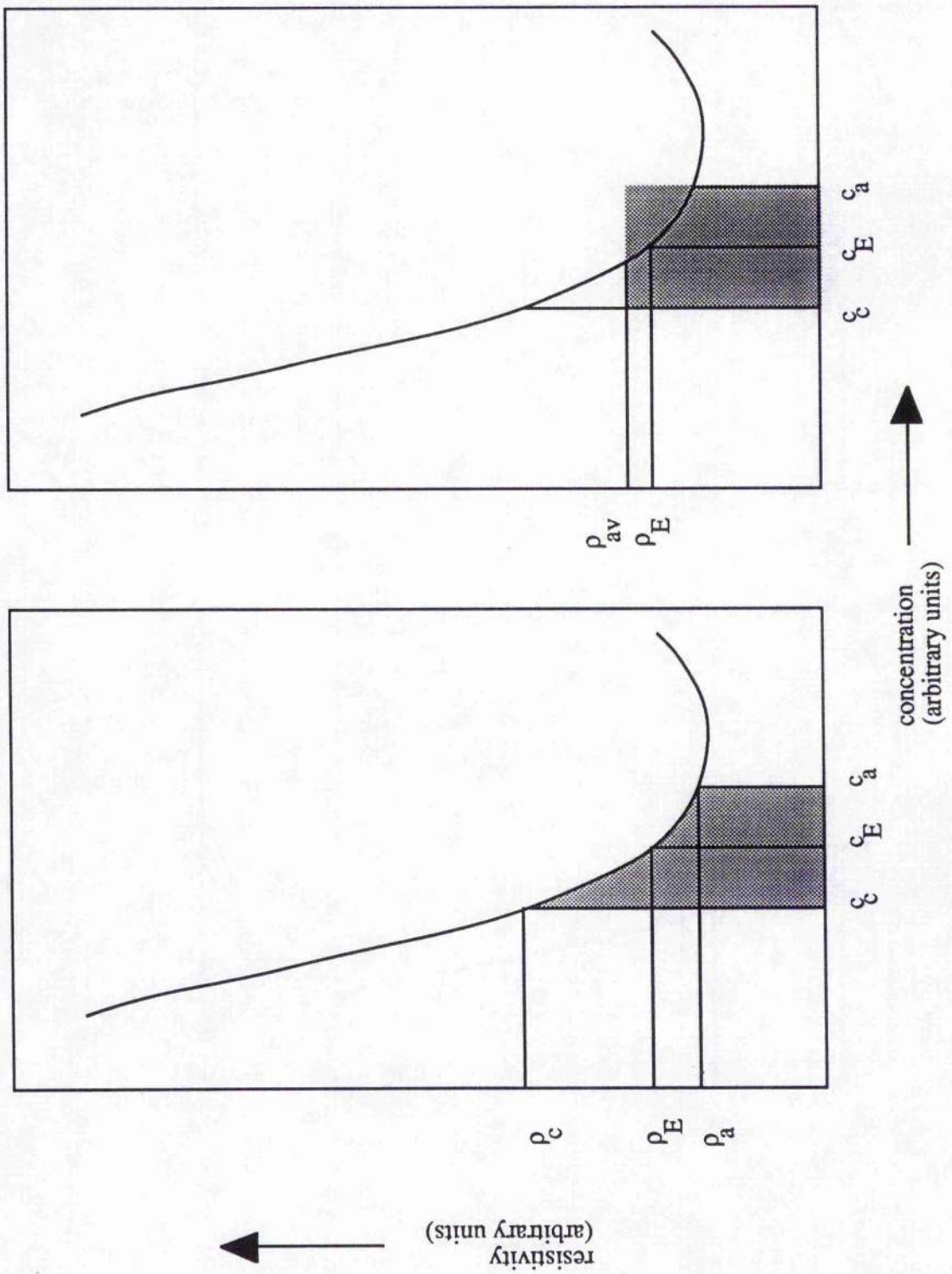

Figure 5-3. Schematic resistivity-concentration graph for $PEO_{36}LiCF_3SO_3$, demonstrating decrease in average resistivity due to polarisation.

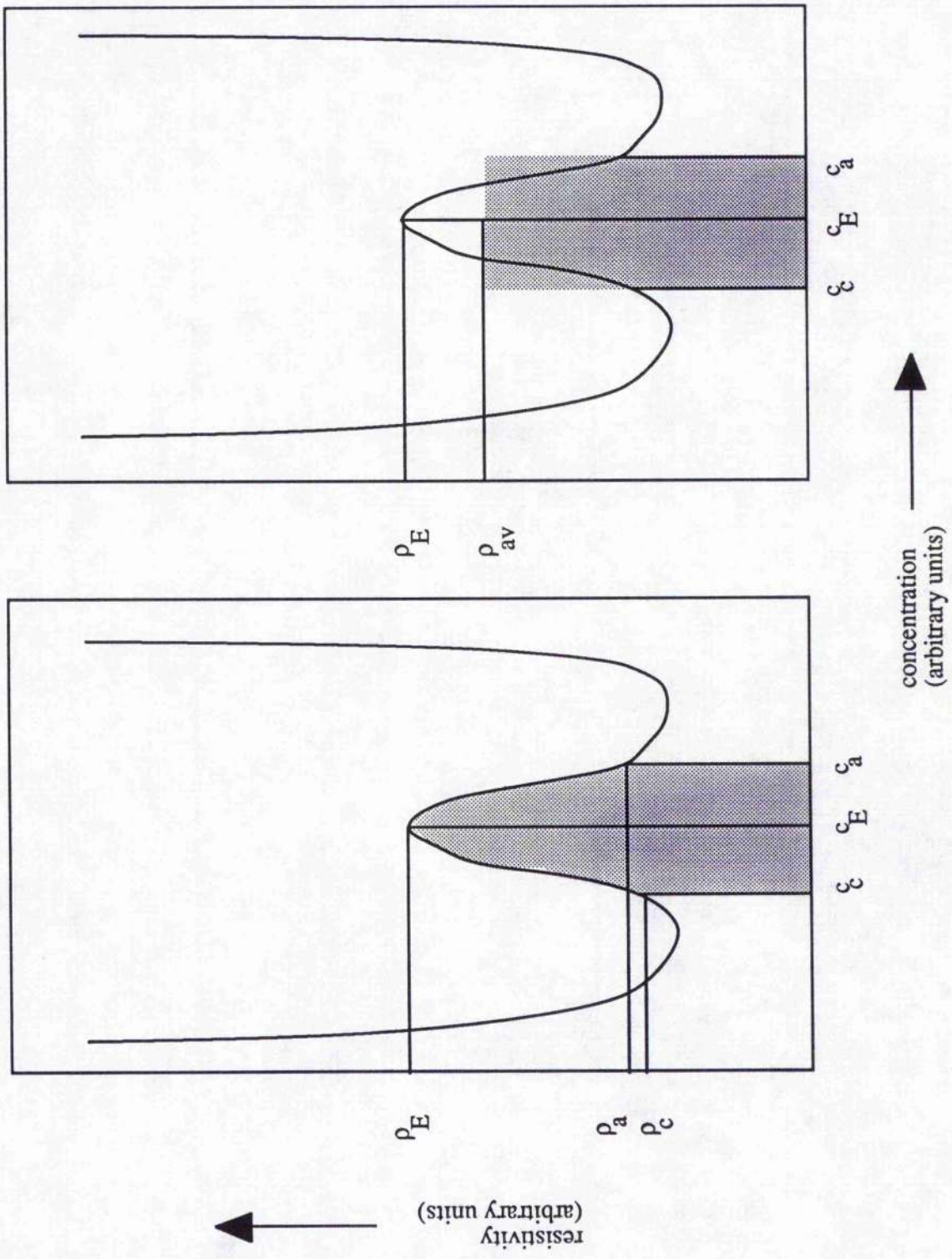

Figure 5-4. Initial and steady-state electrolyte resistances for PEO_xLiClO_4, x = 12, 15, 18, 50, 100.

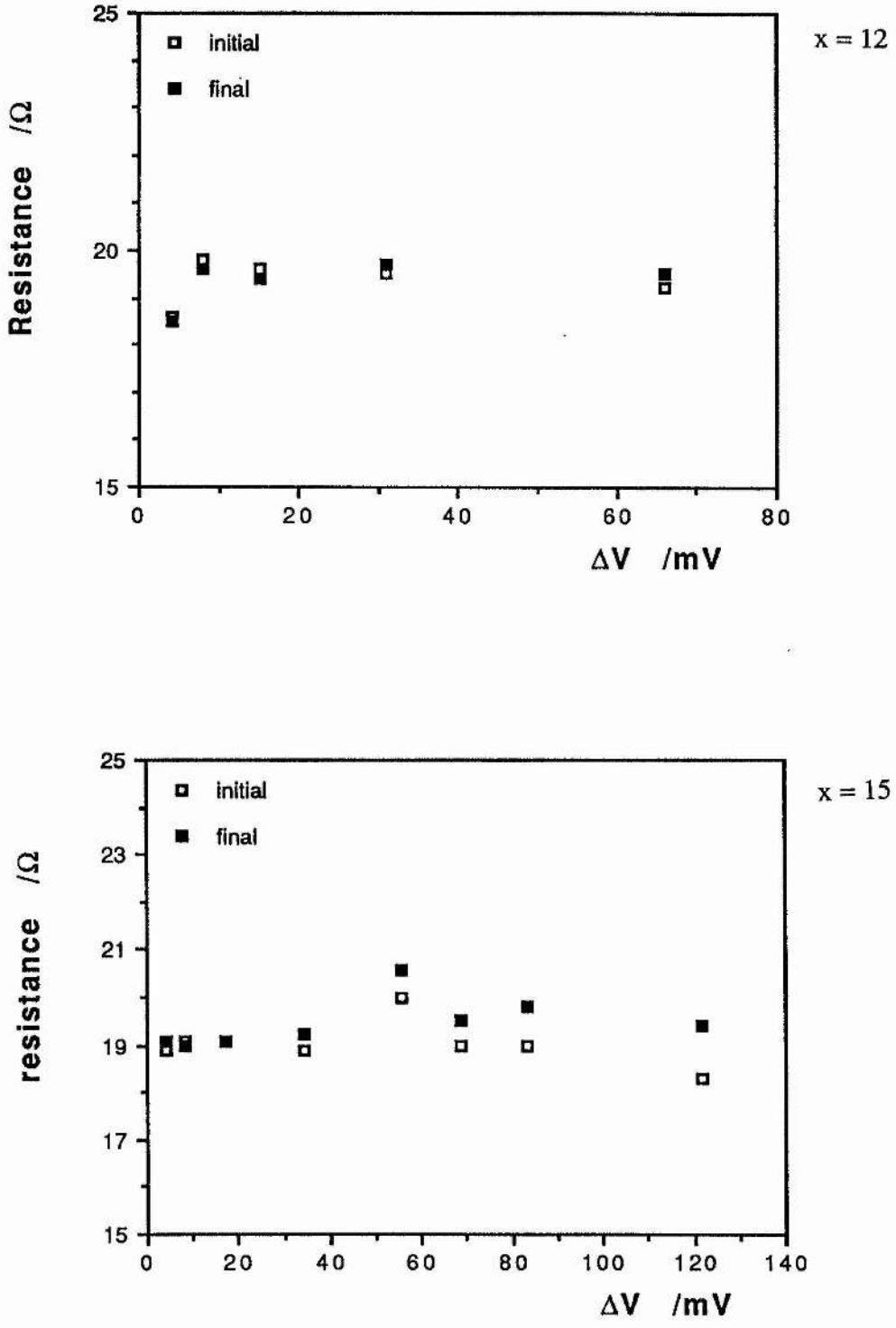

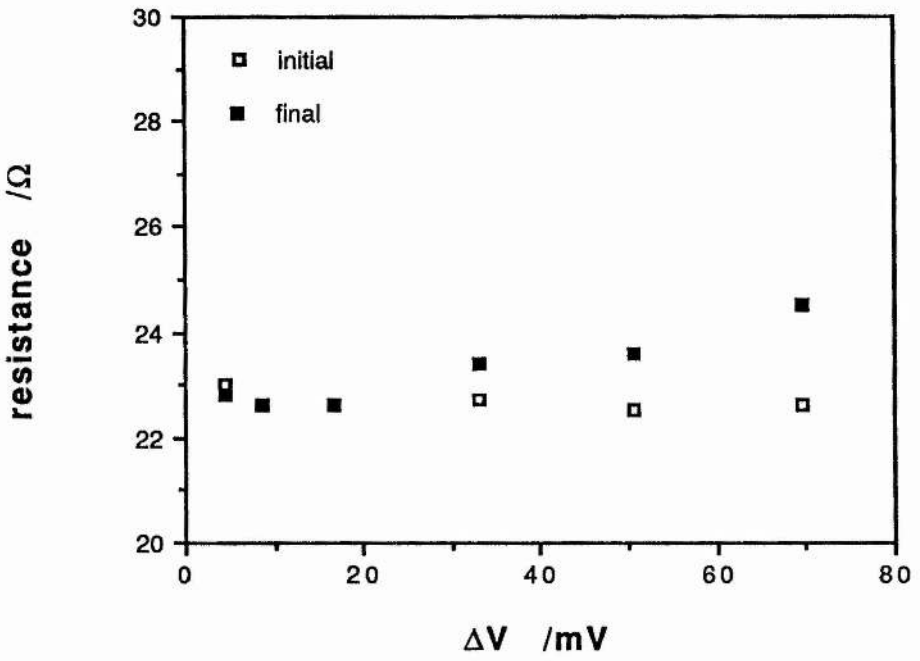
initial
final
resistance /Ω
ΔV /mV
30
28
26
24
22
20
0
20
40
60
80

x = 18

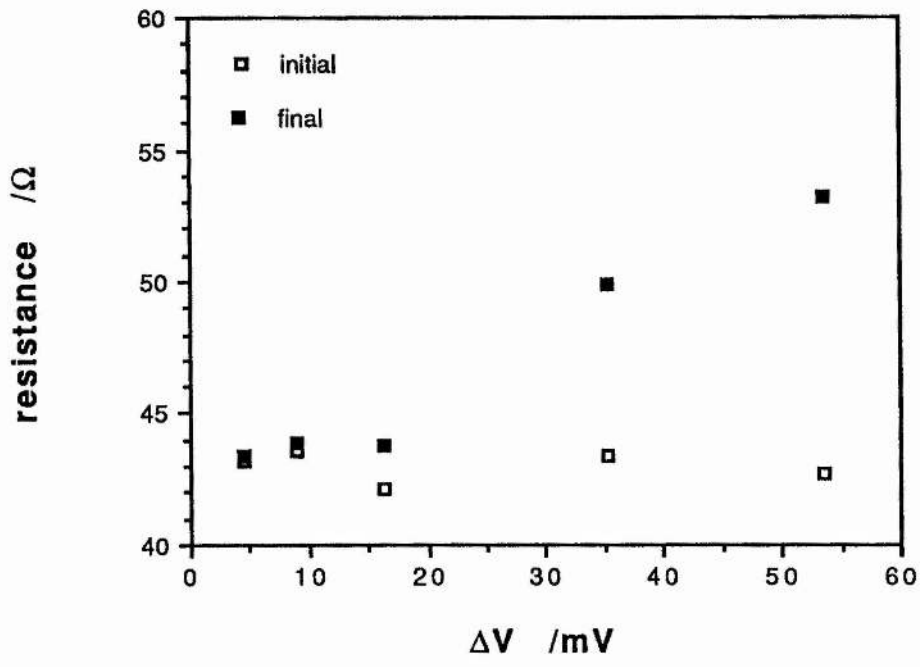
initial
final
resistance /Ω
ΔV /mV
60
55
50
45
40
0
10
20
30
40
50
60

x = 50

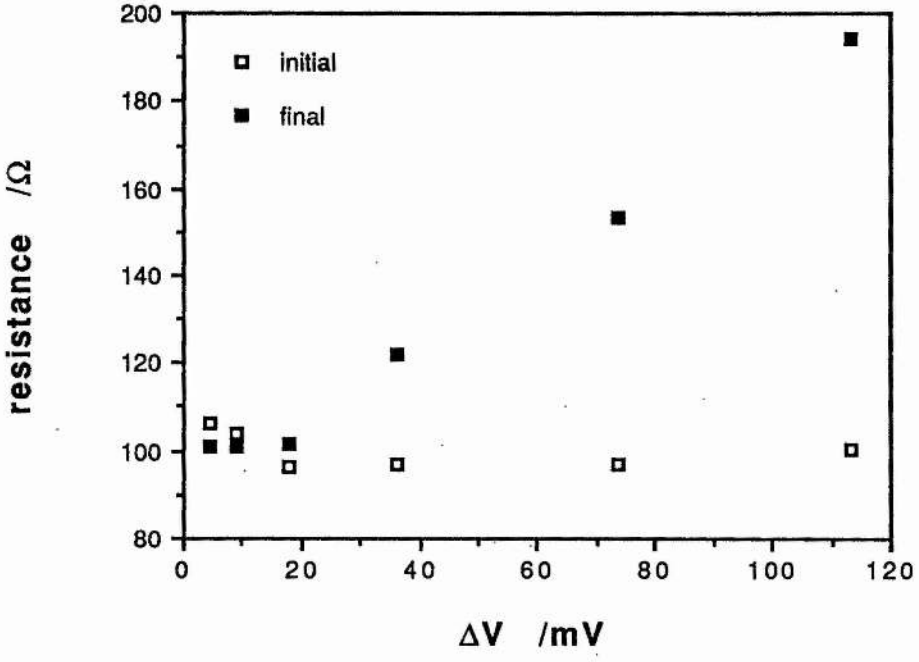
initial
final
resistance /Ω
ΔV /mV
200
180
160
140
120
100
80
0
20
40
60
80
100
120

x = 100

Figure 5-5. Initial and steady-state electrolyte resistances for $PEO_xLiCF_3SO_3$, x = 18, 36, 50, 100.

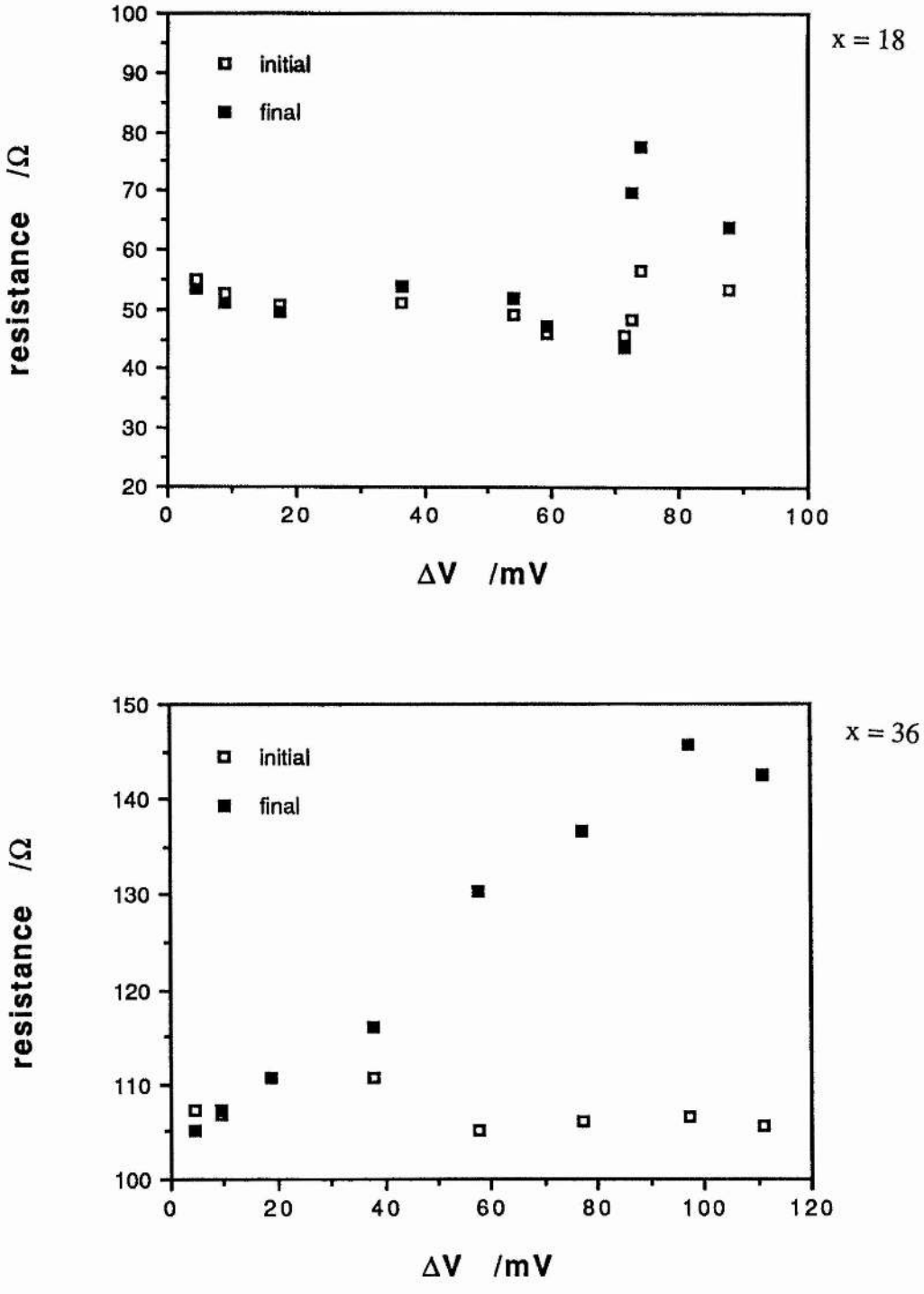

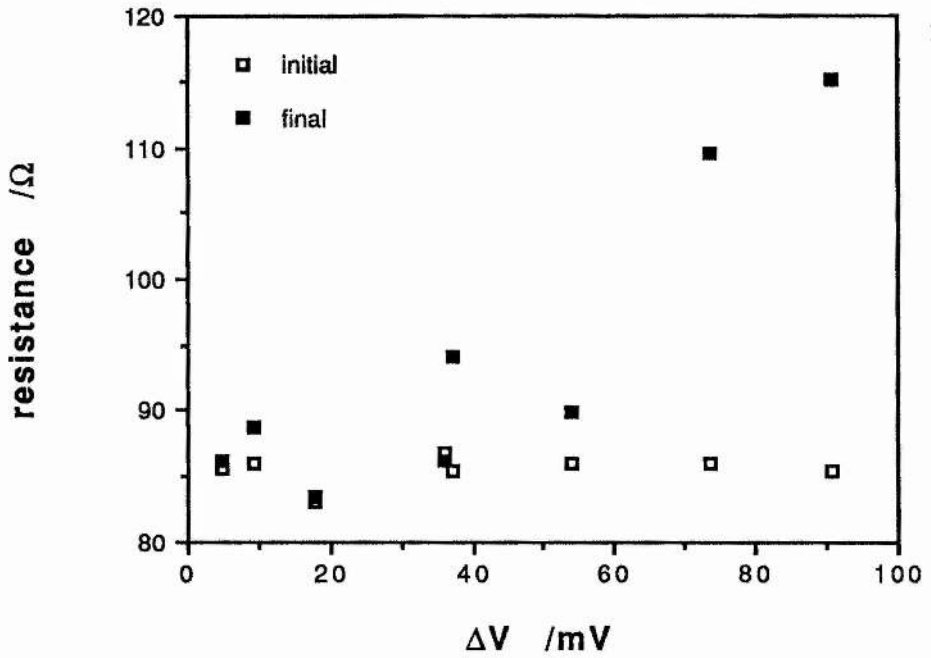
x = 50
initial
final
resistance /Ω
120
110
100
90
80
0
20
40
60
80
100
ΔV /mV

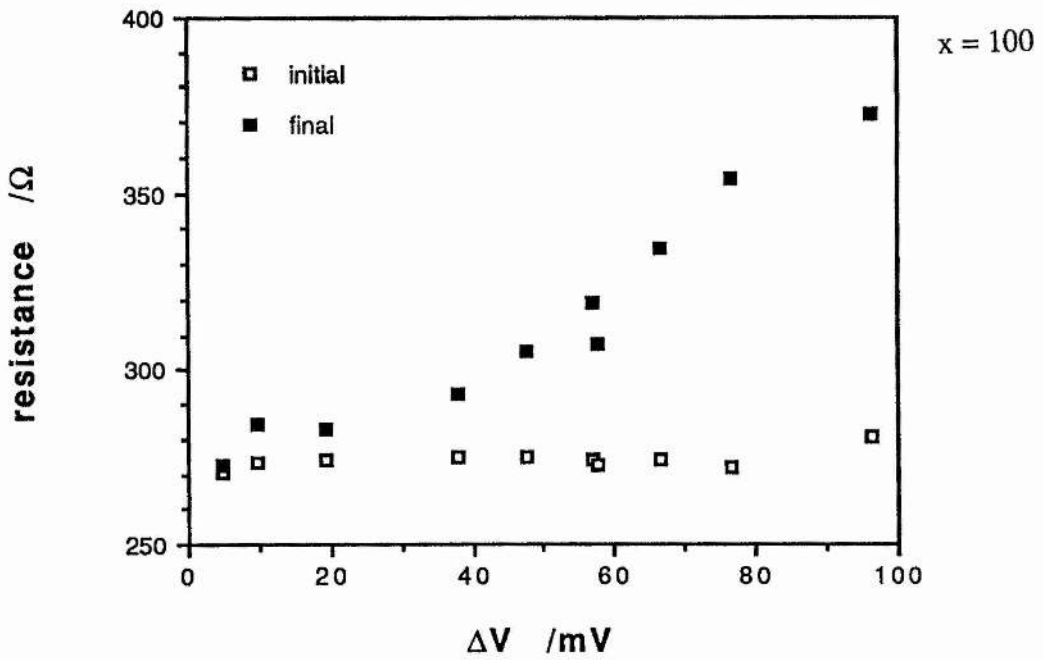
x = 100
initial
final
resistance /Ω
400
350
300
250
0
20
40
60
80
100
ΔV /mV

Figure 5-6. Initial and steady-state electrolyte resistances for PEO_xNaBPh_4, x = 36, 100.

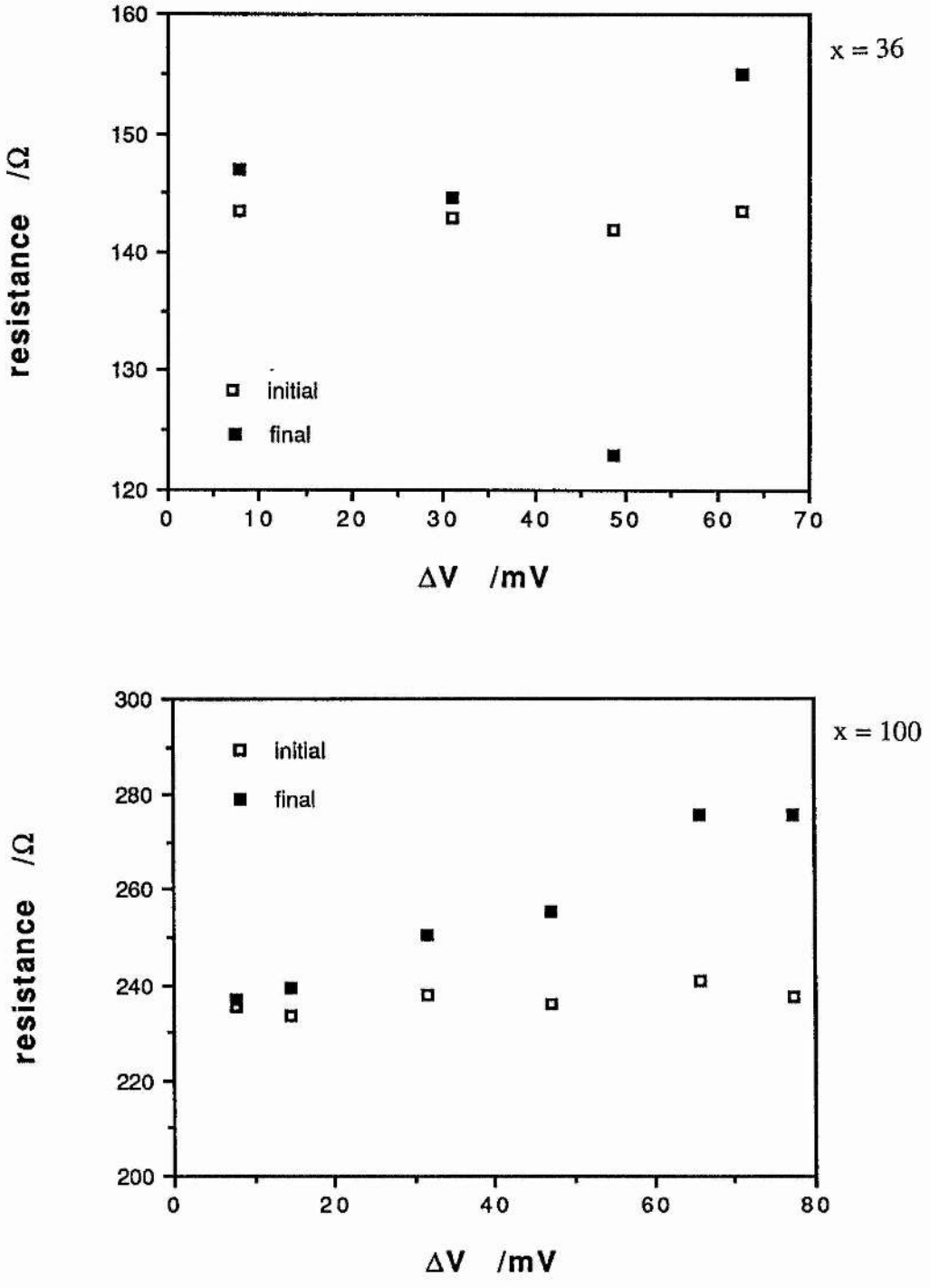

Figure 5-7. Two impedance diagrams differing only in electrolyte resistance, leading to different dc resistances.

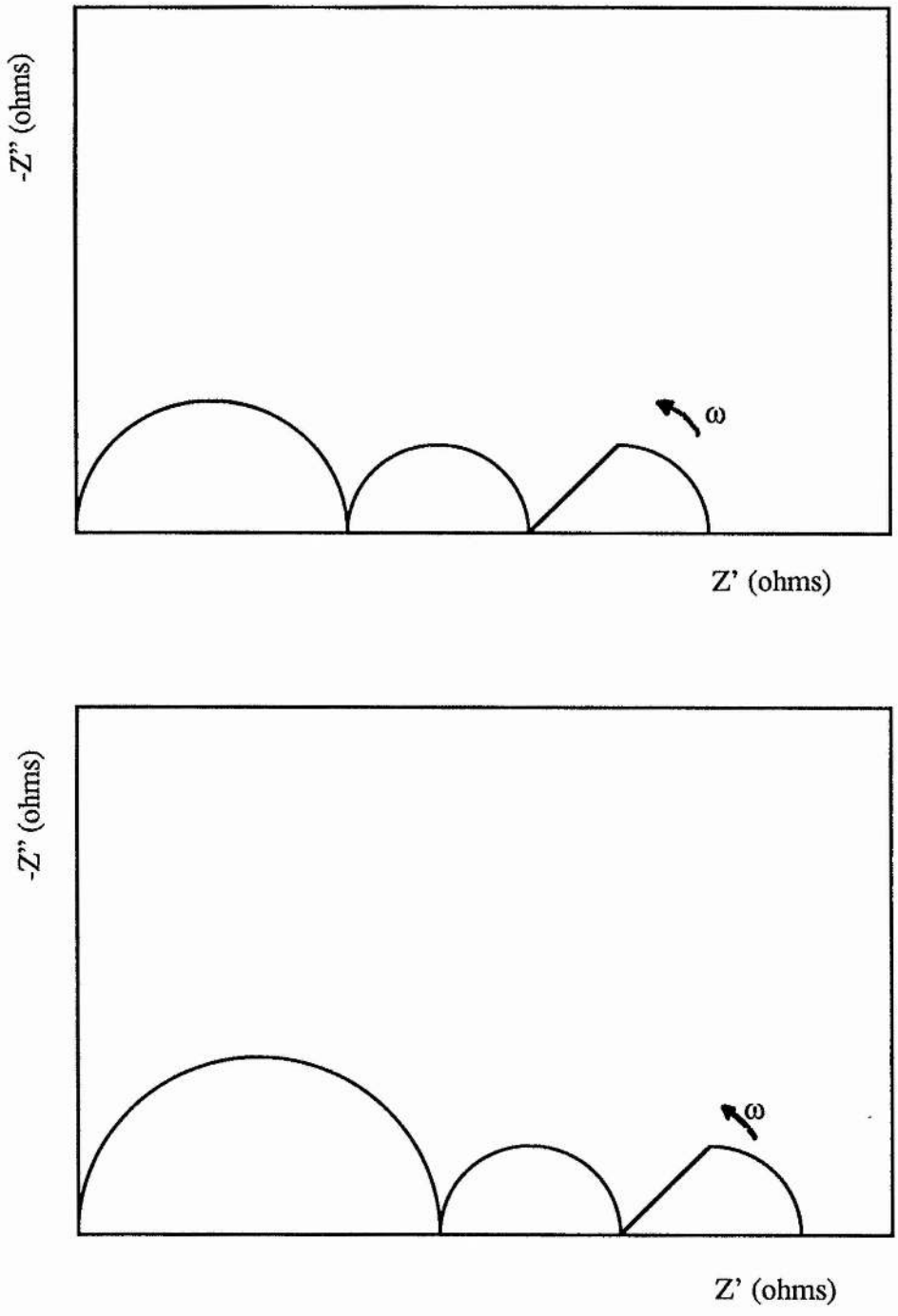

Figure 5-8. Extension of an impedance diagram below the real axis.

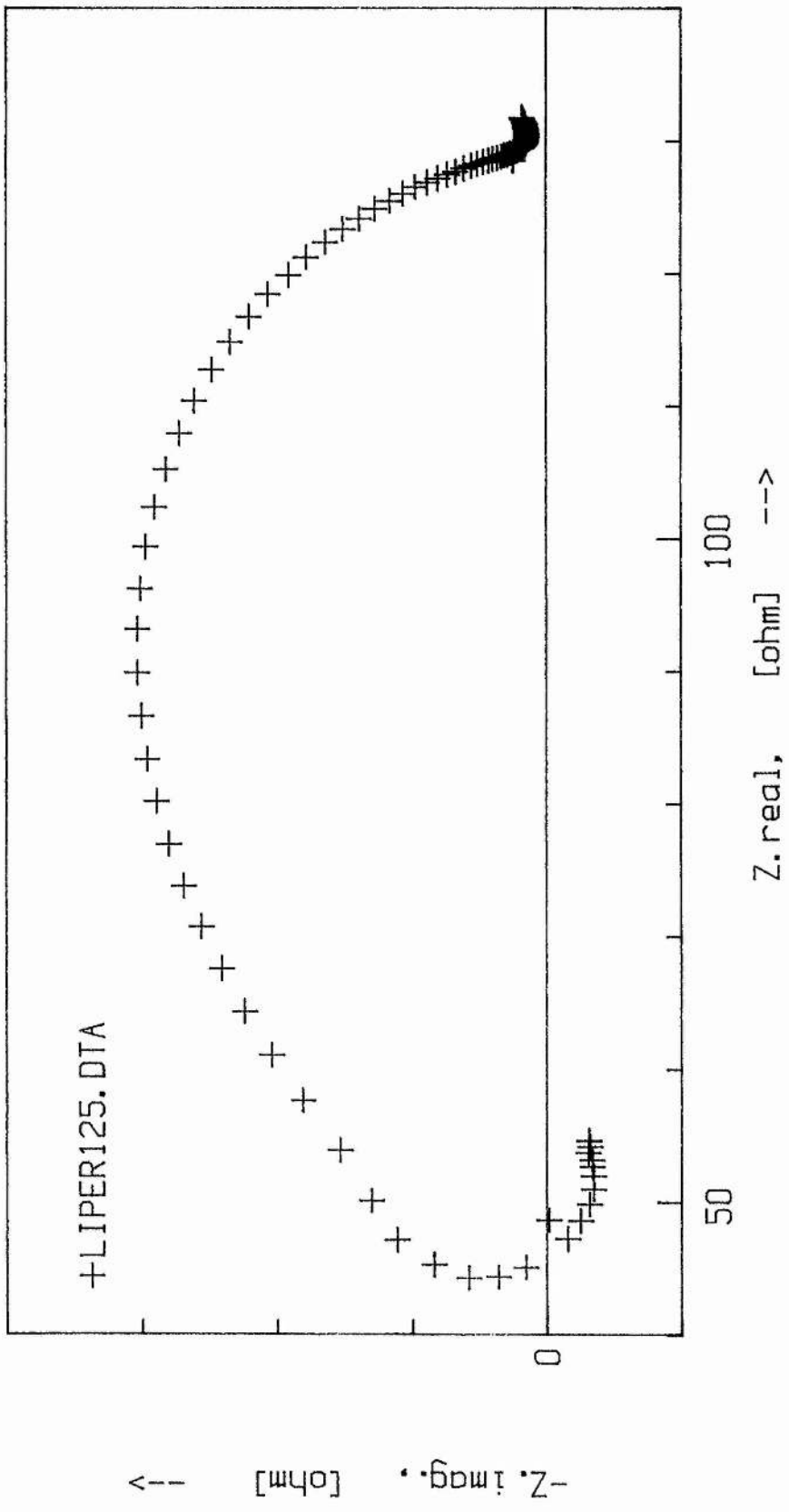

Figure 5-9. Extrapolation of low-frequency impedance data to provide a high frequency intercept.

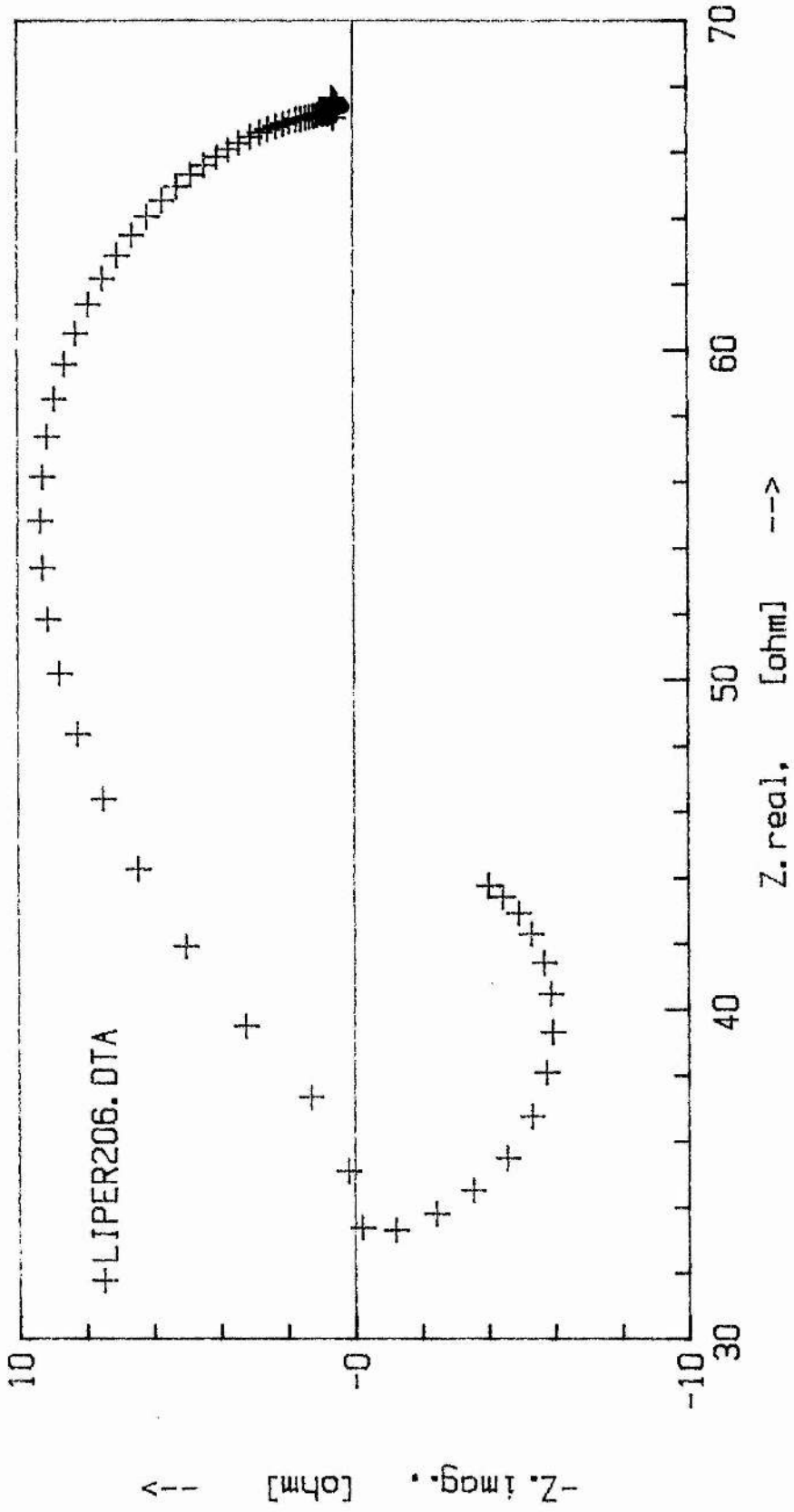

Figure 5-10. Decrease in ΔE with time for a PEO_xLiClO_4 polymer electrolyte at steady-state.

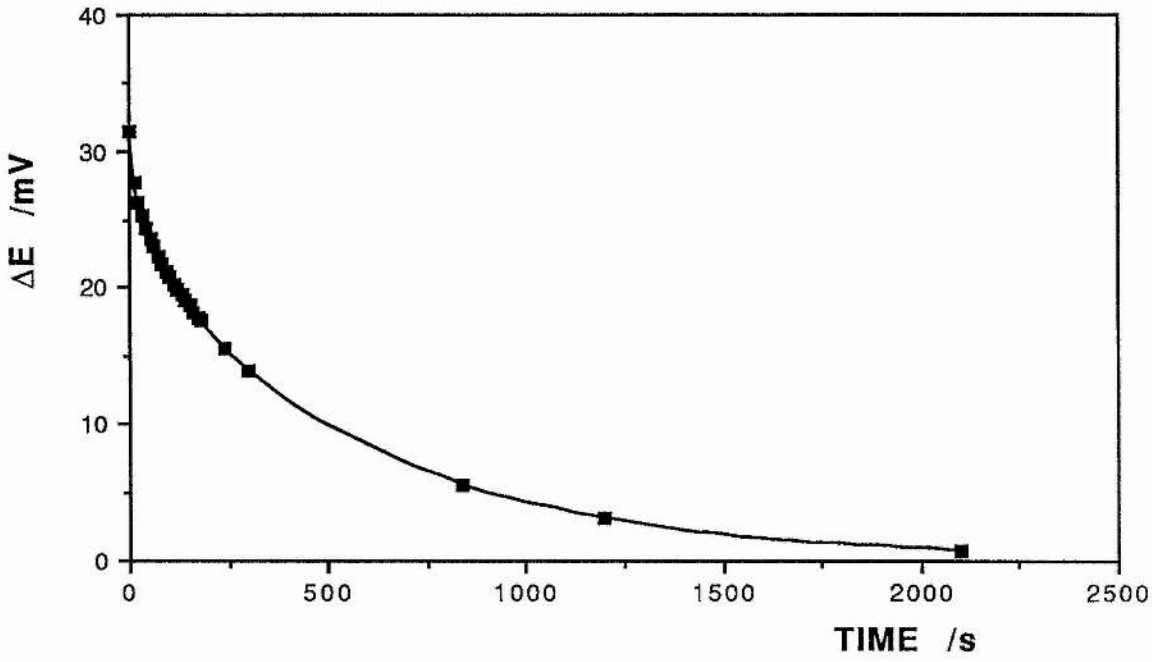

Figure 5-11. Variation in ΔE with ΔV for PEO_xLiClO_4 at 120°C, x = 12, 15, 18, 50, 100.

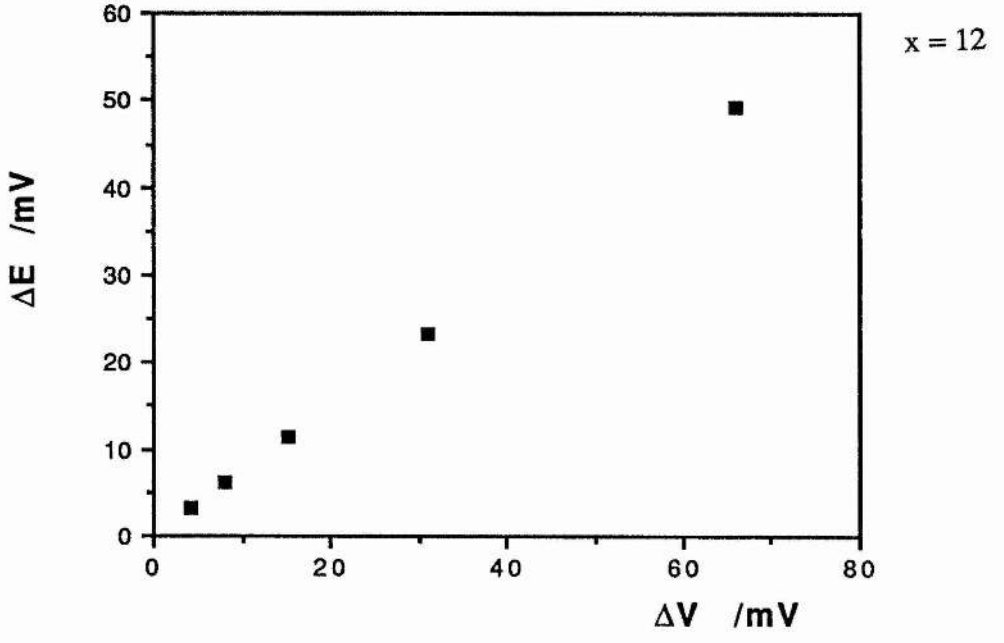

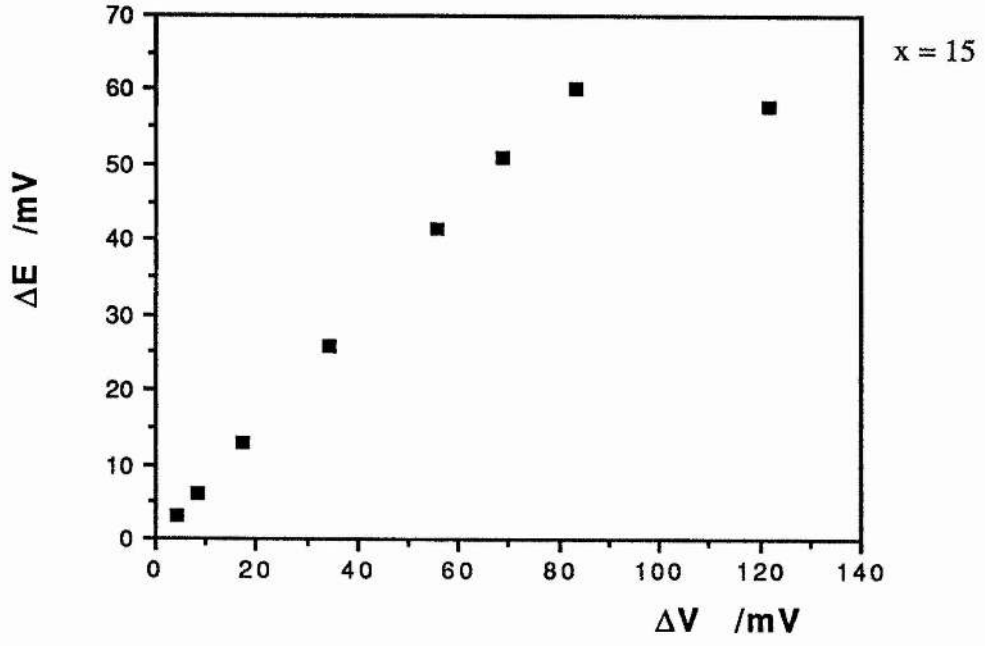

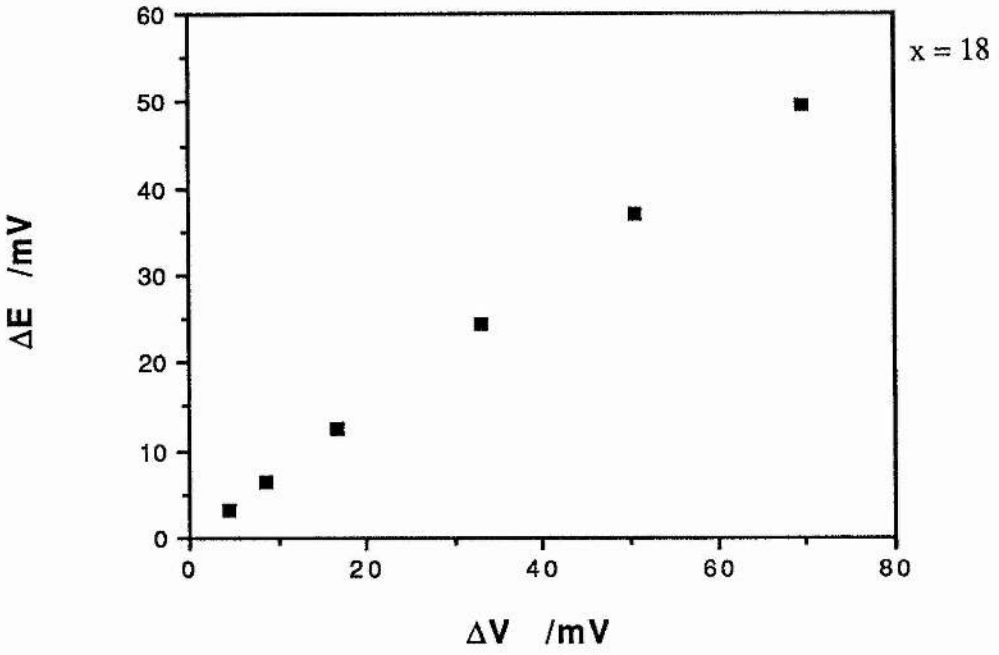
x = 18
ΔE /mV
ΔV /mV
0
10
20
30
40
50
60
0
20
40
60
80

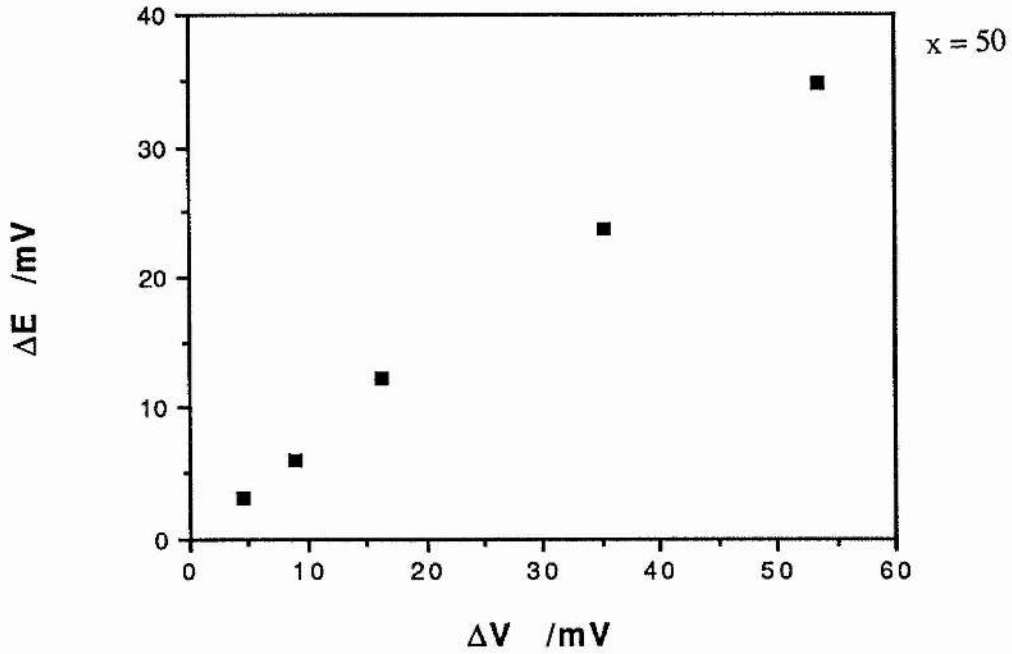
x = 50
ΔE /mV
ΔV /mV
0
10
20
30
40
0
10
20
30
40
50
60

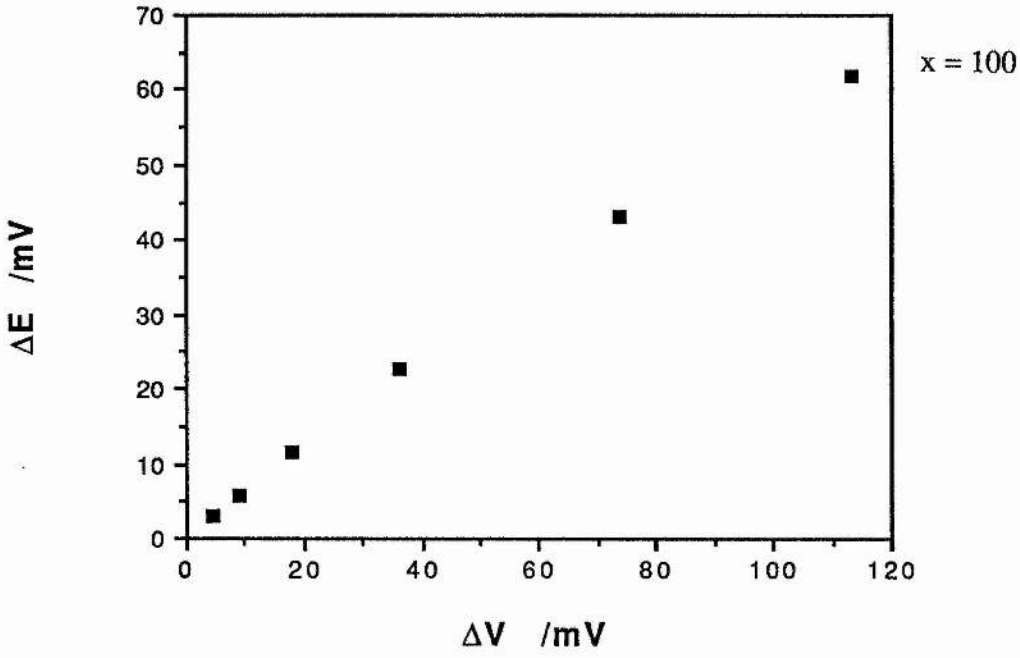
70
60
50
40
30
20
10
0
0
20
40
60
80
100
120
ΔE /mV
ΔV /mV
x = 100

Figure 5-12. Variation in ΔE with ΔV for $PEO_xLiCF_3SO_3$ at 120°C, x = 18, 36, 50, 100.

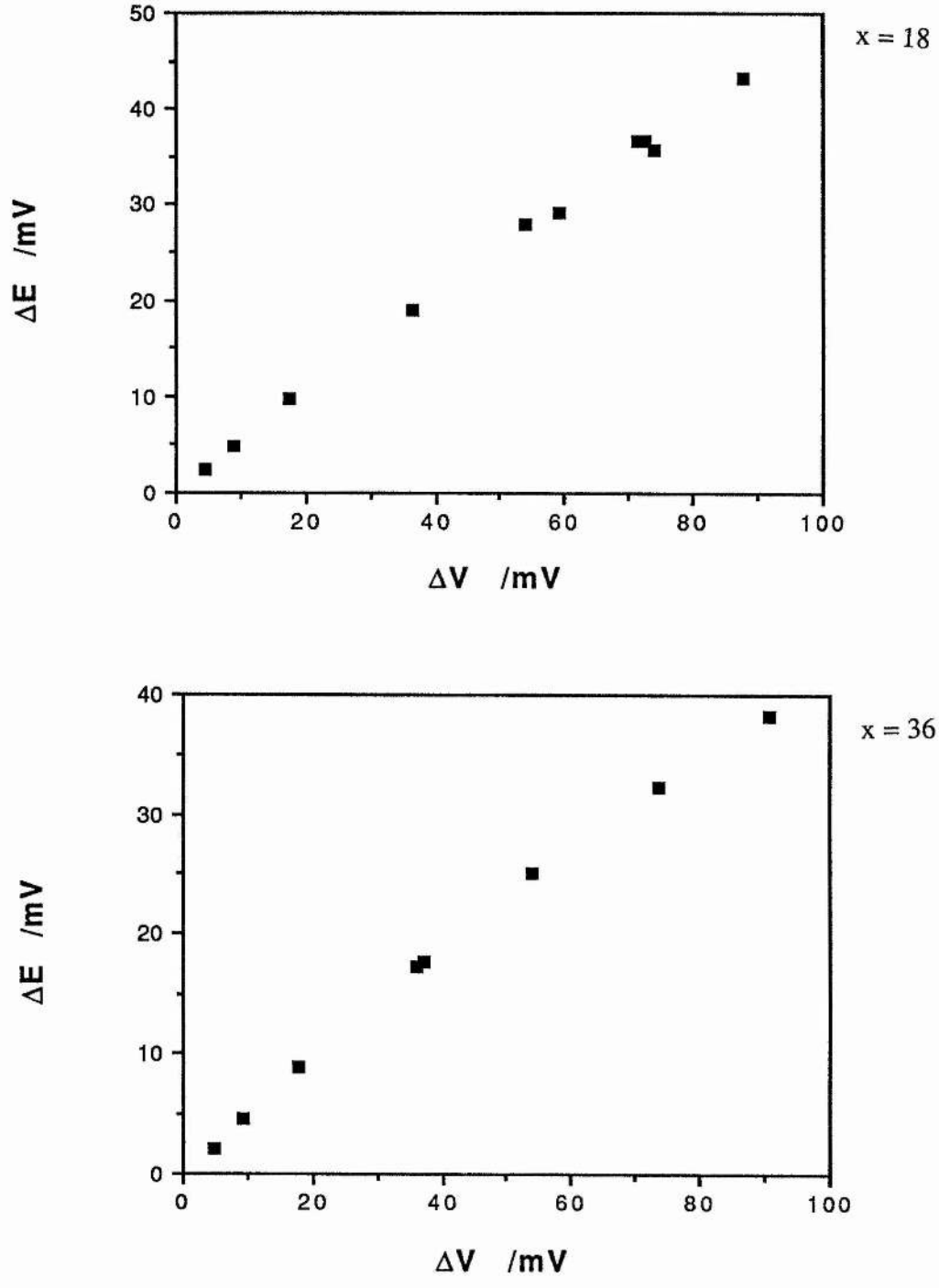

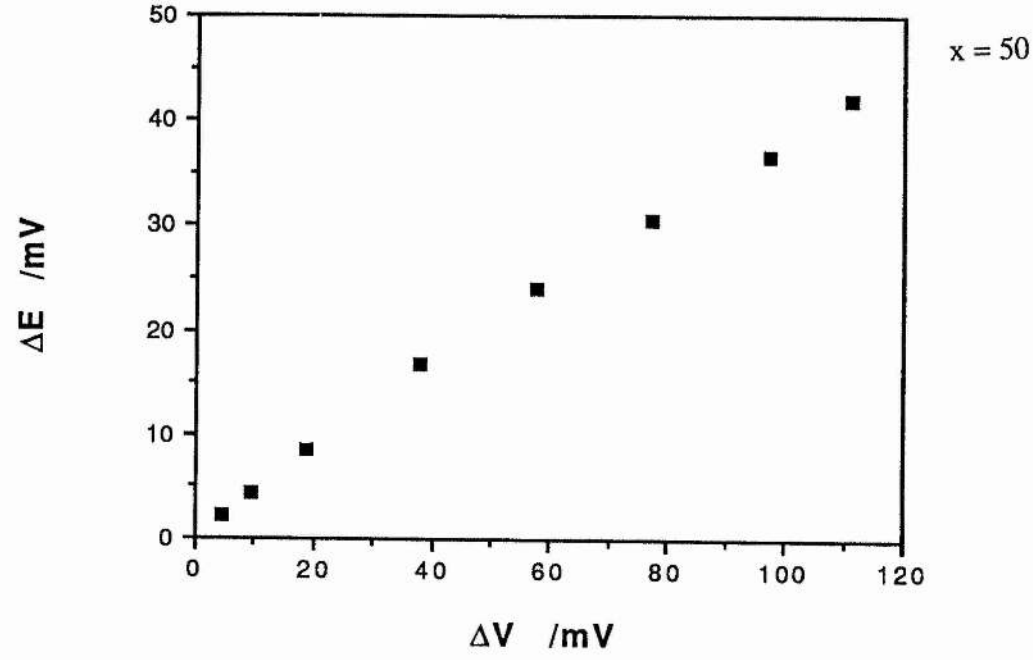
50
40
30
20
10
0
0
20
40
60
80
100
120
ΔE /mV
ΔV /mV
x = 50

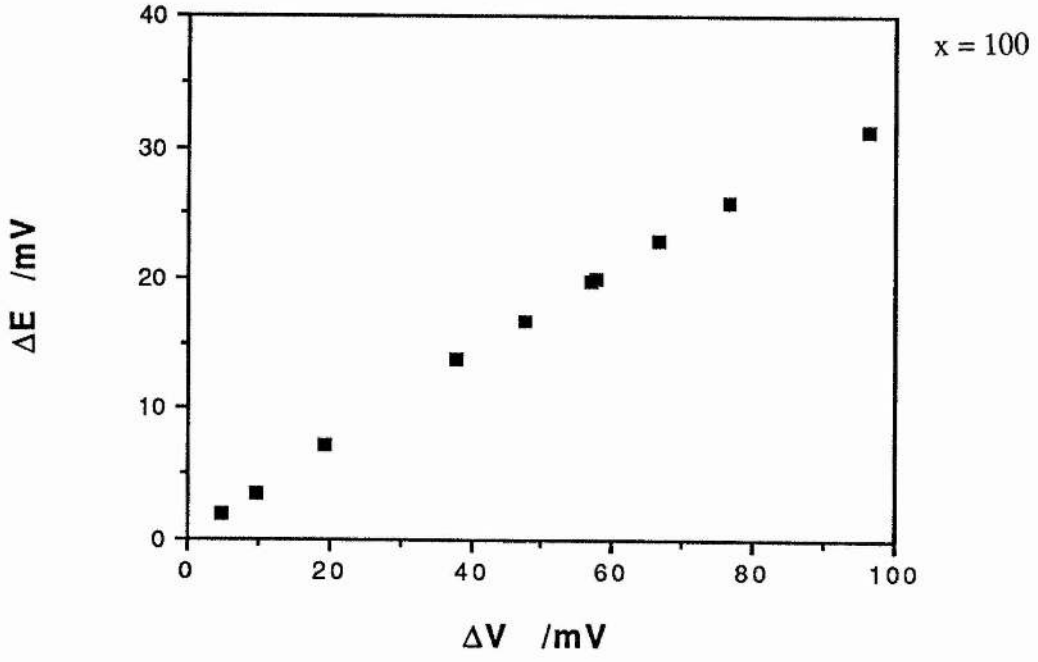
40
30
20
10
0
0
20
40
60
80
100
ΔE /mV
ΔV /mV
x = 100

Figure 5-13. Variation in ΔE with ΔV for PEO_xNaBPh_4 at 85°C, x = 36, 100.

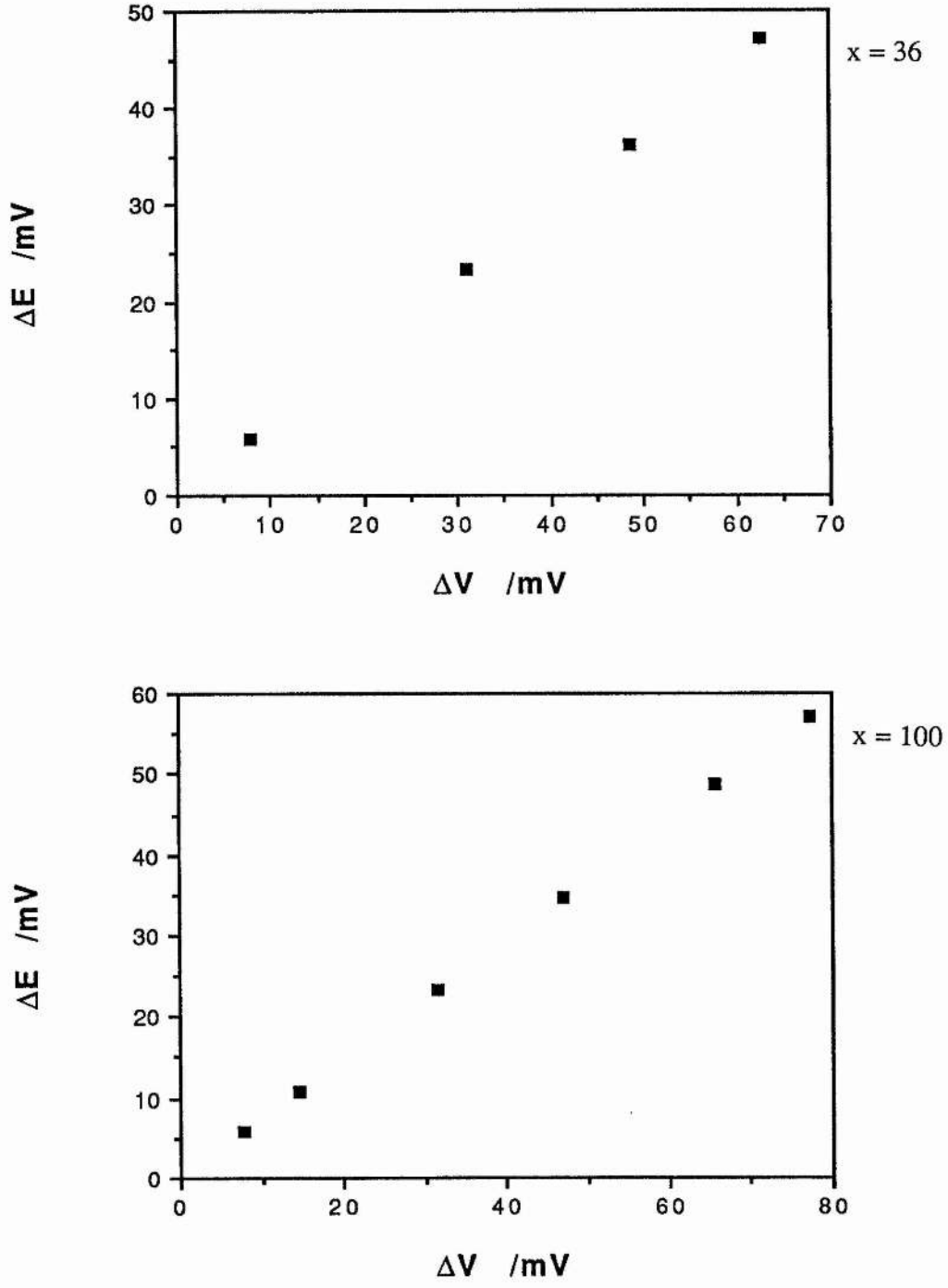

Figure 5-14. Variation in $\Delta E/\Delta V$ with concentration for PEO_xLiClO_4 at 120°C, x = 12, 15, 18, 50, 100; $PEO_xLiCF_3SO_3$ at 120°C, x = 18, 36, 50, 100; and PEO_xNaBPh_4 at 85°C, x = 36, 100.

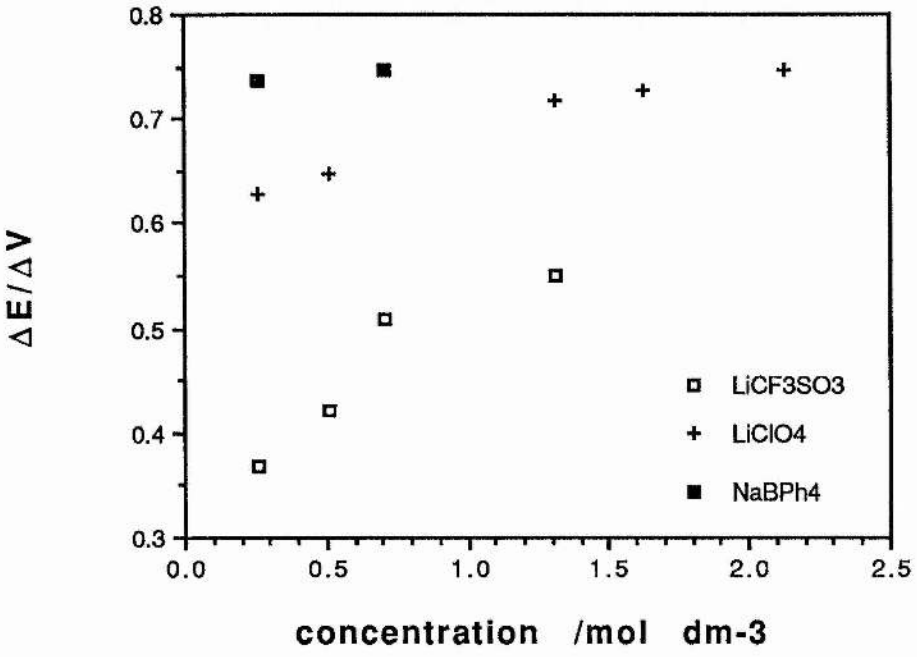

Figure 5-15. Concentration-distance diagram for a polarised electrolyte containing M^+ and X^- ions and MX ion-pairs in the presence of enhanced ion-pair breakdown in the vicinity of the electrodes.

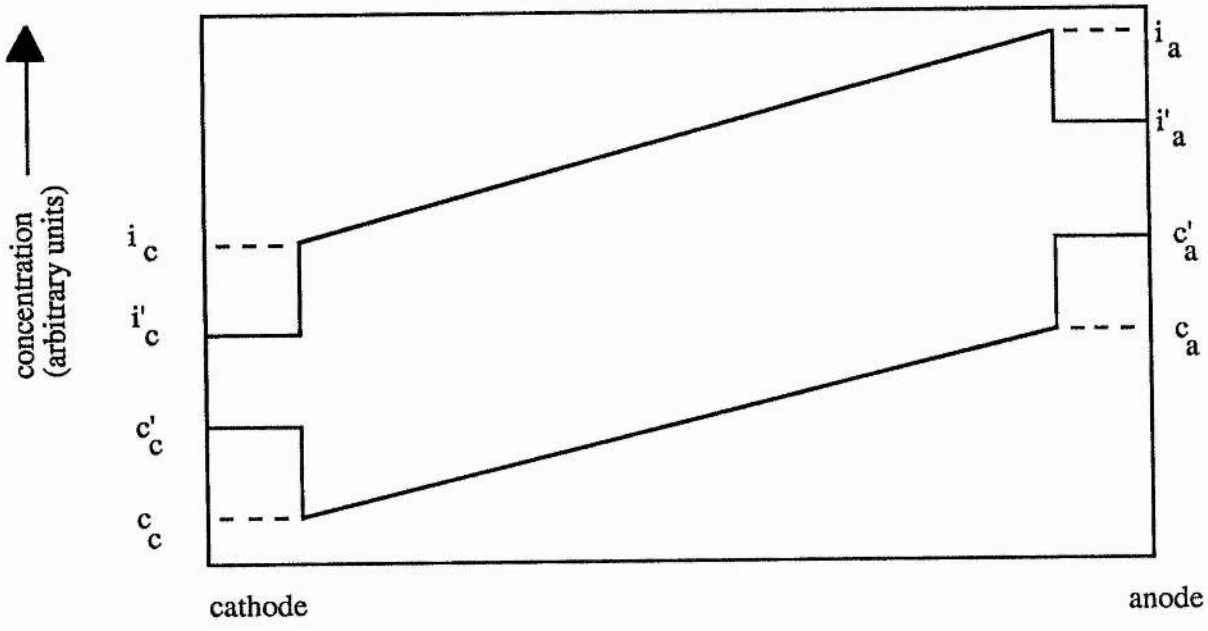

Figure 5-16. Variation in steady-state current with applied potential difference for PEO_xLiClO_4 at 120°C, x = 12, 15, 18, 50, 100.

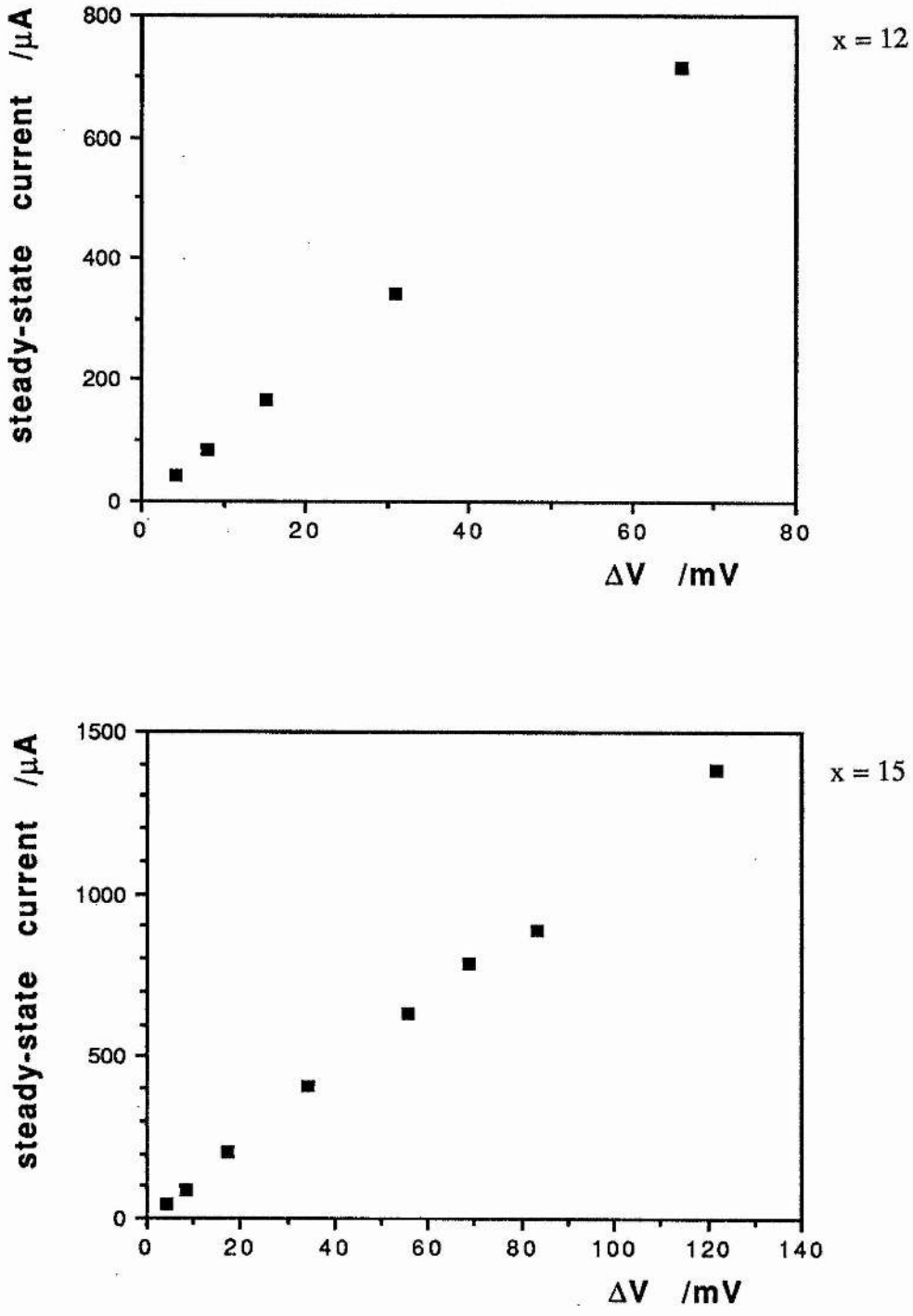

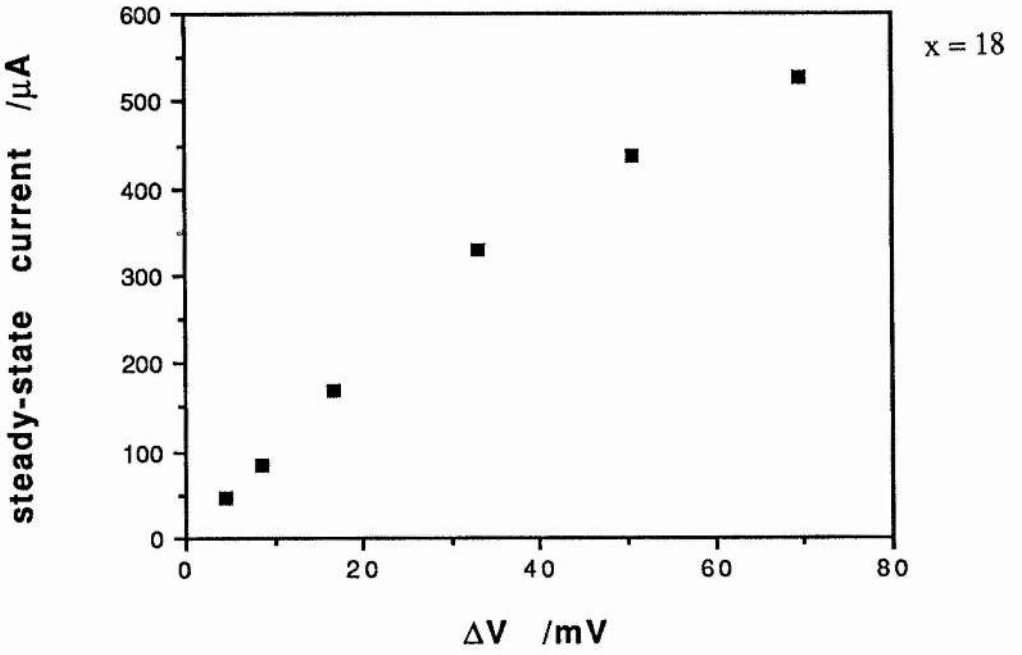
steady-state current /μA
600
500
400
300
200
100
0
0
20
40
60
80
ΔV /mV
x = 18

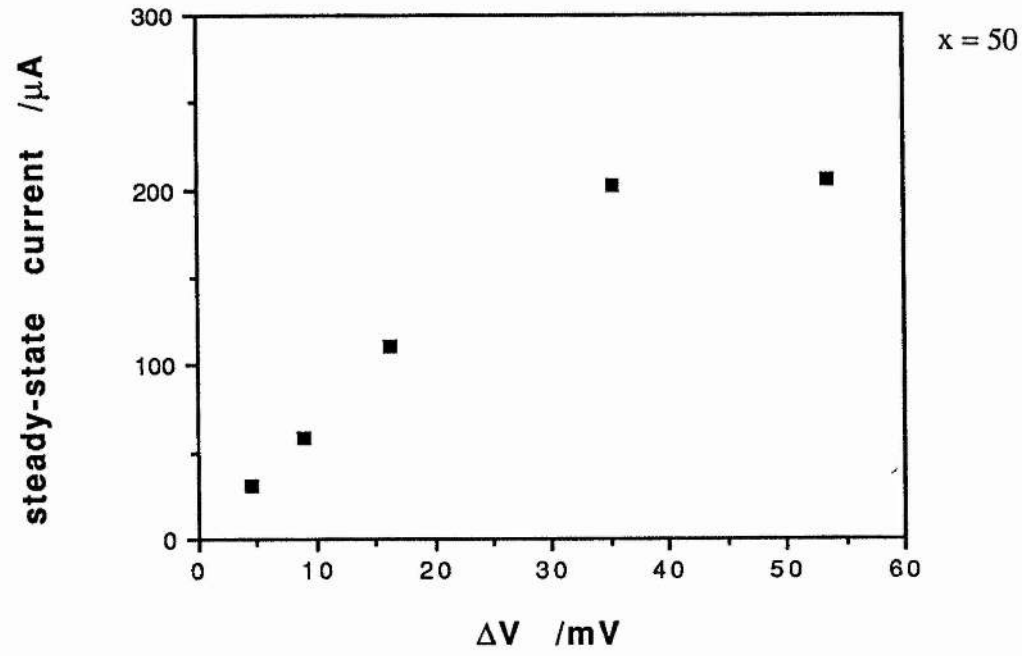
steady-state current /μA
300
200
100
0
0
10
20
30
40
50
60
ΔV /mV
x = 50

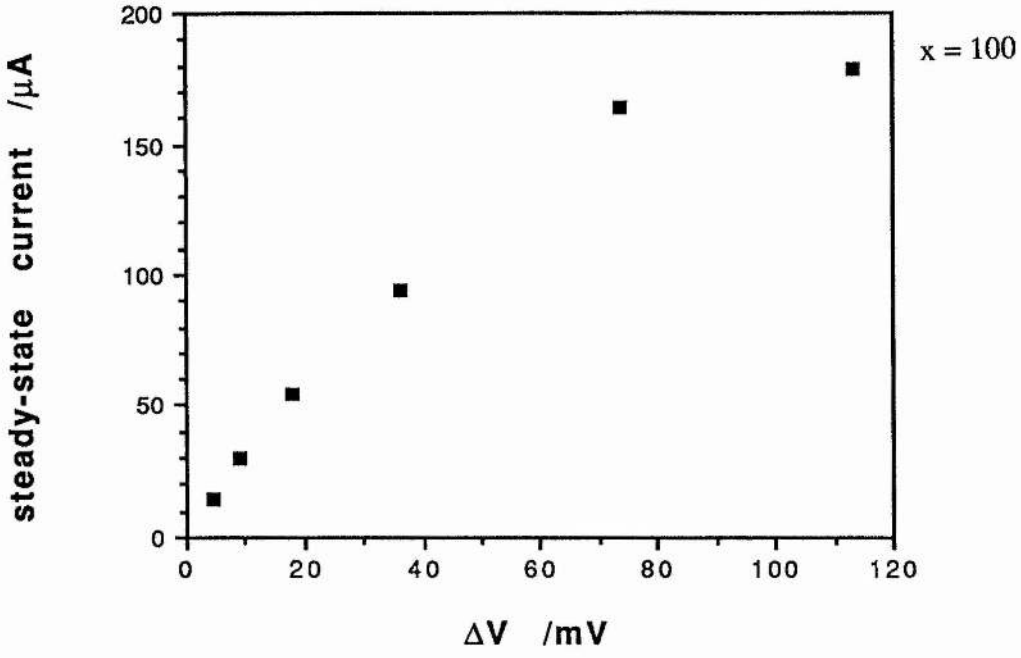
steady-state current /μA
200
150
100
50
0
0
20
40
60
80
100
120
ΔV /mV
x = 100

Figure 5-17. Variation in steady-state current with applied potential difference for $PEO_xLiCF_3SO_3$ at 120°C, x = 18, 36, 50, 100.

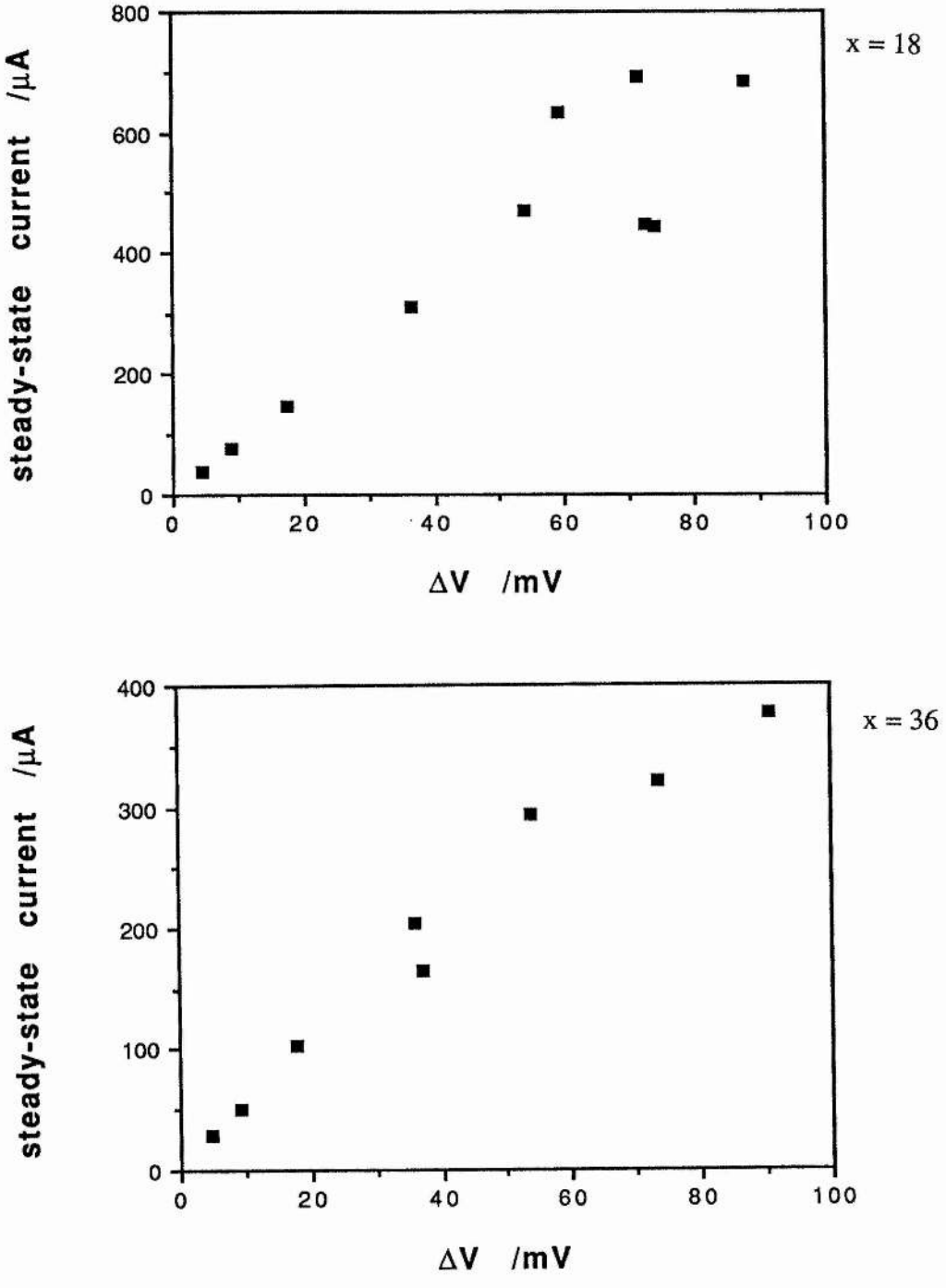

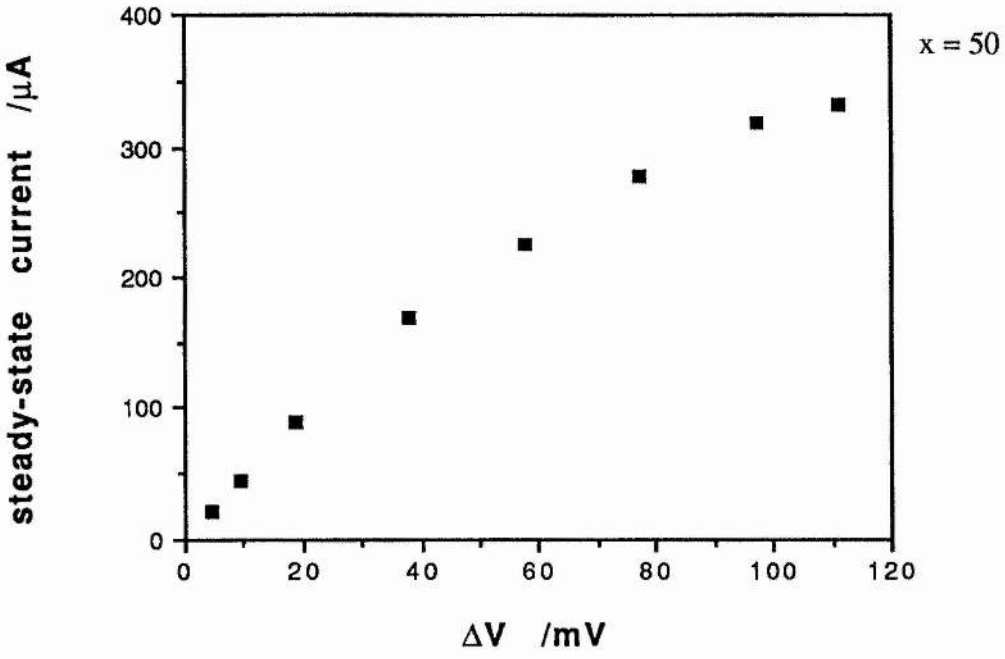
steady-state current /μA
400
300
200
100
0
0
20
40
60
80
100
120
ΔV /mV
x = 50

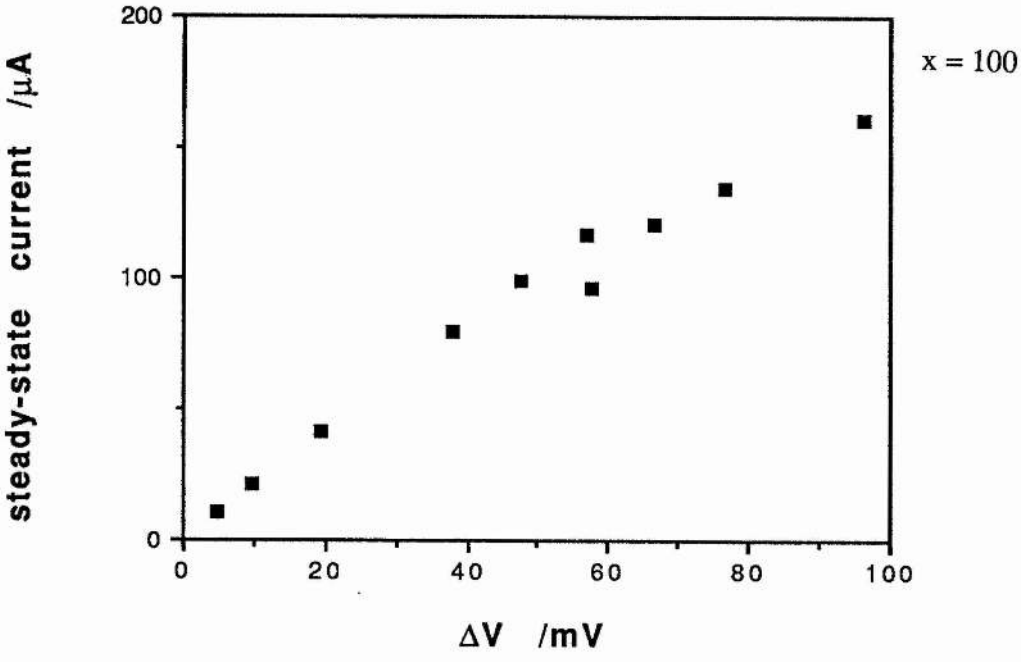
steady-state current /μA
200
100
0
0
20
40
60
80
100
ΔV /mV
x = 100

Figure 5-18. Variation in steady-state current with applied potential difference for PEO_xNaBPh_4 at 85°C, x = 36, 100.

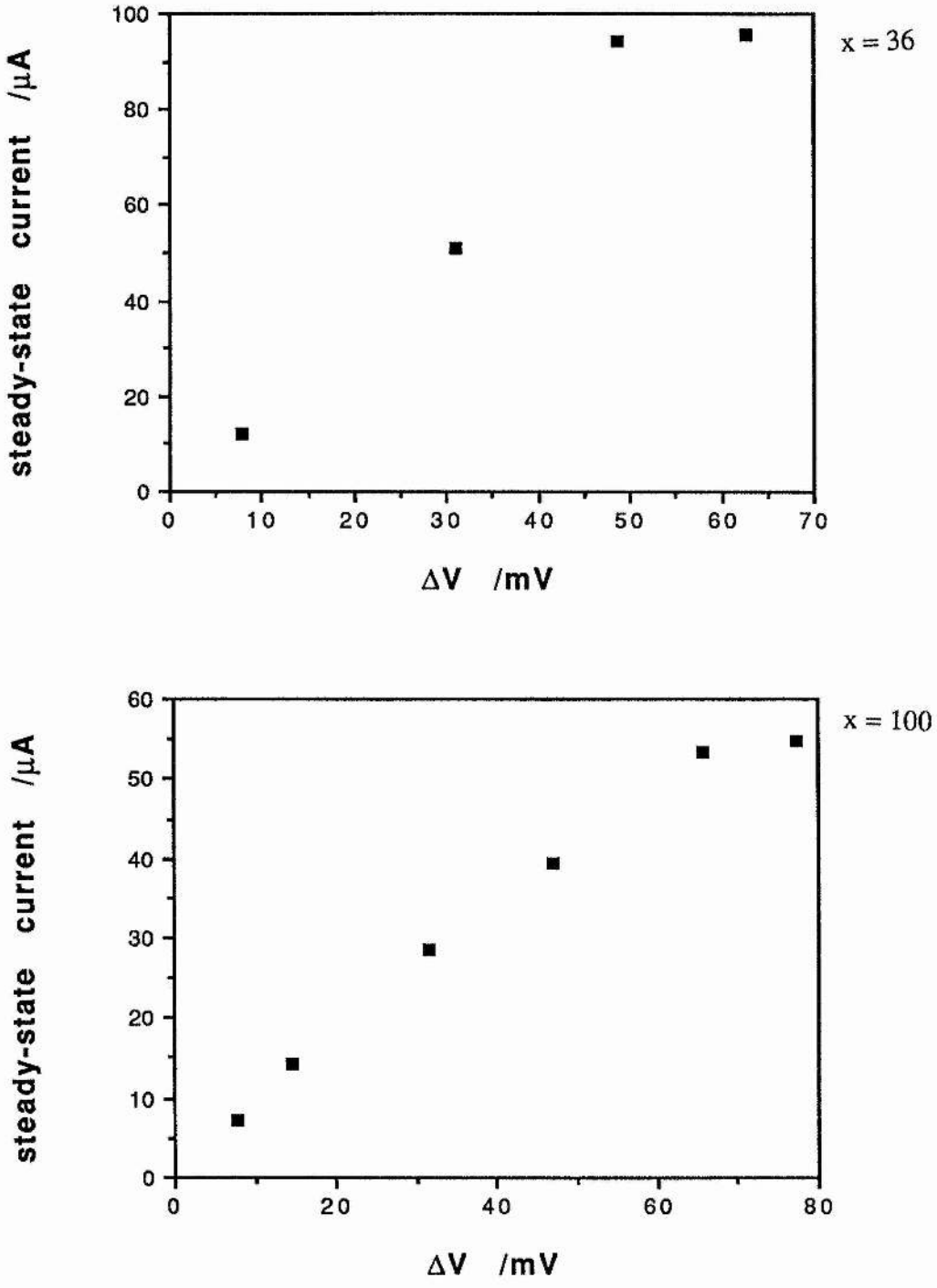

Figure 5-19. Variation in current fraction with applied potential difference for PEO_xLiClO_4 at 120°C, x = 12, 15, 18, 50, 100.

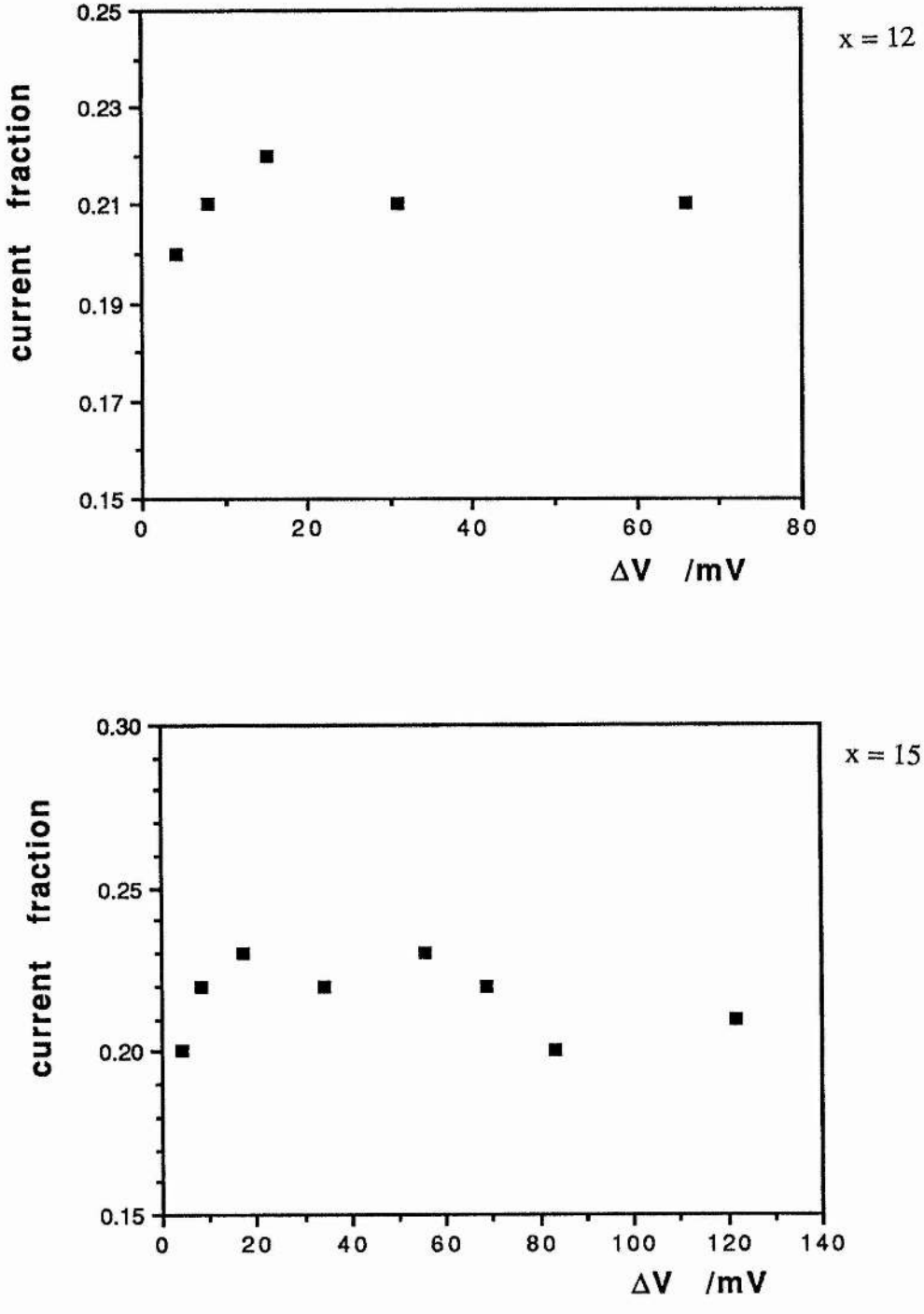

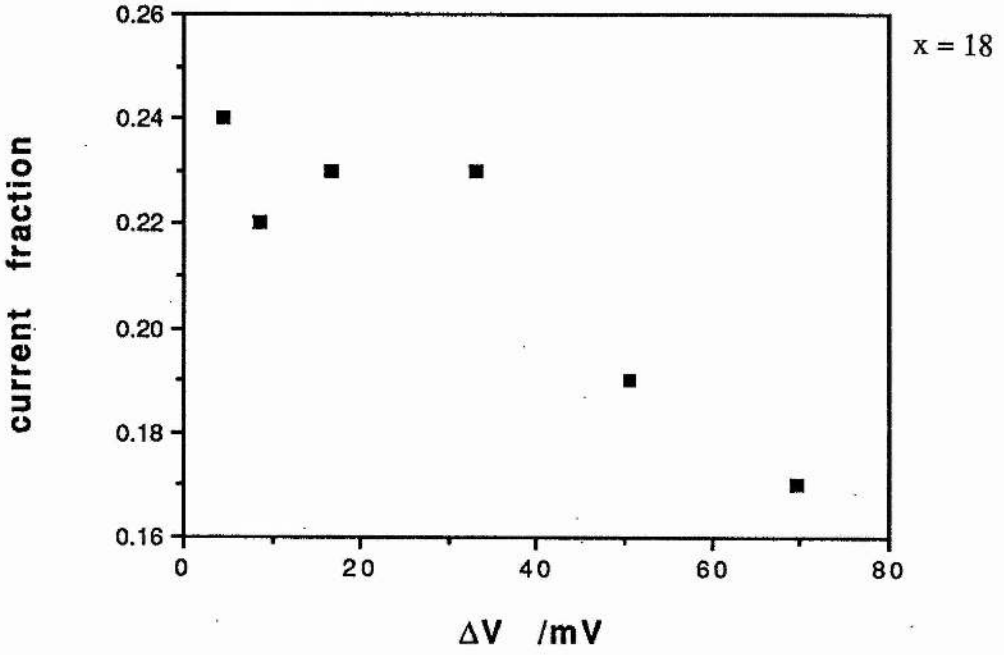
0.26
0.24
0.22
0.20
0.18
0.16
current fraction
0
20
40
60
80
ΔV /mV
x = 18

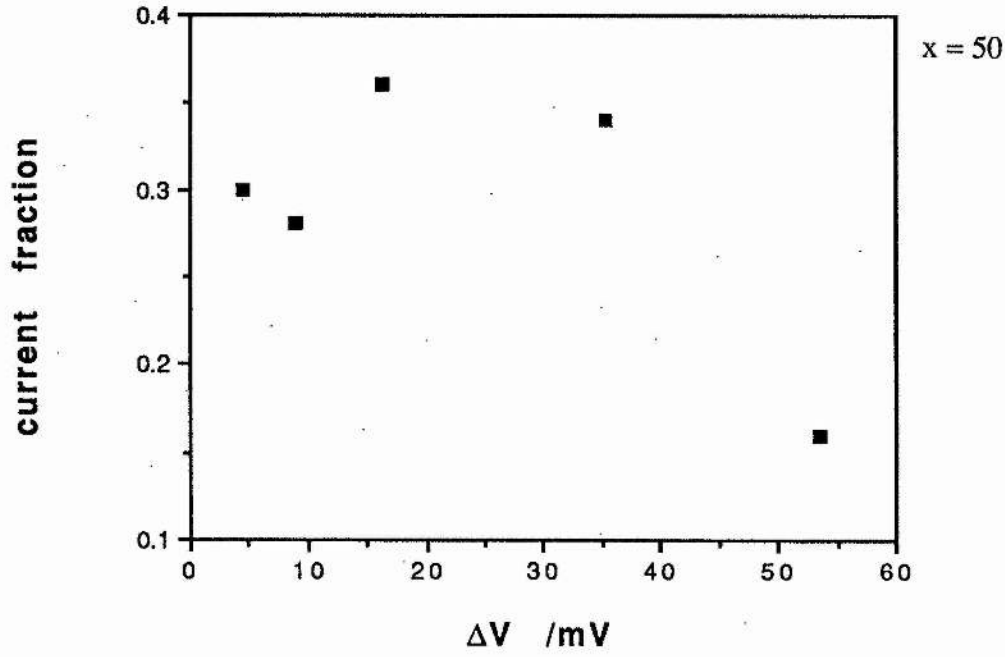
0.4
0.3
0.2
0.1
current fraction
0
10
20
30
40
50
60
ΔV /mV
x = 50

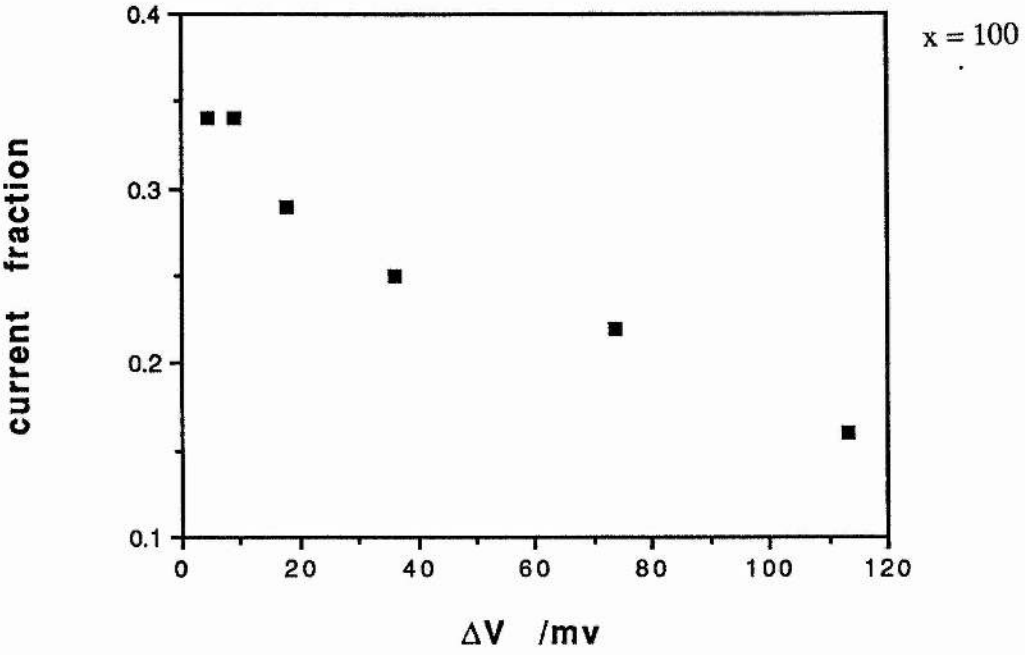
x = 100
current fraction
0.4
0.3
0.2
0.1
0
20
40
60
80
100
120
ΔV /mv

Figure 5-20. Variation in current fraction with applied potential difference for $PEO_xLiCF_3SO_3$ at 120°C, x = 18, 36, 50, 100.

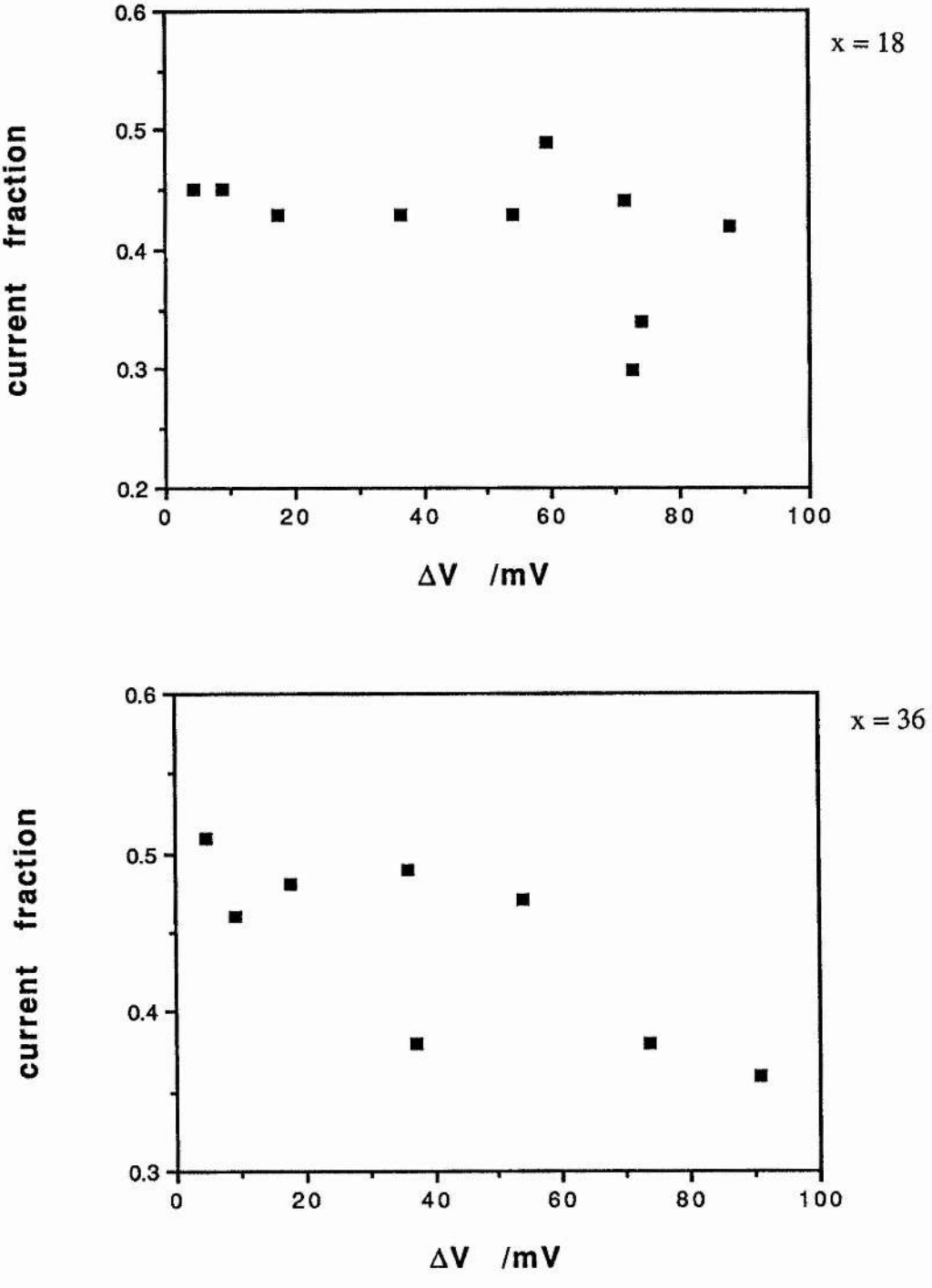

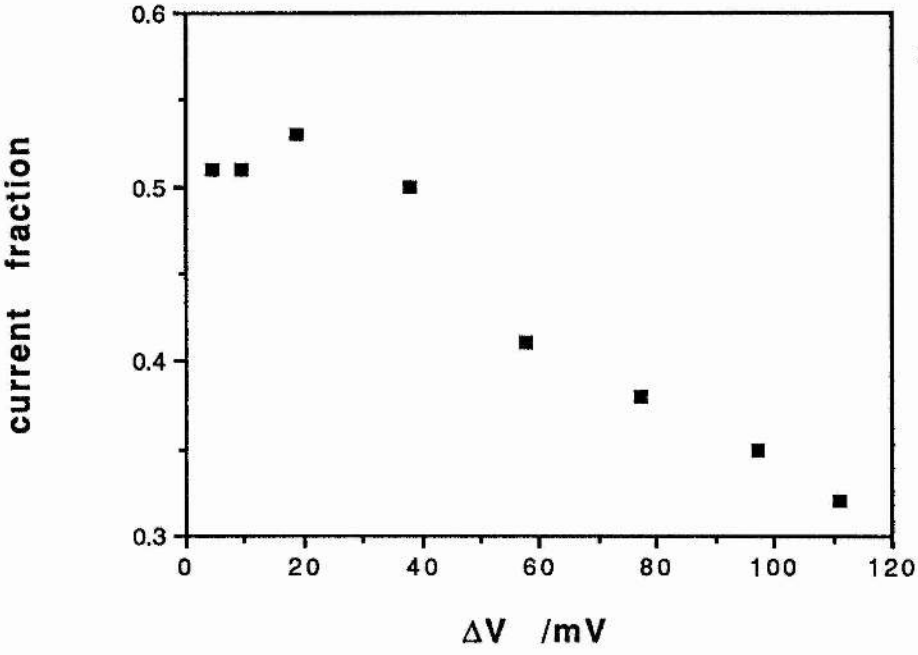
x = 50
current fraction
0.6
0.5
0.4
0.3
0
20
40
60
80
100
120
ΔV /mV

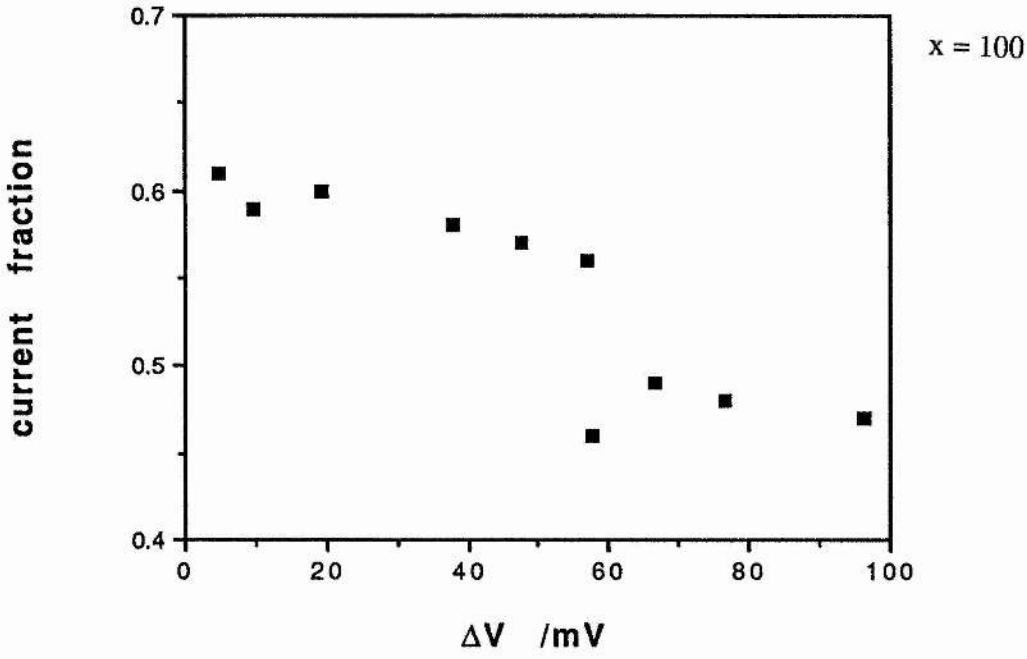
x = 100
current fraction
0.7
0.6
0.5
0.4
0
20
40
60
80
100
ΔV /mV

Figure 5-21. Variation in current fraction with applied potential difference for PEO_xNaBPh_4 at 85°C, x = 36, 100.

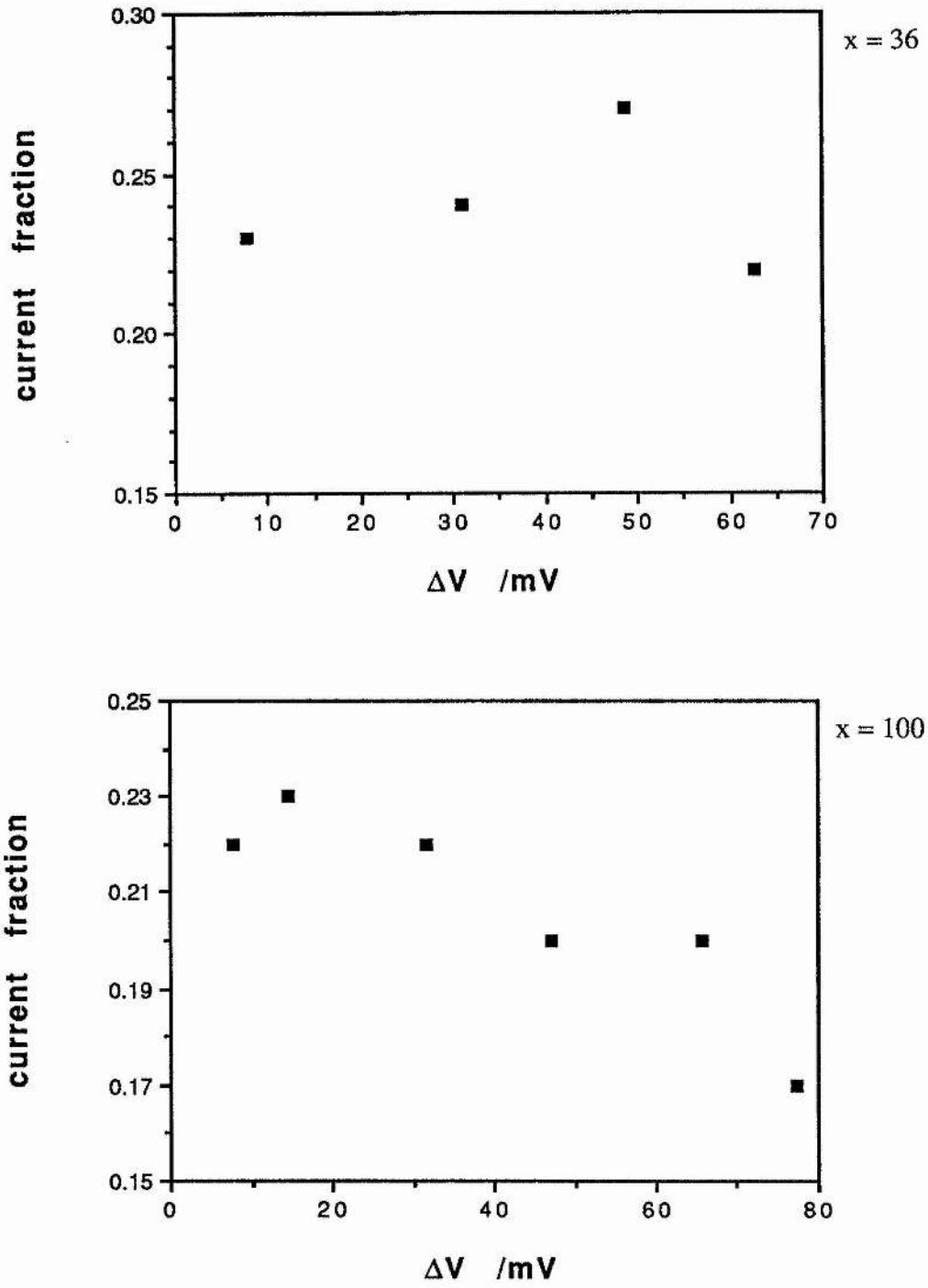

Figure 5-22. Limiting current fractions *vs* concentration at 120°C for PEO_xLiClO_4 x = 12, 15, 18, 50, 100, and $PEO_xLiCF_3SO_3$ x = 18, 36, 50, 100.

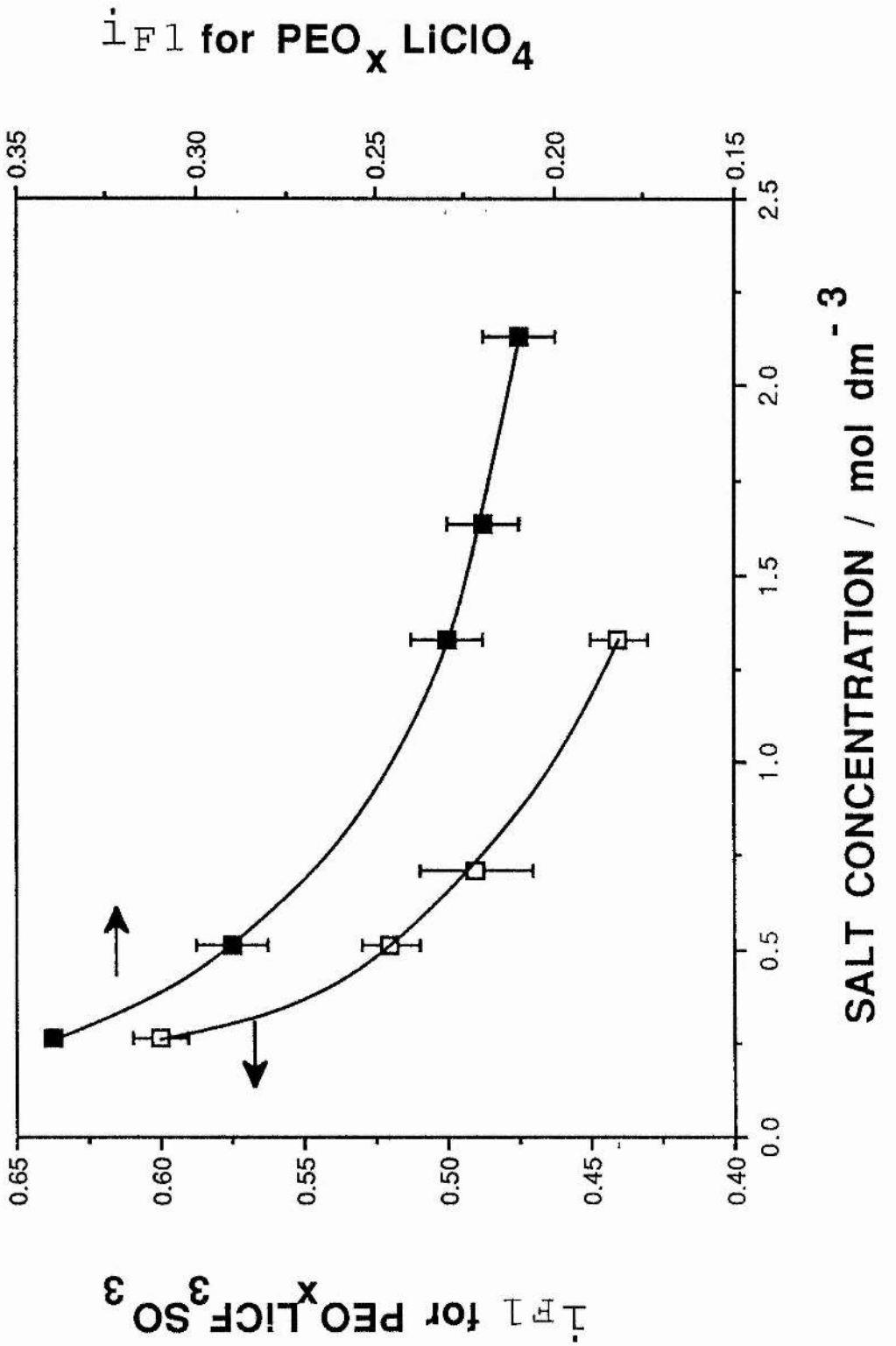

Figure 5-23. Limiting current fraction variation with temperature for PEO_xLiClO_4.

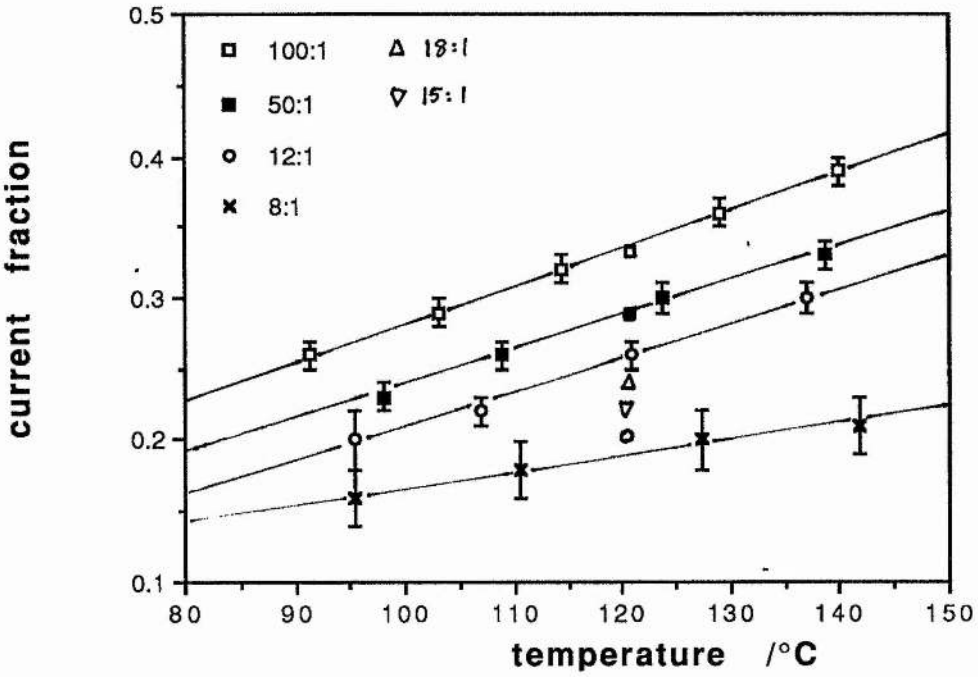

Figure 5-24. Relationship between i_{Fl} and $\Delta E/\Delta V$.

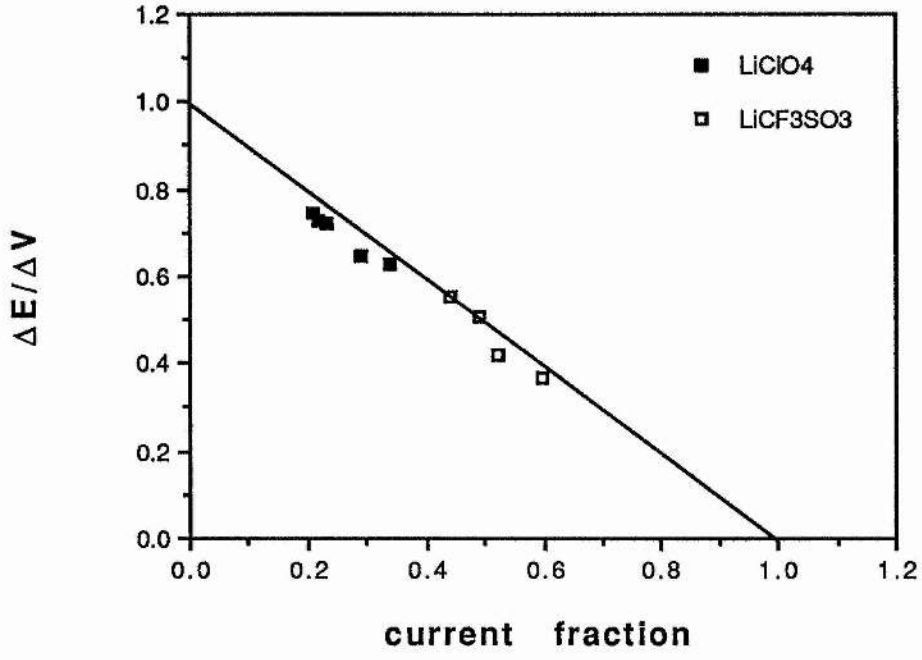

CHAPTER 6

HITTORF ANALYSIS: THE NON-STEADY-STATE DC POLARISATION OF POLYMER ELECTROLYTES

It has been observed in §3.2 that the polarisation of PE cells to steady-state may result in the diffusion of neutral species across the cell, a phenomenon which must be taken into consideration if the mass transport processes constituting the steady-state current are examined. This transport of neutral species prevents the ratio of the steady-state current to the initial current from being used as a measure of the cation transference number in the PE.

The polarisation of a PE cell using the Hittorf procedure is of particular benefit to the study of mass transport in PEs, because only the migration of charged species needs to be considered during the experiment, with no neutral-species transport occurring through all of the electrolyte. Any neutral-species transport in the vicinity of the electrodes is irrelevant, as shown in §6.1, which allows this procedure to determine true ionic transference numbers.

In §6.1.1 a general description is given of the theory and operation of a Hittorf cell for the determination of transference numbers in liquid (typically aqueous) electrolytes. Then in §6.1.2 results from the Hittorf study of liquid PEs [66] are discussed. In §6.1.3 results from the related Tubandt method [103] [104] are discussed for solid cross-linked PEs, and finally in §6.2 the results from this study are presented for some PEO-based solid PEs.

6.1 HITTORF CELLS

A Hittorf cell for the determination of transference numbers in liquid electrolytes is in essence a long tube, filled with the electrolyte under study, with some means of isolating four or more sections of the electrolyte (*e.g.* by taps placed at various points along the tube). A schematic diagram of such a cell is shown in Figure 6-1a. In reality a more complicated design of apparatus may be used (such as that shown in Figure 6-1b) often with several bends in the tube to minimise electrolyte convection, something to which liquid electrolytes are prone. As current is passed though the cell, changes in the electrolyte composition are likely to occur in the vicinity of the electrodes; and if

these changes are limited to the end compartments they may be determined (using some suitable measuring technique) and related to the transference numbers of the ion-constituents. There must be no change of composition in the inner compartments, which are used as internal references to verify that any composition changes are isolated in the electrode compartments.

6.1.1 Theory and Operation of a Hittorf Cell.

If one considers a cell such as that shown in Figure 6-1b, but with two middle sections rather than one, then its mode of operation is as follows: a potential difference is applied to the electrodes in the end compartments of the tube, causing current to flow between them *via* ionic transport through the electrolyte. The cell may be operated in a galvanostatic mode, to allow the easy determination of the amount of charge passed through the cell. After a time the potential difference is removed and the electrolyte sections isolated, drained and analysed.

What occurs in the electrolyte during a polarisation is as follows: consider a cell containing an electrolyte of the salt M^+X^- of uniform composition, in which M^+ and X^- exist in several species (*e.g.* M^+, X^-, MX, M_2X^+, MX_2^-), and in which the electrodes consist of the metal M. When the electrodes are polarised, M^+ ions are injected at the anode and removed at the cathode. If a middle section of the electrolyte is considered, then an amount of M^+ and M_2X^+ ions will enter this section at the anode side whilst an amount will leave at the cathode side. Because the electrolyte is initially of a uniform composition with the same current flowing through both faces of the section, these two fluxes are equal. The same will be true for X^- and MX_2^- ions, except that these enter at the cathode side and leave at the anode side of the section. The relative sizes of all the ion fluxes are determined by the individual ion transport numbers. The neutral species do not migrate in the electric field in the electrolyte, and there is no composition gradient in the central part of the electrolyte in which neutral-species diffusion could occur. The net composition of the middle electrolyte sections thus remains constant *for as long as the electrolyte compositions at the two boundaries of each section remain the*

same.

In the vicinities of the electrodes, however, net compositional changes may occur (they will do if $T^+ \neq 1$, as shown later); and if this is so they will start to happen immediately: at the cathode an amount of M^+ is removed by reduction, and the loss of positively charged species in the compartment is balanced by the influx of M^+ and M_2X^+ ions from the central compartments and outflow of X^- and MX_2^- ions into the central compartments. Because the transport numbers are not pre-determined it is likely that the loss of M as M^+ (to the electrode) and MX_2^- (to the central compartments) from the cathode section will not be exactly balanced by the influx of M^+ and M_2X^+ from the central part of the electrolyte. If this is the case, then the composition of the cathode section begins to change. Likewise, at the anode the gain of M in the form of M^+ ions (from the electrode) and MX_2^- ions (from the central compartments) may not be balanced by the loss of M in the form of M^+ and M_2X^+ to the central compartments.

Thus with time compositional changes which occur at the electrodes start to spread throughout the cell—the cell is slowly moving towards steady-state (which, in a solid electrolyte of length $\approx$ 1 cm., would take many days if not weeks [68]). For a time (which must be greater than the polarisation time) no compositional changes occur in the central part of the electrolyte, simply because the changes have not had time to spread there.

Of course, if composition gradients exist in the vicinity of the electrodes, the diffusion of neutral species may be occurring there; but because the net composition of the electrolyte in the electrode compartments is determined by the oxidation (or reduction) of M (M^+) together with the inflow and outflow of charged species through a boundary with the central compartments of invariant composition, any transport of neutral species within an electrode compartment is irrelevant and does not affect the result (though such transport may be how a supply of M is maintained at the cathode).

The changes in the composition of the compartments may be determined using an appropriate technique (such as titration or conductivity measurements). The change in the number of moles of the electroactive ion-constituent (usually the cation-

constituent) in the appropriate electrode compartment (cathode for cation-constituent and anode for anion-constituent) is related to its transference number, such that:

$$\Delta m_{\pm} = \frac{(1 - T_{\pm})Q}{z_{+}F} \qquad 6\text{-}1$$

Hence determining the amount of charge passed and the composition change in the electrode compartment enables the transference numbers to be calculated. Performing the calculation with data from both electrode compartments is a good evaluation of the internal consistency of the results.

Analysis of the central compartments is undertaken to verify that all composition changes occurring as a result of the passage of charge are retained in the electrode compartments. If this were not the case then the determined change in the number of moles of the cation- or anion-constituent would be less than the actual change in the number of moles, which from equation (6-1) would produce an artificially high cation transference number. It is important to have at least two central compartments, because it may happen that a composition change at one end of a single central compartment may be offset by an equal but opposite composition change at the other end of the compartment, producing no net compositional change in the central compartment and a false verification of the composition changes taking place only in the electrode compartments, giving rise to incorrect transference numbers. With two or more central compartments, a change in the expected composition in one central compartment adjacent to an electrode compartment with respect to the other central compartments would show that the polarisation was carried out for too long.

A schematic diagram illustrating the passage of charge through an electrolyte containing M^+ and X^- ions is shown in Figure 6-2. It is seen that no compositional changes have occurred in the central compartments, because the polarisation has been halted in good time. It is apparent that the passage of much more charge *would* produce composition changes in the central compartments. It may also be seen that if the cation transference number is unity no compositional changes occur, because the loss of M^+ ions from each compartment is exactly balanced by the influx of M^+ ions

from the other compartments or the anode.

Figure 6-3 demonstrates that, although the salt concentration profile may not be simple, the subsequent analysis provides a measure of the average salt concentration in the compartment, which may then be related to the transference numbers. Of course, if the concentration changes are in the vicinity of the electrodes, and the electrode compartments are large, significant salt concentration differences may not arise or may not be distinguished against a large background concentration.

One problem which may limit the length of time for which polarisations may be carried out in liquid electrolytes is convection. This process may cause intermixing between the electrode and reference compartments. Complicated cell designs may reduce the extent to which convection occurs, but fortunately such problems are not likely to occur in solid electrolytes.

When liquid electrolytes are polarised account must also be taken of the change in solvent concentrations in the electrode compartments because solvent coordinated to ionic species may be transported unequally between cations and anions. This solvent is released when ions are discharged at the electrodes, giving rise to a solvent concentration change thus producing a solution composition change not intrinsically due to the passage of charge through the cell. This is a difficult problem to overcome. The addition of an inert substance to the electrolyte whose concentration could be determined at the end of a polarisation (with any change in the concentration related to the transport of coordinated solvent in the electrolyte) is in theory suitable, but Spiro [76] reports that in practice no substance is really unaffected by the passage of charge through an electrolyte. Such problems are of no concern to the polarisation of solid PEs, because no long-range motion of the polymeric solvent can take place.

6.1.2 Transference Numbers in Liquid Polymer Electrolytes

Cameron *et al.* [66] have performed Hittorf experiments on liquid PEs containing sodium salts, using sodium amalgam electrodes, and found an anionic transference number of ≈ 1. This is an initially surprising result when it is considered

that some form of sodium transport must occur in the electrolyte (because the sodium salts may be used to produce solid electrolytes which pass current between non-blocking electrodes at steady-state [105]), but the authors observe that such a result may suggest that ion-pairs are the only means of transporting Na^+ through the electrolyte in a steady-state experiment, with all of the charge actually being carried by the anions. The fact that negative sodium transference numbers were not observed may also indicate that negative triple ions (MX_2^-) are not likely to be present or mobile.

It should also be borne in mind that in this experiment non-labile ions which are tightly bound to the polymer (and which would thus be immobile in solid PEs) may still be transported in the applied electric field by virtue of the fact that long-range translation of the liquid polymeric solvent may occur, though the authors report that NMR data indicate that polymer diffusion is ten times slower than the diffusion of salt species. Nevertheless, the experiment is important because it only examines the transport of ionic species, even if some of the species would be immobile in solid PEs.

6.1.3 Transference Numbers in Network Polymer Electrolytes

Leveque *et al.* [103] [104] have reported ionic transference numbers for lithium perchlorate in various cross-linked polyether networks, determined using the Tubandt method, in which weight changes are related to transference numbers. Several weighed PE discs were stacked between electrodes and current passed through the assembly. The transference numbers were determined by separating and re-weighing the discs. The authors reported T^+ values of around 0.2–0.4, with the actual values being relatively temperature insensitive, but varying with the PEO lengths in the networks.

These T^+ values are quite large, compared with those values found by Cameron *et al.*. Either different species are present or mobile in these network electrolytes, or some other factor such as experimental technique may account for the difference: the applied potential differences for the Tubandt experiments were quite large (of the order of volts) and may have led to the breakdown of the electrolyte at the electrode-electrolyte interfaces, a process by which current could be passed without the transport

of salt species, producing an inflated value of the cation transference number. However, the fact that a single-ion conductor produced a cation transference number of the order of unity would tend to refute this suggestion.

The Tubandt technique would be impossible to perform on ordinary PEO-based PEs, because their adhesive nature makes it impractical to separate thin films which have been in contact under pressure at high temperature. This problem does not occur in a Hittorf cell, where only arbitrary sectioning of the electrolyte after polarisation is necessary (providing that all the composition changes are contained in the electrode sections) and where a gross composition is determined, rather than a net change in weight.

6.2 NON-STEADY-STATE POLARISATION OF PEO_xLiClO_4

Preliminary calculations (§4.5) suggested that the Hittorf technique could be carried out on a simple slab of PE, which would enable transference numbers to be determined for PEs which are commonly reported in the literature (*e.g.* PEO_xLiClO_4), as opposed to PEs which are not so widely used (cross-linked PEO_xLiClO_4).

A Hittorf cell, described in §4.2.1 was devised for the polarisation of solid PEs. In this cell there are four compartments; two central and two electrode. The assembly and operation of the cell has been detailed in §4.2.1. There are both advantages and disadvantages of using solid PEs rather than liquid PEs in Hittorf cells. The advantages are that:

(i) the transport of non-labile charged species cannot occur in a solid PE, so transference numbers measured are for mobile charged species,

(ii) no long-range migration of the polymer may take place in a solid PE, so no solvent correction need be applied, and

(iii) no convection can take place in a solid PE, so quite substantial concentration changes might be produced without dispersion, because it takes a

relatively long time for diffusion to take place over several millimetres.

Disadvantages are that:

(i) the low conductivity of solid PEs requires a long polarisation time for substantial amounts of charge to be passed through the cell without recourse to potentially damaging large potential differences, and

(ii) a solid PE of uniform composition (*i.e.* of uniform background salt concentration) is more difficult to produce than a liquid PE. This also means that the experimental technique might only be performed on amorphous PEs, because it can not be guaranteed that the proportion of any crystalline material is uniform through the electrolyte.

It was anticipated that salt concentration differences of the order of 5–10% could be produced between the reference and electrode compartments (see §4.5). The analytical technique chosen to determine these concentration differences was atomic absorption spectrometry, which could detect lithium concentrations to an accuracy of 0.01 ppm over a concentration range of 0–5 ppm; *i.e.* to an accuracy ≈ 1%. The analytical procedures have been described in Chapter 4.

6.2.1 The Polarisation of Hittorf Cells

The polarisation of several PEO_8LiClO_4 cells at 120°C to produce a constant current of 50 μA resulted in large and irreproducible voltage changes occurring during the polarisation, as shown in Figure 6-4, and it was thought that this current was unsustainable for a long period of time, with the possibility of electrolyte breakdown occurring at the cathode. This electrolyte breakdown could sustain current without the reduction and removal of lithium ions, rendering the experiment worthless. A lead metal cathode was used in subsequent polarisations to allow the formation of a lithium–lead alloy during the passage of current, which could be analysed after the experiment to verify that the current passed was wholly due to the reduction of lithium ions at the cathode.

In cells polarised at 120°C the electrolyte is very rubbery, and it is (usually)

easily removed from the metal electrodes without any apparent contamination by lithium–lead alloy at the cathode, or with little lithium contamination at the anode, providing that such a removal is carried out before the electrolyte cools and hardens. If the electrolyte is allowed to cool in the cell there is also the risk of it cementing the two cell halves together. The lead, being a relatively hard metal, did not fragment and adhere to the electrolyte when the cell was dismantled (as the lithium occasionally did); and conversely no electrolyte adhering to the lead electrode was observed.

Cells with a lead cathode were polarised to pass 10 μA. No voltage transients were observed after the initial rise in potential from the open circuit potential (as shown in Figure 6-5), and when cells were dismantled the lead was seen to be blackened at the electrolyte interface. Lithium–lead alloys are typically dark [45]. It may be seen with the naked eye that the entire interface is not blackened, and under a x 20 microscope the appearance of the surface is very granular (as depicted in Figure 6-6). It may be seen from Figure 6-5 that reproducible voltage–time plots are possible using a current of 10 μA. Slight discrepancies between the plots may be attributed to differing electrolyte resistances, which require different potential differences to drive the same current.

6.2.2 Results from the Hittorf Polarisations of PEO-based Polymer Electrolytes

The Li-AAS analyses of polarised Pb|PEO_xLiClO_4|Li cells are presented in Tables 6-A, 6-C, 6-E and 6-G. The experimental data are the average of two or more readings. It may be seen that the indicated lithium contents of the central reference compartments are lower that the actual lithium content, as determined from the composition of the electrolyte. These reference compositions were used to produce a calibration graph for each experiment, as detailed in §4.5, allowing the conversion of electrode compartment data from the indicated lithium contents (from Li-AAS) to actual lithium contents.

Once calibration graphs were produced, linear or quadratic equations were empirically fitted to the data as appropriate to allow the conversion of the electrode

compartment data. The results of these fits for the experiments reported are contained in Table 6-I. After the actual lithium contents of the electrode compartments had been determined they were used to calculate the transference numbers of the ions in the electrolyte, as shown in §6.2.4. The calibration graphs of indicated *vs* actual lithium contents of samples are shown in Figures 6-7 to 6-10.

Graphs of indicated lithium content *vs* the mass of sample are shown in Figures 6-11 to 6-14 for the electrolytes studied. It is apparent that the cathode compartment samples contain less lithium (weight for weight) than the reference compartments, and the anode compartment samples contain more, showing that compositional changes have occurred as a result of passing current through the cell. The reference samples show a less scattered response than the electrode samples, and this may be due to two factors:

(i) anode samples may have retained small pieces of lithium after cell separation, and

(ii) the sectioning of electrode compartments may not be normal to the electrodes. In Figure 6-16 the random sectioning of a uniform reference compartment is seen not to affect the weight fraction of lithium in the resultant samples; but the uneven sectioning of an electrode compartment, which does not have a uniform salt distribution, is seen to alter the weight fraction of lithium in the resultant samples. Providing all of the electrode compartment samples are analysed and the results taken together, any scatter in the data is not important.

6.2.3 The Lithium Content of the Lead Cathode After Polarisation.

The anticipated lithium contents of the lead cathodes were determined from the amount of charge passed, assuming that this was due wholly to the reduction of lithium ions at the cathode. Again, the value determined from Li-AAS was less than anticipated, but if the same correction was applied to this data as to the electrolyte data then results close to the anticipated values were found, indicating that lithium ion reduction was responsible for the current passed; and consequently that the measured

lithium contents could be confidently related to the lithium transference number. The data are summarised in Table 6-J.

6.2.4 Determination of Transference Numbers from the Amount of Lithium Detected in a Sample.

For a given sample mass and a known amount of charge passed through a cell, it may be shown that generally the transference numbers are a simple function of the mass of lithium detected.

If a PE sample of known composition PEO_xLiX before polarisation, and with a mass of W grams after polarisation, is found, after calibration of the results from Li-AAS, to contain L grams of lithium, then the number of moles of lithium present in the sample is simply given by:

$$\text{moles of Li} = \frac{L}{m} \qquad 6\text{-}2$$

where m is the molar mass of lithium (m = 6.94 g mol^{-1}). If all the lithium is present as the lithium salt LiX (as is most likely to be the case for the cathode compartment, which is not susceptable to lithium metal contamination) there are obviously L/m moles of LiX present, and if S is the molar mass of the salt, the mass of LiX present is given by:

$$\text{mass of LiX} = \frac{LS}{m} \text{ grams} \qquad 6\text{-}3$$

i.e. the mass of PEO present in the sample is given by:

$$\text{mass of PEO} = W - \frac{LS}{m} \text{ grams} \qquad 6\text{-}4$$

If the mass of the repeat unit in PEO is P (P = 44.052 g mol^{-1}), then the number of moles of polymer repeat unit present is simply equation (6-4) divided by P; and because the electrolyte initially had an O:M ratio of x, the number of moles of LiX originally present in this mass of PEO is given by:

$$\text{moles of LiX} = \frac{W - \frac{LS}{m}}{Px} \qquad 6\text{-}5$$

thus the change in the number of moles of LiX brought about by the passage of charge

is the difference between the amount of salt now in the polymer (L/m moles) and the amount of salt originally present in the polymer (equation (6-5)), *i.e.*:

$$\Delta \text{ moles LiX} = \frac{L}{m} - \left(\frac{W - \frac{LS}{m}}{Px} \right) \qquad 6\text{-}6$$

For a positive cation transference number, and considering the cathode compartment, equation (6-6) yields a negative answer; *i.e.* salt is lost from the compartment during the passage of charge through the electrolyte. From equation (6-1), equation (6-6) may be related to the anion transference number in the following equation:

$$T^- = \frac{Fz_-}{Q}\left[\frac{L}{m}\left(1 + \frac{S}{Px}\right) - \frac{W}{Px}\right] \qquad 6\text{-}7$$

Because Q and W are accurately measured, and m, S, P, and x are known, equation (6-7) is a linear equation of the form $T^- = aL + c$, so it may be used to provide an expression for T^- once the amount of lithium in the sample has been found. If a graph of T^- *vs* mass of lithium is plotted it shows visually just how dependant T^- is on the accuracy of the lithium determination. If the gradient of the graph is relatively large, a small range of x-ordinate values (masses of lithium) will give rise to a large range of y-ordinate values (anion transference numbers); and if the gradient is relatively small a small range of x-ordinate values will give rise to a small range of y-ordinate values. This is illustrated in Figure 6-16, and the experimental graphs are shown in Figures 6-17 to 6-20.

6.3 LITHIUM TRANSFERENCE NUMBERS IN PEO-BASED POLYMER ELECTROLYTES

The observed lithium contents of the electrode compartments were corrected using the calibration data contained in Table 6-I. After this adjustment the amount of lithium detected was related to the change in the amount of lithium perchlorate in the compartment by using equations 6-2 to 6-6. The calculations of this for each cell are

shown in Tables 6-B, 6-D, 6-F and 6-H. These changes, together with the amount of charge passed through the cell, were used to determine the transference numbers in the electrolyte. The results of this are shown in Table 6-K.

It is seen that the anionic transference numbers calculated using data from the anode compartments are consistently greater than those calculated using data from the cathode compartments. This may be due to contamination of the anode compartment/anode interface by lithium when the cell was dismantled, and suggests that the results are not as accurate as the cathode compartment data. These values of T^- may be regarded as upper limits.

Of the three polarisations using PEO_8LiClO_4 (H4, H6, H7), two gave reproducible results to within experimental error (H4 and H7). It is believed that the cathode data from H6 are unreliable because the solutions stood for a week after preparation, and it may have come to pass that they started to spoil. Even from the Li-AAS composition *vs* mass of sample graph (Figure 6-13) it is seen that the fall in lithium content of the cathode does not roughly match the gain in lithium content of the anode.

The results from PEO_8LiClO_4 electrolytes indicate cationic transference numbers less than the current fraction found for this electrolyte at the same temperature, suggesting that neutral species transport contributes to the steady-state current in these electrolytes. The cation transference numbers, determined from cathode data, are not as low as those found by Cameron *et al.*, though a different system was examined in that case. The T^+ values are lower than those determined by Leveque *et al.* for the same salt in a different polymer.

The difference between the 50:1 and 8:1 results is interesting in that it follows the same trend as the current fraction measurements, but the errors are such that nothing much should be read into the difference. The errors are larger for the 50:1 sample because the electrolyte itself contains much less lithium than the 8:1 electrolyte (the 50:1 sample has a salt concentration of $\approx$ 0.51 M whilst the 8:1 sample has a salt concentration of $\approx$ 2.85 M). Nevertheless, it has proved possible to perform the

technique on this relatively dilute electrolyte.

6.3.1 Comments

The Hittorf method of determining transference numbers has been demonstrated for two lithium perchlorate-based PEs. Problems with the quantitative detection of lithium using Li-AAS have been overcome by the production of calibration graphs using Hittorf reference compartment data and data from stock electrolyte. The facts that the fits are sometimes linear and sometimes quadratic, with differences between the fitting parameters, requires the production of a fresh calibration graph each time an experiment is performed, though this is not too inconvenient.

Considering the size of the samples used, the data obtained are quite accurate, suggesting that this technique may be performed on other electrolytes. Two electrolytes which should be examined are low concentration lithium triflate electrolytes—these have quite large current fractions, which would contrast with the low cation transference numbers which might be anticipated—and sodium thiocyanate-based electrolytes, in order to see if there is any difference between the solid electrolyte and the liquid.

The technique of AAS may be used to examine other PEs, providing that they contain metal salts which are able to be analysed using AAS, such as sodium or zinc. It should be possible to obtain true and relatively accurate transference numbers for a whole range of PEs using this method, allowing the results to be contrasted with those of other experimental techniques.

Table 6-A: Expected and Observed Lithium Concentrations for Pb|PEO_8LiClO_4|Li Cell (H4) After Passage of 1.082 C (= 11.2 μmol Li).

SAMPLE	SAMPLE MASS / mg	EXPECTED Li CONCENTRATION / ppm	OBSERVED Li CONCENTRATION / ppm
c1	10.411	1.57	1.335
c2	8.164	1.23	1.06
c3	9.642	1.46	1.275
c4	7.268	1.10	0.905
c5	8.528	1.29	1.09
c6	9.431	1.43	1.20
TOTAL	53.444		6.865
mc1	10.196	1.54	1.38
mc2	8.455	1.28	1.17
mc3	8.269	1.25	1.11
mc4	13.888	2.10	1.95
mc5	10.535	1.59	1.42
mc6	9.918	1.50	1.38
TOTAL	61.261		8.41
ma1	9.175	1.39	1.27
ma2	8.799	1.33	1.20
ma3	11.318	1.71	1.56
ma4	11.822	1.79	1.66
ma5	10.931	1.65	1.51
ma6	12.469	1.89	1.70
TOTAL	64.514		8.90
a1	10.429	1.58	1.52
a2	10.192	1.54	1.48
a3	13.247	2.00	1.945
a4	8.846	1.34	1.30
a5	10.516	1.59	1.54
a6	9.847	1.49	1.455
TOTAL	63.077		9.24
Pb	0.078 (i)	0.78	0.68

(i) mass of lithium deposited on the lead cathode calculated from the amount of charge passed.

The sample notation refers to Figure 6-21

Expected lithium contents of electrode samples assumes sample is of unchanged composition

Table 6-B: Calculation of the Change in Lithium Content of the Cell in Table 6-A.

CATHODE:	Total mass	53.444 mg
	Indicated lithium content	0.687±0.005 mg
	Corrected lithium content	0.753±0.005 mg
	Implied $LiClO_4$ content	11.543±0.077 mg
	Implied PEO content	41.901±0.077 mg

41.901±0.077 mg of PEO present as PEO_8LiClO_4 contain 12.649±0.023 mg $LiClO_4$

$\Delta M_{(LiClO4)}$ = (11.543 - 12.649 ± 0.080) mg = -1.106±0.080 mg

ANODE:	Total mass	63.077 mg
	Indicated lithium content	0.924±0.005 mg
	Corrected lithium content	1.014±0.005 mg
	Implied $LiClO_4$ content	15.545±0.077 mg
	Implied PEO content	47.532±0.077 mg

47.532±0.077 mg of PEO present as PEO_8LiClO_4 contain 14.349±0.023 mg $LiClO_4$

$\Delta M_{(LiClO4)}$ = (15.545 - 14.349 ± 0.080) mg = +1.196±0.080 mg

Table 6-C: Expected and Observed Lithium Concentrations for Pb|$PEO_{50}LiClO_4$|Li Cell (H5) After Passage of 0.4587 C (= 4.8 μmol Li).

SAMPLE	SAMPLE MASS / mg	EXPECTED Li CONCENTRATION / ppm	OBSERVED Li CONCENTRATION / ppm
c1	18.900	0.57	0.435
c3	17.483	0.53	0.39
c5	21.450	0.64	0.505
TOTAL	57.833		1.33
mc1	22.786	0.68	0.625
mc3	16.170	0.49	0.435
mc5	18.185	0.55	0.48
TOTAL	57.141		1.54
ma1	22.224	0.67	0.61
ma3	19.913	0.60	0.53
ma5	17.016	0.51	0.455
TOTAL	59.153		1.595
a1	13.779	0.41	0.455
a3	14.361	0.43	0.49
a5	16.162	0.49	0.58
TOTAL	44.302		1.525
p1 †	10.495	0.32	0.30
p2 †	8.731	0.26	0.23
p3 †	3.605	0.11	0.10
p4 †	18.829	0.57	0.515
Pb	0.033 (i)	0.33	0.315

(i) mass of lithium deposited on the lead cathode calculated from the amount of charge passed.

† These samples were taken from excess electrolyte after the production of the electrolyte slab.

The sample notation refers to Figure 6-21, except that a1 in this table denotes the combined 1 and 2 in the Figure, a3 denotes the combined 3 and 4, and a5 denotes the combined 5 and 6. The same holds for the other samples.

Expected lithium contents of electrode samples assumes sample is of unchanged composition

Table 6-D: Calculation of the Change in Lithium Content of the Cell in Table 6-C.

CATHODE:	Total mass	57.833 mg
	Indicated lithium content	0.133±0.004 mg
	Corrected lithium content	0.149±0.004 mg
	Implied $LiClO_4$ content	2.284±0.061 mg
	Implied PEO content	55.549±0.061 mg

55.549±0.061 mg of PEO present as $PEO_{50}LiClO_4$ contain 2.683±0.003 mg $LiClO_4$

$\Delta M_{(LiClO4)}$ = (2.284 - 2.683 ± 0.061) mg = -0.399±0.061 mg

ANODE:	Total mass	44.302 mg
	Indicated lithium content	0.153±0.004 mg
	Corrected lithium content	0.170±0.004 mg
	Implied $LiClO_4$ content	2.606±0.061 mg
	Implied PEO content	41.696±0.061 mg

41.696±0.061 mg of PEO present as $PEO_{50}LiClO_4$ contain 2.014±0.003 mg $LiClO_4$

$\Delta M_{(LiClO4)}$ = (2.606 - 2.014 ± 0.0.061) mg = +0.592±0.061 mg

Table 6-E: Expected and Observed Lithium Concentrations for a Pb|PEO_8LiClO_4|Li Cell (H6) After Passage of 1.662 C (= 17.2 μmol Li).

SAMPLE	SAMPLE MASS /mg	EXPECTED Li CONCENTRATION /ppm	OBSERVED Li CONCENTRATION /ppm
c1	11.759	1.78	1.535
c2	11.897	1.80	1.615
c3	7.962	1.20	1.02
c4	13.904	2.10	1.985
c5	11.699	1.77	1.56
c6	14.389	2.18	2.015
TOTAL	71.610		9.73
mc1	10.436	1.58	1.47
mc2	11.373	1.72	1.63
mc3	6.740	1.02	0.915
mc4	10.180	1.54	1.42
mc5	13.320	2.01	2.305*
mc6	11.172	1.69	1.59
TOTAL	63.221 (49.901*)	9.33 (7.025*)	
ma1	9.917	1.50	1.39
ma2	10.453	1.58	1.465
ma3	12.235	1.85	1.80
ma4	10.563	1.60	1.465
ma5	11.876	1.80	1.695
ma6	9.148	1.38	1.265
TOTAL	64.192		9.08
a1	7.607	1.15	1.135
a2	9.035	1.37	1.485
a3	8.265	1.25	1.29
a4	10.084	1.53	1.66
a5	7.130	1.08	1.08
a6	8.137	1.23	1.31
TOTAL	50.258		7.96
p1 †	2.521	0.38	0.325
p2 †	5.203	0.79	0.70
p3 †	6.559	0.99	0.88
p4 †	10.697	1.62	1.52
p5 †	11.829	1.79	1.655
Pb	0.119 (i)	1.19	1.075

(i) mass of lithium deposited on the lead cathode calculated from the amount of charge passed.

* This sample is anomalous and has been omitted from quantities and calculations marked by an asterisk.

† These samples were taken from excess electrolyte after the production of the electrolyte slab.

The sample notation refers to Figure 6-21

Expected lithium contents of electrode samples assumes sample is of unchanged composition

Table 6-F: Calculation of the Change in Lithium Content of the Cell in Table 6-E.

CATHODE	Total mass	71.610 mg
	Indicated lithium content	0.973±0.005 mg
	Corrected lithium content	1.029±0.006 mg
	Implied $LiClO_4$ content	15.775±0.092 mg
	Implied PEO content	55.835±0.092 mg

55.835±0.092 mg of PEO present as PEO_8LiClO_4 contain 16.856±0.028 mg $LiClO_4$

$\Delta M_{(LiClO4)}$ = (15.775 - 16.856 ± 0.096) mg = -1.081±0.096 mg

ANODE	Total mass	50.258 mg
	Indicated lithium content	0.796±0.005 mg
	Corrected lithium content	0.864±0.006 mg
	Implied $LiClO_4$ content	13.245±0.092 mg
	Implied PEO content	37.013±0.092 mg

37.013±0.092 mg of PEO present as PEO_8LiClO_4 contain 11.174±0.028 mg $LiClO_4$

$\Delta M_{(LiClO4)}$ = (13.245 - 11.174 ± 0.096) mg = +2.071±0.096 mg

Table 6-G: Expected and Observed Lithium Concentrations for Pb|PEO_8LiClO_4|Li Cell (H7) After Passage of 1.692 C (= 17.5 μmol Li).

SAMPLE	SAMPLE MASS /mg	EXPECTED Li CONCENTRATION /ppm	OBSERVED Li CONCENTRATION /ppm
c1	8.657	1.31	1.09
c2	12.027	1.82	1.595
c3	8.257	1.25	1.03
c4	13.125	1.99	1.735
c5	8.653	1.31	1.115
c6	10.113	1.53	1.325
TOTAL	60.832		7.89
mc1	7.806	1.18	1.075
mc2	11.312	1.71	1.635
mc3	7.223	1.09	1.00
mc4	11.732	1.77	1.725
mc5	12.059	1.82	1.76
mc6	10.875	1.64	1.57
TOTAL	61.007		8.765
ma1a	8.340	1.26	1.175
ma1b	5.479	0.83	0.775
ma2	11.592	1.75	1.705
ma3	7.266	1.10	1.01
ma4	9.701	1.47	1.38
ma5a	9.744	1.47	1.41
ma5b	4.280	0.65	0.61
ma6	9.596	1.45	1.35
TOTAL	65.998		9.415
a1	7.096	1.07	1.07
a2	10.139	1.53	1.605
a3	6.867	1.04	1.055
a4	12.269	1.86	2.035
a5	13.768	2.08	2.28
a6	14.854	2.25	2.52
TOTAL	64.993		10.565
Pb	0.122 (i)	1.22	1.095

(i) mass of lithium deposited on the lead cathode calculated from the amount of charge passed.

The sample notation refers to Figure 6-21

Expected lithium contents of electrode samples assumes sample is of unchanged composition

Table 6-H: Calculation of the Change in Lithium Content of the Cell in Table 6-G.

CATHODE	Total mass	60.832 mg
	Indicated lithium content	0.789±0.005 mg
	Corrected lithium content	0.835±0.006 mg
	Implied $LiClO_4$	12.801±0.092 mg
	Implied PEO content	48.031±0.092 mg

48.031±0.092 mg of PEO present as PEO_8LiClO_4 contain 14.500±0.028 mg $LiClO_4$

$\Delta M_{(LiClO4)}$ = (12.801 - 14.500 ± 0.096) mg = -1.081±0.096 mg

ANODE	Total mass	64.993 mg
	Indicated lithium content	1.057±0.005 mg
	Corrected lithium content	1.077±0.006 mg
	Implied $LiClO_4$ content	16.510±0.092 mg
	Implied PEO content	48.483±0.092 mg

48.483±0.092 mg of PEO present as PEO_8LiClO_4 contain 14.636±0.028 mg $LiClO_4$

$\Delta M_{(LiClO4)}$ = (16.510 - 14.636 ± 0.096) mg = +1.874±0.096 mg

Table 6-I: Parameters of Least Mean Squares Fits to Li-AAS Data from Pb|PEO_xLiClO_4|Li Cells.

Cell	Composition	a	b
H4	PEO_8LiClO_4	1.097	not fitted
H5	$PEO_{50}LiClO_4$	1.162	-0.097
H6	PEO_8LiClO_4	1.201	-0.085
H7	PEO_8LiClO_4	1.151	-0.068

Fits were through the origin.

H4 was a linear fit, H5, H6, H7 were quadratic due to curved calibration plot.

Table 6-J. Observed and Corrected Lithium Contents of Lead Cathodes.

Sample	Expected lithium content /ppm	Observed lithium content /ppm	Corrected lithium content /ppm
H4	0.78	0.68	0.75
H5	0.33	0.315	0.34
H6	1.19	1.075	1.19
H7	1.22	1.095	1.19

Table 6-K: Determination of Transference Numbers for the Electrolytes Studied.

Sample	$\Delta_{(LiClO4)}$ cathode /mg	$\Delta_{(LiClO4)}$ anode /mg	Charge passed /C	T^- cathode	T^- anode	
H4	-1.106±0.080	+1.196±0.080	1.082	0.93	1.00	±0.07
H5	-0.399±0.061	+0.592±0.061	0.459	0.79	1.17	±0.12
H6	-1.081±0.096	+2.071±0.096	1.662	0.59	1.13	±0.05
H7	-1.699±0.096	+1.874±0.096	1.692	0.91	1.00	±0.05

Figure 6-1. (a) schematic and (b) actual diagram of a Hittorf cell for the examination of aqueous electrolytes [(b) taken from Wall *et al.* (*J. Phys. Colloid Chem* (1950) **54** 979) quoted by Spiro in reference [76]].

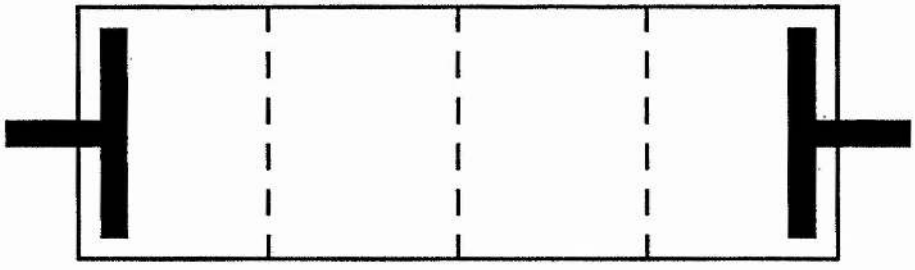

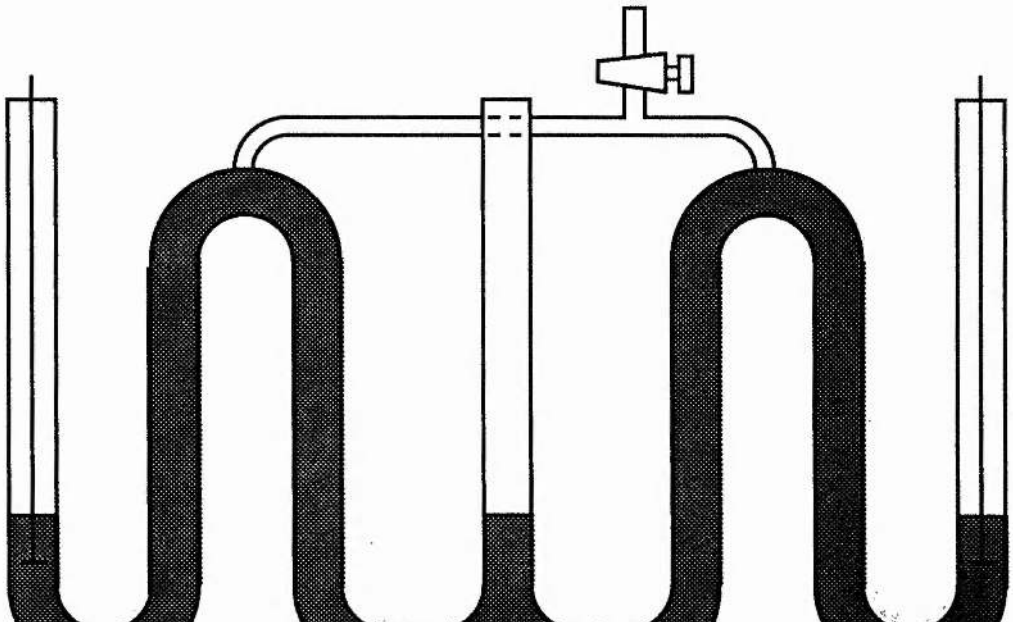

Figure 6-2. Mass transport in a uniform electrolyte of free ions with an anionic transference number of 0.6 (a) before, and (b) after the passage of a charge of 5e.

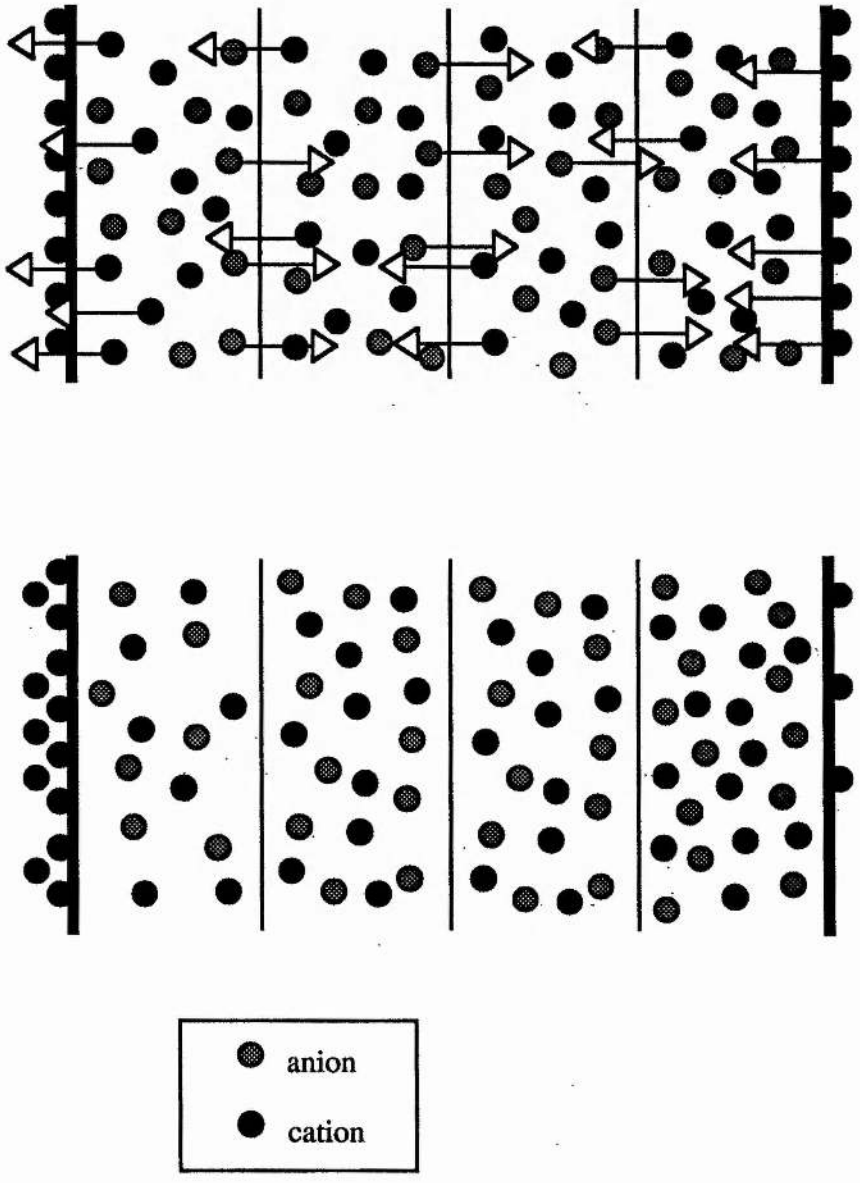

Figure 6-3. Relationship between the actual concentration profile and the bulk concentration as determined by AAS for a four-compartment Hittorf cell.

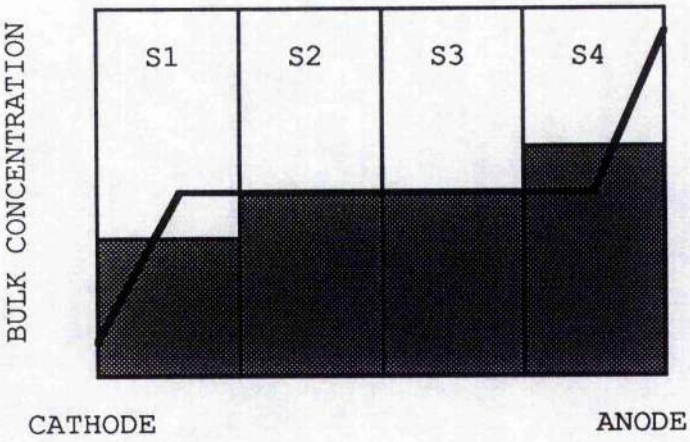

ACTUAL (LINE) AND BULK (SHADED)
CONCENTRATION PROFILE OF POLARISED
HITTORF CELL

Figure 6-4. Voltage transients for two Li|PEO_8LiClO_4|Li Hittorf cells at 120°C passing 50 μA.

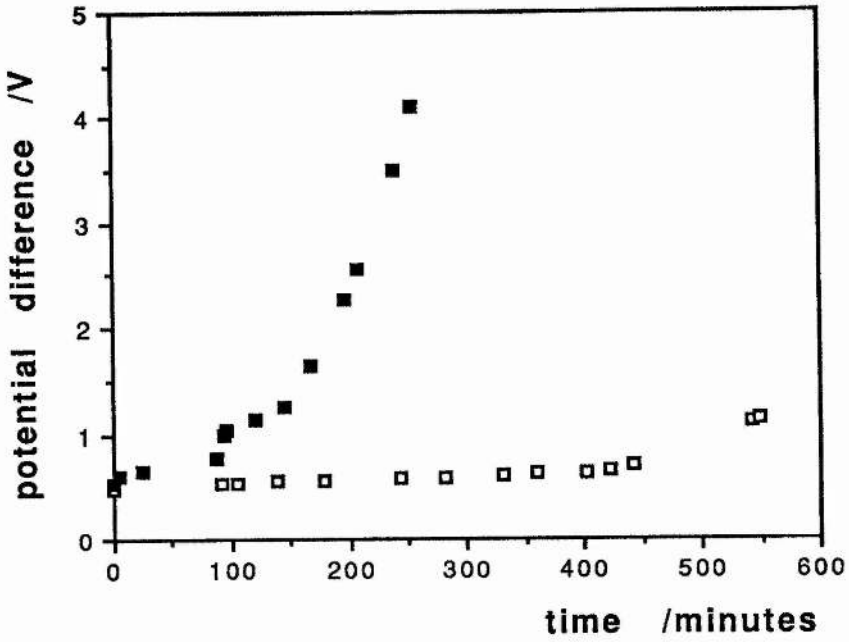

Figure 6-5. Voltage transients for three Li|PEO_8LiClO_4|Li Hittorf cells at 120°C passing 10 μA.

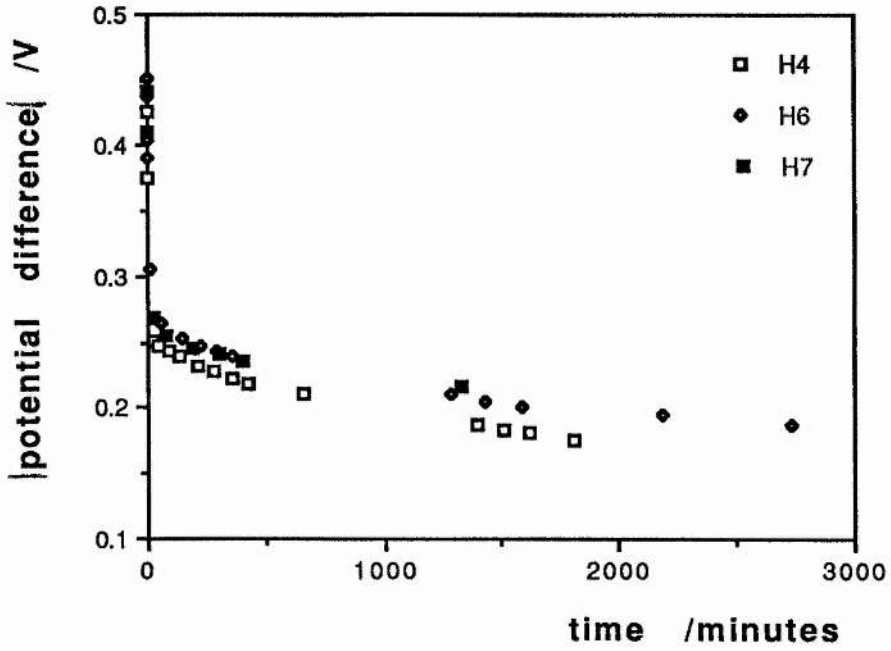

Figure 6-6. Appearance of the lead cathode after polarisation.

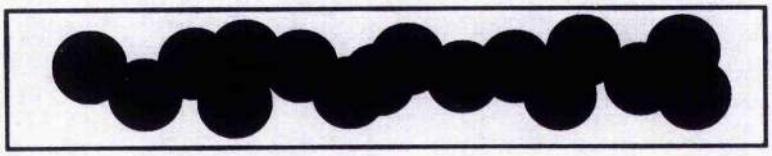

Figure 6-7. Calibration graph for the AAS results from cell H4

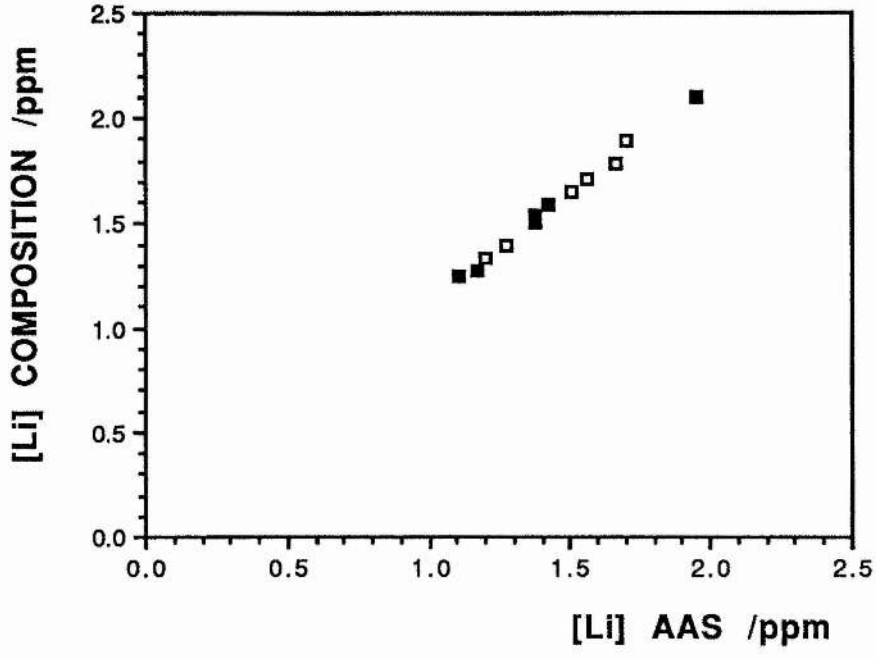

Figure 6-8. Calibration graph for the AAS results from cell H5.

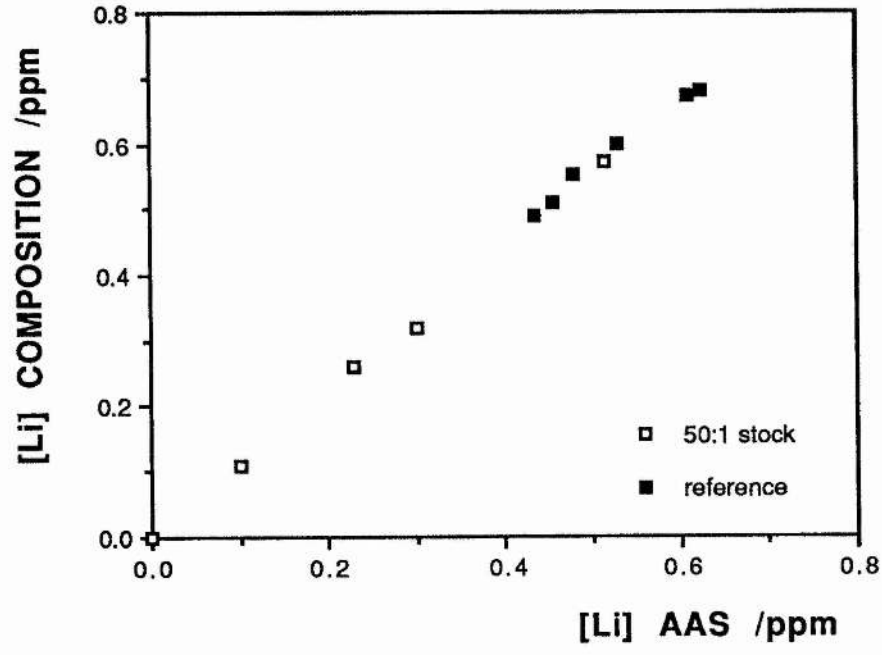

Figure 6-9. Calibration graph for the AAS results from cell H6.

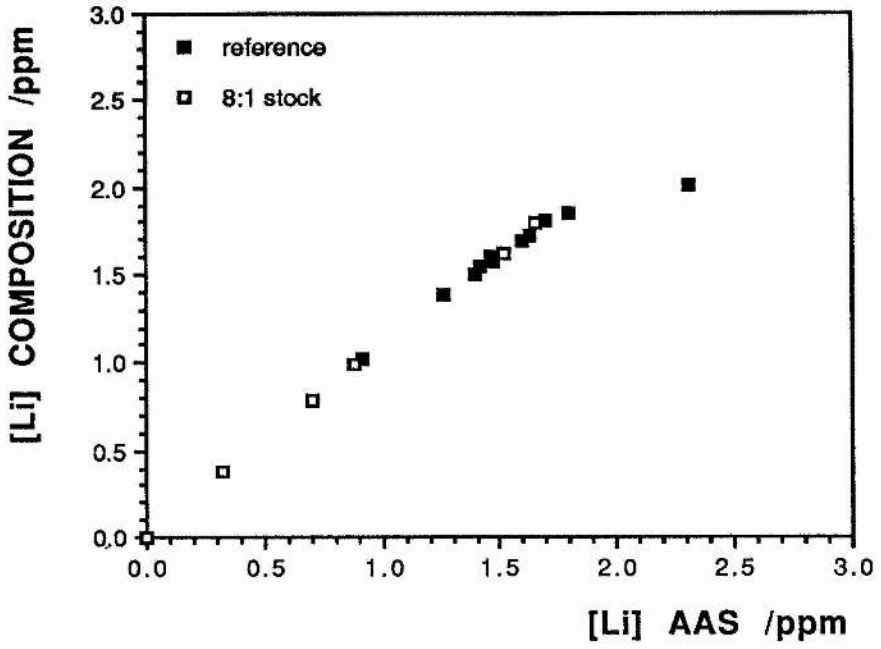

Figure 6-10. Calibration graph for the AAS results from cell H7.

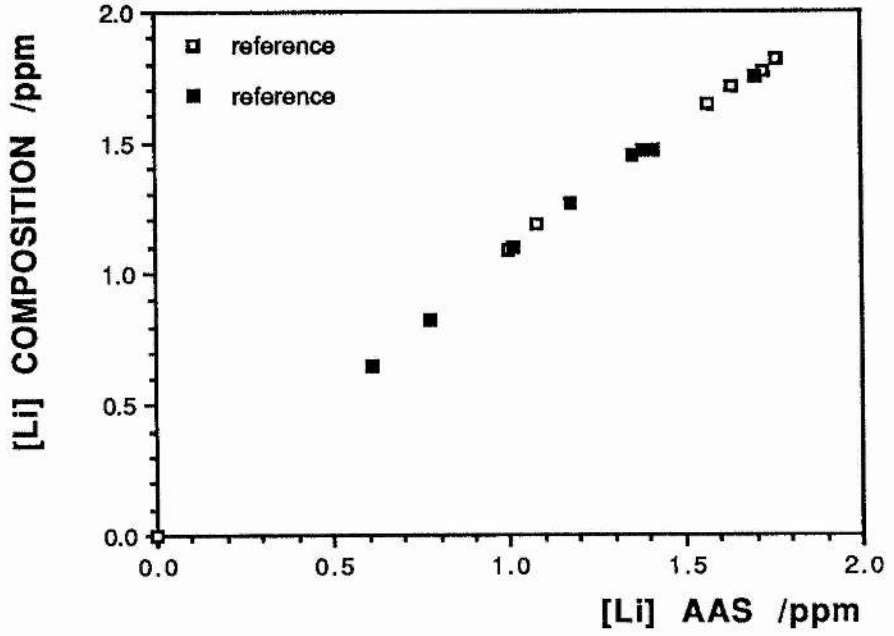

Figure 6-11. Indicated lithium content *vs* sample mass for cell H4.

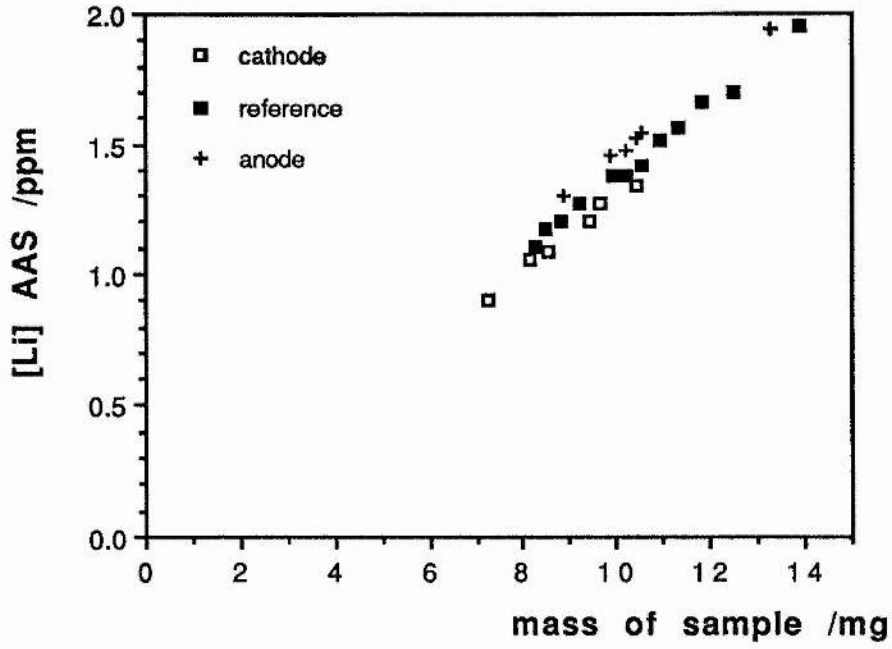

Figure 6-12. Indicated lithium content *vs* sample mass for cell H5.

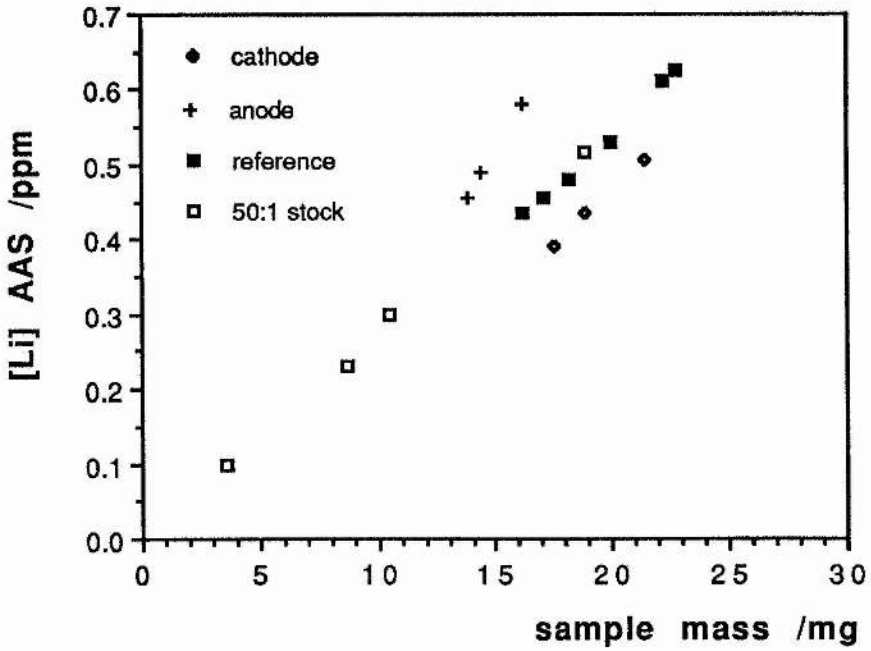

Figure 6-13. Indicated lithium content *vs* sample mass for cell H6.

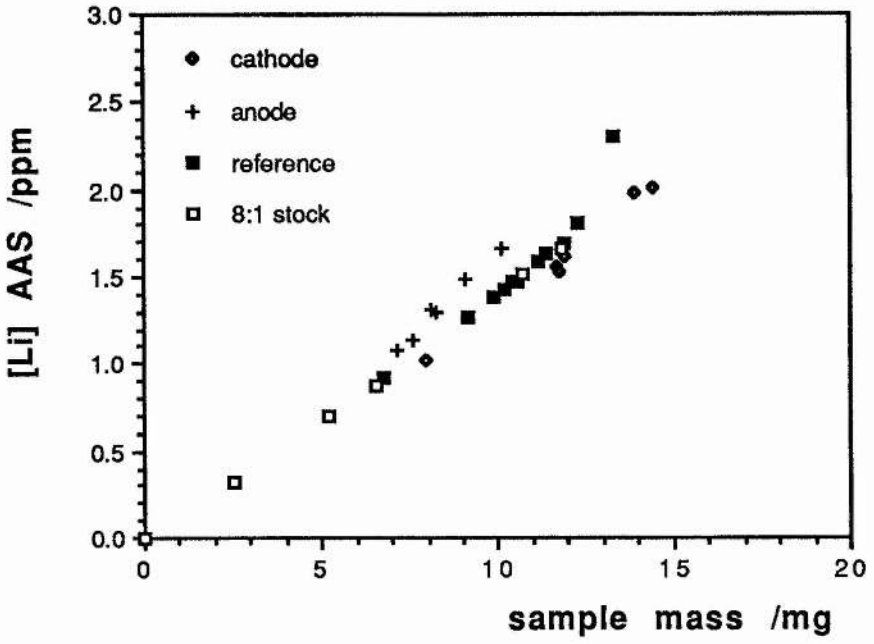

Figure 6-14. Indicated lithium content *vs* sample mass for cell H7.

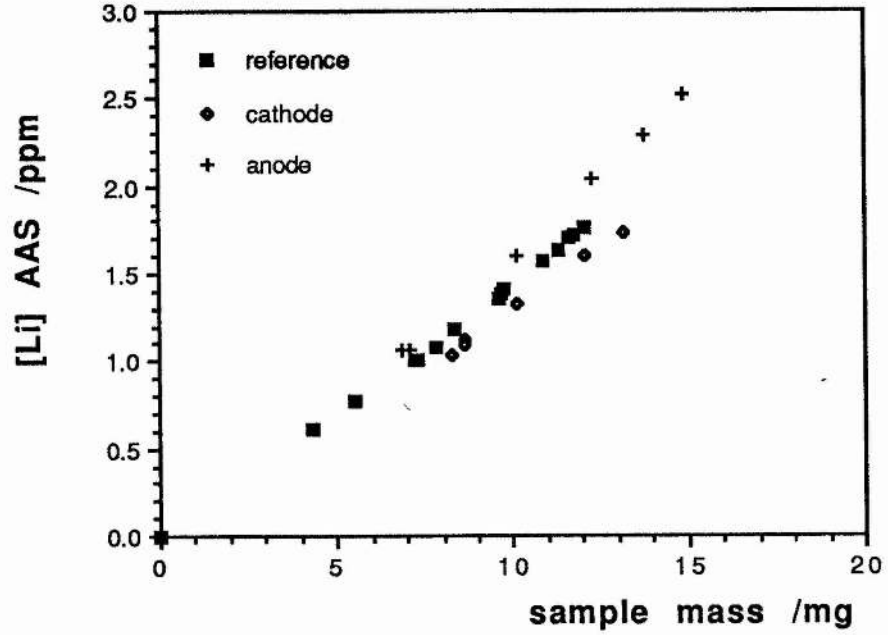

Figure 6-15. Sectioning of polarised and unpolarised electrolyte, demonstrating that the amount of lithium in the sample (weight for weight) is independent of the sectioning for unpolarised electrolyte, but dependent for the polarised electrolyte.
The lighter shading denotes a changed lithium content with respect to the rest of the electrolyte. The average lithium content (*i.e.* uniformity of shading) is constant in the unpolarised case, but is dependent on sectioning for the polarised electrolyte.

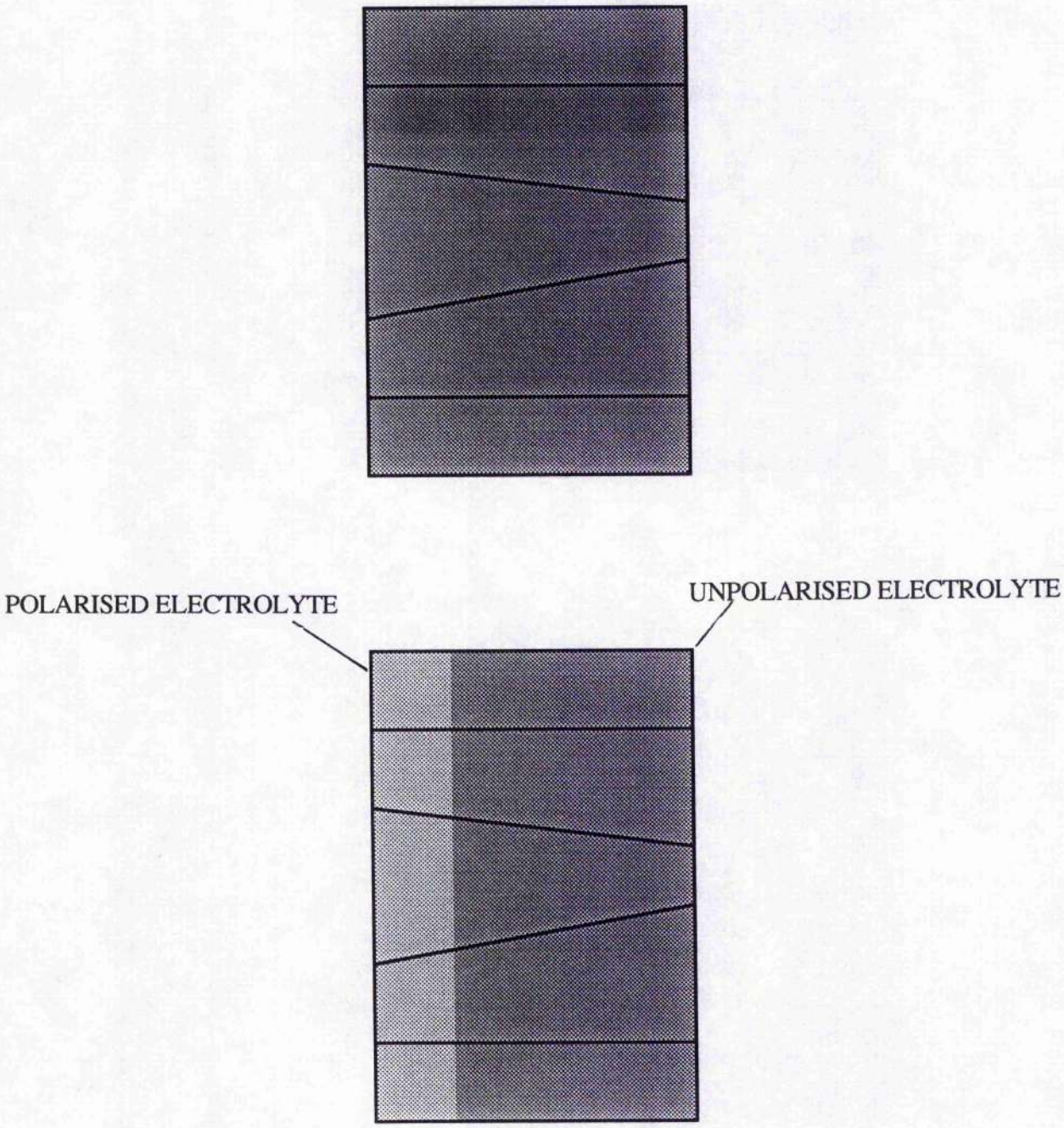

Figure 6-16. Demonstration of the dependence of transference numbers on the mass of lithium determined using equation (6-7).

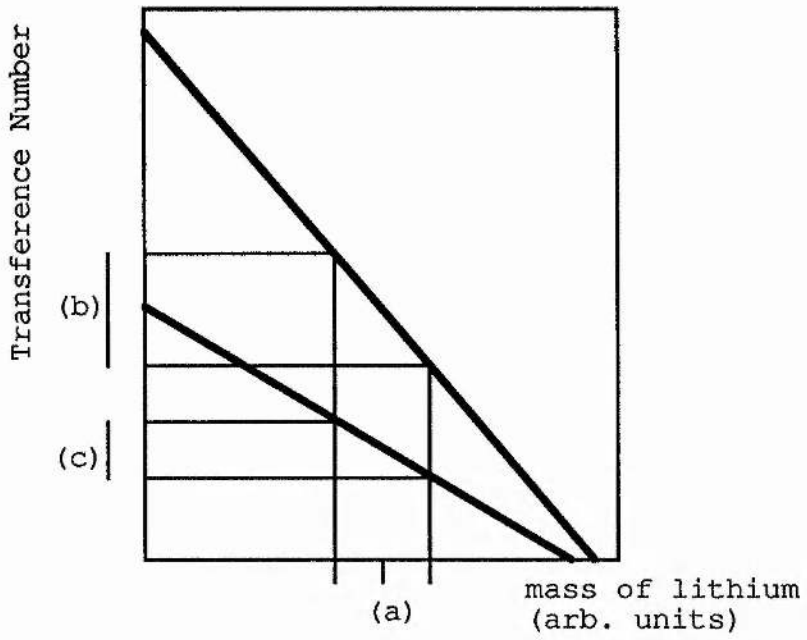

(a) This denotes the measured amount of lithium together with the error range associated with the measurement.

(b) This denotes the error in the transference number arising from the steepness of the gradient (i.e. due to the small value of Q).

(c) This denotes the error in the transference number arising from the lesser gradient (i.e. due to the large value of Q).

Figure 6-17. Graph of anion transference number *vs* mass of lithium for cell H4.

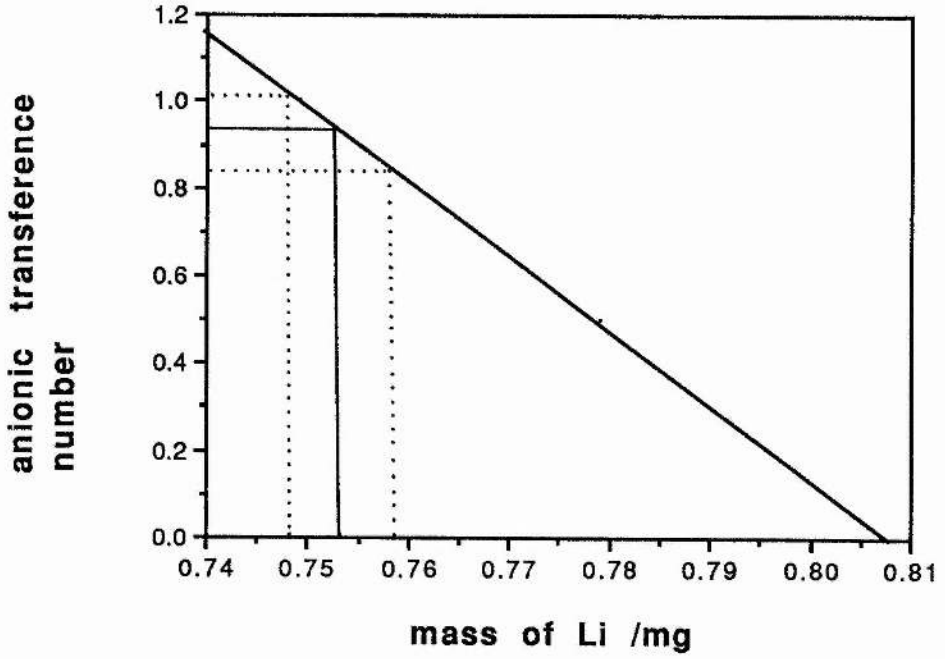

Figure 6-18. Graph of anion transference number *vs* mass of lithium for cell H5.

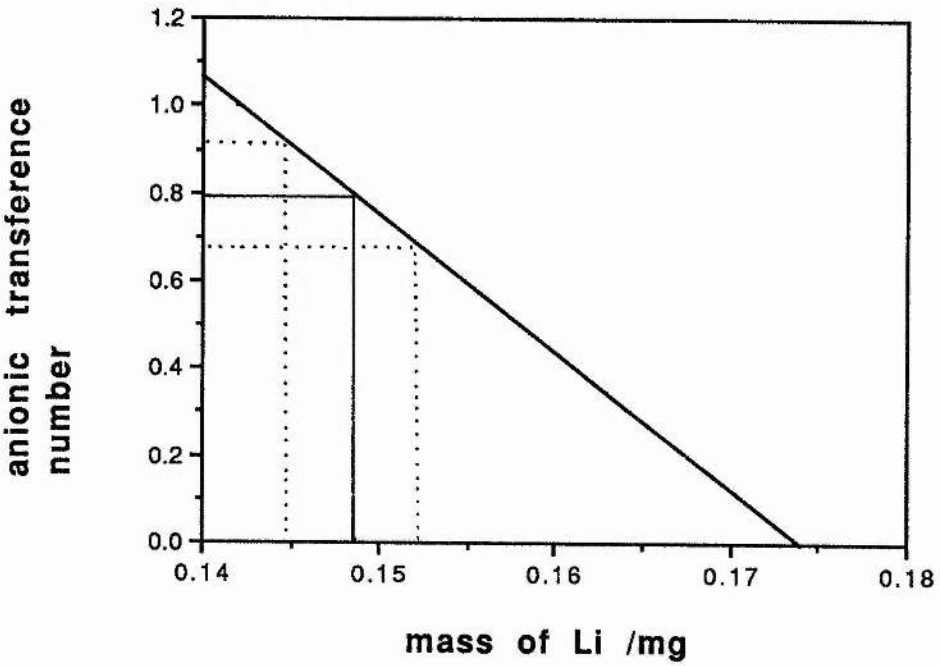

Figure 6-19. Graph of anion transference number *vs* mass of lithium for cell H6.

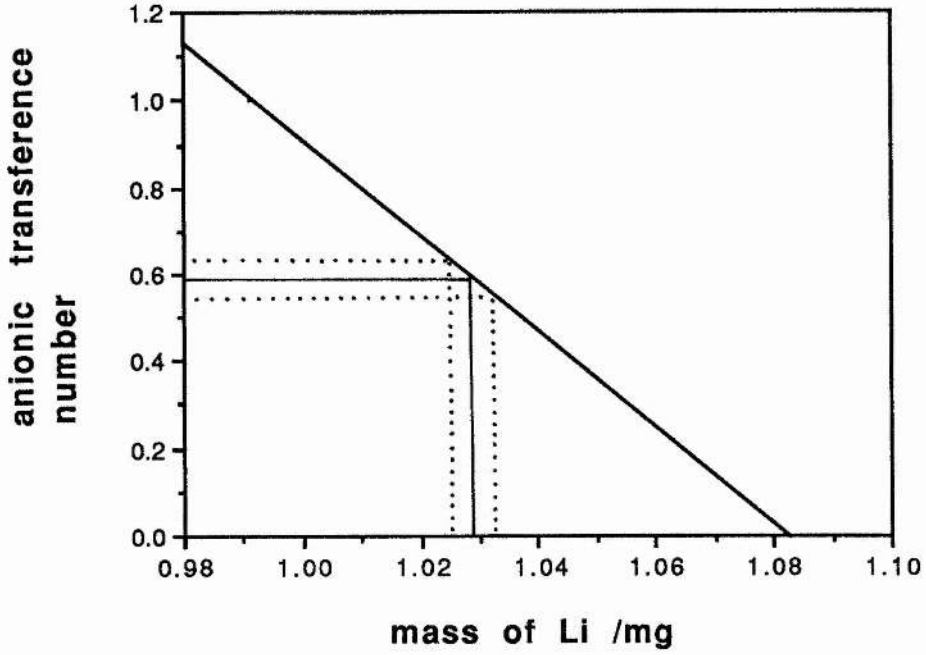

Figure 6-20. Graph of anion transference number *vs* mass of lithium for cell H7.

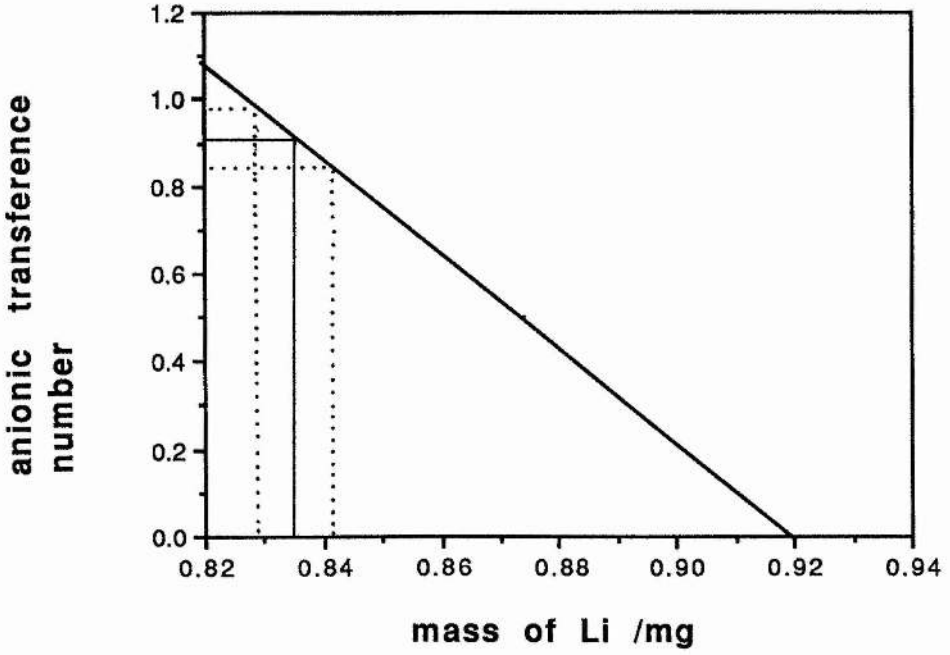

Figure 6-21. Relationship between sample notation and the electrolyte from a Hittorf cell. The compartments denoted C, MC, MA, and A represent the cathode, middle (cathode), middle (anode), and anode electrolyte compartments respectively. The numbers denote the samples produced by the sectioning of each compartment.

	C	MC	MA	A
1				
2				
3				
4				
5				
6				

CHAPTER 7

QUASIELASTIC NEUTRON SCATTERING STUDY OF $PEO_xLiCF_3SO_3$

Quasielastic neutron scattering (QENS) is an experimental technique which may be used to provide information about atomic motions in time and space. Reference [106] provides a thorough description of the physical basis of the technique and of the models of atomic and molecular motion which may be used to interpret the results obtained from this type of experiment. QENS has been used to study protonic conductors based on PEO [107] [108]. In this chapter results of a QENS study of several $PEO_xLiCF_3SO_3$ PEs will be presented and discussed, and a basic explanation of QENS given.

7.1 CONDUCTIVITY VARIATION OF $PEO_xLiCF_3SO_3$

Robitaille and Fauteux [11] [109] reported the conductivity variation with temperature and composition of $PEO_xLiCF_3SO_3$ prepared from commercial PEO, in which several maxima and minima were shown. Subsequently the conductivity variation for $PEO_xLiCF_3SO_3$ prepared from high-purity PEO was reported [109]. The form of conductivity-composition plot for the high purity samples is that of an "inverted parabola", as generally observed for other PEs. It was suggested that the oscillatory nature of the low purity PE conductivity could be due to different polymer motion occurring as the salt concentration changed, or due to a variation in the proportions of salt species present in the PE, with a greater proportion of neutral species present at the conductivity minimum.

It was intended that the polymer motion would be studied by quasielastic neutron scattering (QENS), and the possible changes in salt species present by examining the current-voltage response (as described in Chapters 3 and 5).

The conductivity-composition diagram from reference [109] is shown in Figure 7-1. The conductivities of the samples prepared for the dc study (which was carried out after the QENS study) did not agree with those reported in reference [11], but did agree with those reported in reference [109]. The fact that the hot-pressed samples for the dc study were prepared using unwashed commercial PEO suggests that these

conductivities should be displayed by all $PEO_xLiCF_3SO_3$ electrolytes. It is therefore most probable that the PE samples prepared for the QENS study (solvent cast from acetonitrile) also did not display the oscillatory conductivity behaviour that was supposed to be studied using this technique. Bearing this in mind, the results of the QENS study will now be reported.

7.2 QUASIELASTIC NEUTRON SCATTERING STUDY OF $PEO_xLiCF_3SO_3$

The polymer motion was studied by quasielastic neutron scattering on the IN6 time-of-flight spectrometer at the Institut Laue-Langevin in France under the auspices of Dr. Christiane Poinsignon (Laboratoire d'Ionique et d'Electrochimie du Solide, Saint-Martin d'Hères, Grenoble) and Dr. José Dianoux (Institut Laue-Langevin, Grenoble).

The theoretical model of polymer motion to which the experimental data were fitted was one in which there are two hydrogen environments and two hydrogen motions. The lithium triflate-based electrolytes are known to be a mixture of crystalline and amorphous material over a wide range of compositions and temperatures, so one of the hydrogen environments was chosen to be a "fixed" site (in a crystal) and the other a "mobile" site (in the amorphous material). The two types of motion considered were:

(a) precession of the C-H bond (tracing out a cone in space)

and

(b) large-scale motion of the methylene group in a sphere.

In the crystalline material only motion as in (a) was considered to occur. In the amorphous material both types of motion were considered to be occurring, but that the effect of (b) would be dominant. The assumption that the methylene groups move in a sphere may seem crude (the $-CH_2-$ groups cannot move independently, and motion in a sphere might not be the expected motion of a long "cylindrical" polymer) but it has been applied with some success to the study of long-chain hydrocarbons [110], to which a long-chained polyether may be roughly compared.

The motion of the methylene group provides information about the movement of the oxygen atoms to which these groups are attached; and it was envisaged that the highly conducting PE compositions would display a large volume of motion, allowing ions held by one part of the polymer to be moved closer to another, vacant polymer segment, facilitating the motion of charged species through the polymer thus enhancing the conductivity. It has been shown for protonic conductors [108] that the motion of the mobile protons is directly related to the motion of the polymer.

7.2.1 Experimentation

$PEO_xLiCF_3SO_3$ samples of composition x = 100, 36, 16, and 8 were prepared by solvent casting from acetonitrile. The instrumental arrangement of the IN6 spectrometer is depicted in Figure 7-2. The samples were 5 cm in diameter and 0.2 mm thick—this thickness being chosen to prevent the multiple scattering of neutrons in the sample. Samples were held in an aluminium can which was subsequently exposed in the neutron beam to provide a set of data for subtraction from the sample+can data. Finally, a vanadium standard was exposed; vanadium is a purely incoherent scatterer (see §7.3) and was used to provide a data set for normallising the experimental data. Exposure to the neutron beam was carried out at various temperatures, controlled to ± 5 K. The incident neutron beam is monochromatic, with several possible wavelengths between 4 and 6 Å capable of being produced. A wavelength of 5.9 Å was used in the experiment. At this wavelength neutrons possess an energy of the order of milli-electron volts (meV), which is of a similar magnitude to the energy changes involved in molecular rotation and translation.

By judicious choice of experimental parameters (sample thickness, total scattering cross-section, number of scatterers) it was arranged that the intensity of the transmitted beam was about 90% of that of the incident beam. 10% of the neutrons were thus scattered. This was done to minimise the amount of multiple scattering of neutrons in the sample. As the sample can was at 45° to the incident beam, it masked some of the detectors grouped around 225°. A plot of neutron count against angle is

shown in Figure 7-3, where 0° is taken to be the path of the incident beam. The reduction in neutron count at the masked angles is readily apparent.

Also indicated in Figure 7-3 are small increases in the neutron count above the background level at certain angles. These are Bragg reflections from ordered sites in the sample; which may sometimes appear if the sample is partially crystalline. Because some of the neutrons at these angles have not been randomly scattered there the data at these positions was not considered.

There were 94 individual spectra taken at angles between 0 and 115°, with varying numbers of detectors (up to 9) grouped around their nominal angle. The first 6 spectra (below 10°) are not considered, as they register the 90% of neutrons which are not scattered. There are a number of channels to record the incident neutrons as they impact on each detector, with the zero-energy transfer neutrons being centred on channel 428. All neutron events are recorded between channels 370 and 486, so only data from these channels are used. Figure 7-4 shows the neutron count *vs* channel number for 5 spectra taken from the exposure of a $PEO_{16}LiCF_3SO_3$ sample. It is readily apparent that the neutron counts are indeed all recorded in the range of channels chosen. From these channels which contain data for each detector, diagrams such as Figure 7-3 may be obtained for the whole range of angles available.

What is actually done to obtain a plot of counts *vs* angle, such as that shown in Figure 7-3, is to take the sample counts at a given angle θ normalised for all sample counts, subtract the data obtained for the can alone, and to normalise this against the same data obtained for the vanadium standard, *i.e.*:

$$\frac{\dfrac{\text{sample counts at } \theta}{\text{total sample counts}} - \dfrac{\text{can counts at } \theta}{\text{total can counts}}}{\dfrac{\text{vanadium counts at } \theta}{\text{total vanadium counts}}} \qquad 7\text{-}1$$

Data from small groups of adjacent spectra (*e.g.* spectra 64-66, 67-70, *etc.*) are combined, providing that there is no evidence of non-random data being present. About 10 sets of data above the masked angles were studied in total, with each assigned

the angle around which the constituent groups are centred.

A graph of neutron counts against energy for $PEO_{16}LiCF_3SO_3$ at 105°C and angle 96.5° is shown in Figure 7-5. It is seen that most of the neutrons are scattered elastically (*i.e.* with zero energy change), with some quasielastic scattering around zero energy. A lorentzian corresponding to elastic scattering and one corresponding to quasi-elastic scattering are shown in Figure 7-5.

7.3 NEUTRON SCATTERING

Neutron scattering may be either coherent or incoherent. In coherent scattering the influence of nuclear spins is small or absent, and the waveform properties of the neutron predominate on collision. Thus, interference phenomena may give rise to diffraction and scattering patterns indicative of the sample structure.

Incoherent scattering is complex: the neutrons behave more like particles than waves when interacting with nuclei of nuclear spin $I > 0$. The scattering angle and amplitude depend on whether the spins are parallel or antiparallel, and also on the magnitude of I. As the alignment of spins through a sample is random, the incoherent scattering intensity is equal at all angles.

The scattering may be described in terms of a parameter b, the scattering length, and b is dependent on the spin-state of the nucleus-neutron system. For a nucleus of spin s and neutron of spin (1/2) there are two possible spin states: s + (1/2) and s – (1/2), so there are also two scattering lengths. The coherent scattering length is given by $\langle b_i \rangle$, where $\langle b_i \rangle$ is the average of all scattering lengths b_i; and the incoherent scattering length is given by:

$$\left[\langle b_i^2 \rangle - \langle b_i \rangle^2 \right]^{1/2} \qquad 7\text{-}2$$

where the first term is the average of the squares of all the b_i, and the latter the square of the average of all the b_i's. The scattering cross-sections are related to the scattering

lengths by the following equations:

$$\sigma_{coh} = 4\pi\langle b\rangle^2 \qquad 7\text{-}3$$

and

$$\sigma_{inc} = 4\pi\left(\langle b^2\rangle - \langle b\rangle^2\right) \qquad 7\text{-}4$$

Samples containing hydrogen are predominantly incoherent neutron scatterers, because the incoherent scattering cross-section of hydrogen is ≈ 80 barns, a value which is much larger than either the coherent or incoherent cross-sections of other elements.

Figure 7-6 is similar to Figure 7-2, but the momenta of the incident and scattered neutrons are indicated. The incident neutron beam is of fixed wavelength and collimated (*i.e.* the energy of the incident beam E_o and the wavevector $\underline{K}_o$ are constant, where:

$$E_o = \frac{\hbar^2 K_o^2}{2m} = \hbar\omega_o \qquad 7\text{-}5$$

The momentum of the incident neutrons, being a vector quantity, is given by:

$$\underline{p} = \hbar\underline{K}_o \qquad 7\text{-}6$$

After scattering from the sample a neutron will possess an energy E, given by:

$$E = \frac{\hbar^2 K^2}{2m} = \hbar\omega \qquad 7\text{-}7$$

and a new wavevector $\underline{K}$. In a QENS experiment therefore, the energy change and wavevector change must be measured.

The change in wavevector is represented by the scattering vector $\underline{Q}$, where:

$$\underline{Q} = \underline{K} - \underline{K}_o \qquad 7\text{-}8$$

as shown in Figure 7-7. For no change in the magnitude of the wavevector, Q is given by:

$$Q = \frac{4\pi}{\lambda_o}\sin\vartheta \qquad 7\text{-}9$$

so Q may be used as a measure of the angle through which scattering has occurred, and data is quoted at different Q values.

Thus, after scattering the neutron may be moving in a solid angle $\underline{\Omega}$ with energy E, and in a scattering experiment one is measuring the change in scattering cross-section, σ, with $\underline{\Omega}$ and E; *i.e.*:

$$\frac{\partial^2\sigma}{\partial\underline{\Omega}\,\partial E} = \frac{1}{\hbar}\frac{\partial^2\sigma}{\partial\underline{\Omega}\,\partial\omega} \qquad 7\text{-}10$$

and this in turn may be represented in terms of a scattering law (or scattering function), S, which must be a function of direction and energy, *i.e.* $S(\underline{Q},\omega)$.

If the coherent and incoherent terms are both considered then it may be written that:

$$\frac{\partial^2\sigma}{\partial\underline{\Omega}\,\partial E} = \frac{1}{\hbar}\frac{K}{K_o}\left[\sigma_{coh}S_{coh}(\underline{Q},\omega) + \sigma_{inc}S_{inc}(\underline{Q},\omega)\right] \qquad 7\text{-}11$$

The scattering laws depend only on the properties of the system and are independent of the experiment [106]. If a sample is predominantly hydrogenous then only the incoherent scattering law will be important, and the only important coherent scattering will arise from elastic Bragg reflections.

The scattering function is the time Fourier transform of the intermediate scattering function, $I(\underline{Q},t)$:

$$S(\underline{Q},\omega) = \frac{1}{2\pi}\int_{-\infty}^{\infty} e^{-i\omega t}\, I(\underline{Q},t)\, dt \qquad 7\text{-}12$$

and $I(\underline{Q},t)$ may be derived for various types of motion (*e.g.* rotation over a sphere, jumps over n equidistant points on a circle *etc.*) [106].

It is useful to separate $S(\underline{Q},\omega)$ into an elastic and quasielastic term, because the quasielastic part contains information about reorientational motions. Leadbetter and Lechner [111] show that:

$$S(\underline{Q},\omega) = A_o(\underline{Q})\delta(\omega) + S^{qe}(\underline{Q},\omega) \qquad 7\text{-}13$$

where $\delta(\omega)$ is a δ-function. Thus $S(\underline{Q},\omega)$ contains an elastic component, $A_o(\underline{Q})\delta(\omega)$,

superimposed on a quasielastic component, $S^{qe}(\underline{Q},\omega)$. $A_o(\underline{Q})$ is called the *elastic incoherent structure factor* (EISF), and it gives information about the time-averaged distribution of the scatterer in space. If the time-averaged distribution is bounded the scatterer's position will be its starting position, and A_o tends to 1 as Q tends to zero. If this is found experimentally not to be the case, then it is known that the motion of the scatterers is not localised.

$S^{qe}(\underline{Q},\omega)$ may be written as:

$$S^{qe}(\underline{Q},\omega) = A_n(\underline{Q}) \sum L_i \qquad 7\text{-}14$$

where $A_n(\underline{Q})$ is the quasielastic structure factor. The lorentzians, L_i, arise from the different types of motion considered to occur in the sample. The ratio:

$$\frac{A_o(Q)}{A_o(Q) + A_n(Q)} \qquad 7\text{-}15$$

is determined experimentally and compared to the same ratio provided by the theoretical scattering law.

7.4 EXPERIMENTAL RESULTS

The handling of data and fitting of a motional model were performed using computer programs and subroutines available at the ILL. The presence of a mixed phase made it difficult to interpret the data obtained, because the crystalline material present was found to have a great effect on the results obtained. It did not prove possible to compare the experimental and theoretical EISFs in equation (7-14), because the presence of crystalline material made the procedure relatively insensitive to the amount of amorphous material present. Figure 7-8 shows the experimentally determined structure factor for an 8:1 electrolyte at various temperatures. It is seen that even at high Q values (*i.e.* large angles) and high temperatures the structure factor is large, due to the presence of crystalline material. Figure 7-9 shows the same type of plot for a less crystalline 16:1 electrolyte where the structure factor is not as great.

One of the parameters required for a simulation of the experimental data is the fraction of "fixed" sites in the sample, *i.e.* the proportion of the sample which is crystalline. It was remarked in Chapter 2 that this may not be confidently found from the phase diagram of the system. Eventually, only the high temperature data were examined in detail, to minimise the proportions of crystalline material present. The 8:1 sample was used to provide fitting parameters for the crystalline material present in the other samples.

The presence of crystalline material has been shown to give rise to Bragg peaks in Figure 7-3. It also results in diagrams of counts *vs* energy being predominantly elastic, especially at low temperatures. Figure 7-10 shows a plot of counts *vs* energy for an 8:1 electrolyte at 27°C. The form of the plot is very elastic, with most of the counts occurring close to zero energy change. The same sample at 117°C produces a plot which shows a more significant, but still very small, quasielastic response, as shown in Figure 7-11.

The model of motion was applied to data from three angles for each composition, each angle being examined separately at first in order to obtain a suitable fit, and then all three were examined together. The radii of diffusion that this treatment gave for the 100:1, 36:1, and 16:1 samples showed a slight decrease as the salt concentration increased, as might be expected due to the introduction of more transient cross-linking cations, and were about 2.5 Å (the difference between the 100:1 to 16:1 samples only being 0.2 Å), a value which is similar to that found for methylene groups in long-chained hydrocarbons [110].

The presence of crystalline material in the $PEO_xLiCF_3SO_3$ system complicated the interpretation of results from these systems, but together with the results from the polarisation study (*i.e.* the electrolyte conductivities) such results as were obtained suggest that the conductivity-composition diagram of Robitaille and Fauteux [11] is not the typical displayed conductivity-composition diagram for this material.

Figure 7-1. Conductivity-composition diagram of $PEO_xLiCF_3SO_3$ from reference [11].

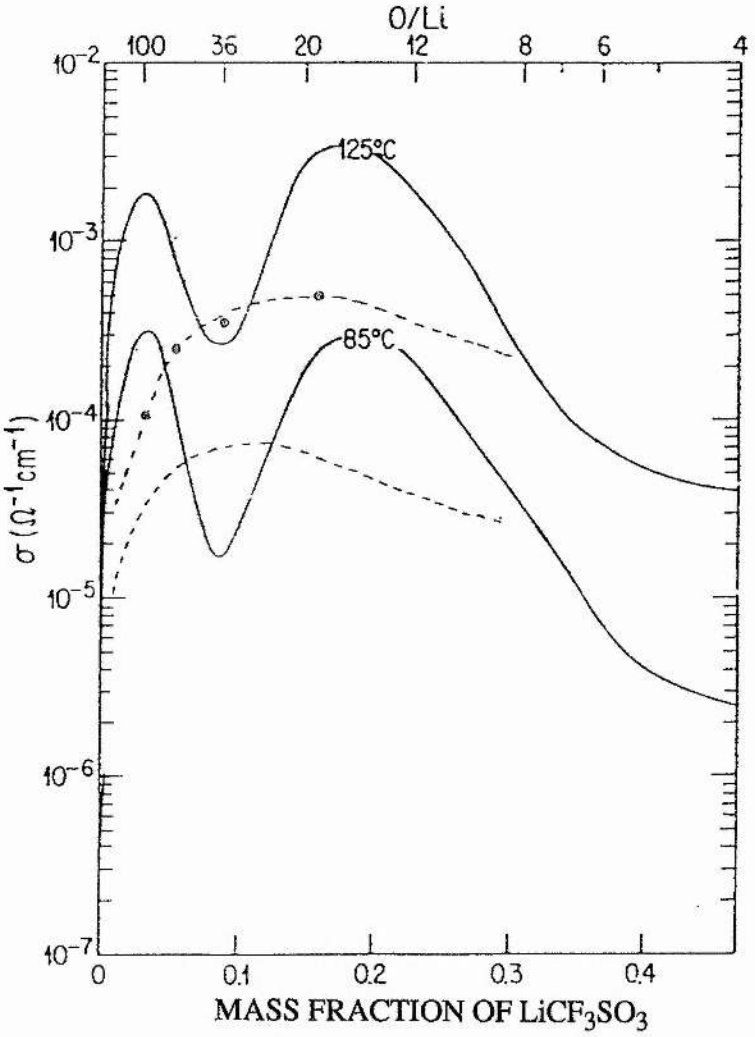

Fig. 1. Isothermal variation of the ionic conductivity as a function of salt weight fraction for C-PEO–$LiCF_3SO_3$ (——) and HP-PEO–$LiCF_3SO_3$ (- - -) systems at 85 and 125 °C.

(•) THIS STUDY AT 120°C

Figure 7-2. Representation of the instrumental arrangement of the IN6 t-o-f spectrometer at the ILL, Grenoble.

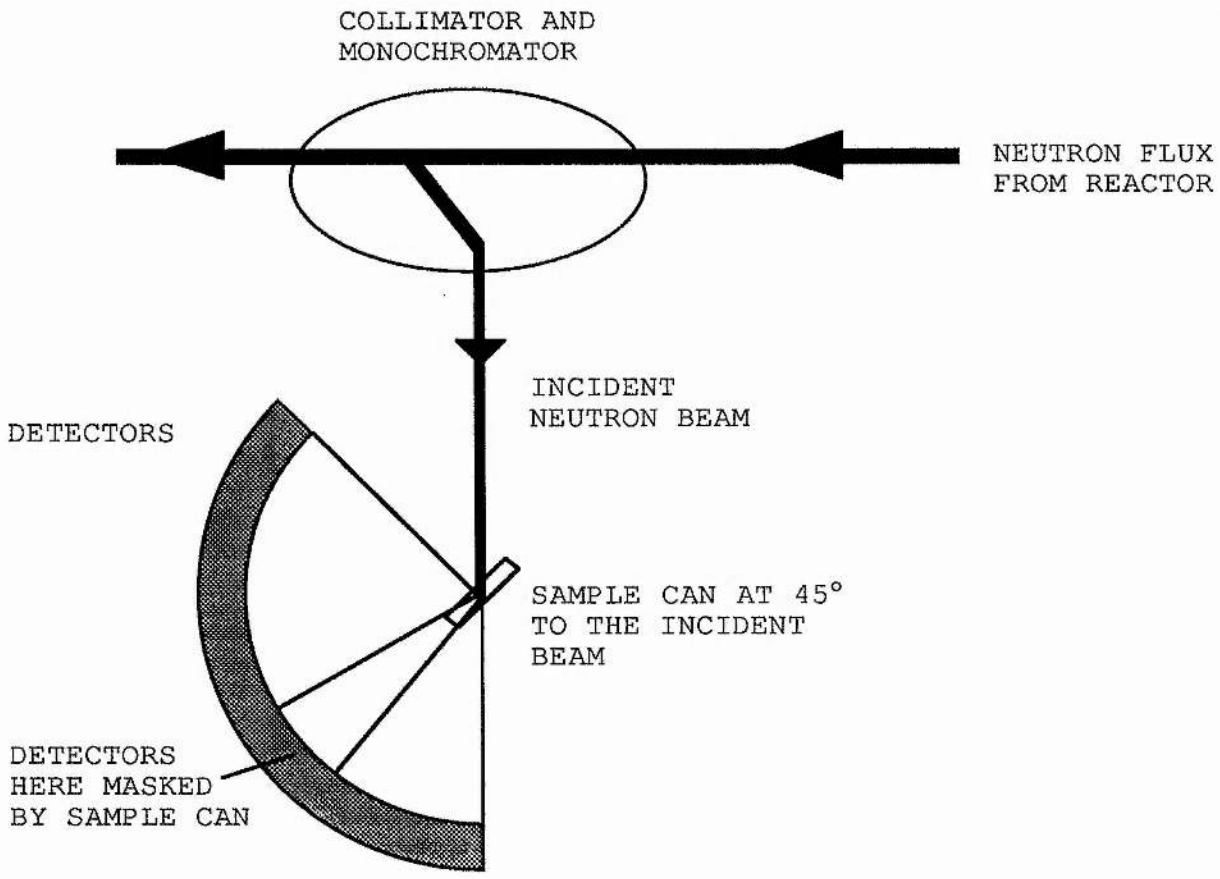

Figure 7-3. Plot of neutron counts *vs* angle for a $PEO_8LiCF_3SO_3$ electrolyte displaying masked angles and Bragg peaks (*).

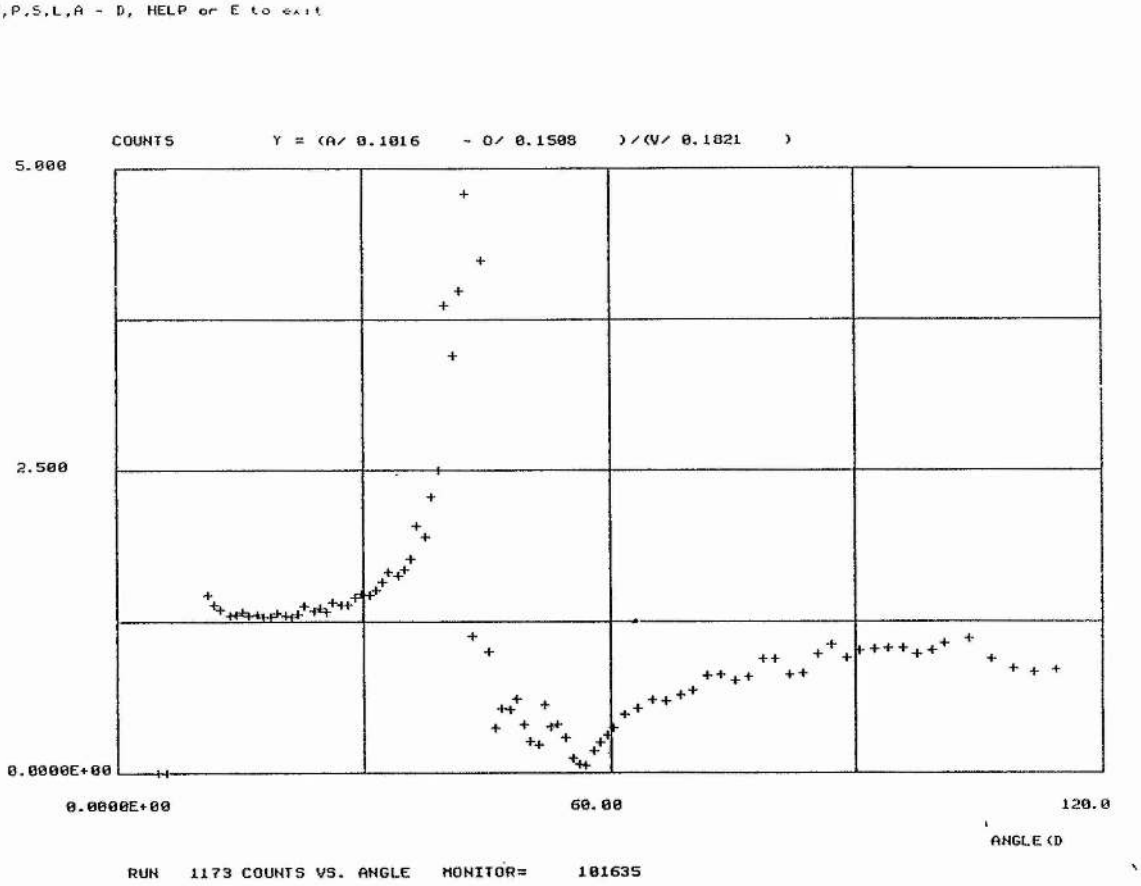

Figure 7-4. Plot of neutron counts *vs* channel number from the exposure of a $PEO_{16}LiCF_3SO_3$ sample.

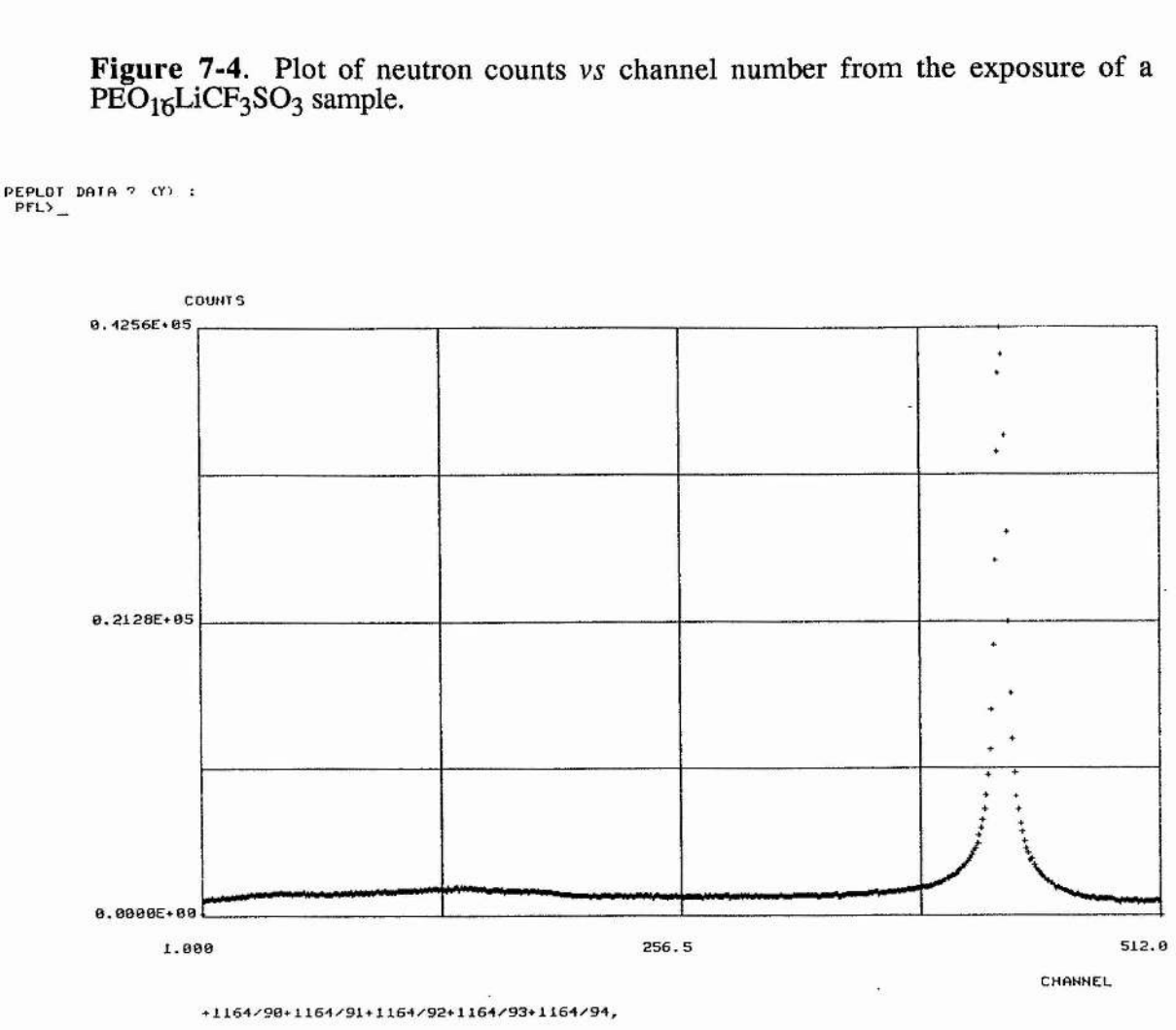

Figure 7-5. Plot of neutron counts *vs* energy for a $PEO_8LiCF_3SO_3$ sample at 378K at angle 96.5°.

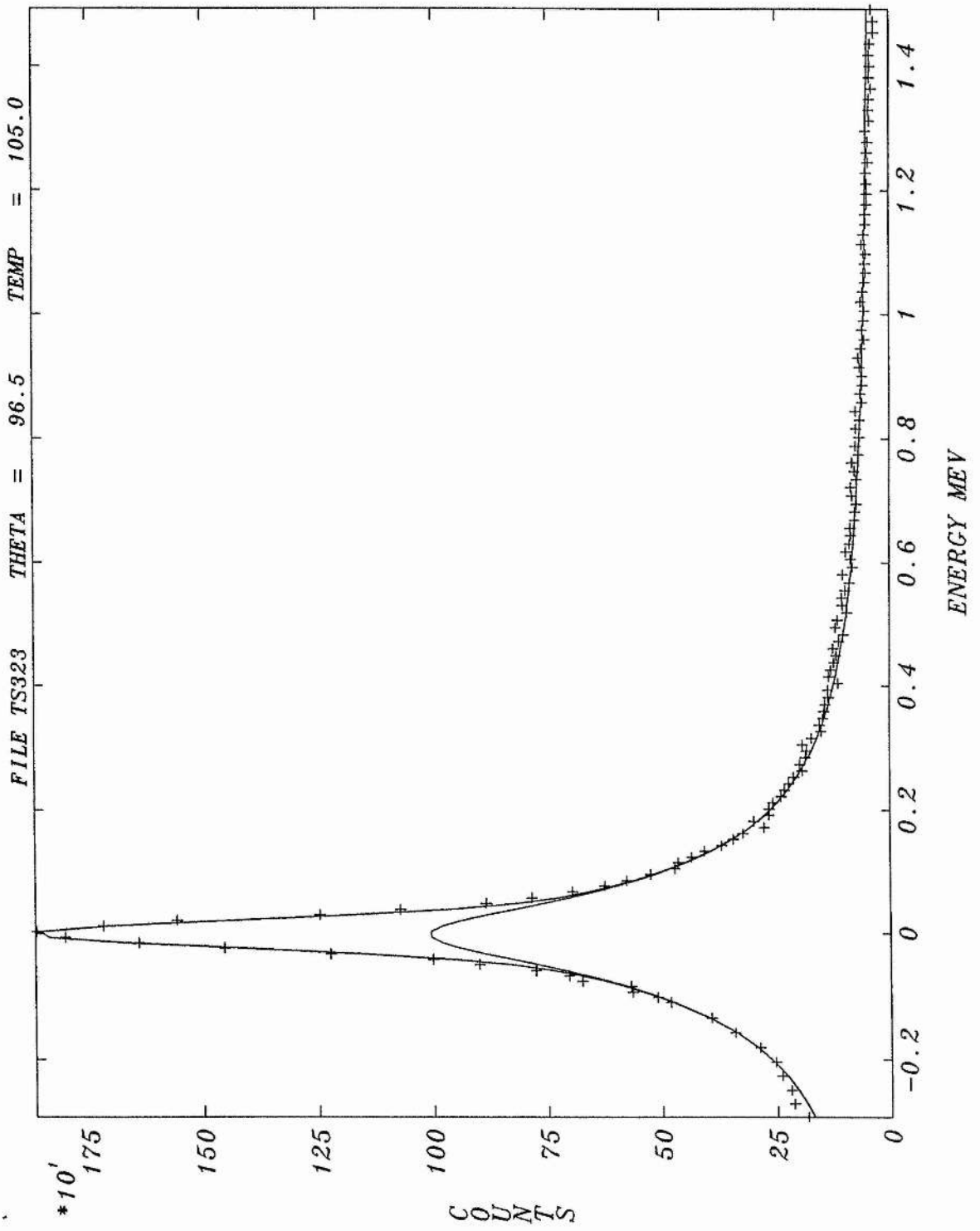

Figure 7-6. Representation of the momenta of incident and scattered neutrons.

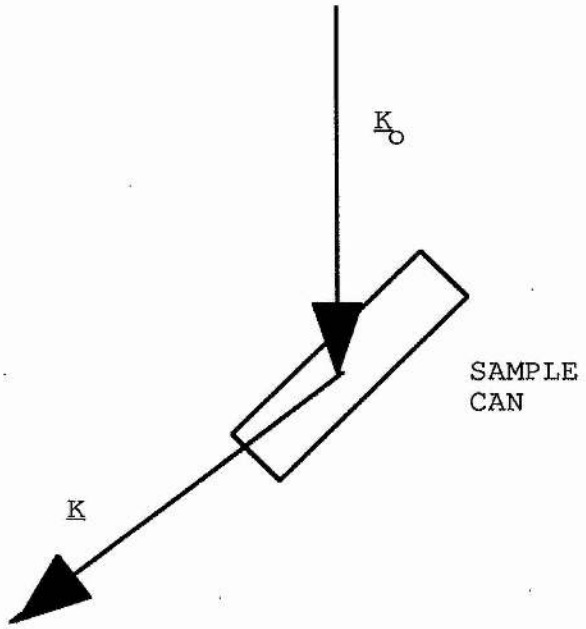

Figure 7-7. Determination of the scattering vector Q from the incident and scattered neutrons.

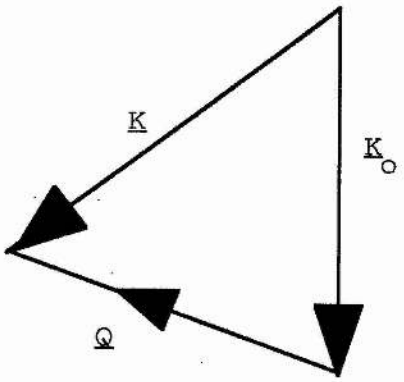

Figure 7-8. Experimentally observed EISF for $PEO_8LiCF_3SO_3$ at various temperatures.

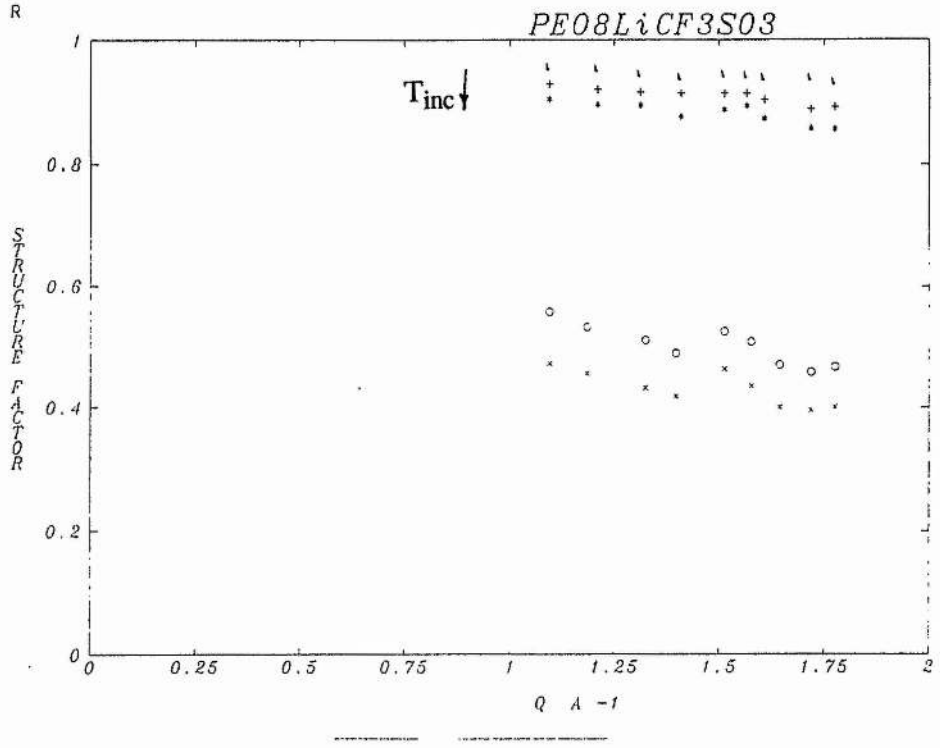

Figure 7-9. Experimentally observed EISF for $PEO_{16}LiCF_3SO_3$ at various temperatures.

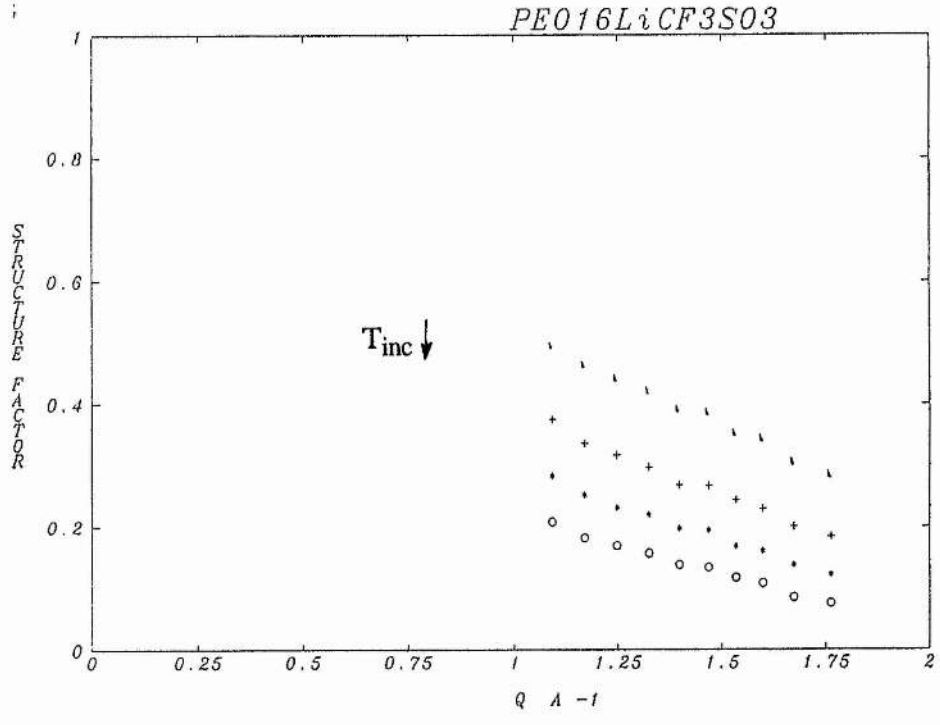

Figure 7-10. Plot of counts against energy change for $PEO_8LiCF_3SO_3$ at 27°C

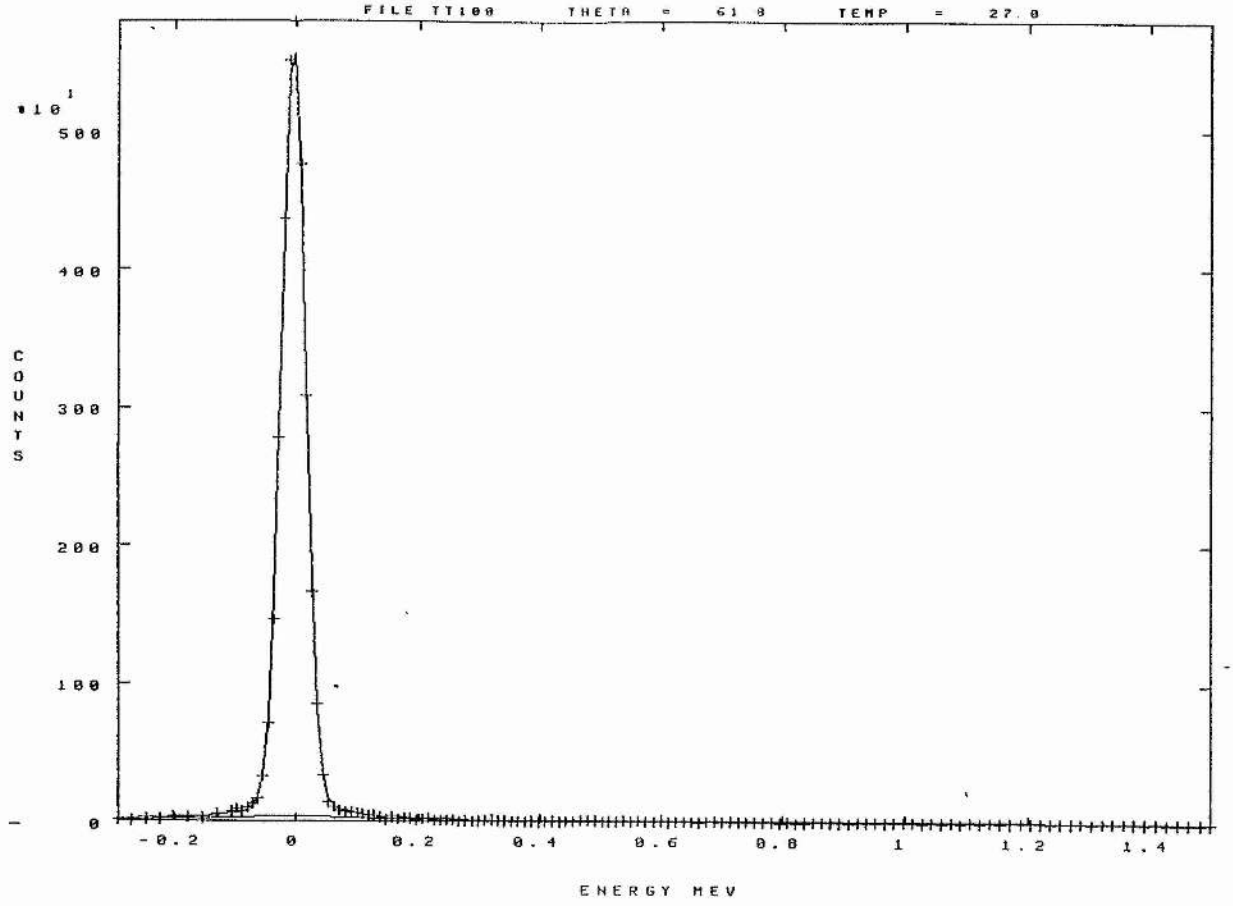

Figure 7-11. Plot of counts against energy change for $PEO_8LiCF_3SO_3$ at 117°C

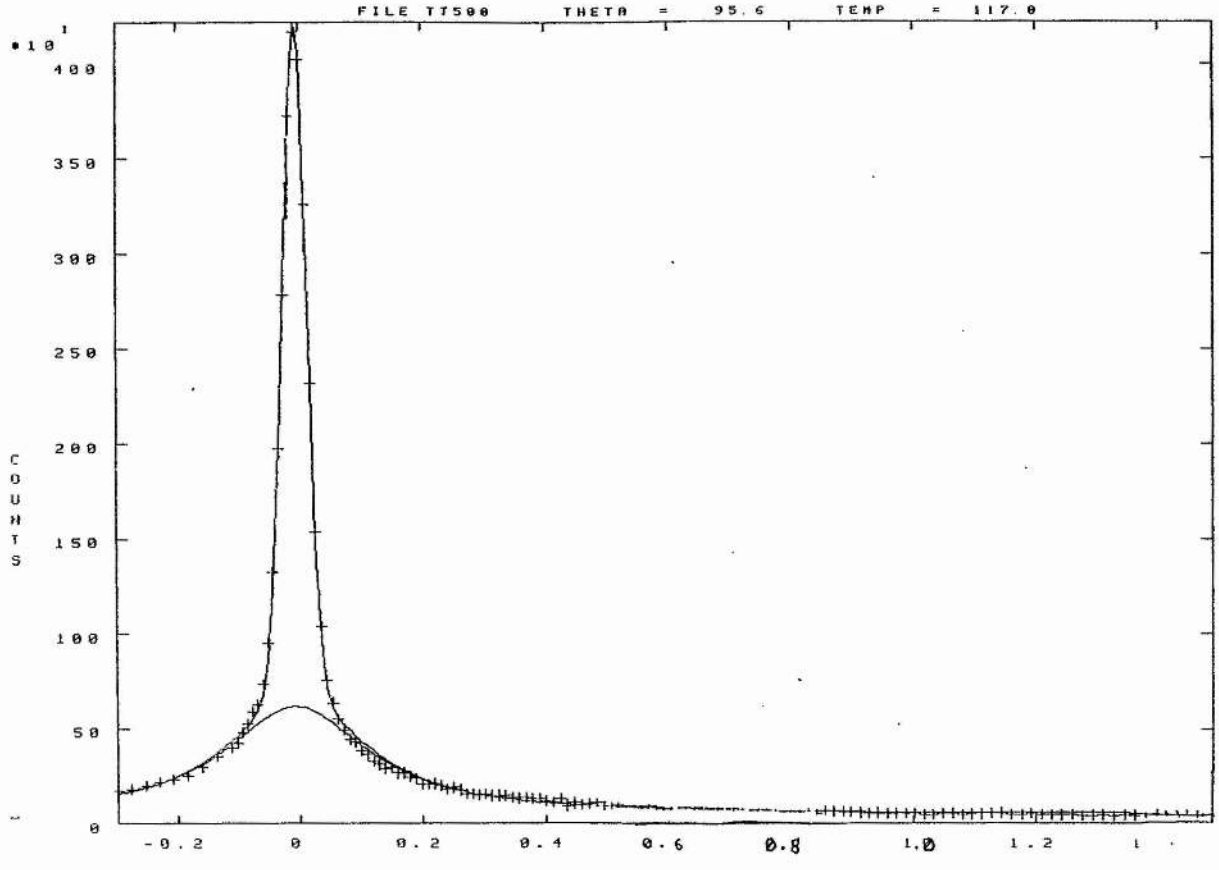

CHAPTER 8

DISCUSSION

There are three main parts to this thesis: the theoretical and experimental examination of two-electrode cells at steady-state, and the non-equilibrium experimental study of electrolytes using the Hittorf technique. The important points which have arisen in this thesis will now be summarised and discussed.

8.1 THEORETICAL TREATMENT

The extension of the treatment of an ideal PE containing free ions to a PE containing ion-pairs as well as free ions resulted in three major differences between the results provided by each examination; these are in terms of the potential difference distribution, steady-state current, and applied potential difference range of linear I^s-ΔV response.

(i) *Potential Difference Distribution.* Neglecting (or correcting for) an interface resistance, the applied potential difference is evenly distributed over the concentration potential difference and electrolyte potential difference when the electrolyte only contains free ions. If ion-pairs are present this distribution is uneven, with the electrolyte potential difference being the greater of the two.

(ii) *Steady-state Current.* When this is found at a potential difference for which a linear I^s-ΔV response occurs, it is the cation contribution to the initial current when only free ions are present. The diffusion of the cations exactly balances the reduction in cation migration arising from the fall in the electrolyte potential difference during the experiment. This allows the ratio of the steady-state to initial current to be used as a measure of the cation transport number. However, this measurement must be performed in the linear I^s-ΔV region because a fall in the anticipated steady-state current occurs at higher potentials, preventing the ratio from being used as a measure of the transport number.

When ion-pairs are present the steady-state current is not that part of the initial current arising from the cations, because the mass transport of cation-containing species must consider the effect of ion-pair diffusion. The use of I^s/I^o as a measure of the

cation transport number is thus invalid when mobile ion-pairs exist in the electrolyte. However, this use of the ratio of the currents provides a practical means of assessing an electrolyte's suitability for use in a battery, but paradoxical results may occur if the equation is cited as a transport number or transference number. This led to the ratio being termed the "current fraction".

(iii) *Applied Potential Difference Range of Linear I^s-ΔV Response.* When free ions alone are considered this limit of an ohmic response of steady-state current to applied potential difference only holds up to 20 mV, if deviation from linearity of 1% is taken to be the limit. This arises from the approximation of a logarithmic term by a linear term, which is only valid in the limit of small potential differences (which is to say small concentration differences at the electrodes).

When ion-pairs are present this applied potential difference range may be as large as tens of volts. This difference is due to the rapid diffusion of neutral species in the electrolyte, preventing a large ionic concentration difference from being established between the electrodes. As well as their mobility, the presence of a large amount of ion-pairs will also contribute to the size of the neutral species flux. The approximation of a logarithmic term by a linear term is still used, but its breakdown does not occur.

The effects of non-ideality on PEs containing free ions were shown to be similar to those of the presence of ion-pairs; that is, a decrease in ΔE with respect to $\Delta\phi$, and an increase in the potential difference range over which the I^s-ΔV response is linear.

When triple ions are present only a limited number of models may be examined fully. In these cases, when M^+ ions are present, the concentration potential difference is again less than the electrolyte potential difference. The postulation of electrode reactions when M^+ ions are not present in the electrolyte may give rise to an electrolyte potential difference less than the concentration potential difference, though none were found. A modification of the free ions and ion-pairs model was shown to do this.

The difference between transport numbers and transference numbers was discussed, and it was shown that the steady-state polarisation experiments may not usually be used to measure these parameters. It was suggested that the parameter measured in steady-state current measurements be called the "current fraction". This shows what proportion of the initial current may be maintained at steady-state, in the absence of interface resistances. The parameter is dependent on any electrolyte resistance changes and breakdowns in approximations used to relate the current and potential difference, hence it is a very practical parameter. At low applied potential differences the parameter is constant, and referred to as the "limiting current fraction". Because resistance changes and approximation breakdowns serve to decrease the steady-state current from the value it would take in their absence, the limiting current fraction represents the maximum proportion of the initial current which may be maintained at steady-state.

If experimental determinations of this parameter are to be performed, which is desirable (because a high ac conductivity may not be due to the non-blocked species in a steady-state experiment; *e.g.* magnesium-based PEs which display a tolerable ac conductivity but almost non-existent dc conductivity when magnesium electrodes are employed) the potential difference range over which the determinations were made should be stated. For example, in Table 5-Q a current fraction of 0.04 is obtained for $PEO_{100}LiClO_4$, which is an almost meaningless statement if the potential difference at which the measurement was made is not stated. The fact that this is the current fraction at nearly 600 mV might lead one to expect that a larger current fraction may be obtained at lower potential differences, which is found to be the case—the limiting current fraction is 0.34 for this electrolyte.

It is also of vital importance for the effects of interface resistances to be corrected for—it might be the case that in practical devices these resistances exist, but they are not properties of the electrolyte *per se*, and their presence and magnitude depend on many circumstances (electrode materials, thermal history *etc.*); so to have

any meaningful discussion about the electrolyte alone they must be corrected for.

Verification of the theoretical predictions has been sought in the literature. Extended ranges of linear I^s-ΔV response have been found, though one can not always be sure that interface resistances have been corrected for. Results by Gray and by Watanabe suggest that resistance changes do not occur to a great extent at very low concentration (O:M » 100:1) and that extended ohmic responses between the steady-state current and applied potential differences occur. It is possible that the examination of these low concentration electrolytes may provide results which can be interpreted in terms of the presence of simple salt species, and allow the interpretation of data from higher concentration electrolytes. However, though it is easy to predict what type of polarisation response should occur for these systems (for example, if the minimum in the molar conductivity plot in Figure 2-4 is due to the presence of ion-pairs, then mobile ion-pairs will tend to extend the ohmic range and make ΔE less than $\Delta\phi$, but immobile (solvent-separated) ion-pairs will simply reduce the free ion concentration, resulting in a low ohmic range and ΔE being equal to $\Delta\phi$) it is likely that one cannot proceed to lower and lower concentrations using the theory in Chapter 3, because a point will be reached where a substantial space-charge will exist in the vicinity of the electrodes, making it difficult to separate the potential difference into identifiable ΔE and $\Delta\phi$ terms.

8.2 EXPERIMENTAL STUDY

The experimental examination of PEs has been hampered by the fact that electrolyte resistance changes occurred at large polarisation potentials for most of the electrolytes examined. In the case of $PEO_{18}LiCF_3SO_3$, high polarisation potentials produced an erratic response, which is suggested to be due to the salt concentration at the anode rising to a point at which electrolyte crystallisation occurred. Mixed-phase systems are known to produce more erratic results. The distribution of the applied potential difference between concentration and electrolyte potential differences is also not constant with potential, so changes in these proportions will have an effect on the

current passed by the electrolyte. Because the electrolytes studied are relatively highly conducting short-circuiting was a frequent problem.

The potential difference range of linear I^s-ΔV response was experimentally limited by changes in the electrolyte resistance, so it was not possible to determine the potential at which mathematical approximations broke down.

The determination of current fractions and limiting current fractions was performed for the two lithium electrolytes most used in the production of PEs. The variation with temperature of the limiting current fractions was determined for $LiClO_4$-based electrolytes, and an empirical relationship between the current fractions and the proportion of the applied potential difference existing as the concentration potential difference was found.

8.3 HITTORF STUDY

The results from the Hittorf experiments demonstrate that such experiments might be performed on a wide range of electrolytes. Unlike the situation in the Tubandt method, electrolyte slabs do not have to be separated undamaged. Only an arbitrary sectioning of the electrolyte needs to be performed, providing that all of the concentration changes are retained in the electrode compartments. Problems with contamination of the anode compartments remain to be overcome, but the problem is not so great with lithium as it is expected to be for sodium.

The analytical technique chosen to detect the lithium has proved to be of sufficient accuracy, though the experimental procedure was time-consuming. AAS may be used to determine the concentrations of other salts which are of interest, such as sodium- and zinc-based PEs.

The use of a lead metal cathode allowed the verification of the current being due to the reduction of lithium ions, and not due to any electrolyte breakdown at the

interface. The use of a relatively low current permitted reproducible polarisations to be made. Low currents require long polarisation times, but this is possible in solid PEs because of the lack of convection.

Using this technique the cation transference numbers were found to be low—lower than the current fractions, but greater than the cation transference numbers reported for liquid PEs containing a different salt.

8.4 CONDUCTIVITY OF LITHIUM TRIFLATE-BASED POLYMER ELECTROLYTES

The results of the polarisation of the lithium triflate-based PEs suggest that the anomalous conductivity-concentration behaviour of this system is not generally observed for this electrolyte, because the conductivities of hot-pressed samples prepared from commercial polymer were the same as those prepared from purified polymer. The results of a quasielastic neutron scattering experiment agreed with this observation, inasmuch as a reduction of polymer motion with increasing concentration was observed, presumably caused by increasing viscosity.

8.5 FUTURE WORK

The results of this thesis suggest that the determination of current fractions should be carried out over a stated potential difference range, to see if the measured parameters are constant. The measurement itself is of practical use, more so than measurements using NMR or radiotracer techniques, because it is a property of the electrolyte under conditions which will occur in batteries. The electrolytes studied were chosen because of their widespread use and amorphous compositions, so the results obtained are relatively reproducible. Results from mixed-phase materials may vary from sample to sample; nevertheless, these types of measurement for other PEs would be desirable.

The determination of transference numbers may be performed for relatively firm electrolytes using the technique detailed in Chapter 6. Such measurements mean that at last a straightforward way of determining these somewhat elusive parameters exists, enabling these measurements to be compared with steady-state results and results from "non-invasive" techniques such as NMR and radiotracer diffusion.

REFERENCES

[1] D. E. Fenton, J. M. Parker and P. V. Wright
Polymer **14** (1973) 589

[2] M. Armand, J. M. Chabagno and M. Duclot
Abstract 6-5, *Second International Meeting on Solid Electrolytes.*
St Andrews, Scotland, 1978.

[3] *Polymer Electrolyte Reviews—I*
ed. J. R. MacCallum and C. A. Vincent
Elsevier Applied Science, London, 1987.

[4] *Polymer Electrolyte Reviews—II*
ed. J. R. MacCallum and C. A. Vincent
Elsevier Applied Science, London, 1990.

[5] C. A. Vincent
Progress in Solid State Chemistry **17** (1987) 145-261

[6] M. A. Ratner and D. F. Shriver
Chemical Reviews **88** (1988) 109-124

[7] P. G. Bruce, J. Nowinski, F. M. Gray and C. A. Vincent
Solid State Ionics **38** (1990) 231-234

[8] T. M. A. Abrantes, L. J. Alcacer and C. A. C. Sequeira
Solid State Ionics **18/19** (1986) 315-320

[9] R. Huq and G. C. Farrington
Solid State Ionics **28-30** (1988) 990-993

[10] S. Passerini, R. Curini and B. Scrosati
Applied Physics A **49** (1989) 425-429

[11] C. D. Robitaille and D. Fauteux
Journal of Electrochemical Society **133** (1986) 315-325

[12] M. Z. A. Munshi and B. B. Owens
Solid State Ionics **38** (1990) 87

[13] M. Z. A. Munshi and B. B. Owens
Solid State Ionics **38** (1990) 95

[14] M. Z. A. Munshi and B. B. Owens
Solid State Ionics **38** (1990) 103

[15] D. G. H. Ballard, P. Cheshire, T. S. Mann and J. E. Przeworski
Macromolecules **23** (1990) 1256-1264

[16] M. Gauthier, D. Fauteux, G. Vassort, A. Belanger, M. Duval, P. Ricoux, J. M. Chabagno, D. Muller, P. Rigaud, M. B. Armand and D. Deroo
Journal of Power Sources **14** (1985) 23-26

[17] A. Gilmour, M. Z. A. Munshi, B. B. Owens and W. H. Smyrl
Materials and Processes for Lithium Batteries 358-372
K. Abraham and B. Owen, eds

[18] M. Gauthier, D. Fauteux, G. Vassort, A. Belanger, M. Duval, J. M. Chabagno, D. Muller, P. Rigaud, M. B. Armand and D. Deroo
Journal of the Electrochemical Society **132** (1985) 1333-1340

[19] T. Skotheim and I. Lundström
Journal of the Electrochemical Society **129** (1982) 894-895

[20] A. F. Sammells and P. G. P. Ang
Journal of the Electrochemical Society **131** (1984) 617-619

[21] S. Pantaloni, S. Passerini and B. Scrosati
Journal of the Electrochemical Society **134** (1987) 753-755

[22] O. Bohnke, C. Bohnke and S. Amal
Materials Science and Engineering **B3** (1989) 197-202

[23] K. Honda, M. Fujita, H. Ishida, R. Yamamoto, K. Ohgaki
Journal of the Electrochemical Society **135** (1988) 3151-3154

[24] B. Marsan, D. Fauteux and A. K. Vijh
Solid State Ionics **28-30** (1988) 1058-1061

[25] P. G. Bruce and C. A. Vincent
Journal of Electroanalytical Chemistry and Interfacial Electrochemistry **225** (1987) 1-17

[26] C. Berthier, W. Gorecki, M. Minier, M. B. Armand, J. M. Chabagno and P. Rigaud
Solid State Ionics **11** (1983) 91-95

[27] E. A. Rietman and M. L. Kaplan
Journal of Polymer Science Part C, Polymer Letters **28** (1990) 187-191

[28] K. E. Doan, S. Ganapathiappan, K. Chen, M. A. Ratner and D. F. Shriver
Materials Research Society Symposium Proceedings **135** (1989) 343-349

[29] P. M. Blonsky, D. F. Shriver, P. Austin and H. R. Allcock
Journal of the American Chemical Society **106** (1984) 6854-6855

[30] B. L. Papke, M. A. Ratner and D. F. Shriver
Journal of the Electrochemical Society **129** (1982) 1694-1701

[31] R. D. Armstrong and M. D. Clarke
Solid State Ionics **11** (1984) 301-303

[32] F. M. Gray
Personal Communication

[33] F. Bonino, S. Pantaloni, S. Passerini and B. Scrosati
Jounal of the Electrochemical Society **135** (1988) 1961-1965

[34] A. Magistris, G. Chiódelli, K. Singh and P. Ferloni
Solid State Ionics **38** (1990) 235-240

[35] S. Smart
Honours Research Project, University of St. Andrews, 1989.

[36] J. E. Weston and B. C. H. Steele
Solid State Ionics **7** (1982) 81-88

[37] R. Huq and G. C. Farrington
Journal of the Electrochemical Society **135** (1988) 524-528

[38] B. L. Papke, M. A. Ratner and D. F. Shriver
Journal of the Physical Chemistry of Solids **42** (1981) 493-500

[39] L. L. Yang, A. R. McGhie and G. C. Farrington
Journal of Electrochemical Society **133** (1986) 1380-1385

[40] P. G. Bruce, F. Krok and C. A. Vincent
Solid State Ionics **27** (1988) 81-88

[41] M. Eigen
Pure and Applied Chemistry **6** (1963) 97

[42] H. Yang and G. C. Farrington
Second International Symposium on Polymer Electrolytes pp 265-272
ed. B. Scrosati, Elsevier Applied Science, London and New York, 1990.

[43] J. W. Lorimer
Journal of Power Sources **26** (1989) 491-502

[44] J. R. MacCallum, A. S. Tomlin and C. A. Vincent
European Polymer Journal **22** (1986) 787-791

[45] F. M. Gray
Solid State Ionics **40/41** (1990) 637-640

[46] L. M. Torell and S. Schantz
in reference [4]

[47] A. S. Tomlin
PhD Thesis, University of St Andrews 1988

[48] S. Bhattacharja, S. W. Smoot and D. H. Whitmore
Solid State Ionics **18/19** (1986) 306-314

[49] P. G. Bruce and C. A. Vincent
Faraday Discussions of the Chemical Society **88** (1989) 43-54

[50] S. E. Lindsay, D. H. Whitmore, W. P. Halperin and J. M. Torkelson
Polymer Preprints **30** (1989) 442

[51] A. V. Chadwick
Journal of the Chemical Society, Faraday Transactions **86** (1990) 1157-1165

[52] A. V. Chadwick, A. A. Al-Mudaris and C. Bridges
Polymer Preprints **30** (1989) 418

[53] G. G. Cameron, J. L. Harvie and M. D. Ingram
Solid State Ionics **34** (1989) 65-68

[54] P. G. Bruce, M. T. Hardgrave and C. A. Vincent
Journal of Electroanalytical Chemistry and Interfacial Electrochemistry **271** (1989) 27-34

[55] R. P. Buck
Journal of Electroanalytical Chemistry and Interfacial Electrochemistry **271** (1989) 1-14

[56] A. Bouridah, F. Dalard and M. Armand
Solid State Ionics **28-30** (1988) 950-953

[57] A. Bouridah, F. Dalard, D. Deroo and M. B. Armand
Journal of Applied Electrochemistry **17** (1987) 625

[58] A. Bouridah, F. Dalard, D. Deroo and M. B. Armand
Solid State Ionics **18/19** (1986) 287-290

[59] E. A. Rietman, M. L. Kaplan and R. J. Cava
Solid State Ionics **17** (1985) 67-73

[60] J. R. MacCallum, M. J. Smith and C. A. Vincent
Solid State Ionics **11** (1984) 307

[61] M. L. Wiliams, R. F. Landel and J. D. Ferry
Journal of the American Chemical Society **77** (1955) 3701-3706

[62] The independent references of Vogel, Tamman and Fulcher are contained in reference [24] of M. A. Ratner's Chapter in reference [3]

[63] M. Kakihana, S. Schantz, B-E. Mellander and L. M. Torell
Second International Symposium on Polymer Electrolytes pp 23-33
ed. B. Scrosati, Elsevier Applied Science, London and New York, 1990.

[64] L. J. van der Pauw
Philips Research Reports **13** (1958) 1-9

[65] P. G. Bruce, J. Evans and C. A. Vincent
Solid State Ionics **25** (1987) 255-262

[66] G. G. Cameron, M. D. Ingram and J. L. Harvie
Faraday Discussions of the Chemical Society **88** (1989) 55-64

[67] M. Kakihana, J. Sandahl, S. Schantz and L. M. Torell
Second International Symposium on Polymer Electrolytes pp 1-16
ed. B. Scrosati, Elsevier Applied Science, London and New York, 1990.

[68] S. Atlung
Progress in Batteries and Solar Cells **2** (1979) 96-97

[69] R. P. Buck
Journal of Membrane Science **17** (1984) 1-62

[70] D. Fauteux
Journal of the Electrochemical Society **135** (1988) 2231-2237

[71] P. R. Sørensen and T. Jacobsen
Electrochimica Acta **27** (1982) 1671-1675

[72] J. Evans, C. A. Vincent and P. G. Bruce
Polymer **28** (1987) 2324-2328

[73] A. Katchalsky and P. F. Curran
Non-Equilibrium Thermodynamics in Biophysics
Harvard University Press, Cambridge, Massachusetts, 1967

[74] G. J. Dudley and B. C. H. Steele
Journal of Solid State Chemistry **31** (1980) 233-247

[75] P. G. Bruce and C. A. Vincent
New Polymeric Materials

[76] M. Spiro, in
Physical Methods of Chemistry Part IIA, Electrochemical Methods
ed. A. Weissberger and B. W. Rossiter
Wiley-Interscience, New York, 1971.

[77] D. F. Shriver, S. Clancy, P. M. Blonsky and L. C. Hardy
Proceedings of the 6th RISO International Symposium on Metallurgy and Materials Science.
F. W. Poulsen, N. Hessel Anderson, K. Clausen, S. Skaarup and O. T. Sorensen, eds.
RISO National Laboratory, Roskilde, 1985.

[78] J. Evans
Personal Communication

[79] F. M. Gray
European Polymer Journal **24** (1988) 1009-1012

[80] F. M. Gray, J. R. MacCallum and C. A. Vincent
Solid State Ionics **18/19** (1986) 282-286

[81] F. M. Gray, J. R. MacCallum and C. A. Vincent
British Patent Application No. 8619049

[82] D. Fauteux
Solid State Ionics **17** (1985) 133-138

[83] Computer programs written in Turbo Pascal by F. M. Gray

[84] W. I. Archer and R. D. Armstrong
Electrochemistry, volume 7
The Royal Society of Chemistry

[85] J. R. Macdonald
Journal of Chemical Physics **61** (1974) 3977-3996

[86] B. Boukamp
University of Twente

[87] Z. Ogumi, Y. Uchimoto, Z. Takehara and F. R. Foulkes
Journal of the Electrochemical Society **137** (1990) 29-34

[88] Z. Ogumi
Personal Communication

[89] E. L. Henn
Analytica Chimica Acta **73** (1974) 273-281

[90] S. S. M. Hassan
Organic Analysis Using Atomic Absorption Spectrometry
Ellis Horwood Limited, Chichester, 1984.

[91] P. T. Crisp, J. M. Eckert and N. A. Gibson
Analytica Chimica Acta **104** (1979) 93-98

[92] G. D. Christian and F. J. Feldman
Analytica Chimica Acta **40** (1968) 173-179

[93] A. S. Horned and B. B. Owen
The Physical Chemistry of Electrolytic Solutions
Reinhold Publishing Corporation, New York, 1958

[94] P. M. Blonsky, D. F. Shriver, P. Austin and H. R. Allcock
Solid State Ionics **18/19** (1986) 258-264

[95] L. L. Yang, R. Huq, G. C. Farrington and G. Chiodelli
Solid State Ionics **18/19** (1986) 291-294

[96] H. Yang, R. Huq and G. C. Farrington
Polymer Preprints **30** (1989) 412

[97] R. Huq, G. Chiodelli, P. Ferloni, A. Magistris and G. C. Farrington
Journal of the Electrochemical Society **134** (1987) 364-369

[98] M. Watanabe, S. Nagano, K. Sanui and N. Ogata
Solid State Ionics **28-30** (1988) 911-917

[99] P. G. Bruce, J. Evans and C. A. Vincent
Solid State Ionics **28-30** (1988) 918-922

[100] A. Killis, J.-F. LeNest, A. Gandini and H. Cheradame
Macromolecules **17** (1984) 63-66

[101] J. S. Lundsgaard, S. Yde-Anderson, R. Koksbang, D. R. Shackle, R. A. Austin and D. Fauteux
Second International Symposium on Polymer Electrolytes pp 395-410
ed. B. Scrosati, Elsevier Applied Science, London and New York, 1990.

[102] J. Shi
Personal Communication

[103] M. Leveque, J.-F. LeNest, A. Gandini and H. Cheradame
Makromolecular Chemistry, Rapid Communications **4** (1983) 497-502

[104] M. Leveque, J.-F. LeNest, A. Gandini and H. Cheradame
Journal of Power Sources **14** (1985) 27-30

[106] M. Bée
Quasielastic Neutron Scattering—Principles and Applications in Solid State Chemistry, Biology, and Materials Science
Adam Hilger, Bristol and Philadelphia, 1988

[107] C. Poinsignon
Solid State Ionics **35** (1989) 107-113

[109] D. Fauteux, J. Prud'homme and P. E. Harvey
Solid State Ionics **28-30** (1988) 923-928

[110] F. Guillaume, G. Coddens, A. J. Dianoux, W. Petry, M. Rey-Lafon and C. Sourisseau
Molecular Physics **67** (1989) 665-679

[111] A. J. Leadbetter and R. E. Lechner
Neutron Scattering Studies, in "The Plastically Crystalline State"
ed. J. N. Sherwood, J. Wiley & Sons, 1979.

[112] S. Besner, A. Vallée and J. Prud'homme
Polymer Preprints **30** (1989) 406

APPENDIX A

PHYSICAL AND ELECTROCHEMICAL PARAMETERS OF POLYMER ELECTROLYTES

This section contains data which have been used to determine other parameters pertinent to the study of mass transport in polymer electrolytes, such as the conductivity values reported in Chapter 7, as well as other parameters such as equivalent conductivities which could be calculated from the data. Properties such as the electrolyte concentrations are included because they tend not to be reported in the literature.

A1 CONCENTRATIONS OF SALTS IN POLYMER ELECTROLYTES

The concentrations of salts in the PEs used in this study were determined by cold-pressing a large 5 mm diameter pellet of the particular PE in a Specac press to two tonnes and determining its length and mass. The mass was determined to three decimal places using a Sartorius Microbalance, and it was generally of the order of 250 mg. The length was determined using a micrometer screwguage (accurate to 0.005 mm) and was usually of the order of 1 cm. From the mass the number of moles of salt present are determined, and the concentration is determined from this and the volume of the sample. Salt concentrations were used in the evaluation of equivalent conductivities and as a parameter against which other data were plotted. Some voidage is likely to occur by cold-pressing, but comparisons between cold-pressed samples and thick hot-pressed samples (used in the Hittorf experiments) suggest that this is negligible

The following Tables (Tables A-A to A-C) report the salt concentrations found for PEs used in this study: PEO_xLiClO_4 (x = 8,12,15,50,100), $PEO_xLiCF_3SO_3$ (x = 18,36,50,100) and PEO_xNaBPh_4 (x = 36,100). A graph of concentration *vs* the oxygen:metal ratio is shown (Figure A-1).

Table A-A. Concentration of PEO-$LiClO_4$ electrolytes.

O:M ratio	Concentration /mol dm^{-3}
8	2.83
12	2.13
15	1.63
18	1.36
50	0.51
100	0.26

Table A-B. Concentration of PEO-$LiCF_3SO_3$ electrolytes.

O:M ratio	Concentration /mol dm^{-3}
18	1.31
36	0.71
50	0.51
100	0.26

Table A-C. Concentration of PEO-$NaBPh_4$ electrolytes.

O:M ratio	Concentration /mol dm^{-3}
36	0.69
100	0.25

A2 CONDUCTIVITY

The following Tables (Tables A-D to A-G) contain conductivity data for PEO_xLiClO_4 (x = 8,12,50,100) over a range of temperatures, and for PEO_xLiClO_4 (x = 8, 12, 15, 18, 50, 100) (Table A-H) and $PEO_xLiCF_3SO_3$ (x = 18, 36, 50, 100) (Table A-I) at 120°C.

A graph of log(conductivity /Scm^{-1}) *vs* 1/T (K) (Figure A-2) for the data in Tables A-D to A-G show the curved response typically found for this system. The conductivity *vs* composition diagrams of PEO_xLiClO_4 and $PEO_xLiCF_3SO_3$ of Robitaille and Fauteux are included in Figure A-3 for comparison with the data obtained at 120°C.

Table A-D. Conductivity Variation of PEO_8LiClO_4 with Temperature.

Temperature /°C	Bulk resistance /Ω	Cell constant /10^{-2} cm^{-1}	Conductivity (σ) /10^{-4} S cm^{-1}	log(σ)
95.4	55.3±4.6	2.67	4.87±0.42	-3.32±0.04
110.5	31.1±2.3	2.67	8.63±0.64	-3.07±0.03
127.5	18.9±1.1	2.67	14.18±0.83	-2.85±0.03
141.8	12.5±0.7	2.67	21.43±1.20	-2.67±0.03

Table A-E. Conductivity Variation of $PEO_{12}LiClO_4$ with Temperature.

Temperature /°C	Bulk resistance /Ω	Cell constant /10^{-2} cm^{-1}	Conductivity (σ) /10^{-4} S cm^{-1}	log(σ)
95.5	57.9±3.2	2.67	4.63±0.26	-3.34±0.03
107.0	39.8±0.8	2.67	6.70±0.14	-3.17±0.01
121.0	29.6±0.5	2.67	9.04±0.14	-3.04±0.01
137.0	21.9±0.3	2.67	12.19±0.17	-2.91±0.01

Table A-F. Conductivity Variation of $PEO_{50}LiClO_4$ with Temperature.

Temperature /°C	Bulk resistance /Ω	Cell constant /10^{-2} cm^{-1}	Conductivity (σ) /10^{-4} S cm^{-1}	log(σ)
98.0	50.5±1.2	2.67	5.29±0.13	-3.28±0.01
108.8	42.4±0.9	2.67	6.30±0.14	-3.20±0.01
123.7	34.7±0.5	2.67	7.68±0.13	-3.12±0.01
138.6	30.8±0.4	2.67	8.66±0.10	-3.06±0.01

Table A-G. Conductivity Variation of $PEO_{100}LiClO_4$ with Temperature.

Temperature /°C	Bulk resistance /Ω	Cell constant /10^{-2} cm^{-1}	Conductivity (σ) /10^{-4} S cm^{-1}	log(σ)
91.2	121.8±1.2	2.67	2.19±0.02	-3.66
103.2	101.6±1.0	2.67	2.63±0.03	-3.58±0.01
114.5	87.2±0.9	2.67	3.06±0.03	-3.51±0.01
129.0	73.3±0.4	2.67	3.64±0.02	-3.44
140.0	68.1±0.4	2.67	3.92±0.02	-3.41

Table A-H. Conductivity Variation with Salt Content of PEO_xLiClO_4 at 120°C.

O:M ratio	Conductivity (σ) / 10^{-4} S cm^{-1}	log(σ)
12	15.00±0.55	-2.83±0.02
15	15.26±0.81	-2.82±0.02
18	12.42±0.43	-2.91±0.02
50	6.72±0.08	-3.17±0.01
100	3.34±0.21	-3.48±0.03

Table A-I. Conductivity Variation with Salt Content of $PEO_xLiCF_3SO_3$ at 120°C.

O:M ratio	Conductivity (σ) / 10^{-4} S cm^{-1}	log(σ)
18	5.71±0.37	-3.24±0.03
36	3.38±0.04	-3.47±0.01
50	2.70±0.09	-3.57±0.01
100	1.06±0.03	-3.98±0.01

Figure A-1. Graph of salt concentration *vs* O:M ratio for PEO_xLiClO_4 and $PEO_xLiCF_3SO_3$.

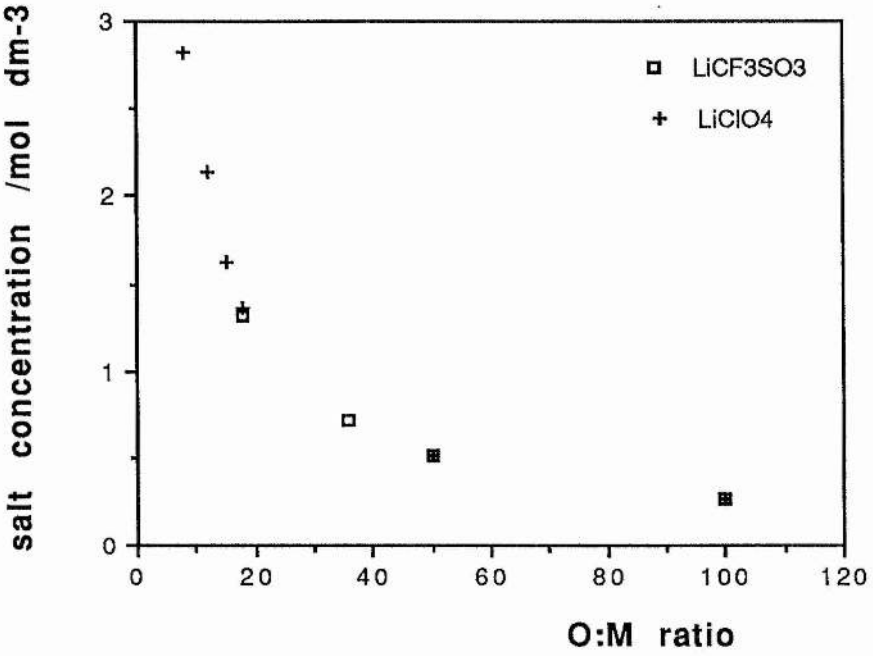

Figure A-2. Graph of conductivity *vs* inverse temperature for PEO_xLiClO_4.

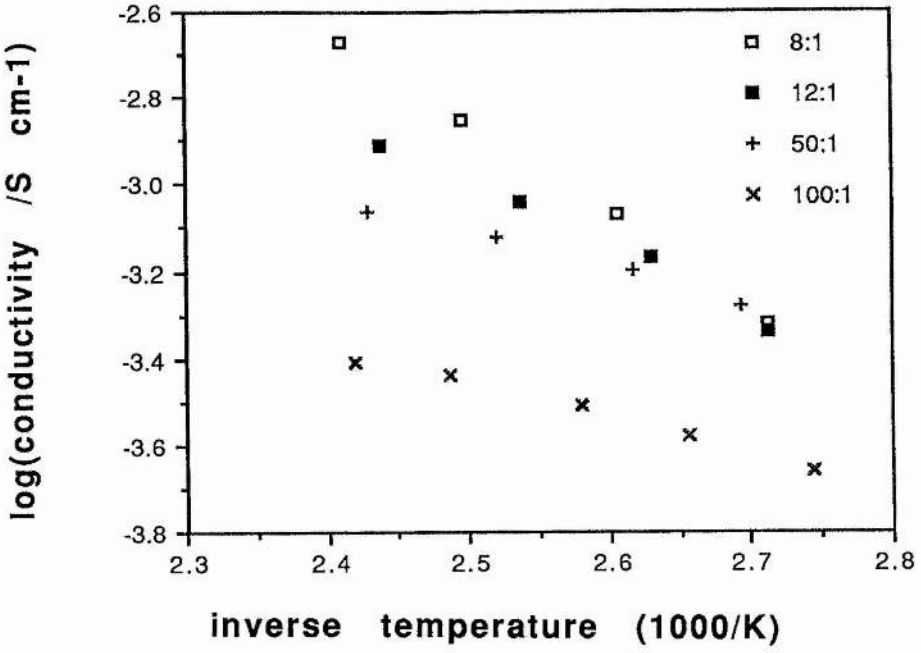

Figure A-3. Graph of conductivity *vs* temperature for PEO_xLiClO_4 (from reference 11).

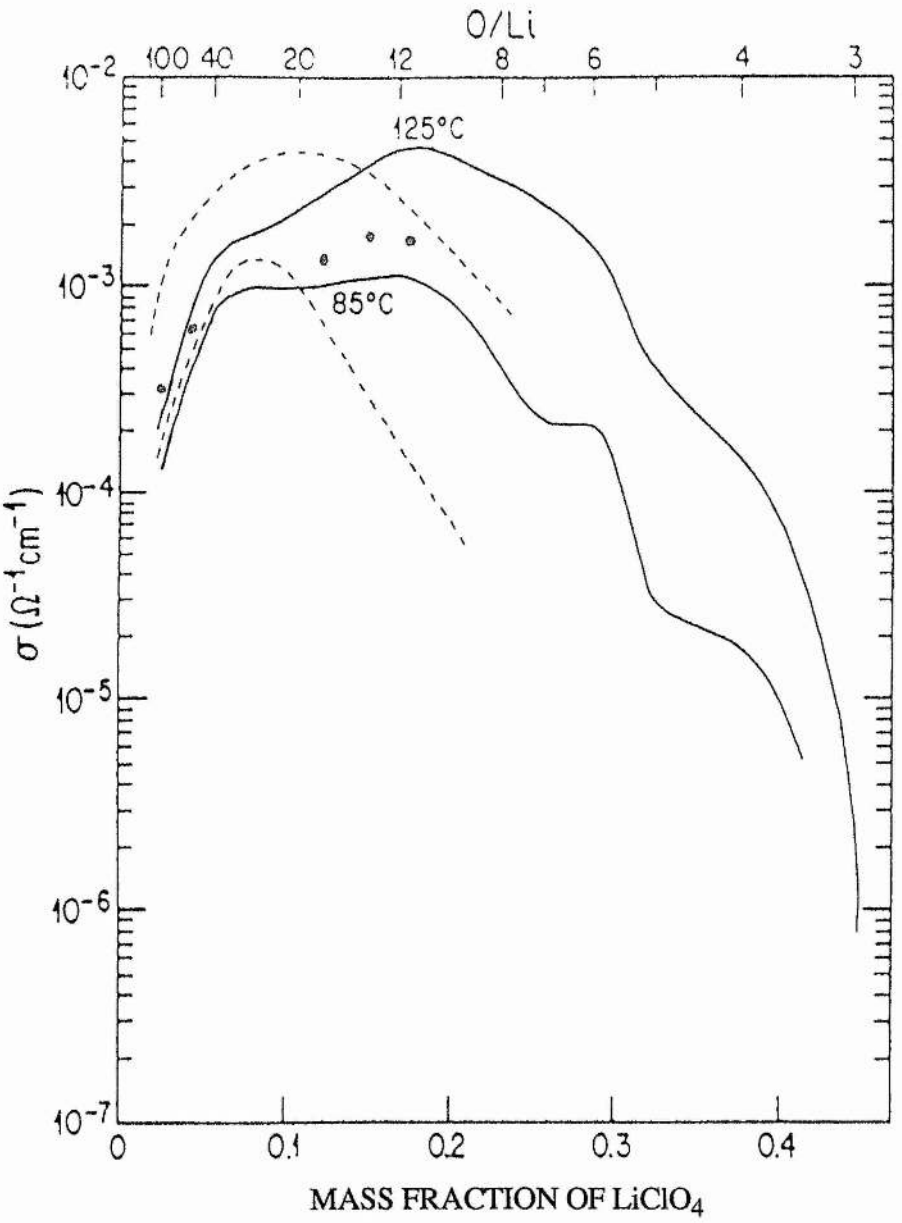

(⊙) THIS STUDY AT 120°C